Università degli Studi di Ferrara

DOTTORATO DI RICERCA IN
SCIENZE DELL'INGEGNERIA

CICLO XXXIV

COORDINATORE Prof. Stefano Trillo

UNCERTAINTY QUANTIFICATION IN STRUCTURAL ENGINEERING:

APPLICATIONS TO HISTORIC MASONRY STRUCTURES

Settore Scientifico Disciplinare ICAR/08

Dottorando

Dott. Ing. Marco Nale

_____

Tutori

Prof.ssa Ing. Elena Benvenuti

_____

Prof. Ing. Fabio Minghini

_____

Col.o. Prof. Ing. Antonio Tralli

_____

Anni 2018/2021

Abstract

Masonry structures constitute a large part of the building heritage present in Italy. This type of structure is particularly vulnerable to seismic action and has been found to be the structural type most responsible for the economic losses and social impacts following the recent earthquakes in central Italy. The vague and imprecise information on the structures, the materials used, the changes that have occurred over the centuries and the load conditions etc., make the assessments of their reliability and stability uncertain.

This doctoral thesis presents a methodology for the quantification of uncertainties for the structural elements of masonry structures.

The first part presents the state of the art on quantification of uncertainty by exposing the various probabilistic methods and related procedures. In particular, we focus on the use of fuzzy methods for quantifying uncertainties as they are more general and computationally efficient to describe the various and complex uncertainties that characterize existing masonry structures. The state of the art of risk assessment is also discussed, examining the aspects concerning the quantification of uncertainties and the reliability of existing structures.

The second part shows the creation of fragility curves for local collapse mechanisms considering the out-of-plane response. In particular, a classical procedure is applied for the evaluation of the fragility curves for a historical aggregate of the city of Ferrara, Italy, starting from the CARTIS database. For the assessment of vulnerability, the associated uncertainties are treated both through a classic Monte Carlo procedure and through fuzzy methods. Results obtained through linear kinematic analysis and dynamic analysis for some of the main local mechanisms are presented and a comparison with the results reported non-analytically in the technical literature is presented.

The third part critically exposes the assessment of the structural reliability of a masonry column of the cathedral of Saint George the Martyr in Ferrara. The uncertainties based on the data relating to the material coming from the experimental

tests are considered and the uncertainty on the horizontal thrusts of the arches discharged onto it is taken into account and therefore the variability of the pressure curve. For this purpose, simplified procedures are developed which allow taking into account the incomplete solidarity of the two parts, medieval and baroque, which make up the column.

keywords: uncertainty quantification; fuzzy set theory; stochastic methods; historic masonry structures.

Sommario

Le strutture in muratura costituiscono una grande parte del patrimonio edilizio presente in Italia. Questo tipo di struttura è particolarmente vulnerabile all'azione sismica ed è risultata la tipologia strutturale maggiormente responsabile delle perdite economiche e degli impatti sociali a seguito dei recenti eventi sismici nell'Italia centrale. Le informazioni vaghe ed imprecise sulle strutture, sui materiali utilizzati, le modifiche avvenute nei secoli e le condizioni di carico etc., rendono incerte le valutazioni sulla loro affidabilità e stabilità.

In questa tesi di dottorato si presenta una metodologia per la quantificazione delle incertezze per gli elementi strutturali delle strutture in muratura.

Nella prima parte si presenta lo stato dell'arte sulla quantificazione dell'incertezza esponendo i vari metodi probabilistici e le relative procedure. In particolare, ci si sofferma in particolare sull'uso di metodi fuzzy per la quantificazione delle incertezze in quanto più generali e computazionalmente efficienti per descrivere le diverse e complesse incertezze che caratterizzano le strutture esistenti in muratura. Viene inoltre discusso lo stato dell'arte della valutazione dei rischi, esaminando gli aspetti riguardanti la quantificazione delle incertezze e l'affidabilità delle strutture esistenti.

La seconda parte mostra la creazione di curve di fragilità per meccanismi di collasso locale considerando la risposta fuori piano. In particolare, viene applicata una procedura classica per la valutazione delle curve di fragilità per un aggregato storico della città di Ferrara, Italia, a partire dalla banca dati CARTIS. Per la valutazione della vulnerabilità, le incertezze associate vengono trattate sia attraverso una procedura classica alla Monte Carlo che attraverso metodi fuzzy. Vengono presentati risultati ottenuti sia attraverso analisi di tipo cinematico lineare e non che di tipo dinamico per alcuni dei principali meccanismi locali e viene presentato un confronto con i risultati riportati in modo non analitico nella letteratura tecnica.

La terza parte espone in modo critico la valutazione dell'affidabilità strutturale di una colonna in muratura della cattedrale di San Giorgio Martire a Ferrara. Si considerano le incertezze basate sui dati relativi al materiale provenienti dalle prove sperimentali e

si tiene conto dell'incertezza sulle spinte orizzontali degli archi che si scaricano su di essa e quindi della variabilità della curva delle pressioni. A tale scopo si sviluppano delle procedure semplificate che consentono di tenere conto della non completa solidarietà delle due parti, medievale e barocca, che compongono la colonna.

parole chiave: quantificazione dell'incertezza; metodi fuzzy; metodi stocastici; strutture storiche in muratura.

Acknowledgment

I would like to express my gratitude to my advisors Professor Elena Benvenuti, Professor Fabio Minghini and Professor Antonio Tralli for their valuable help, feedback and support during this research. In particular, I would like to thank Professor Tralli for his guidance in this work throughout the period of this Ph.D.

I would also like to acknowledge Dr. Andrea Chiozzi for his feedback, his constant support of this work.

I would like to thank Professor Michael Beer for having the opportunity to work and investigate these issues as visiting scholar at the Institut für Risiko und Zuverlässigkeit - Leibniz Universität Hannover. I also want to express my gratitude to other members of his research team Dr. Eng. Matteo Broggi, Professor Marcos Valdebenito and Professor Pengfei Wei for introducing me to uncertainty quantification in the presence of vague and imprecise information and stochastic methods.

This thesis was partially funded by the Regional Agency of Civil Protection of Regione Emilia – Romagna under research grant no. DGR n.686 del 14/05/2018 and the University of Ferrara. These supports are gratefully appreciated and acknowledged.

Contents

List of Figures

List of Tables

1 Introduction

1.1 Motivation and background

Recent and past earthquakes (e.g., in Italy: Friuli 1976, Irpinia 1980, Umbria-Marche 1996, L'Aquila 2009, Emilia 2012 and Central Italy 2016), have shown that unreinforced masonry buildings (URM) are prone to damage by seismic actions also causing a large number of casualties, injuries and economic loss.

The seismic assessment of these structures, mainly historical ones, is a very challenging task since their response may be affected by various aspects, such as masonry mechanical behavior, complex structural and geometric arrangement, changes of intended use and structural changes that occurred over the centuries.

A very large number of papers have dealt with this topic over the past fifty years and nowadays several methods are available in the literature for the structural assessment of existing masonry buildings, from simple analytical methods to more advanced numerical methods such as finite element methods and discrete element methods. Among the review articles on this topic are mentioned (D'Altri et al., 2020; ReLUIS, 2020; Roca et al., 2010; Tralli et al., 2014).

The evaluation of the reliability of existing masonry structures is therefore of enormous importance both under the usual vertical operating loads and for resistance to any future earthquakes. Strictly speaking, all variables in engineering structures are stochastic to a certain degree and structural reliability analysis has to deal with the rational treatment of random variables and uncertainties. However, despite some pioneering works of Italian researchers (Augusti et al., 1984; Augusti and Ciampoli, 2000; Caddemi et al., 2002) on probabilistic limit analysis, only very few applications to monuments and masonry structures have been published and generally led only to qualitative results.

The main reason is probably that in the case of existing masonry structures we are faced with too great uncertainties on the mechanical and also geometrical parameters and too large variability of them. Actually, mainly because masonry is a heterogeneous

material consisting of units of different types, such as bricks, ashlars, adobes, regular or irregular stones etc., and joints made of clay, bitumen, chalk, lime or cement-based mortar, glue etc. Both units and joints can have completely different mechanical, chemical and physical behaviors and the number of their possible combinations, in terms of geometry, assembling and characteristics can be sensibly high, to raise some doubts about the pertinence of the term "masonry". Nevertheless, the different types of masonry, even though exhibit diverse mechanical behaviors have broadly a very low tensile strength as a common feature and this property has always been so important to influence the shape of ancient constructions. Furthermore, there are many challenges in performing advanced mechanical tests in ancient structures because of the great variety of masonries, the variability of the masonry itself in a specific structure and the impossibility of reproducing such variability in just one specimen.

The structures belonging to the Architectural Heritage, namely, by their very nature and history (materials and assembling), provide many very interesting challenges in conservation, diagnosis, analysis, monitoring and strengthening. The recently published Guidance on Heritage Impact Assessments for Cultural World Heritage Properties by ICOMOS (International Council on Monuments and Site, 2011) and the Italian Guidelines for cultural heritage buildings in seismic zones by MIBAC (Ministero della Cultura, 2010) recommends an iterative process between data acquisition and diagnosis on one hand and structural behavior and safety on the other. In particular, diagnosis and evaluation of structural safety are two sequential and related steps that establish the effective need for some interventions and their extent. However, as a matter of fact, in the evaluation of the reliability of masonry buildings or structural elements practitioners make use of the regulations in force (CEN, 2005a; MIT, 2018, 2019) that allow a deterministic evaluation and the use of safety coefficients that generally require a reduction in the compressive strength of the masonry up to a factor of three.

An engineering problem has to contend with the level of knowledge available. In general, in engineering, its purpose can be divided into two categories: the analysis of the behavior of the structure under known conditions and the design of a structure that satisfies a minimum safety criterion established by the codes and guidelines.

These categories have to deal with the data of the structure and the loads that are not exactly known but are affected by intrinsic uncertainties. This problem can be solved

by reducing uncertainties by increasing knowledge.

The primary goal of structural engineering is life safety to hazard and collapse prevention. Currently, the possible assessment of the risk of collapse allows us to evaluate the safety of a structure thanks to advances in computational power and in the development of models that can reproduce the behavior of any structural element of a structure. These structures, systems and infrastructure require proper measures and approaches to allow and verify their reliable performance.

The available and the required information to describe structures and systems is the major problem in this context due to their discrepancy. Due to limited, vague and imprecise information, the reliability and performance analysis of complex structures or systems becomes increasingly complicated. It has therefore become a key question how to model this uncertainty for quantification despite significant developments in generalizing approaches. Certainly, depending on the purpose of the analyzes and the information available, the analyst can dispose of a series of developments. It is, therefore, necessary to use a probabilistic approach to the problem. In most cases, an expert expresses a belief in the form of a subjective probability distribution, which can be implemented in a Bayesian approach. Set theoretical descriptors can be used if only ranges or limits are available for some parameters. All this leads to non-probabilistic approaches which combined with probabilistic information give imprecise probabilities. By aggregating the quantification of generalized uncertainty with developed and emerging concepts and techniques from the traditional probabilistic domain, in particular with advanced stochastic modeling and Monte Carlo simulation, it is now possible to obtain reliability assessments for the most complex structural problems.

The reliability analysis of structural elements in industrial, aerospace and nuclear engineering has evolved in a completely different way in the last decades (Ang and Tang, 2007; Zio, 2013). Non-deterministic reliability analysis methods classified as probabilistic, for instance, the Monte Carlo simulation (MCS) method, first-order reliability method (FORM), and response surface method (RSM) are currently employed together with possibilistic methods such as interval analysis and fuzzy analysis.

1.2 Objectives and scope

This dissertation is focused on developing a methodology to characterize the response

of the structures under uncertainty and the implication of collapse for some structural elements of historic masonry structures. The research includes some case study applications of out-of-plane failure of masonry walls of the historic center in Ferrara, Italy, and the columns of the Cathedral of Saint George the Martyr in Ferrara, Italy.

First of all, only one type of masonry is considered consisting of fired clay bricks and lime mortar typical of the Po Valley and in particular of the city of Ferrara. Moreover, simple structural elements are also considered: load-bearing walls and columns. As for the walls, the derivation of fragility functions for local failure mechanisms in unreinforced masonry buildings starts from the data processing of the CARTIS database (created with an expeditious method). A qualitative description of the building stock and associated relevant uncertainties (material, geometrical, loads) are initially considered. Epistemic uncertainties are included using logical trees. Mechanical models, the validity of which is documented in the literature also from results of experimental campaigns, are introduced to analyze the out-of-plane response of masonry walls. A dynamic approach is used, adopting a multiple stripe analysis method to derive punctual fragilities. Finally, fragility functions are fitted to the computed fragilities, showing the moderate quality of the building stock.

Subsequently, the uncertain quantities are treated as fuzzy sets and the statistical deviations obtained are represented in the same context, even reaching the definition of the relative influence of the various uncertain parameters. Then the columns of the cathedral of Ferrara currently undergoing reinforcement and restoration are considered. The problem is very complex, the original medieval (of the XII century) columns were incorporated into new large columns in the XVIII century, about 2.20 by 4.20 m. The quality of the masonry is in both cases fair but the two parts that constitute the column are substantially disconnected and the internal texture uncertain and cannot be investigated with certainty. Finally, the loads transmitted by the heavy vaulted roofs, in particular the horizontal thrusts, cannot be accurately determined given the age of the structure and the nature of the subsequent interventions. The standard application of the technical regulations does not appear satisfactory and is of doubtful applicability, for example, the column is subject to variable loads along the heights well as the use of finite element techniques given the irregularity of the internal texture. Therefore, also to apply statistical procedures such as the Monte Carlo simulation or the fuzzy

sets that require a large amount of analysis, appropriate generalizations of the beam theory have been developed.
The main objectives of this research are:

- to develop a stochastic methodology upon which can be quantified seismic structural response in presence of vague and imprecise information using simplified mechanical models;
- to identify, investigate and evaluate the various uncertainties inherent in structural elements in masonry structures;
- to evaluate with a sensitivity analysis, the parameters that influence the structural response and the collapse of these elements under seismic actions.

1.3 Organization

This dissertation deals with the uncertainty quantification in structural engineering with applications to historic masonry structures, focusing on modeling uncertainty, quantification of its impacts on structural response, and implications on collapse safety under different load conditions.
It is organized into seven chapters which are described in the following paragraphs:

Chapter 2 presents probabilistic methods and procedures for modeling and evaluating uncertainties in parameters. The main issues are addressed on the sources of uncertainty, the mathematical description of uncertain data, generalized methods for the propagation of uncertainty, Monte Carlo simulation and sensitivity analysis.
Furthermore, we present a summary of risk assessment in engineering. The main issues that compose a robust risk assessment are addressed: the role of data knowledge, the role of quantifying uncertainty and the reliability of existing structures.

Chapter 3 presents typological fragility functions for local failure mechanisms for Unreinforced Masonry buildings (URM). URM buildings undergoing seismic actions often exhibit local failure mechanisms which represent a serious life-safety hazard, as recent strong earthquakes have shown. Compared to new buildings, older unreinforced masonry buildings are more vulnerable, not only because they have been designed without or with limited seismic loading requirements, but also because

horizontal structures and connections amid the walls are not always effective. Also, Out-Of-Plane (OOP) mechanisms can be caused by the significant slenderness of the walls even if connections are effective.
The purpose of this chapter is to derive typological fragility functions for unreinforced masonry walls considering OOP local failure mechanisms. In the case of slender walls with good material properties, the OOP response can be modeled concerning an assembly of rigid bodies undergoing rocking motion. In particular, depending on its configuration, a wall is assumed either as a single rigid body undergoing simple one-sided rocking or a system of two coupled rigid bodies rocking along their common edge. A set of 44 ground motions from earthquake events that occurred from 1972 to 2017 in Italy is used in this study. The likelihood of collapse is calculated via Multiple Stripe Analysis (MSA) from a given wall undergoing a specific ground motion. Then, the single fragility functions are suitably combined to define a typological fragility function for a class of buildings. The procedure is applied to a historical aggregate in the city center of Ferrara (Italy) as a case study. The fragility functions developed in this research can be a helpful tool for assessing seismic damage and economic losses in unreinforced masonry buildings on a regional scale.

Chapter 4 presents a method to quantify the effect of the uncertainty with which parameters such as geometric data, mechanical characteristics and the entity and position of the loads are known on local out-of-plane failure mechanisms in existing unreinforced masonry buildings (URM).
The chapter discusses the modeling of uncertainties by fuzzy methods and references is made to good quality masonry made with bricks baked in clay and lime mortar, as typical of buildings in the Po Valley, such as those hit by the 2012 earthquake in Emilia. In the frequent case of slender elements with good material properties, the wall response can be modeled as an assembly of rigid bodies and linear kinematic limit analyses, as defined in Italian standard, or dynamic analyses for studying the rocking motion are employed to provide the “fuzzy” fragility curves as a function of peak ground acceleration (PGA). A probabilistic evaluation of the collapse loads under seismic actions and a sensitivity analysis are also presented for all these procedures and different local collapse mechanisms.

Chapter 5 presents a procedure for the safety assessment of the masonry columns of the Cathedral of Saint George the Martyr in Ferrara, Italy. The current state of the column is detailed with the relative information on the mechanical properties of the materials, the loads and their application. Particular attention is given to the creation of simplified mechanical models useful to obtain a fair compromise between computational times and the robustness of the results. These simplified models are validated with analytical solutions and numerical models (i.e., FEM models).

Chapter 6 presents a procedure for quantifying the uncertainties encountered in the structural analysis of masonry pillars of the cathedral of Ferrara. This method is applied where the main sources of uncertainties are vague and imprecise information such as the characterization of the behavior of the material and the loads and their application. The purpose of quantifying uncertainties is to determine adequate safety margins. In this chapter, the uncertainties are quantified through fuzzy theories that allow deriving the interval bounds and the mean structural response.

Chapter 7 summarizes the main conclusions of this dissertation. The limitations of the studies are presented and provide some suggestions for future work in this field.

2 Review of basic probabilistic methods and risk assessment procedures

This chapter introduces very concisely the probabilistic methods and procedures for modeling and evaluating uncertainties in data. The main issues are addressed on the sources of uncertainty, the mathematical description of uncertain data, generalized methods for the propagation of uncertainty, Monte Carlo simulation and sensitivity analysis.

Furthermore, this chapter focuses on risk assessment in engineering. The main issues that compose a robust risk assessment are addressed: the role of data knowledge, the role of quantifying uncertainty and the reliability of existing structures.

For these issues, the characteristic terminology and equations are recalled from various textbooks present in literature (Ang and Tang, 2007; Benjamin and Cornell, 1970; Zio, 2007).

2.1 Mathematical description of uncertain data

The following paragraphs show the various mathematical models for the stochastic description of uncertain data and with greater precision, of the input parameters of the model. The purpose of this section is not to give complete coverage of the mathematics used but to provide a minimum formalism required below.

2.1.1 Classic probability theory

The probability space $(\Omega, \mathcal{F}, \mathbb{P})$ is defined by the event space Ω (also known as sample space, universal set, or outcome space) equipped with the σ-algebra $\mathcal{F}$ and a probability measure $\mathbb{P} \in [0,1]$.

2.1.1.1 Axioms

The foundations of probability theory were formalized by Andrey Kolmogorov in 1933 and are known as Kolmogorov's axioms which are:

1. the probability of an event is a non-negative real number

$$\mathbb{P}(\Omega) \geq 0 \qquad \forall \Omega \in \mathcal{F} \tag{2.1}$$

2. the probability that at least one of the elementary events in the entire sample space will occur is 1 (unitary)

$$\mathbb{P}(\Omega) = 1 \tag{2.2}$$

3. any countable sequence of disjoint sets (synonymous with mutually exclusive events) $\{\omega_1, \omega_2, \ldots, \omega_n\} \in \Omega$ satisfies (σ – additivity)

$$\mathbb{P}\left(\bigcup_{i=1}^{\infty} \omega_i\right) = \sum_{i=1}^{\infty} \mathbb{P}(\omega_i) \tag{2.3}$$

2.1.1.2 Random variable

A random variable *X* is defined by a map $X(\omega): \Omega \mapsto \mathcal{D}_X \subset \mathbb{R}$ that connects a fundamental event $\omega \in \Omega$ from a value $X(\omega)$ to $\mathcal{D}_X$ which is the support domain of *X*. A *cumulative distribution function* (CDF) describes the random variable X denoted by a function $F_X(x)$ that assigns a probability to an event i.e., $F_X(x) = \mathbb{P}(X \leq x)$.

$$\mathbb{P}(a \leq x \leq b) = \int_a^b f_X(x)\, dx \tag{2.4}$$

In the case that *X* is a continuous function the first derivative of CDF is the *probability density function* (PDF) denote by $f_X(x)$, where $f_X(x)$ is the non-negative Lebesgue integrable function.

$$f_X(x) = \frac{dF_X(x)}{dx} \tag{2.5}$$

In the presence of data from a random variable *X*, a useful tool for the estimation of the CDF can be the *empirical cumulative distribution function* (eCDF).

$$F_X^{emp}(x) = \frac{1}{N}\sum_{i=1}^{N} \mathbb{I}_{x \geq \mathcal{X}^{(i)}}(x) \tag{2.6}$$

where $\mathbb{I}$ is an indicator factor that is equal to 1 when a true condition is verified otherwise it is equal to 0. The $\mathcal{X}^{(i)}$ is the i^{th} realization of the random variable *X*.

It is useful to exploit the definitions of the first moment of a random variable *X* which is commonly defined as the mean (a.k.a. expected value) and that of the second central moment (a.k.a. variance). The mean $\mathbb{E}[\mathcal{X}]$ and variance $\mathrm{Var}[\mathcal{X}]$ are defined as follows:

$$\mathbb{E}[\mathcal{X}] = \frac{1}{N}\sum_{i=1}^{N} \mathcal{X}^{(i)} \qquad \mathrm{Var}[\mathcal{X}] = \frac{1}{N-1}\sum_{i=1}^{N} \left(\mathcal{X}^{(i)} - \mathbb{E}[\mathcal{X}]\right)^2 \tag{2.7}$$

where the parameter $\boldsymbol{\theta}$ describes a vector that represents the shape of CDF, are extracted by solving: $\mu(\theta) = \mathbb{E}[\mathcal{X}]$, $\sigma^2(\theta) = \mathrm{Var}[\mathcal{X}]$.

2.1.1.3 Limitation

It is not possible to distinguish between epistemic and aleatory uncertainty and it is not possible to precisely identify the sources of uncertainties separately. Above all, in cases of lack of data, where the judgment of the expert and/or the information are imprecise, the probability depends a lot on the initial assumptions (Rocchetta et al., 2018).

2.1.2 Evidence Theory

The theory of evidence can be seen as a generalization of the classical theory of probability also called the Demster-Shafer theory (Dempster, 1967; Shafer, 1976).

The evidence theory manages to represent both aleatory and epistemic uncertainty with a range from plausibility to belief in which probability theory represents only one value.

Two measures are considered in the theory of evidence for every event $\mathcal{E}$ in the event space Ω: plausibility and belief. To define these two measures is introduced *m* which is defined as the basic probability assignment (BPA):

$$m(\mathcal{J}) = \begin{cases} > 0 & \text{if } \mathcal{J} \in \mathcal{F} \\ 0 & \text{if } \mathcal{J} \subset \mathcal{F} \text{ and } \mathcal{J} \notin \mathcal{F} \end{cases} \tag{2.8}$$

where $\mathcal{F}$ is a subset Ω.

$$\sum_{\mathcal{J} \in \mathcal{F}} m(\mathcal{J}) = 1 \tag{2.9}$$

The $m(\mathcal{J})$ represents the probability masses that are associated with an event $\mathcal{J}$. This can be interpreted as a sum of likelihood weights. The maximum amount of likelihood that can be associated with an event $\mathcal{E}$ is defined as the plausibility measure while the minimum amount of likelihood that can be associated with an event $\mathcal{E}$ corresponds to the belief measure. These are defined as follows:

$$\text{Pls}(\mathcal{E}) = \sum_{\mathcal{J} \cap \mathcal{E} \neq \emptyset} m(\mathcal{J}) \tag{2.10}$$

$$\text{Bel}(\mathcal{E}) = \sum_{\mathcal{J} \subseteq \mathcal{E}} m(\mathcal{J}) \tag{2.11}$$

From the Eqs. (2.10) and (2.11), it follows that $\text{Bel}(\mathcal{E}) + \text{Bel}(\mathcal{E}^C) \leq 1$, $\text{Pls}(\mathcal{E}) + \text{Pls}(\mathcal{E}^C) \geq 1$, and complementary property $\text{Bel}(\mathcal{E}) + \text{Pls}(\mathcal{E}^C) = 1$, where $\mathcal{E}^C$ is the complementary event $\mathcal{E}$. When $\text{Bel}(\mathcal{E}) = \text{Pls}(\mathcal{E})$ there is the special case of traditional probability. A Demster-Shafer structure (DS) occurs with the construction of $\text{Bel}(\cdot)$, $\text{Pls}(\cdot)$, $\mathcal{J}$ and $m(\mathcal{J})$. The theory of evidence has been applied in various fields of application and theoretical developments (Helton and Oberkampf, 2004). The fields of application vary from optimization and design, decision making, simulation, system responses and model predictions and uncertainty quantification. In the fields of civil engineering, it has been used for applications including structural reliability (McGill and Ayyub, 2008; Oberguggenberger and Fellin, 2008), structural optimization (Tonon and Bernardini, 1998) and geotechnical stability investigations (Hall et al., 2004).

2.1.2.1 Limitation

The ability to determine bounds for specific events constitutes one of the limitations for the trivial application of this theory. In practical applications, the definition of bounds is a non-trivial procedure.

2.1.3 Probability boxes

A probability box is a robust mathematical instrument commonly deployed to characterize uncertain factors affected by mixed sources of aleatory and epistemic uncertainty.

Probability boxes (p-boxes) specify the CDF of a variable X by lower and upper bounds identified by $\underline{F}_X$ and $\overline{F}_X$, each (Beer et al., 2013; Ferson and Ginzburg, 1996).

$$\left\{P \in \mathbb{P} \middle| \forall p \in \mathbb{R},\ \underline{F}_X(x) = P\left(\left(-\infty, x\right]\right) \leq \overline{F}_X(x)\right\} \tag{2.12}$$

the real but unknown CDF is inside these bounds which are defined $\underline{F}_X(x) \leq F_X(x) \leq \overline{F}_X(x)$ for any value $x \in \mathcal{D}_X$. The intermediate area is formed by the two boundary curves; it is called by the name: probability-box. Figure 2.1 shows a clear example of a p-box.

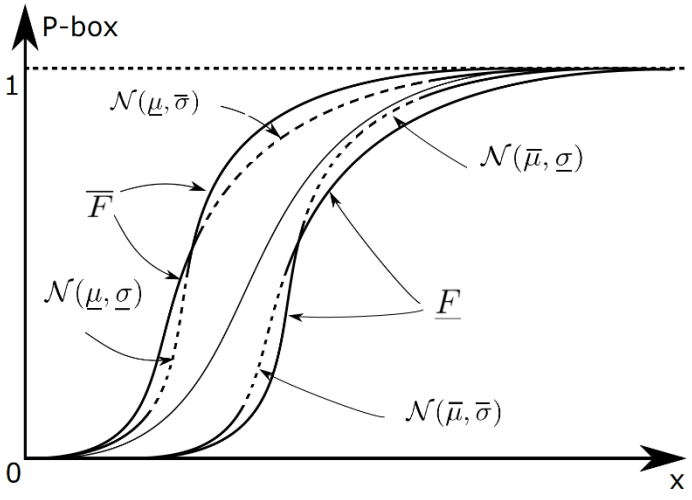

Figure 2.1: example of probability box.

In literature, two kinds of p-boxes are considered, specifically free and parametric p-boxes. Lower and upper bounds on the CDF determine free p-boxes. This means that the true CDF can have an arbitrary shape as long as it realizes the feature of a generic

CDF and it is attributable to the bounds of the p-box. Free p-boxes are a peculiar case of Dempster-Shafer structures when considering the event $\{X \le x\}$. Then, the plausibility function $\mathrm{Pls}(X \le x)$ is the same to $\overline{F}_X(x)$ and the belief function $\mathrm{Bel}(X \le x)$ is the same $\underline{F}_X(x)$, for all $x \in \mathcal{D}_X$.

Parametric p-boxes, also known as distributional p-boxes, are determined as distribution function groups where the parameters belong to intervals. Parametric p-boxes provide an explicit division of aleatory and epistemic uncertainties. The epistemic uncertainty is depicted by the intervals in the distribution parameters, although aleatory uncertainty is reproduced by the distribution function family. Nevertheless, parametric p-boxes are more limiting than free p-boxes because they need knowledge of the distribution family.

2.1.3.1 Limitation

While p-boxes may allow dealing with epistemic and aleatory uncertainties one of the crucial aspects of this tool for quantifying uncertainty lies in defining the bounds of epistemic uncertainty (Bi et al., 2019; Faes et al., 2021).

2.1.4 Fuzzy theories

Fuzzy variables are deeply connected to the set theory. In the following, the fundamental definitions of sets are introduced here by Möller and Beer (2004). Given a fundamental set Ω and *x* an element of this fundamental set, a fuzzy variable $\tilde{A}$ is defined:

$$\tilde{A} = \left\{ \left(x, \mu_{\tilde{A}} \right) \middle| x \in \Omega \right\} \tag{2.13}$$

where $\mu_{\tilde{A}}$ is the membership function of the fuzzy variable. The membership function describes the uncertainty. This function can be continuous or discrete.

$$\mu_{\tilde{A}} \ge 0 \tag{2.14}$$

When the values of this function belong to the range [0,1], it refers to a normalized membership function. Only normalized membership functions will be considered

below.

$$\sup_{x \in X} \left[\mu_{\tilde{A}}(x) \right] = 1 \tag{2.15}$$

A crisp set is called when the membership function is binary, i.e. {0,1}, otherwise when the membership function is not binary is called fuzzy set. Figure 2.2 shows how a fuzzy set and crisp set are defined.

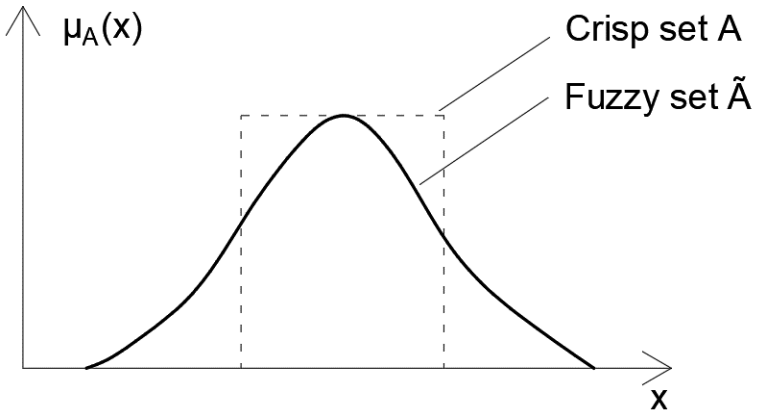

Figure 2.2: fuzzy variable $\tilde{A}$ with membership function $\mu_{\tilde{A}}$ (Möller and Beer, 2004).

Fuzzy is a generalization of the epistemic uncertainty modeled by a crisp set (i.e., intervals) and can represent the imprecision in measurements. When α = 0 the relative interval *A* denoted the maximum possible interval for the event with high uncertainty. Otherwise, when α = 1 the value of the measurement is very precise.

2.1.4.1 α-level set (α-cut)

The α-level interval is defined as:

$$A_\alpha = \left\{ x \in X \middle| \mu_{\tilde{A}}(x) \geq \alpha \right\} \tag{2.16}$$

where $\alpha \in [0,1]$ is the α-cut level. Remark that the α-cuts provide nested intervals. Each α-level set is a connect interval $\left[x_{\alpha_k l}, x_{\alpha_k r} \right]$ when the fuzzy set is convex.

$$x_{\alpha_k, l} = \min \left[x \in X \middle| \mu_A(x) \geq \alpha_k \right] \tag{2.17}$$

$$x_{\alpha_k,r} = \max\left[x \in X \middle| \mu_A(x) \geq \alpha_k \right]$$

2.1.4.2 Extension principle

The extension principle allows you to map the fuzzy set to a result space (Zadeh, 1975). The result membership function $\tilde{B}$ is obtained from those of input fuzzy numbers $x_1,\ldots, x_n$ as

$$\tilde{B} = \left\{ \left(z, \mu_B(z) \right) \middle| z = f(x_1,\ldots,x_n) \right\} \quad z \in \mathbb{Z} \quad (x_1,\ldots,x_n) \in X_1 \times \ldots \times X_n \tag{2.18}$$

with membership function

$$\mu_B(z) = \begin{cases} \sup\limits_{z=f(x_1,\ldots,x_n)} \min\left[\mu(x_1),\ldots,\mu(x_n) \right] & \text{if } \exists\, z = f(x_1,\ldots,x_n) \\ 0 & \text{otherwise} \end{cases} \tag{2.19}$$

Figure 2.3 shows the process of mapping to a new fuzzy output using the extension principle.

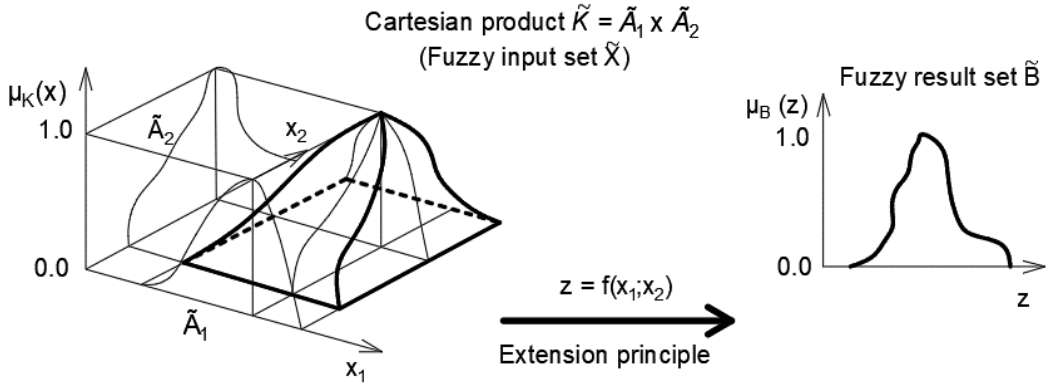

Figure 2.3: mapping two fuzzy (A_1, A_2) set into fuzzy set B using the extension principle (Möller and Beer, 2004).

2.1.4.3 Fuzzy distributions

A probability distribution associated with a fuzzy interval for every value $x \in \mathcal{D}_X$ creates a fuzzy distribution that permits explicit the CDF of this distribution.

$$F_X(x) \in \Xi_X(x,c) \tag{2.20}$$

where $F_X(x)$ is a fuzzy interval, $\Xi_X(x,c)$ represent the membership function for variable X and CDF value $c \in [0,1]$. The construction of a fuzzy distribution can be seen as a generalization of a free or parametric p-box, as shown in Figure 2.4. The associated membership function is shown in red, for a given value $x^{(0)}$. More, the lower and upper bounds of the CDF have been derived analytically for a given level $\alpha^{(0)}$. This method can be replicated for every value $x \in \mathcal{D}_X$.

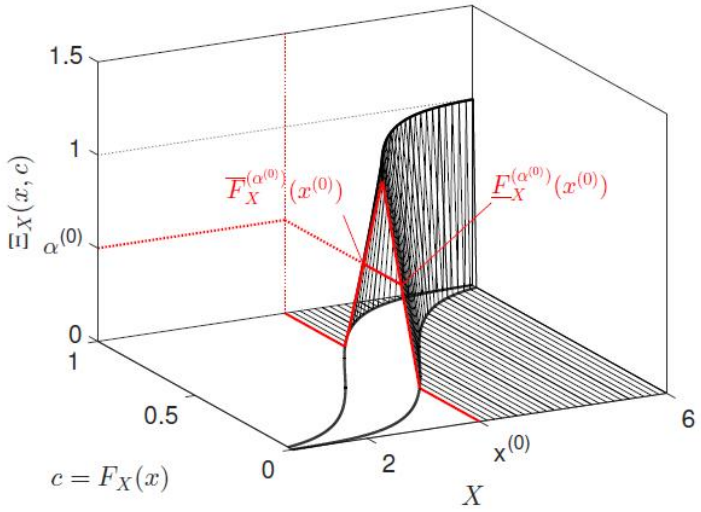

Figure 2.4: fuzzy distribution: a generalization of a p-box (Schöbi, 2017).

2.1.5 Additional methodologies

Other methodologies for modeling uncertainty are available in the literature to model uncertainty in addition to the methods presented here (for more details see (Beer et al., 2013)). These include info-gap theory (Ben-Haim, 2006), credal sets (Karlsson et al., 2010), lack of knowledge theory (Barthe et al., 2003; Ladevèze et al., 2006) and possibility theory (de Cooman et al., 1995; Dubois and Prade, 1988). All these methodologies are part of information theory as strictly described in Klir (2006).

2.1.6 Comparison

Different concepts exposed in previous sections are connected and visualized in Figure 2.5. The various concepts are placed inside a rectangular box. The Dempster-Shafer (DS) structures and the p-boxes are shown inside a single rectangular box due to due

to their equivalence. Starting from the higher level and following the arrows, it is possible to increase the knowledge of the data to choose the best model of uncertainty. The most general uncertainty representations are shown in the highest level, i.e. all three aspects of uncertainty models are included. When you pass to a lower level, an aspect of uncertainty modeling is removed. For instance, if a fuzzy distribution will reduce to a free p-box, the uncertainty model removes fuzziness. Therefore, the free p-box decreases to an interval when removing aleatory uncertainty. Lastly, the interval eases to a constant when disregarding any epistemic uncertainty.

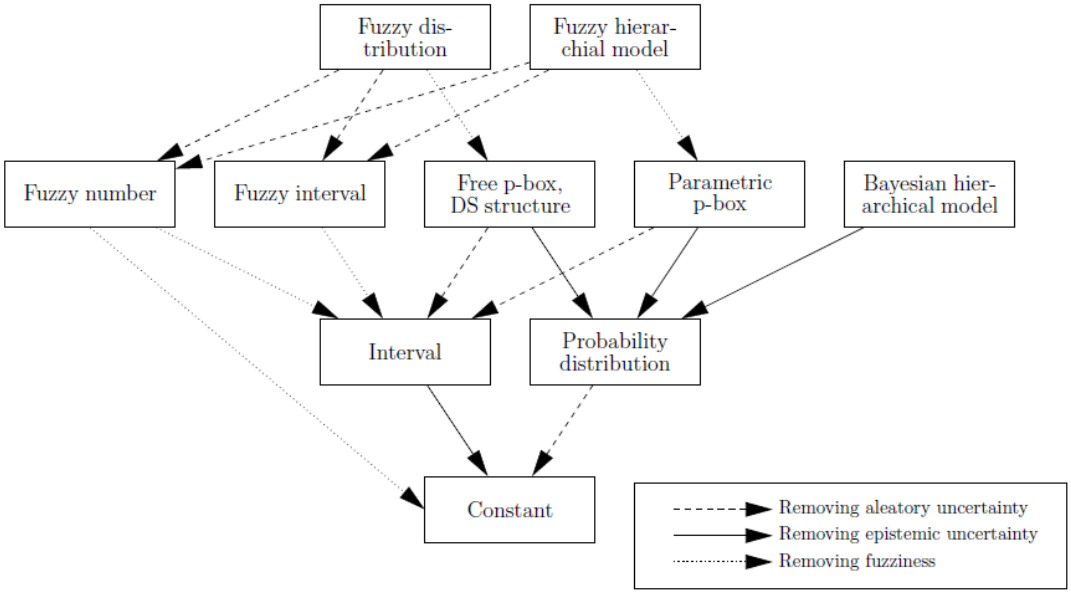

Figure 2.5: links between different notions of uncertainty modeling (image from Schöbi (2017)).

Table 2.1: comparison of different concepts of uncertainty modeling for a variable X.

Concept	Uncertainty model	Aleatory uncertainty	Epistemic uncertainty	
			Interval-valued	Fuzzy sets
Constant	x	-	-	-
Probability theory	$F_X(x)$	$X \sim F_X(x)$	-	-
Interval	$x \in [\underline{x}, \overline{x}]$	-	$x \in [\underline{x}, \overline{x}]$	
Dempster-Shafer structure	$\mathrm{Bel}(X \le x), \mathrm{Pls}(X \le x)$	$X \sim F_X(x)$	$\mathrm{Bel}(X \le x) \le F_X(x) \le \mathrm{Pls}(X \le x)$	-
P-box	$\underline{F}_X(x),\ \overline{F}_X(x)$	$X \sim F_X(x)$	$\underline{F}_X \le F_X(x) \le \overline{F}_X$	-
Fuzzy number	$\xi_X(x)$	-	$x \in \mathcal{D}_X^\alpha$	$\xi_X(x)$
Fuzzy distribution	$\Xi_X(x,c)$	$X \sim F_X(x)$	$\underline{F}_X^\alpha \le F_X(x) \le \overline{F}_X^\alpha$	$\Xi_X(x,c)$

2.2 Uncertainty's sources

Aleatory and epistemic uncertainty are defined as the two principal sources of uncertainty in the literature (Eldred et al., 2011; Ellingwood and Kinali, 2009; Helton et al., 2004; Helton and Burmaster, 1996; Kiureghian and Ditlevsen, 2009; Oberkampf et al., 2004).

Aleatory ("*alea*" is Latin for "dice") uncertainty describes the natural/intrinsic variability of a quantity of interest and is hence non-reducible. It refers to a property of the system associated with fluctuations or variability. Aleatory uncertainty is a stochastic variation that results from an underlying random experiment and corresponds to the traditional frequentist definition of probability theory.

Epistemic ("*επιστημη*" is Greek for "knowledge/science") uncertainty describes the lack of knowledge and is potentially reducible by acquiring more data. Epistemic uncertainty remains as a collection of all problematic cases and does not imply a specific mathematical model (Beer et al., 2013).

Uncertainties in experiment and simulation can be separated into three sources (Bi et al., 2019):

- Uncertainties in parameterization
  The input parameters of the numerical model are inaccurately determined, such as the materials properties, geometry sizes and random boundary conditions (e.g. winds or earthquakes).
- Uncertainties in modeling
  The numerical model always includes simplifications and approximations (e.g., linearization of nonlinear behaviors).
- Uncertainties in experiments
  The measurements are difficult to control by different random events (e.g., measurement system errors or human personal judgments). More insights into experimental uncertainty can be found in Bi et al. (2018).

The input model parameters can be divided into four categories according to the participation of aleatory uncertainty (natural variation) or/and epistemic uncertainty (lack of knowledge) (Bi et al., 2019):

I) parameters without any uncertainty, appearing as constants;

II) parameters with solely epistemic uncertainty, appearing as unknown-but-fixed constants, delimited by a specific interval;

III) parameters with only aleatory uncertainty are random variables with completely delineated probability characteristics (e.g. distribution type, mean, variance, etc.);

IV) parameters with either aleatory and epistemic uncertainties are imprecise probability variables with only vaguely uncertain properties.

Figure 2.6 shows the four categories shown above. This classification of parameters implies a different treatment and propagation of uncertainties. For more details see Bi et al. (2019).

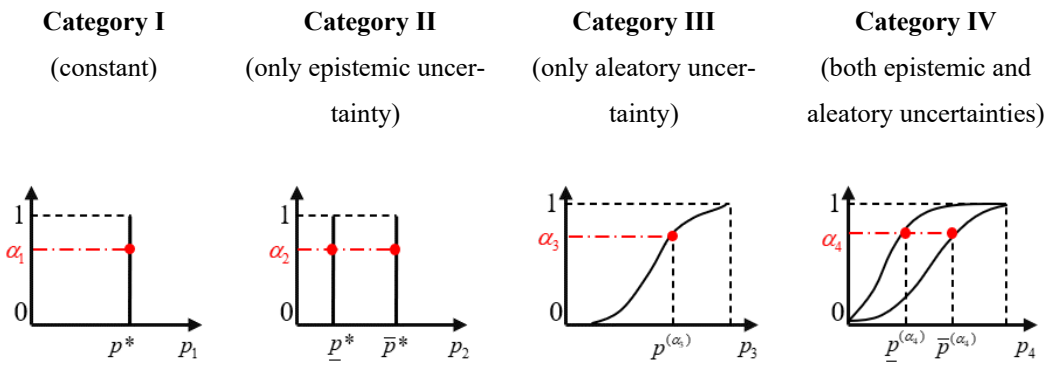

Figure 2.6: different forms of parameter categories (Bi et al., 2019).

2.3 Generalized methods for uncertainty propagation

Deterministic analyzes are widely used to assess the response of structures under any action and condition but provide insufficient information to represent the variability of the quantities of interest. It is accepted that stochastic analysis can explicitly take into account the effect of uncertainties by evaluating the variability of the parameters of interest. This methodology has multiple advantages. Allows you to assess the reliability and sensitivity of responses by providing more realistic predictions and information for decision analysis. Sensitivity analysis is a tool that provides information on which quantities influence the response of a structure (Section 2.5). Figure 2.7 shows a simplified diagram of the difference between deterministic and stochastic analysis.

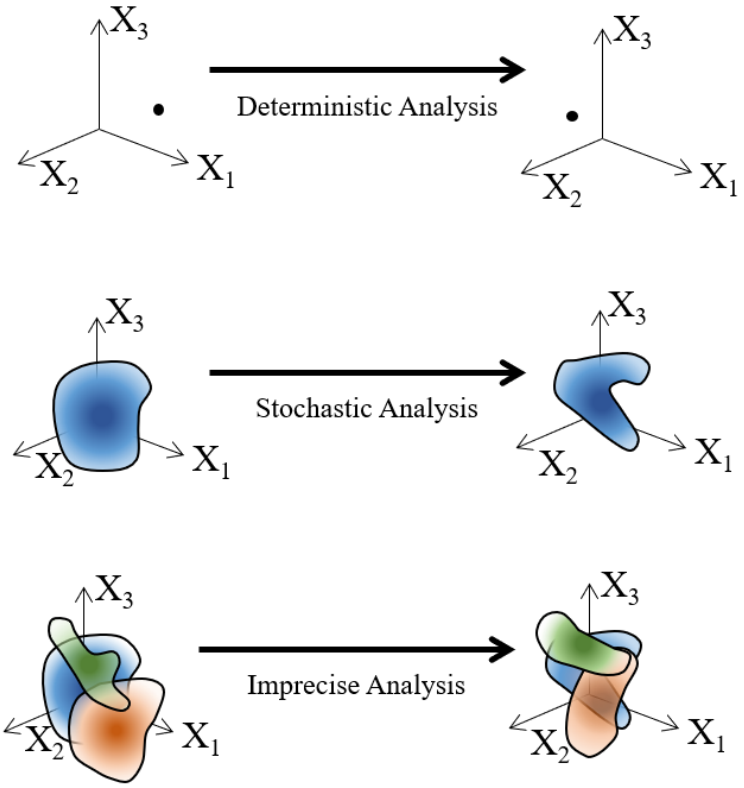

Figure 2.7: computational cost of the stochastic analysis versus deterministic analysis (Patelli, 2017).

The deterministic analysis presents a map between a single point in the input space representing the model parameters and a point in the output space representing the system response. The stochastic analysis extends this map to a region of points in both the input space and the output space. This is done by repeating the deterministic analysis many times. At this point, it is crucial to assess how uncertainties propagate. In the following paragraphs, we will deal with the machine that carries out the passage between the inputs and the outputs called black box and we will briefly explain the classes and advanced methods for the evaluation of uncertainties.

2.3.1 Black-box models

A computational model $M_{\mathcal{V}}$ can be identified as a map from an *m*-dimensional input space **x** to an *o*-dimensional output space of a multidimensional quantity **V**. Formally, it is written as follows:

$$M_{\mathcal{V}} : x \in \mathcal{J}_X \subset \mathbb{R}^m \rightarrow \mathbf{V} = M_{\mathcal{V}} \in \mathbb{R}^0 \tag{2.21}$$

where the input and output vectors are $\mathbf{x} = (x_1, ..., x_M)$, and $\mathbf{V} = (\mathcal{V}_1, ..., \mathcal{V}_O)$, each. This

computational model can be processed as a black box of which only the input and output vectors can be seen to perform uncertainty quantification.

If **x** is influenced by aleatory uncertainty, this will be characterized by an appropriate probability distribution function (and corresponding CDF). Employing the computational model M_v (for instance using the classic Monte Carlo method) which propagates the uncertainties, will distinguish the output in a well-defined CDF.

In the case where **x** is influenced by epistemic or mixed aleatory-epistemic uncertainty, their characterization will take place using suitable generalized probabilistic tools (e.g., p-box). The outputs will have limits on the vulnerability CDF (i.e., p-box) due to the propagation of uncertainty.

2.3.2 Classical and advanced method

A simple comparison between a classical probabilistic method to an advanced uncertainty quantification (UQ) method is shown in Figure 2.8. Here is an example where the vulnerability of a system is measured. The vulnerability model M_v adopts the sum of the quantities A and B. Input A has an aleatory behavior (it is distributed like a normal PDF) while input B is a parameter influenced by a purely epistemic uncertainty (e.g. an interval). In particular, it is possible to see how the parameter B does not have a stochastic behavior but is rather imprecise.

If a classic Monte Carlo method is performed, it should be assumed that a PDF characterizes the uncertainty for B. A uniform distribution within the interval is commonly assumed, adopting the so-called Laplace indifference principle.

When the probabilistic model is delineated and the uncertainty is propagated, the output will have a precise probabilistic description (i.e. a crisp CDF in a dashed line).

This may be incorrect for two main reasons: the assumptions may be difficult to justify and may produce erroneous results. Furthermore, analysts will not be capable to discern between the role of epistemic uncertainty and aleatory uncertainty to the output.

To surmount this limit, classical probabilistic methods can be coupled with advanced uncertainty quantification which allows distinguishing between epistemic and aleatory uncertainty in the output without introducing hypotheses (i.e. uniform random behavior of a parameter within a tolerance range) and with weaker or lesser hypotheses than the classical equivalent.

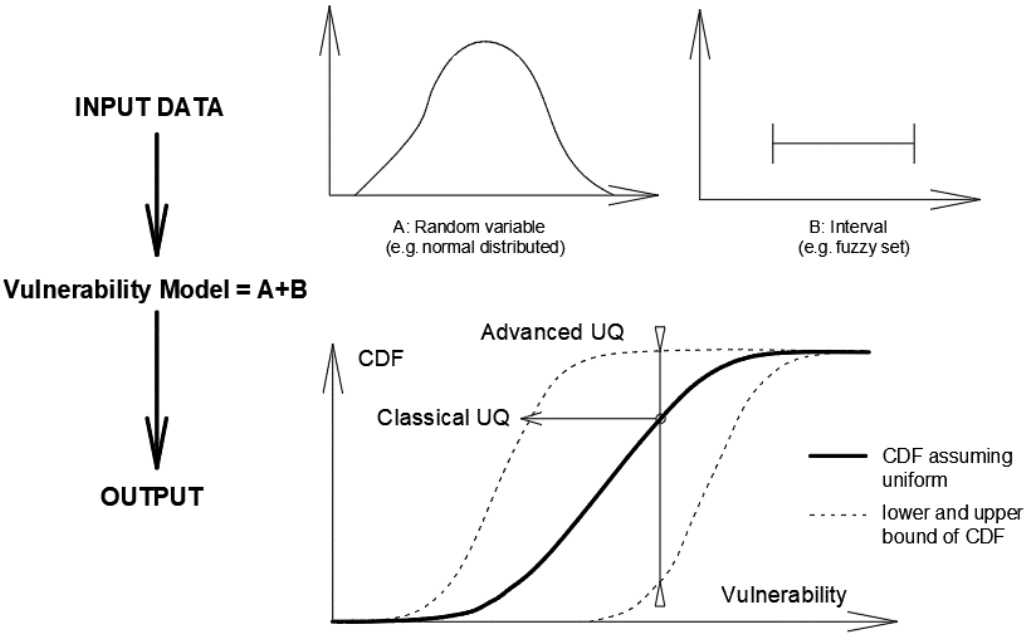

Figure 2.8: comparative of classical and advanced uncertainty quantification (Rocchetta, 2018).

The resulting output will be described e.g., ranges or the lower and upper bounds on the CDF.

Those methods are generally higher computational costs (Patelli, 2017; Patelli et al., 2014) and they have an imprecise probabilistic description of the output (Beer et al., 2013). Nonetheless, generalized probabilistic frameworks offer a valuable viewpoint of the results. Furthermore, they apply to any computational model being non-intrusive (Patelli et al., 2018).

2.4 Monte Carlo Simulation

The Monte Carlo simulation (MCS) method is a robust technique for the assessment of the stochastic response where the input is modeled by a large number of random variables (Zio, 2013).

2.4.1 Basic principles

The Monte Carlo method exploits the basic principles of sampling and the laws of statistics to obtain information on the variability of the response (Figure 2.9). Statistically independent samples are generated for each input using an appropriate number generator following probability distributions for uncertain parameters.

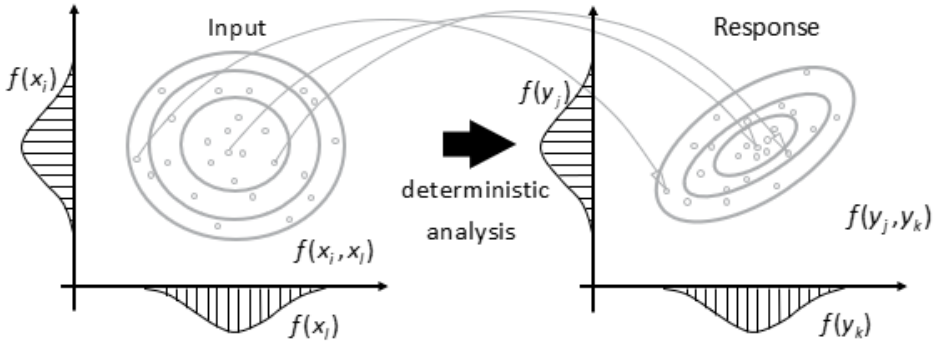

Figure 2.9: Monte Carlo sampling for stochastic analysis (Schenk and Schuëller, 2005).

Wanting to describe the system by an operator L, this is defined by a vector x in an m-dimensional vector space that represents a set of causal input variables that maps the y outputs to an r-dimensional vector space. This is expressed as follows:

$$Lx = y \tag{2.22}$$

However, each sample generated by the input $x^{(i)}$ is calculated as the corresponding output $y^{(i)}$ using Monte Carlo as a simulation. This simple form of Monte Carlo simulation is often referred to as a direct Monte Carlo simulation. So, a finite number n of independent samples $\left\{x^{(i)}\right\}_{i=1}^{n}$ is represented according to statistical laws of distribution of inputs $f\left(x_1, x_2, \ldots, x_m\right)$. Each vector for each uncertain parameter represents a deterministic value and therefore deterministically defines the response that could be represented by the vector

$$y^{(i)} = Lx^{(i)} \tag{2.23}$$

Therefore, in literature to provide the mapping given by Eq. (2.23) traditional deterministic finite element analyzes can be used between input and response (Schenk and Schuëller, 2005).

All uncertainties can be justified as independent in simple cases. Such an assumption is proper as far as this assumption does not belie experience and physical properties. Each component can be obtained by available random number generators where its parameters and distribution must be provided when the components are reputed as

independent. In the cases of stochastic processes or random fields, it is necessary to consider correlations between random variables.

2.4.2 Error assessment

The estimator of the response, that is a random variable, is defined by

$$\bar{y}_k = \frac{1}{n}\sum_{i=1}^{n} y_k^{(i)} \tag{2.24}$$

The mean ($E\{\bar{y}_k\}$) and the variance ($\mathrm{Var}\{\bar{y}_k\}$) of the estimator of the response are defined as follows:

$$\begin{aligned} E\{\bar{y}_k\} &= \frac{\sum_{i=1}^{n} E\left[y_k^{(i)}\right]}{n} = \mu_{y_k} \\ \mathrm{Var}\{\bar{y}_k\} &= E\left\{\left(\bar{y}_k - E\{\bar{y}_k\}\right)^2\right\} = \frac{\sigma_{y_k}^2}{n} \end{aligned} \tag{2.25}$$

A basis for the evaluation of error is provided by Chebyshev's inequality

$$P\left\{\left|\bar{y} - \mu_y\right| < \epsilon\right\} \geq 1 - \frac{1}{\epsilon^2}\frac{\sigma_y^2}{n} \tag{2.26}$$

where ϵ indicates a tolerance. The minimum sample size can be defined as follows considering a confidence level $1-\delta$.

$$n_{\min} \geq \frac{\sigma_{y_k}^2}{\epsilon^2}\frac{1}{\delta} \tag{2.27}$$

This condition is valid for any y_k probability distribution and any sample size larger than necessary. Comparing the statistical error made by estimating the function using the MCS method with N trials, and the numerical error derived from a quadrature formula in which the integrand function is calculated in N points, it results in any case, analog or biased, that the MC error varies with $N^{-1/2}$ (Amster and Djomehri, 1976; Booth and Amster, 1978):

$$\varepsilon_{MC} \sim N^{-\frac{1}{2}} \tag{2.28}$$

The error in quadrature differs like Δ^k with Δ equal to the integration interval and k a small integer that relies on the numerical method applied in the quadrature formula in the case of a regular function. k increases with the complexity of the rule but is at most 2÷3.

In the case of a hypercube with n dimensions and side length 1, the number of points on one edge is Δ^{-1} so that the total number of points is $N = \Delta^{-n}$ and the numerical quadrature error is

$$\varepsilon_q \sim \Delta^k \sim N^{-\frac{k}{n}} \tag{2.29}$$

The MCS estimate is suitable ($\varepsilon_{MC} \leq \varepsilon_q$), if $n \geq 2k = 6$. Therefore, the method is effective if it is necessary to evaluate an integral in a domain that should have at least 6-dimensional (Zio, 2013).

2.4.3 Advanced methods

A large number of simulations and high computational expenses are required for standard Monte Carlo Simulations. This problem is particularly important for cases in which the model behavior is computationally very intensive, that it is compulsory to recourse to approaches for increasing the efficiency of sampling for Monte Carlo methods.

The use of efficient Monte Carlo-based methods to quantify uncertainty in reliability and risk analyzes has led to recent developments with advanced variance reduction techniques (Pedroni et al., 2017). In the literature, there are several techniques e.g., importance sampling (IS) (de Angelis et al., 2017), subset simulation (SS) (Jia et al., 2017), and orthogonal plain sampling (OPS)(Wang and Kiureghian, 2017), metamodels (e.g., kriging and polynomial expansions) (Schöbi et al., 2017).

2.5 Sensitivity analysis

The relative importance of each input of a model can be measured by Sensitivity Analysis (SA). In literature, a wide variety of SA methods can be found such as reviews of various methods in (Helton et al., 2006; Saltelli, 2008; Xu and Gertner, 2008). This method can be divided into two main categories: local and global.

The *local sensitivity analysis* focuses on the local impact of the inputs on the model. The *global sensitivity analysis* focuses on the entire variation of the input or a combination of different input variables.

2.5.1 Variance-based sensitivity analysis

A form of global sensitivity analysis is variance-based sensitivity analysis. The procedure for the variance-based sensitivity analysis is briefly reported. For more details see Saltelli (2008). Define $X(i) \in [0,1]$, as a set $i = 1,2,\ldots,d$ of model inputs distributed in the hypercube unit and Y as an output of a model M (in case of multiple outputs, these can be evaluated by several independent sensitivity analyzes) as follows

$$M : \mathcal{X} \to \mathcal{Y}, \quad \mathbf{X} \to Y = M(\mathbf{X}) \tag{2.30}$$

The model can be expressed as follows:

$$Y = f_0 + \sum_{i=1}^{d} f_i\left(X(i)\right) + \sum_{i=1}^{d} f_{i,j}\left(X(i), X(j)\right) + \cdots + f_{1,2,\ldots,d}\left(X_1, X_2, \ldots, X_d\right) \tag{2.31}$$

where f_0 is a constant and f_i is a function of X_i, f_{ij} is a function of X_i and X_j. The functional decomposition orthogonal can be written as conditional expected values:

$$\begin{aligned} f_0 &= \mathbb{E}[Y] \\ f_i\left(X(i)\right) &= \mathbb{E}\left[Y \middle| X(i)\right] - f_0 \\ f_{ij}\left(X(i), X(j)\right) &= \mathbb{E}\left[Y \middle| X(i), X(j)\right] - f_0 - f_i - f_j \end{aligned} \tag{2.32}$$

where M_i is the effect of variation *X(i)* (also described as the main effect of factor *i*), and M_{ij} is the effect of variation *X(i)* and *X(j)* together, more to the effect of their single variations. This is so-called second-order interaction. Higher-order terms have similar notions. The functional decomposition can be traced back to the variance decomposition equation as follows:

$$Var(Y) = \sum_{i=1}^{d} V_i + \sum_{i<j}^{d} V_{ij} + \cdots + V_{1,2,\ldots,d} \tag{2.33}$$

where V_i and V_{ij} are:

$$V_i = Var_{X_i}\left[\mathbb{E}_{\mathbb{X}_{\sim i}}\left[Y\middle|X_i\right]\right]$$
$$V_{ij} = Var_{X_{ij}}\left[\mathbb{E}_{\mathbb{X}_{\sim ij}}\left[Y\middle|X_i, X_j\right]\right] - V_i - V_j \tag{2.34}$$

The notation $\mathbf{X}_{\sim i}$ denotes the group of all variables apart *X(i)*. The variance decomposition displays how the variance of the model output can be decomposed in relation to each input and the interaction effects among them. Jointly, all terms grow the total variance of the model output.

2.5.2 Sobol's indices

The first order sensitivity coefficient that quantifies the effect of each input factor on the model output is defined as follows (Sobol, 1993):

$$S_i = \frac{Var_{X_i}\left[\mathbb{E}_{\mathbb{X}_{\sim i}}\left[Y\middle|X(i)\right]\right]}{Var\left[Y\right]} \tag{2.35}$$

where $X(i)$ is the *i*th uncertain input factor, $\mathbf{X}_{\sim i}$ is the matrix of all uncertain factors, $\mathbb{E}_{\mathbb{X}_{\sim i}}\left[Y\middle|X_i\right]$ is the prediction of the model output *Y* taken over all possible values of $\mathbf{X}_{\sim i}$ while removing the $X(i)$ uncertainty (i.e. keeping X_i fixed), $Var_{X_i}[\ ]$ is the variance taken over all possible values of $X(i)$ and $\mathrm{Var}\left[Y\right]$ is the total variance of the output *Y*. The indices S_i can be used to reveal the importance of the input factor $X(i)$ on the variance of the output and it is a normalized index, that is $\sum_i S_i = 1$.

The total effect index S_{T_i} is also known as the higher-order Sobol's effects (second and higher-order interactions). All the interactions with other uncertain factors are accounted for by this variance-based measure of the influence of input *i*. It is defined as follows:

$$S_{T_i} = \frac{\mathbb{E}_{\mathbb{X}_{\sim i}}\left[Var_{X_i}\left[Y\middle|\mathbf{X}_{\sim i}\right]\right]}{Var\left[Y\right]} = 1 - \frac{V_{X_{\sim i}}\left[\mathbb{E}_{X_i}\left[Y\middle|\mathbf{X}_{\sim i}\right]\right]}{Var\left[Y\right]} \tag{2.36}$$

where S_{T_i} report the involvement to the total variance of the output $\mathrm{Var}[Y]$ when the first-order effect $\mathbf{X}_{\sim i}$ is deleted. Instead S_i, we have generally $\sum_i S_{T_i} \geq 1$ as the input factor effects are included multiple times because of interactions into the model ($\sum_i S_{T_i} = 1$ in case of merely additive models).

2.6 Risk assessment in engineering

2.6.1 Procedure for risk assessment

Risk assessment has become a very popular and widely practiced topic in the industry in recent years. The National Academy of Science "Red Book" captures the fundamental principles of risk assessment where the assessment and decision making are maintained separately. Risk assessment is considered as a scientific task restricted by the available knowledge and the uncertainty intrinsic in risk, whereas the decision-making process is treated as a political act, risk assessment being one part of input but never the only purpose for decision making (National Research Council, 1983). For the decision-maker, quantifying the risk is useful for preventing the risk, implementing the mitigation and prevention measures and defining the various priorities. Defining levels of acceptability of risk is also important for safety analysis and rational decision-making.

The basic idea of this evaluation is to model a system using the information and knowledge available and define a threshold for which it is acceptable. If the knowledge of the event and of the elements that constitute the response of the system is limited, the evaluation will be affected by uncertainty (Zio, 2018).

Generally, the frameworks describing this uncertainty are based on Bayesian probability theory where combined information from databases and expert opinions are combined to assess risk (Kelly and Smith, 2009, 2011).

In the literature today, these approaches are commonly referred to as Probabilistic Risk Assessment (PRA), albeit Probabilistic Safety Assessment (PSA) and Quantitative Risk Assessment (QRA).

The basics of risk quantification based on probabilistic analysis (Rechard, 1999, 2000) have still been applied for more than 35 years since their first application to nuclear power plants in the early 1970s (NRC, 1975).

These approaches have also been extended to civil engineering and especially to earthquake engineering. The applications in the seismic field are connected to the C. Allin Cornell and Haresh C. Shah groups of Stanford University, who applied typical principles of nuclear risk engineering to civil structures.

As it is well known, in this field the risk can be defined as the product of the seismic hazard A, vulnerability V and exposure E.

$$\text{Risk} = (A, V, E) \tag{2.37}$$

The seismic risk was then extended to a probabilistic assessment using the Performance-based Earthquake Engineering (PBEE) framework (Deierlein et al., 2003; Krawinkler and Miranda, 2004).

In this thesis, we will focus mainly on the vulnerability component and the related uncertainty. In the PBEE, vulnerability is described utilizing the fragility curve. This curve, which is mathematically a cumulative probability function, describes the probability of overcoming an assigned parameter (e.g. limit load, limit displacement, etc.) at an intensity measure.

In recent decades we are trying to expand beyond the concept of risk. In addition to the concepts of robustness, safety and reliability already widely present in the literature, the resilience of a system is also evaluated. Table 2.2 shows the classic terminology present in the risk.

Of course, all of these risk-related concepts are in turn correlated with the role that knowledge and robustness of data play. Any analysis that can be done is quite accurate the more the uncertainty due to the models and data is reduced.

Therefore the definition of risk can be expressed as follows (Aven and Renn, 2010):

$$\text{Risk} = \left(\mathcal{A}, \mathcal{C}, \mathcal{L}, \mathcal{K}\right) \tag{2.38}$$

where $\mathcal{A}$ denotes the hazard scenarios that may occur, $\mathcal{C}$ indicates the set of consequences, $\mathcal{L}$ represents the metrics of uncertainty quantification and $\mathcal{K}$ is the knowledge of the risk assessment.

The formulation of risk reported clearly explains the role of knowledge in the output variable. This shows the knowledge conditions the risk. The knowledge available can

be classified into four categories (Flage and Aven, 2015; Zio, 2018):

1. *Unknown-unknown* that identifies those events and scenarios that were unknown to everyone, at the time of the risk assessment;
2. *Unknown-known* indicates those events and scenarios unknown to the risk analysts performing the assessment, but known to someone else;
3. *Known-unknown* identifies situations of awareness where the background knowledge is weak but there are indications or justified beliefs that a new, unknown type of event or scenario (new in the context of the activity posing the risk) could occur in the future;
4. *Known-known* indicates events and scenarios that are known to the analysts performing the risk assessment, and for which evidence exists.

Risk models must evaluate two fundamental aspects with the use of simulation models: the identification of the hazardous conditions for the system, i.e., using Eq. (2.38) must consider the triplet $(\mathcal{A},\mathcal{C},\mathcal{K})$. This triplet represents the critical conditions of the system. Finally, it is fundamental to estimate the probability of occurrence of rare critical scenarios, i.e., $(\mathcal{L},\mathcal{K})$ in Eq. (2.38).

Table 2.2: state of art of the risk terminology related to the systems.

Term	**Definition**
Hazard	an act or phenomenon posing potential harm to some person or thing and its potential consequences (Ayyub, 2014).
Reliability	the ability to fulfill its design functions under designated operating or environmental conditions for a specified period (Ayyub, 2014)
Risk	the potential of losses and rewards resulting from exposure to a hazard or as a result of a risk event (Ayyub, 2014)
Safety	the judgment of risk acceptability for the system (Ayyub, 2014)
Robustness	strength, or the ability of elements, systems, and other measures of analysis to withstand a given level of stress or demand without suffering degradation or loss of function (Bruneau and Reinhorn, 2007);
Vulnerability	the lack of robustness (Rocchetta, 2018)
Resilience	The ability to withstand high impact-low probability events, rapidly recovering and improving operations and structures to mitigate the impact of similar events in the future (Panteli and Mancarella, 2015)

Any risk model that is addressed presents several ways to assess that risk. Different simulation models are possible. The main ones are:

- *High-dimensional*, i.e., with a large number of inputs and/or outputs.
- *Black box* without an explicit input and/or output relation. Coded in a computer program or using meta-model (e.g., data and artificial intelligence).
- *Dynamic* because the system changes in time
- *Computational depending* indeed for a single test simulation, as an effect of the above specifics of the models and the numerical methods utilized for their solution.

Risk science like reliability engineering is plagued with old problems and new challenges:

- the modeling and the representation of the problem;
- the quantification of the model;
- the quantification, propagation and representation of the uncertainty of model behavior.

In particular, this thesis focuses on the quantification, propagation and representation of uncertainties. In seismic engineering as well as in structural engineering, attention has always been focused on the first two points and the third point has been analyzed only concerning the seismic input. In reality, quantifying and describing the uncertainties deriving from a model is the most relevant challenge as their understanding allows to improve the models currently in use and allows the decision-maker to be aware of the tool he uses.

2.6.2 Uncertainties in risk analysis

Management problems that evolve many risks and have limited knowledge of fundamental phenomena lead to uncertainties in valuations. Clarifying what is known and what is not can only be helped by identifying and quantifying uncertainties.
Depending on the decision and management rules to be applied, different levels of risk assessment can be applied to the entity of the outcomes and their probabilities.
Six levels are defined for the treatment of uncertainties (Figure 2.10):

- Level 0: hazard detection and failure modes identification
- Level 1: “worst-case” approach
- Level 2: quasi-worst cases and plausible upper bounds
- Level 3: best estimates and central values
- Level 4: probabilistic risk assessment, single risk curve
- Level 5: probabilistic risk analysis, multiple risk curves

The various levels of treatment of uncertainty and risk assessment are now briefly described. For more details see Paté-Cornell (1996).

Level 0 involves identifying a potential hazard or possible ways in which a system can collapse, without quantitatively assessing the risk. In theory, this approach can support rigorous zero-risk decisions, i.e. when costs are low and the decision is clear.

Level 1 presents the so-called “worst-case” approach. This approach has no notion of probability and is based on worst-case assumptions and in theory the maximum loss level is obtained. This approach is applicable when the loss is sufficient to support the decision.

Level 2 has “plausible upper bounds” and is also called the “near worst-case” approach).
This method is a first attempt to assess risk by considering some uncertainty about the worst-case or that is unlikely or rare such that it is meaningless to consider it. We begin to think about possible scenarios.

Level 3 provides a "best estimate" on a central value, e.g. average. We begin to think about the distribution of the result through the “best estimates” of the variables considered. This approach is currently a major direction of the legislator and various government agencies.

Level 4 includes probabilistic risk analysis (PRA). PRA in its simplest form can be performed to obtain a distribution of the probabilities of the different states of the system based on the best estimates of the models and the values of the parameters. This procedure is widespread in the literature and applied in the last decades in all fields.

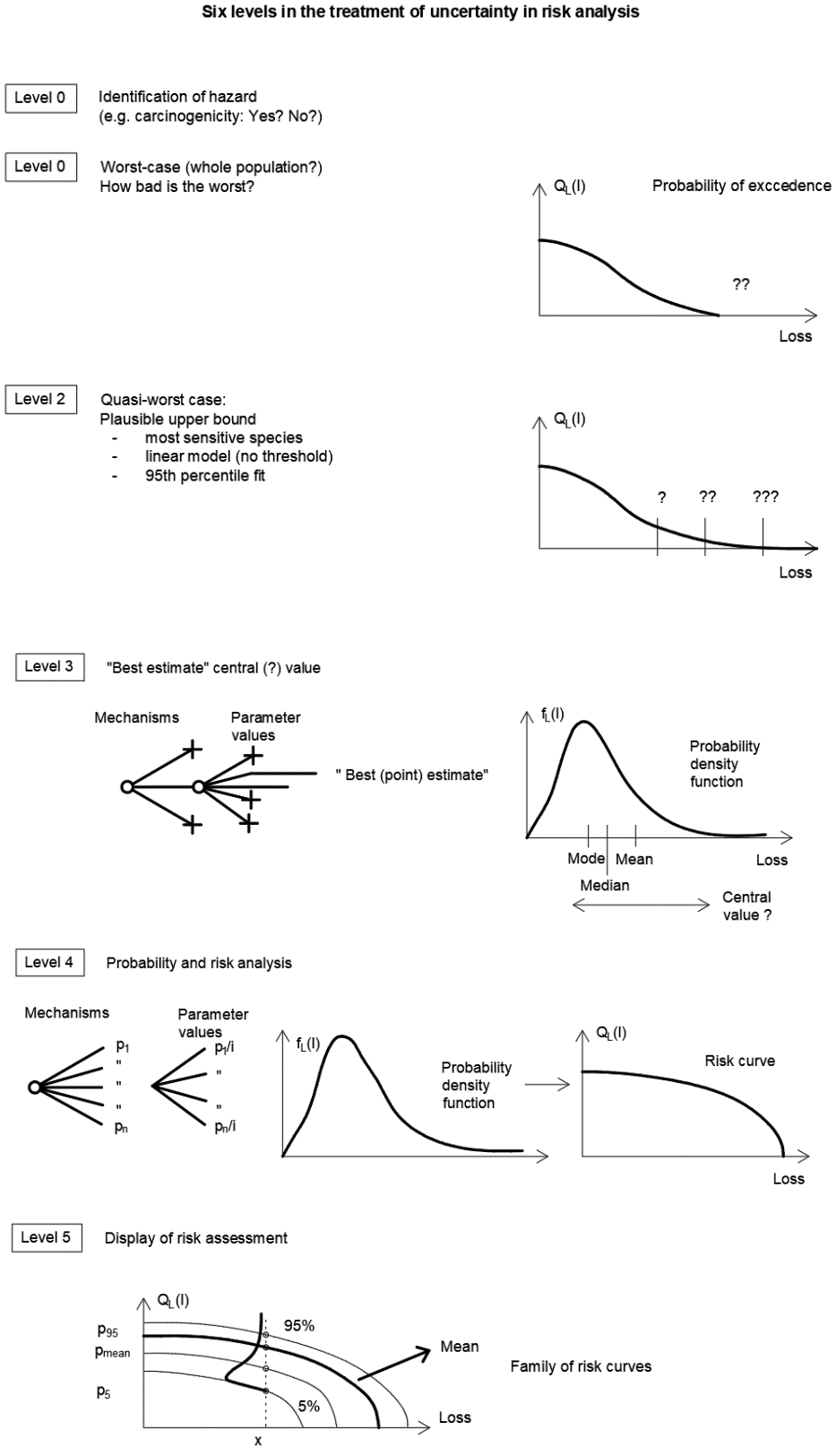

Figure 2.10: six levels of treatment of uncertainties in risk analysis (Paté-Cornell, 1996).

Level 5 represents the most comprehensive level for a risk assessment. This level allows you to expose the uncertainties of various model inputs and their outputs using a family of curves. Carrying out a statistical treatment of existing data, which is employing Bayesian inference, allows a more targeted and congruent risk assessment with the data in possession and with the models adopted.

Therefore, this level represents the best compromise to give the decision-maker all the tools and information for the problem posed. This level can be achieved with all the techniques described in Chapter 2.

2.7 Structural Reliability in existing structures

The evaluation of the probability of a structure having an appropriate performance in its useful life can be defined as the reliability of a system. This probability of failure allows us to estimate its reliability with generally incomplete information.
The evaluation phase of an existing building compared to one in the design phase differs mainly from the information that can be obtained. Therefore, evaluating the reliability of an existing structure must also incorporate the relative uncertainties and the relative lack of information. It is quite true that most existing structures do not have all the information that a new project requires.
For this reason, the evaluation of the reliability of a structure that leads to the evaluation of its index should not be considered an absolute number but a nominal value.
Structures are generally designed to meet some coded security requirements. These criteria are codified by the various codes using formal calculation models. All this is formalized through a reliability index $\left(\beta_{\text{prior}}\right)$ that must be higher than that specific to the code $\left(\beta_{\text{target}}\right)$.

$$\beta_{\text{prior}} \geq \beta_{\text{target}} \tag{2.39}$$

The same condition must be maintained if the information provided by the data and experimental tests is integrated. Therefore, a new a posteriori reliability index is defined which must be higher than the one fixed by the code.

$$\beta_{\text{posteriori}} \geq \beta_{\text{target}} \tag{2.40}$$

The reliability index depends a lot on the type of structure considered, the material and the actions to which it is subject. For example, structures under seismic action have a different reliability index than structures under wind action.

The reliability of a structure is evaluated based on probabilistic models for loads and resistances and can have a limited correlation with the real reliability of the structure. This modeling is strongly influenced by the assumptions made a priori and therefore this measure. This benchmark is established through best practices.

What is defined as best practice is defined according to conventions defined by the goal set. Normally, reference values are defined for the annual probabilities of exceeding in the range of 10^{-6} - 10^{-7}. This interval varies according to the structure and modalities of the limit state considered. Furthermore, these analyzes, to be defined based on the objective set and the mode of damage set, consider socio-economic aspects.

Table 2.3 – 2.4 show the reliability reference values for the ultimate limit state and the service limit state defined for the structures by JCSS (2001). Note how the reliability indices and the annual probability of collapse vary according to the consequences of collapse and the cost of the measures to guarantee its safety.

Table 2.3: target reliability index β and failure probabilities P_F related to ultimate limit states.

Relative cost of safety measure	Minor consequences of failure	Moderate consequences of failure	Large consequences of failure
High	$\beta = 3.1 \left(P_F \approx 10^{-3}\right)$	$\beta = 3.3 \left(P_F \approx 5 \cdot 10^{-4}\right)$	$\beta = 3.7 \left(P_F \approx 10^{-4}\right)$
Normal	$\beta = 3.7 \left(P_F \approx 10^{-4}\right)$	$\beta = 4.2 \left(P_F \approx 10^{-5}\right)$	$\beta = 4.4 \left(P_F \approx 5 \cdot 10^{-5}\right)$
Low	$\beta = 4.2 \left(P_F \approx 10^{-5}\right)$	$\beta = 4.4 \left(P_F \approx 10^{-5}\right)$	$\beta = 4.7 \left(P_F \approx 10^{-6}\right)$

Table 2.4: target reliability index β and failure probabilities P_F related to irreversible serviceability limit states.

Relative cost of safety measure	Target index
High	$\beta = 1.3 \left(P_F \approx 10^{-1}\right)$
Normal	$\beta = 1.7 \left(P_F \approx 5 \cdot 10^{-2}\right)$
Low	$\beta = 2.3 \left(P_F \approx 10^{-2}\right)$

3 Out of-plane local failure of masonry walls

The chapter deals with the evaluation of fragility functions for unreinforced masonry walls in the presence of local failure mechanisms considering the out-of-plane response. This chapter is partially contained in the following publication:

Nale M., Minghini F., Chiozzi A., Tralli A. (2021) "Fragility functions for local failure mechanisms in unreinforced masonry buildings: a typological study in Ferrara, Italy" *Bullettin Earthquake Engineering*. https://doi.org/10.1007/s10518-021-01199-6

3.1 Overview

Unreinforced Masonry (URM) buildings represent a large part of the Italian building stock. Compared to new buildings, existing URM buildings tend to be more vulnerable to earthquakes. In Italian historical centers, this is essentially due to the following causes:

1) Old buildings frequently have strong changes over time, often resulting in a reduction of cross-section areas of masonry walls, a general weakening of mutual connections between walls and floors, and sometimes a significant increase in the seismic masses.

2) Materials may be seriously degraded due to weathering, rising damp, and poor maintenance.
3) In some territories, such as a large part of the Po River plain, seismic design has become mandatory only since 2005, and most of the buildings have been designed in the absence of specific provisions for earthquake resistance.

Recent seismic events (Decanini et al., 2004; Indirli et al., 2013; Penna et al., 2014; Sorrentino et al., 2019) have provided evidence that Out-Of-Plane (OOP) collapse mechanisms in URM structures still represent a serious life-safety hazard.

In fact, under seismic actions, existing URM buildings are often subjected to local collapse mechanisms involving partial or whole OOP failure of façade walls (D'Ayala, 2005, 2013; D'Ayala and Speranza, 2003; Maio et al., 2016). Both activation and evolution up to the collapse of these mechanisms strictly depend on the stiffness and strength of connections between facade walls and other structural elements such as partition walls, floors and roofs.

It is worth observing that, despite the recalled vulnerability of existing URM buildings to OOP collapse mechanisms, the European standard (CEN, 2005b) lacks information about the procedure to be used to assess the OOP behavior of masonry walls.

In Italy, the seismic analysis of historical URM buildings based on the assessment of collapse mechanisms starts with Giuffré (1996). Linear kinematic analysis is considered one of the most reliable tools to assess the activation of OOP failure of masonry walls and is currently adopted by the Italian building code (MIT, 2018).

It is based on the use of the kinematic theorem of limit analysis to select, among various OOP mechanisms, that lead to the minimum seismic load multiplier (α_0). This multiplier may be rewritten in terms of acceleration capacity (a_0). If $W = Mg$ indicates the generic gravitational load associated with mass M and gravity g, the activation load is given by $\alpha_0 W = a_0 Mg/g = a_0 M$. Then, for the safety check, acceleration capacity a_0 is compared with acceleration demand a_{ref} provided by the building code for the selected limit state. Yet, when the mechanism evolution is of interest, a displacement-based (nonlinear) approach should be used.

This approach, usually referred to as kinematic nonlinear analysis, is based on the following steps (MIT, 2018):

1) imposition, for the selected mechanism, of equilibrium conditions corresponding to a generic, deformed configuration;
2) evaluation of the capacity curve for the mechanism as a continuous function of the horizontal displacement of a control point;
3) transformation of the capacity curve for the mechanism into the capacity curve corresponding to an equivalent Single Degree-Of-Freedom (SDOF) system;
4) location, on the SDOF curve, of a limiting displacement corresponding to the considered limit state and comparison with the displacement demand.

This analysis method provides an approximation of the envelope of acceleration-displacement rocking cycles for the mechanism, and results then to be more suitable to catch the Ultimate Limit State (ULS) conditions of masonry walls than the linear method. It can happen, for example, that the mechanism with the smallest displacement capacity does not coincide with the mechanism with the minimum activation acceleration. It can be the case of vertical bending mechanisms of slender walls, which usually provide activation loads significantly larger than simple overturning mechanisms, but tend to experience a very low displacement capacity prior to collapse. That said, the rocking behavior of rigid blocks is highly influenced by ground motion characteristics, which cannot be taken into due account without a nonlinear time-history analysis. Various authors showed the drawbacks related to the use of kinematic analysis methods, which often underestimate the actual capacity of URM walls (Giresini et al., 2015; Shawa et al., 2012; Sorrentino et al., 2016).

There are several numerical methods that allow to evaluate the structural response through nonlinear dynamic analyses. For example they were used FEM with different constitutive relationships (e.g., Concrete Damage Plasticity (CDP), Total strain-based crack (TSC)), discontinuous methods (e.g., Non-Smooth Contact Dynamics (NSCD), Discrete Element Method (DEM)) (Clementi, 2021; Clementi et al., 2019; Ferrante et al., 2021) and Discrete Macro-Element Modeling (DMEM) (Chácara et al., 2019). The simplest and one of the better performing approaches appears to be the nonlinear dynamic analysis of the walls considered as rocking rigid blocks.

The study of rocking oscillators began with the seminal paper by Housner (1963), that derived a SDOF equation of motion for the OOP response of a parapet wall. Following that study, the research focused on the description of the dynamic response of rocking blocks subjected to either earthquake excitations or pulse (Spanos and Koh, 1984; Yim et al., 1980). It has been found that this response may be characterized by dynamic instability and strong nonlinearity. Later, other models were adopted introducing equivalent SDOF models to govern the dynamic behavior of complex multi-block rocking systems (DeJong and Dimitrakopoulos, 2014; Sorrentino et al., 2008). A SDOF force-displacement idealization of the rocking behavior of URM walls was proposed by Doherty et al. (2002).

A unified, probabilistic approach taking account of uncertainties, vulnerability, and

risk can provide, with the use of nonlinear dynamic analysis, a better estimate of structural safety levels. One of the main tools in PEER - PBEE framework (Deierlein et al., 2003; Krawinkler and Miranda, 2004) is the fragility function.

For the rocking block, various studies provided fragility functions in terms of different intensity measures (Chiozzi et al., 2017; Dimitrakopoulos and Paraskeva, 2015; Lagomarsino, 2015). The methods available in the literature to derive fragility functions can be divided into four categories (Pitilakis et al., 2014; Silva et al., 2019): analytical, empirical, expert judgment, and hybrid. Fragility functions have also been proposed to describe the global behavior of masonry structures (Lagomarsino and Giovinazzi, 2006; Rota et al., 2010; Spillatura et al., 2014). Most of these researches consider only the in-plane response of masonry walls (Chiozzi and Miranda, 2017). More recent studies propose fragility functions for OOP mechanisms based on kinematic limit analysis (Zuccaro et al., 2017). Simões et al. (Simões et al., 2019a, 2019b, 2020) developed fragility functions for URM buildings combining in- and out-of-plane wall responses. In particular, for the OOP response, nonlinear kinematic analyses were used in that work. In addition, (Ferreira et al., 2017) developed fragility curves for OOP walls calibrated with observed damage.

This chapter presents a procedure to derive fragility functions for OOP mechanisms in URM buildings based on nonlinear dynamic analyses adopting a rigid block model. Fragility functions are derived considering the uncertainties associated with the peculiarities of masonry structures. These uncertainties are both aleatory and epistemic. The aleatory variables involved, such as wall geometry, masonry mass density, loads transferred from floors and roof, are treated by the Monte Carlo method (Zio, 2013). Epistemic uncertainty is treated through the use of logical trees (Simões et al., 2019b). In the end, the individual fragility functions obtained are combined to define a typological fragility function for a class of masonry buildings.

The approach adopted for the derivation of fragility functions is described in detail in the following sections. The method is then applied to a case study concerning a historical aggregate in the city center of Ferrara, Italy (Figure 3.1).

Some preliminary results of this research have been recently presented by Nale et al. (2020).

Figure 3.1: the historical aggregate in the center of Ferrara, Italy (aerial view).

3.2 Seismic performance of masonry structures in 2012 Emilia earthquake

In 2012 northern Italy was hit by a seismic sequence in the Emilia area i.e., the provinces of Bologna, Ferrara and Modena and some municipalities of the provinces of Mantua and Rovigo. This seismic sequence is characterized by two main shocks, one on May 20 and the second on May 29.

The first event, that of May 20 at 02.03 UTC (04:03 local time), is characterized by a local magnitude M_L = 5.9. The main damages occurred in San Felice sul Panaro and Finale Emilia.

The second earthquake of May 29th at 07.00 UTC (09.00 local time) was characterized by a magnitude of M_L = 5.8 at a distance of 12 km from the event of May 20th and near Felice sul Panaro. Figure 3.2 shows the relative ShakeMaps in macroseismic intensity (Mercalli Cancani Sieberg scale, MCS) for the two main shocks. For more details on seismic sequences see Chioccarelli et al. (2012a, 2012b).

This earthquake is particularly interesting because it hit structures made of fired clay brick masonry with lime mortar compared to the earthquakes of the past in Italy that had affected structures built with stone masonry (Carocci, 2012; Decanini et al., 2004).

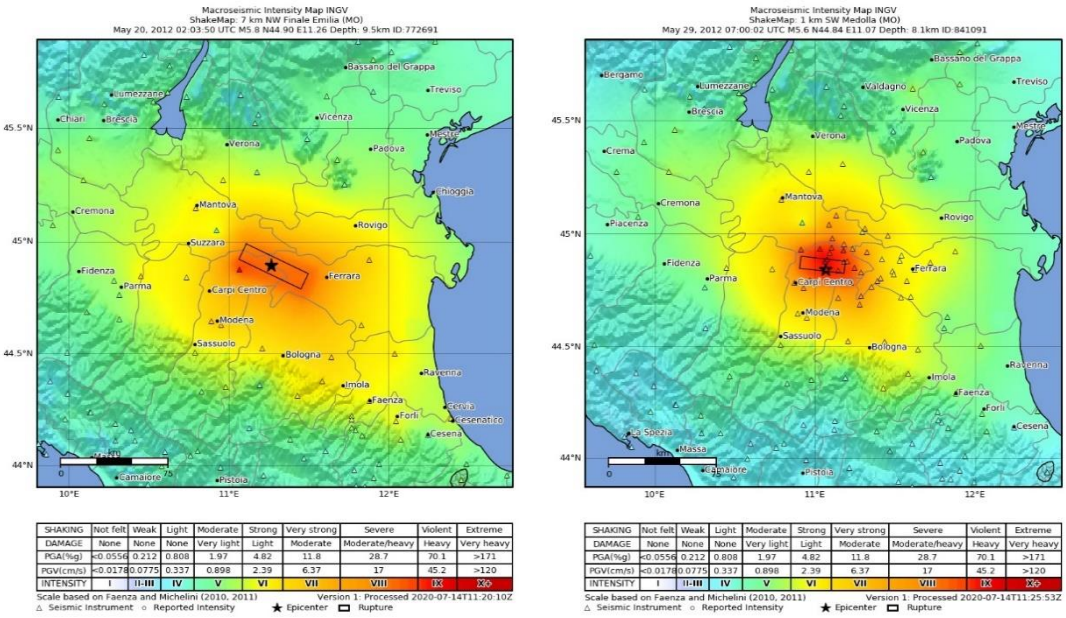

Figure 3.2: Shake Maps of the seismic events of May 20th (M_w = 5.8) and May 29th (M_w = 5.6) from INGV Shake Map Archive (http://shakemap.ingv.it/shake4/archive.html).

The seismic sequence caused various damages to the existing and cultural building heritage (Cattari et al., 2012; Penna et al., 2014; Valente and Milani, 2018). The historical masonry structures constitute an important part of the building stock in the area. Existing masonry buildings often show typical defects and lack of adequate details which increase their seismic vulnerability since the affected area has only been classified as potentially seismic since 2003.

A common feature of these buildings is the limited thickness of the walls. Due to the mechanical resistance properties of brick walls that are usually better than stone masonry, the use of double-leaf walls (about 25 cm) usually does not create concern in the case of residential buildings, where the height of the floor is about 3 m and the perpendicular walls are quite close together. In the case of churches, towers and buildings where the height between the floors can be significant this can produce high criticalities with an increase of vulnerability. Figure 3.3 shows some examples of wall sections. These cross-sections of the walls are characterized by a limited thickness, scarce and in some cases with no connection between the leaf walls.

A further important aspect found in residential and agricultural structures was the scarce and ineffective connection between the floor and the walls and between the walls and the floor. In particular, a series of local collapses were found in the presence of thrust or unstable wooden roofs (Sorrentino et al., 2014).

a) b) c) d) e)

Figure 3.3: cross-sections of walls present in Emilia (images from Cattari et al. (2012)).

The case of poorly maintained wooden roofs has been found quite widely. These roofs have allowed and, in some cases, favored out-of-plane mechanisms on the top of the buildings. Figure 3.4 reveals some of the damage, mainly OOP mechanisms, found in masonry buildings in Emilia. A particular case of severe and anomalous damage is that observed in the municipality of Sant'Agostino (Figure 3.4c). The damages are characterized among other things by the presence of a double volume of about 8 meters with an external wall with two heads.

However, recent masonry buildings should have been designed to prevent the main vulnerabilities of old masonry structures. The national design standards encourage some basic rules for reducing vulnerability such as regular and robust units, the limitation of the slenderness of the walls, the effectiveness of the connections between walls and between floor or roof, a sufficient in-plane stiffness of the floor or roof diaphragms and the regularity of the structure. Before the 2003 revision of seismic classification, most of the modern masonry structures were erected only to resist vertical loads. These buildings present an inadequate lateral strength for an insufficient area of masonry walls, potential irregularities in plan and elevation and divergence in the compulsory structural details and minimum mechanical properties of units and mortar. In most of the cases, the post-earthquake inspections have illustrated a good seismic performance and the absence of considerable damage, in structural and non-structural elements, even in zones near to the epicenters of the seismic events for buildings designed after 2003.

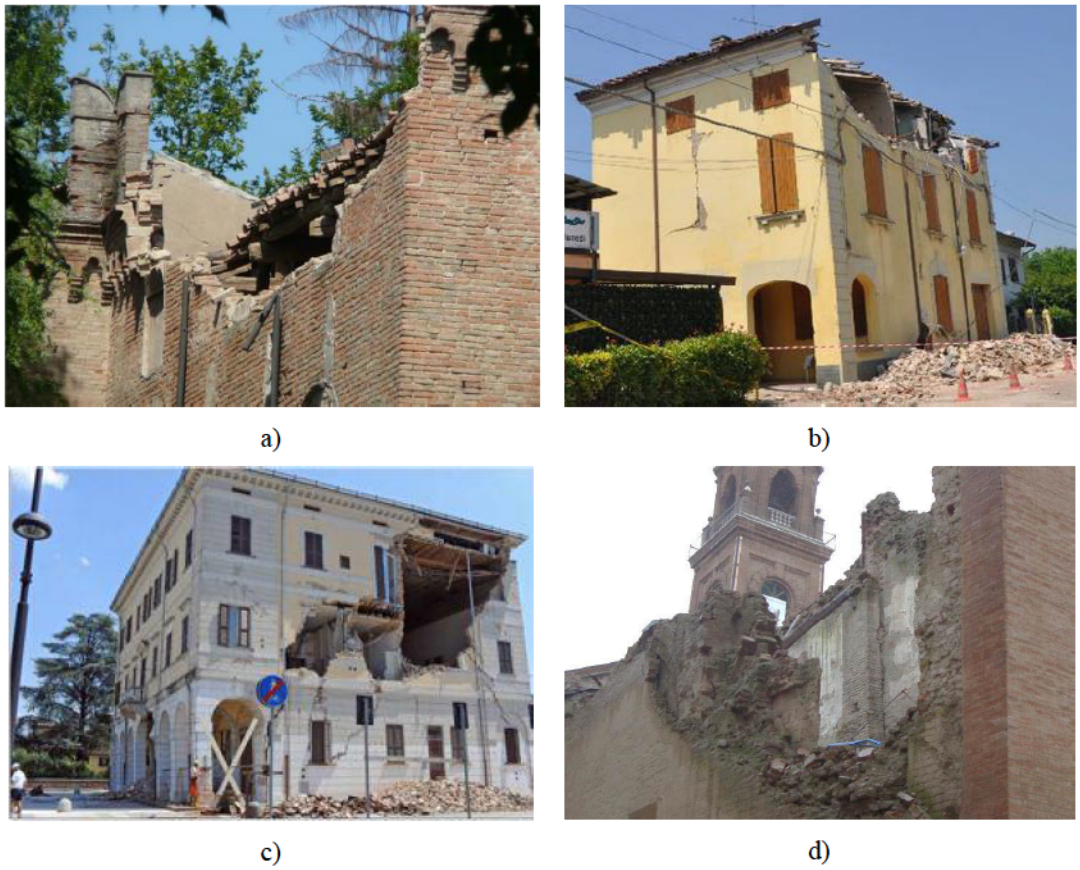

Figure 3.4: examples of damage to the walls of masonry buildings in the Emilia earthquake (images from Ferretti and Tralli (2013)).

3.3 State of art of out-of-plane assessment method

The evaluation of the out-of-plane response of masonry walls represents one of the crucial aspects for the evaluation of the vulnerability of existing URM buildings. This behavior under dynamic action (e.g., earthquake) under inertial forces is particularly complex and difficult to understand, due to the non-homogeneous and discontinuous nature of the masonry and the interaction with the building (Priestley, 1985).

Some international codes and guidelines provide simplified methods for assessing local collapse mechanisms (e.g., ASCE / SEI 41-06 2006; NZSEE 2006; AS3700 2011, NTC 2018). In particular, in this section, the main procedures codified by the Italian standard will be exposed (MIT, 2018), which includes methods based on forces and displacements for out-of-plane mechanisms for URM structures.

For further details see (Lagomarsino and Resemini, 2009; Magenes and Penna, 2011; Penna, 2015; Sorrentino et al., 2016). Finally, the dynamic analysis method will be

exposed which allows idealizing the walls as rigid blocks (Doherty et al., 2002; Housner, 1963; Lagomarsino, 2015). Figure 3.5 shows an example of possible out-of-plane mechanisms for the walls of masonry buildings.

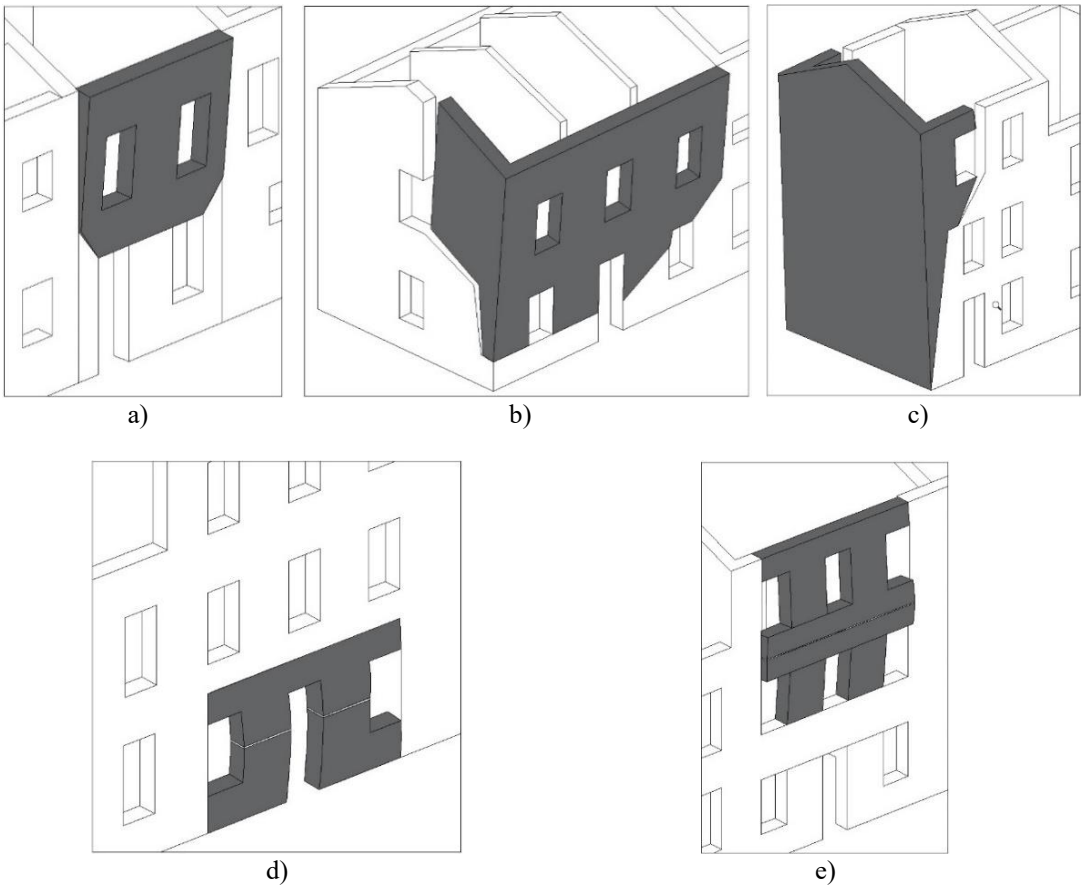

Figure 3.5: example of out-of-plane wall overturning in unreinforced masonry buildings (D'Ayala and Speranza, 2003): a) overturning of a wall at first-floor b) partial overturning of the facade, c) total overturning of the facade, d) flexural mechanism of a wall, e) flexural mechanism of the façade.

3.3.1 Capacity curve

Each mechanism is evaluated by means of an incremental kinematic analysis which allows to derive a pushover curve. For each configuration, the displacement d_k of a control point is defined and the collapse load multiplier α is estimated using the Virtual Works theorem.

The pushover curve obtained is characterized by a static horizontal multiplier α_0. This multiplied is a dimensionless acceleration necessary to activate the mechanism. This describes how capacity changes as the mechanism evolves (Figure 3.6). The curve is defined until the collapse multiplier value is 0 and gravity instability is reached.

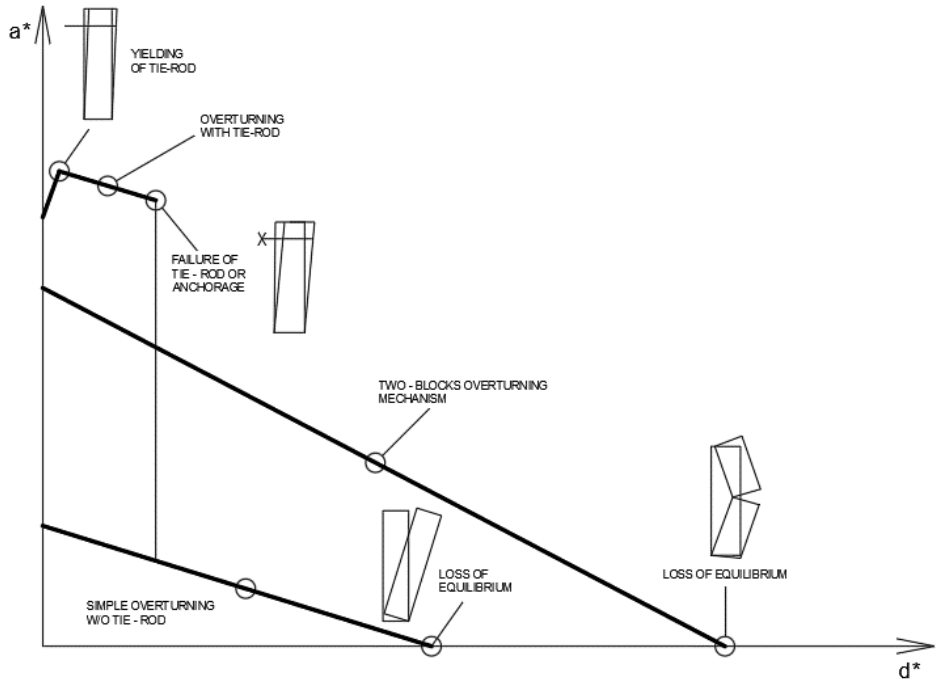

Figure 3.6: examples of the acceleration-displacement capacity curve obtained by nonlinear kinematic analysis as proposed by Italian standard (Magenes and Penna, 2011).

The Italian standard suggests for a more refined calculation to consider the compressive strength of the masonry with a recess of the pin inside the contact section and with possible frictional stresses due to the interlocking with the transverse structures.
The capacity curve is obtained from the pushover curve obtained from the kinematic incremental analysis. Equivalent displacement d^* and equivalent acceleration a^* are required to describe the relative single degree of freedom (SDOF). The equivalent displacement d^* is defined as follows:

$$d^* = \frac{d}{\delta} \frac{\sum_{n=1}^{N} W_n \delta_n^2}{\sum_{n=1}^{N} W_n \delta_n} \tag{3.1}$$

while equivalent acceleration a^* is defined as follows:

$$a^* = \frac{\alpha g}{e^*} \tag{3.2}$$

The aforementioned equations are defined by W_n is the mass of n element

(macroblock), δ_n is the horizontal displacement at the point of application, g is the gravity acceleration, α is the load multiplier and e^* is the ratio between the modal mass and the total mass.

3.3.2 Force-based approach

The force-based approach (FBA) verification consists of verifying that the capacity is greater than the demand according to the force-based control by satisfying the following inequality:

$$a_0^* \geq \frac{a_g S}{q} \tag{3.3}$$

where a_g is the ground acceleration on stiff soil (class A (CEN, 2004)) for the chosen limit state, S is the soil coefficient and q is the behavior factor. In this case q = 2.0 according to Eurocode 8 (CEN, 2004, Table 4.4). This behavior factor is suitable for partitions and facades.

3.3.3 Displacement-based approach

Force-based approach (FBA) is widely recommended for URM buildings because it is perceived as having very limited ductility. However, experimental tests have shown that seismically excited walls can sustain accelerations well above their capacity defined by static calculation (ABK, 1981; Doherty et al., 2002).

The displacement-based approach (DBA) consists of:

$$d_u^* \geq S_{De}(T_S) \tag{3.4}$$

where d_u^* is determined as:

$$d_u^* = \min\left(0.40 d_o^*; d_{ins}^*\right) \tag{3.5}$$

where d_{ins}^* is the displacement corresponding to any situations that could affect the stability of the mechanism and $S_{De}(T_S)$ is the elastic displacement spectrum evaluated at the secant period T_s. The secant period T_s of mechanism is defined as:

$$T_S = 2\pi\sqrt{\frac{d_s^*}{a_s^*}} \tag{3.6}$$

where $d_s^* = 0.4 \cdot d_u^*$ and a_s^* is the relative pseudo-acceleration of the bilinear response curve.

3.3.4 Dynamic approach

Modeling unreinforced masonry walls, subjected to seismic loads, represents an important challenge for both engineers and researchers because of its complexity of being described with nonlinear dynamic analysis. In this study, a single degree of freedom (SDOF) numerical model is used for the analysis of their dynamic behavior under seismic action.

3.3.4.1 Modeling strategy

The equation of motion for a rocking block associated with a given local mechanism can be derived using Lagrange's equation (DeJong and Dimitrakopoulos, 2014):

$$\frac{d}{dt}\left(\frac{\partial T\left(\phi,\dot{\phi}\right)}{\partial\dot{\phi}}\right) - \frac{\partial T\left(\phi,\dot{\phi}\right)}{\partial\dot{\phi}} + \frac{\partial V\left(\phi\right)}{\partial\dot{\phi}} = -B\left(\phi\right)\ddot{u}_g + Q\left(\phi\right) \tag{3.7}$$

where ϕ is the lagrangian parameter that describes the motion, T and V indicate kinetic and potential energy, respectively, $-B\left(\phi\right)\ddot{u}_g$ is the generalized inertial force induced by earthquake ground acceleration $\ddot{u}_g$, Q is the generalized force provided by static loads and overdot stands, as usual, for time derivative. Equation (3.7) can be rewritten in the following form:

$$I\left(\phi\right)\ddot{\phi} + J\left(\phi\right)\dot{\phi}^2 + G\left(\phi\right) = -B\left(\phi\right)\ddot{u}_g + Q\left(\phi\right) \tag{3.8}$$

where $I\left(\phi\right), J\left(\phi\right), G\left(\phi\right)$ and $B\left(\phi\right)$ are nonlinear functions of ϕ. It is also possible to derive from Equation (3.8), for different local mechanisms, the load multiplier that activates the rocking motion from a resting position, i.e. from a state with null acceleration and velocity ($\ddot{\phi} = 0,\ \dot{\phi} = 0,\ \phi = 0$):

$$\lambda = -\frac{Q|_{\phi=0} - G|_{\phi=0}}{g\,B|_{\phi=0}} \tag{3.9}$$

where g is the gravity acceleration. The same load multiplier can be obtained by the limit analysis approach. In rocking systems, the energy dissipation is associated with the impact of the blocks at the base (Housner, 1963; Spanos and Koh, 1984; Yim et al., 1980). The restitution coefficient is defined, indeed, as the ratio of angular velocity after and before the n^{th} impact.

This formulation, reported in Sections 3.3.4.2 and 3.3.4.3, is widely used in the literature (Liberatore and Spera, 2001; Makris and Konstantinidis, 2003; Sorrentino et al., 2011). In the adopted models it is assumed that the rigid block is rocking on a rigid foundation (this is not completely true). The coefficient strongly depends on the contact interface as shown in experimental tests (ElGawady et al., 2011). If the role of the base is considered, a possible shifting rotation point defined based on the interface (compressive behavior of interface and accounting of crushing effects) should be considered (Mehrotra and DeJong, 2018).

3.3.4.2 One-sided rocking

A one-sided rocking can be assumed for a wall even though the presence of internal constraints such as transverse walls and floor slabs. The governing equation for the one-sided rocking of a rigid body can be written similarly to that for two-sided rocking:

$$I_0\ddot{\phi} + gM_bR\sin(\alpha-\phi) = -M_bR\ddot{u}_g\cos(\alpha-\phi) \tag{3.10}$$

where I_0 is the polar moment of inertia with the pivot point 0, M_b is the mass of the block and α is the internal angle and R is the length of the half-diagonal. In the case of vertical restraint, the rotation ϕ of the system remains positive (Figure 3.7). For one-sided cases, the experimental evidence shows that energy dissipation depends on the interface between the rigid block and its external constraint through the coefficient (Sorrentino et al., 2011):

$$\eta_{1s} = \left(1-\frac{3}{2}\sin^2\alpha\right)^2\left(1-\frac{3}{2}\cos^2\alpha\right) \tag{3.11}$$

For better and more accurate modeling of the seismic behavior of the wall, a tri-linear moment-curvature relationship with a finite initial stiffness can be assumed on the basis of experimental tests (Doherty et al., 2002).

The tri-linear function takes into account initial imperfections, non-linear material behavior, and second-order effects. If this configuration is assumed with the tri-linear moment-rotation relationship, the motion equations can be written as follows (Boscato et al., 2014):

$$\begin{aligned}
\ddot{\phi} &= -\frac{WR}{I_0}\left[\frac{k_i}{WR}\phi + \frac{\ddot{x}_g(t)}{g}\cos\left(\alpha - |\phi|\right)\right] && \text{if } |\phi| \le \alpha_1 \\
\ddot{\phi} &= -\frac{WR}{I_0}\left[\operatorname{sgn}(\phi)\frac{k_i}{WR}\alpha_1 + \frac{\ddot{x}_g(t)}{g}\cos\left(\alpha - |\phi|\right)\right] && \text{if } \alpha_1 < |\phi| \le \alpha_2 \\
\ddot{\phi} &= -\frac{WR}{I_0}\left[\operatorname{sgn}(\phi)\frac{k_f}{WR}\left(\alpha - |\phi|\right) + \frac{\ddot{x}_g(t)}{g}\cos\left(\alpha - |\phi|\right)\right] && \text{if } |\phi| > \alpha_2
\end{aligned} \tag{3.12}$$

where R is the distance of the center of gravity from the rotation pivot, k_i is the initial stiffness $\left(k_i = \frac{WR\sin(\alpha)}{\alpha}\cdot\frac{\alpha-\alpha_2}{\alpha_1}\right)$; and k_f is the final stiffness $k_f = \frac{WR\sin(\alpha)}{\alpha}$ with parameter $\alpha_1 = \tan^{-1}\left(3\frac{\Delta_1}{2H}\right)$ (Table 3.1). The ultimate normalized rotation (Δ_u) of the SDOF system is equal to 1. The ultimate normalized rotation corresponds to the Engineering Demand Parameter (EDP, see Section 3.7.2.3).

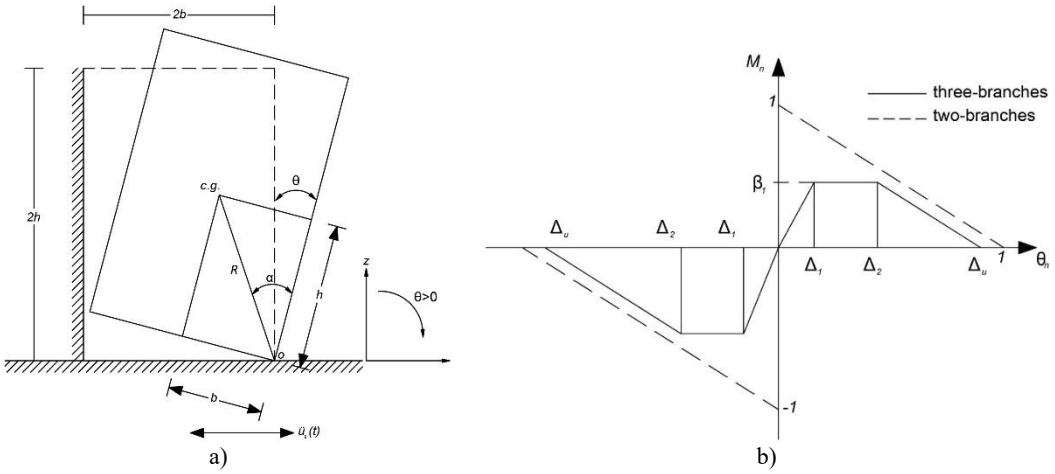

Figure 3.7: a) geometry of a rigid block under the one-sided rocking under ground motion, b) normalized moment-rotation relationship (Sorrentino et al., 2016).

Table 3.1: the trilateral moment rotation curves parameters.

State of degradation	Δ_1/Δ_u	Δ_2/Δ_u
New	6 %	28 %
Moderate	13 %	40 %
Severe	20 %	50 %

3.3.4.3 Two block mechanism

The two-block mechanism can be used to describe the dynamic behavior of a wall that is characterized by the formation of the classical pivot interface at the wall top, bottom, and mid-height. The top and bottom pivot can rotate if they are under a ground motion excitation. The mechanism is described by these main parameters: α_1 and α_2 the describe the slenderness of the two blocks; I_{01} and I_{02} that are the polar moment of inertia regarding the relative mass centers M_{b1} and M_{b2} that are the masses of the bottom and the top blocks (Figure 3.8).

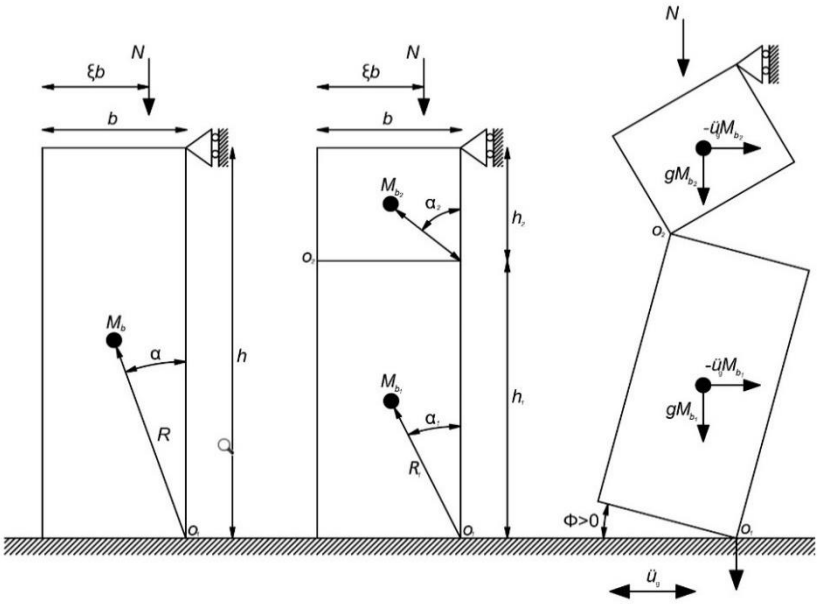

Figure 3.8: (a) wall parameters, (b) cracked vertical spanning strip wall parameters, (c) displaced configuration and ground acceleration component acting in the mass centers of the two bodies.

The resulting equation of motion is equivalent to those proposed in the literature (DeJong and Dimitrakopoulos, 2014; Mauro et al., 2015; Sorrentino et al., 2008) and can be written as follows;

$$\begin{aligned}&\left(I_{01}+B_1 I_{02}+B_2 M_{b2} R_2^2\right)\ddot{\phi}+\left(C_1 I_{02}+C_2 M_{b2} R_2^2\right)\dot{\phi}^2+gAR_2\left[M_{b1}+M_{b2}\left(1+\frac{B_2}{4A^2}\right)\right]= \\ &-A\left(M_{b1}+M_{b2}\right)R_2\cot\left(\alpha_1-\phi\right)\ddot{u}_g+Q\end{aligned} \tag{3.13}$$

with the following system coefficients that are not constant but are functions of rotation ϕ.

$$A=\frac{\sin\left(\alpha_2\right)}{\sin\left(\alpha_1\right)}\sin\left(\alpha_1-\phi\right)$$

$$B_1=\frac{\mathrm{A}^2\cot^2\left(\alpha_1-\phi\right)}{1-A^2}$$

$$B_2=4A^2\left[1+\sqrt{B1}\right]$$

$$C_1=\left[1-\frac{A^2}{\sin^2\left(\alpha_1-\phi\right)}\right]\left(\frac{A}{1-A^2}\right)^2\cot\left(\alpha_1-\phi\right) \tag{3.14}$$

$$C_2=\frac{B_2}{2}\left[\frac{A}{\sqrt{1-A^2}}-\frac{A^2-2}{\left(1-A^2\right)}\cot\left(\alpha_1-\phi\right)\right]$$

$$Q=-2ANR_2\sqrt{B_2}\cos^2\left(\alpha_2\right)\left[\frac{1}{\sqrt{B_2}\cos^2\left(\alpha_2\right)}+1+\xi\tan^2\left(\alpha_2\right)+\frac{\left(\xi-1\right)\tan\left(\alpha_2\right)\sqrt{1-A^2}}{A}\right]$$

The critical rotation and the horizontal load multiplier of the system become:

$$\phi_{cr,0}=\alpha_1$$

$$\lambda=\tan\left(\alpha_1\right)\frac{M_{b1}+\left(M_{b2}+\frac{N}{g}\right)\left(2+\frac{\tan\left(\alpha_2\right)}{\tan\left(\alpha_1\right)}\right)+\left(2\xi-1\right)\frac{N}{g}\frac{\tan\left(\alpha_2\right)}{\tan\left(\alpha_1\right)}}{M_{b1}+M_{b2}} \tag{3.15}$$

and the coefficient of restitution η_{tb} is defined as follows:

$$\eta_{tb} = \frac{M_{b1}R_1^2 + I_{01}\dfrac{\tan\alpha_2}{\tan\alpha_1} - 2M_{b1}R_1^2\sin^2\alpha_1 + M_{b2}R_1^2\left[2 + \dfrac{\sin\alpha_1\cos\alpha_1}{\tan\alpha_2} - \sin^2\alpha_1\left(4 + \dfrac{\tan\alpha_2}{\tan\alpha_1}\right)\right]}{M_{b1}R_1^2 + I_{01} - I_{02}\dfrac{\tan\alpha_2}{\tan\alpha_1} + M_{b2}R_1^2\left[2 + \sin\alpha_1\cos\alpha_1\left(\dfrac{1}{\tan\alpha_2} + \tan\alpha_2\right)\right]} \tag{3.16}$$

The coefficient of restitution depends on the slenderness of the wall and the position of the hinge. For the stockier wall and lower intermediate hinge, the energy dissipation will decrease. For this type of mechanism, the value of the coefficient of restitution is between 0.84 and 0.90 from experimental tests (Graziotti et al., 2016). This model does neither include progressive damage (Doherty et al., 2002) nor an energy damping term (Tomassetti et al., 2019). In this chapter, the analytical formulation (eq. 10) is used for the analyzes. The rocking response results are obtained from a MATLAB code that numerically solves the nonlinear equations by means of a 4th-5th order Runge-Kutta integration technique (The Mathworks Inc., 2016).

3.3.5 Comparison between the linear, non-linear kinematic approach and non-linear dynamic analysis

In this section, a critical review of seismic response assessment techniques for local collapse mechanisms in existing masonry structures is discussed. To have statistically robust results, three types of walls with the two different configurations of constraints are subjected to non-linear dynamic analyses (Table 3.2).

Each wall was subjected to 44 accelerograms with 2 constraint configurations for 10 different amplitude scales of ground motion. A total of 1320 non-linear dynamic analyses were performed. The results of the dynamic analysis are expressed by the ratio between energy demand (E_D) and capacity (E_C) (Shawa et al., 2012; Sorrentino et al., 2016). The energy demand (E_D) is calculated as the maximum potential energy during the seismic action or as the sum of the potential and kinetic energy at instability.

The capacity energy (E_C) is calculated as the difference in the potential energy of the system.

In Figure 3.9, the results obtained from the non-linear dynamic analyses are compared with the methods proposed by the Italian code (MIT, 2018, 2019). In the Italian code, the evaluation of local collapse mechanisms is recommended with two approaches: the force-based approach and the displacement-based approach.

Table 3.2: block used in the analysis, *b* is the thickness of the wall whereas *h* is the height of the wall.

Wall	b [m]	h [m]	boundary conditions
1	0.25	4	one-sided rocking
			two-block mechanism
2	0.25	7.5	one-sided rocking
			two-block mechanism
3	0.25	11.2	one-sided rocking
			two-block mechanism

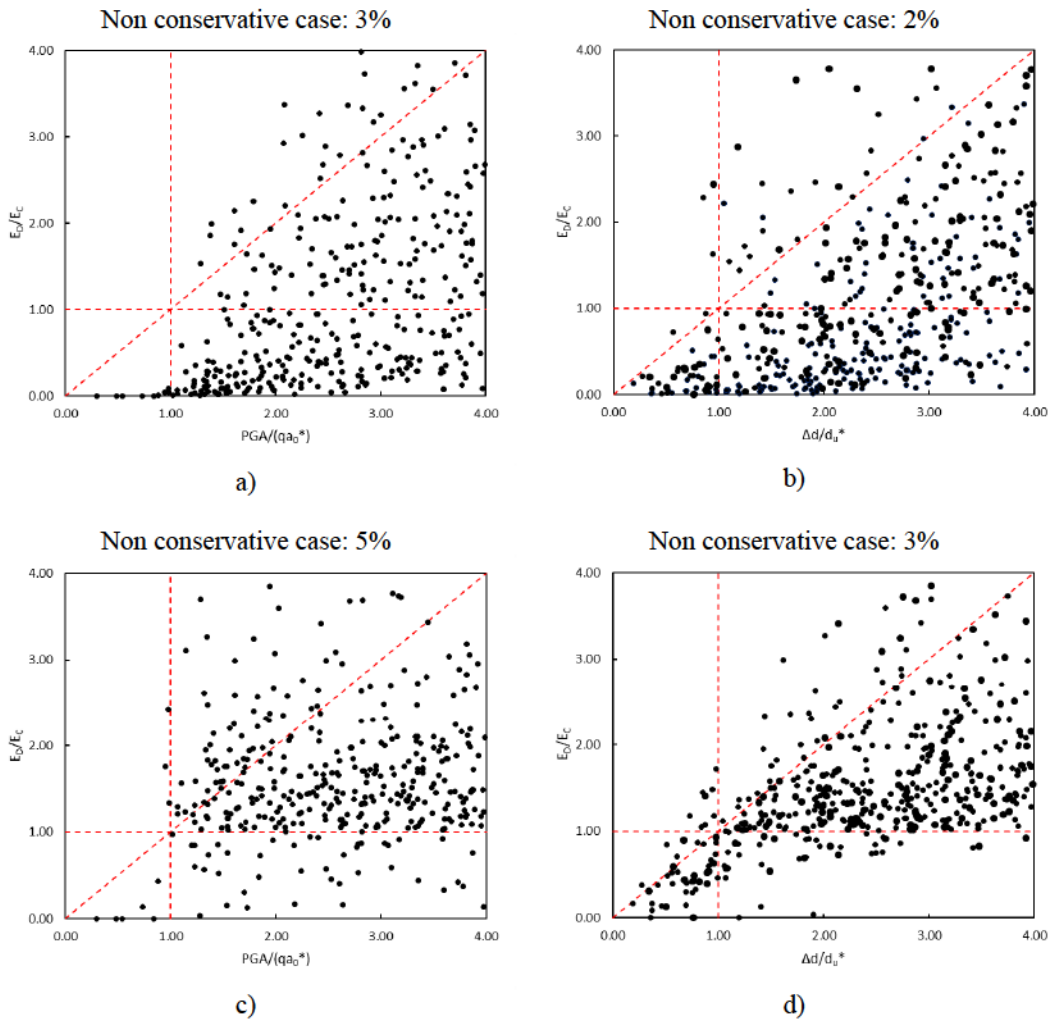

Figure 3.9: Comparison between Italian code (NTC 2018) and non-linear dynamic analysis: a) force-based approach for one-sided rocking, b) displacement-based approach for one-sided rocking, c) force-based approach for two block mechanism, b) displacement-based approach for two block mechanism.

The force-based approach defines the acceleration capacity (a_0*). The acceleration demand is defined as the peak ground acceleration (PGA) divided by behavior factor q = 2.0. The ratio between demand acceleration (PGA at the base of the block) and capacity acceleration is used to compare the force-based approach to the ratio of energy

demands and capacity from dynamic approach that are presented in Figure 3.9a-c.
The displacement-based approach, on the other hand, defines a displacement capacity (d_u*). The corresponding demand displacement is evaluated using the spectral displacement ($S_{De}(T_S)$) at the secant period (T_S) of the local mechanism. The ratio between displacement demand and capacity is used to compare the displacement-based approach to the ratio of energy demands and capacity from the dynamic approach that are presented in Figure 3.9b-d.
As it can be observed in Figure 3.9, the number of non-conservative cases is less for the one-sided mechanism, while it increases in the case of the two-blocks mechanism. Furthermore, it is possible to see how a displacement-based approach can reduce the number of non-conservative cases. Both code approaches confirm that they are in some cases non-conservative.

3.4 Description of approach

Under seismic actions, the local response is related to the activation of out-of-plane collapse mechanisms of parts of the buildings insufficiently connected to the rest of the structure (Figure 3.5). Furthermore, fragility curves were used to describe the local response in a probabilistic context. These curves are useful for defining related vulnerability models.
The intensity measure (IM) adopted in this work is the peak ground acceleration (PGA) as required by the Italian building code (MIT, 2018) and which represents a common choice in the case of URM buildings.
Epistemic uncertainty was treated using a logic tree approach that allows describing the vulnerability of each mechanism (Section 3.6.1). The aleatory uncertainty of each mechanism deriving from the properties of the materials, the geometry of the elements, and the loads applied on the mechanism have been treated with the Monte Carlo method (Section 3.6.2).
The input parameters for a given mechanism were treated as one of the possible combinations of existing walls. To create a group of walls representative of the type of structures considered, a number of 1000 walls have been created. Such walls are the final result of all the uncertainties considered deriving from the epistemic and aleatory ones.

To create the topological fragility curves, we proceeded as follows:

i) identification of all possible configurations of the collapse mechanisms and relative weights (Section 3.6.1);
ii) extrapolation of the main collapse mechanisms from the logic tree (Section 3.6.1);
iii) generation of walls for the various mechanisms (Section 3.6.2);
iv) multiple stripe analysis and creation of fragility curves (Section 3.7.2.4);
v) typological fragility curves by combining the weights of mechanisms (Section 3.7.2.5).

3.5 Building Database

3.5.1 CARTIS database

The structural-Typological and Seismic ChARacterization database, referred to in the following as CARTIS (Zuccaro et al., 2016), is an inventory of building typologies funded by the Italian National Civil Protection Department and implemented by the Italian University Network of Seismic Engineering Laboratories (ReLUIS) with the purpose of a seismic vulnerability assessment at a territorial scale. To date, the database collects information on 506 municipalities. For any given municipality involved, the data collection is mainly based on an interview to municipality technicians informed on historical events of city planning. This generally allows subdividing the urban center into homogeneous building compartments and filling out a form with data (i.e., age of structures, types of vertical structures, floor slabs and roofs, geometrical data) on the various structural typologies contained into them. To validate the datasets, several buildings for each structural typology are also accurately surveyed on site.
The resulting information is more detailed than that provided by available standard methods (ISTAT data, Census Database) and can more effectively support the creation of vulnerability models. In this chapter, the CARTIS database is used to develop typological fragility functions for local failure mechanisms in URM structures.

3.5.2 Case study

3.5.2.1 The historic center of Ferrara

The historic center of Ferrara is made up of 92% masonry buildings and the remainder is made up of reinforced concrete and mixed structures. The structures are of less than 3 stories for 83%, albeit unevenly distributed concerning the construction periods of the city from the 14th to the 19th century (Dolce et al., 2015).

The historical-urban development of the historic center of the city can be traced back to three main additions (Figure 3.10).

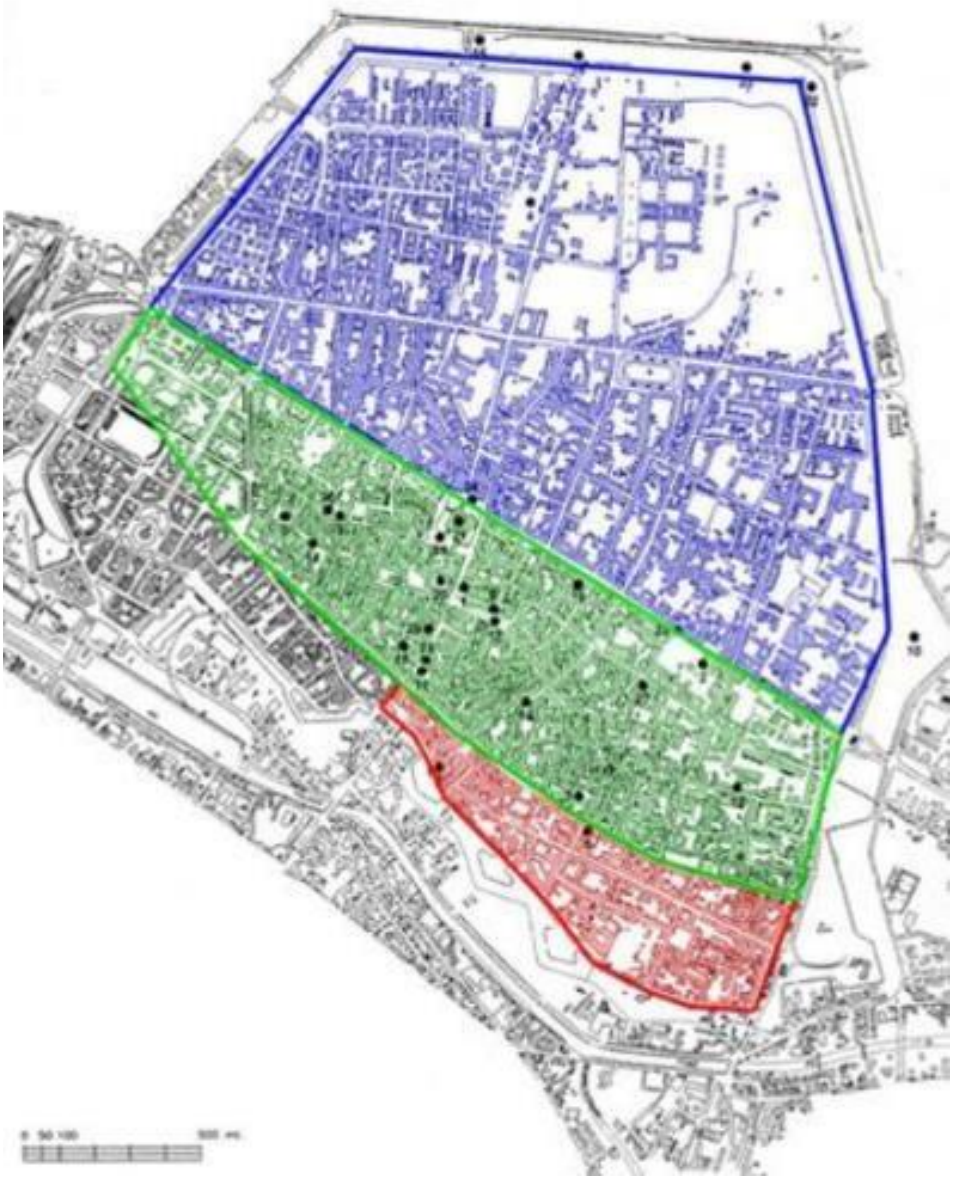

Figure 3.10: urban evolution of the city of Ferrara.

The historic center consists of the first medieval nucleus up to the 12th century. In that period the cathedral was built and the first network of streets running perpendicular to the Po di Ferrara with the current streets of Porta Reno, Vignatagliata and San Romano, represented by the green area.

Subsequently, there was the addition of Borso d'Este (1450) in the southern part of the city (Figure 3.10, red area). The last and most important addition was the one desired by Duke Ercole I d'Este made by the architect Biagio Rossetti in 1492. This addition is known as Addizione Erculea. This affects the northern part of the city with a new Renaissance structure (Figure 3.10, blue area).

The area under study focuses on an area south of the city, which includes the medieval core and the addition of Borso d'Este. For the aggregate considered, we conduct accurate analyzes for each structural unit belonging to the pathway, relating to the first mode most significant mechanisms. In addition, an accurate visual analysis was carried out for each case study in order to characterize the individual facades and highlight the main critical issues. In this study, all private buildings were considered, excluding historic buildings and churches. Buildings made of reinforced concrete were also excluded. To highlight the prominence that local overturns can take on in the central area of the city, we briefly report the results of linear kinematic analyses performed for the facades in one street of the area, via Porta d'Amore.

A three-dimensional model of the facade of all the masonry structural units identified in the street under study was created, for each model various simulations were then performed according to the global and local kinematics whose study was considered significant (Figure 3.11).

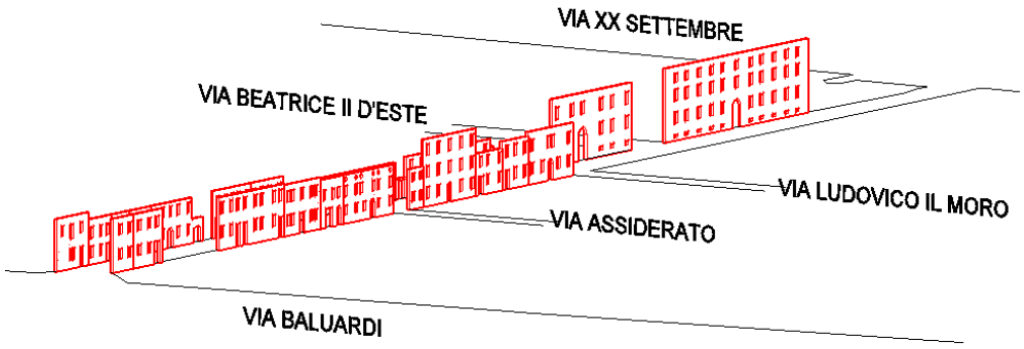

Figure 3.11: a three-dimensional model of the facades for Porta d'Amore street.

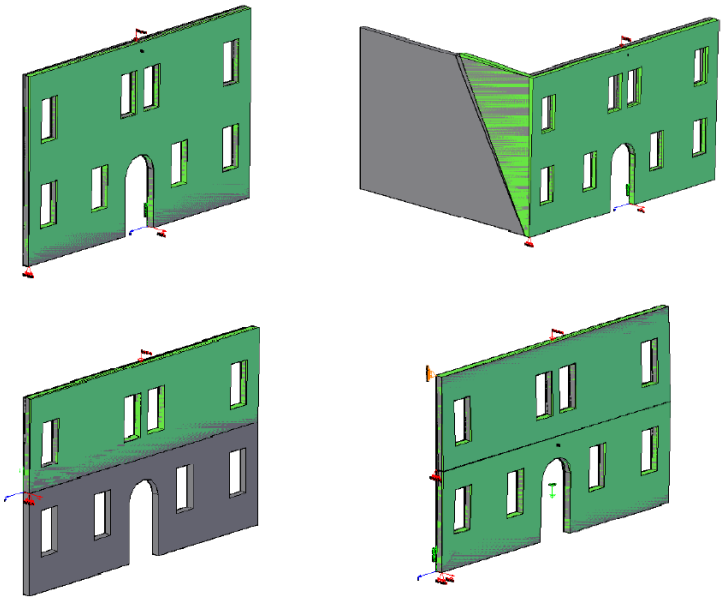

Figure 3.12: possible combinations of mechanisms for the walls.

The first mode mechanisms that have been studied are simple global overturning, global compound overturning (only for sidewalls that showed an adequate degree of clamping), simple overturning and vertical bending (Figure 3.12).

For each wall, the safety coefficient ρ was calculated as the ratio between the maximum acceleration expected on the ground in the a_{SLV} life-saving limit state condition and the collapse acceleration of the kinematics a_0^*:

$$\rho = \frac{a_{SLV}}{a_0^*} \tag{3.17}$$

where a_{SLV} is defined as Eq. (3.3).

The safety factor ρ when it is between 0 and 1 indicates a safety situation as the maximum expected acceleration is lower than that necessary for the activation of the kinematics itself. If it is greater than 1, the danger of the kinematics is greater and therefore unsafe. In fact, the kinematics will be able to activate with a much lower acceleration than the maximum expected on the ground.

To define the degree of danger we divided the coefficient ρ into intervals, in order to represent the results obtained with a chromatic scale and to be able to analyze them in a more intuitive way (Table 3.3).

Table 3.3: safety classification by means of the ρ safety coefficient.

Range coefficient ρ	degree of safety	Color tag
$\rho < 1$	safe	green
$1 \leq \rho < 2$	low unsafe	yellow
$2 \leq \rho < 4$	medium unsafe	blue
$\rho \geq 4$	high unsafe	red

The most critical issues concern the simple global overturning of the walls. This condition is particularly burdensome, especially for aggregate buildings. The presence of clamping with the sidewalls can be considered reliable in most cases; obviously, it involves a considerable decrease in the risk of overturning.

The local overturning checks, carried out for the various floors, do not generally present high criticalities. Verification of vertical bending are satisfied almost everywhere. The distribution of the capacity factors is therefore quite homogenous and no buildings have been identified in particular situations of isolated criticality compared to others.

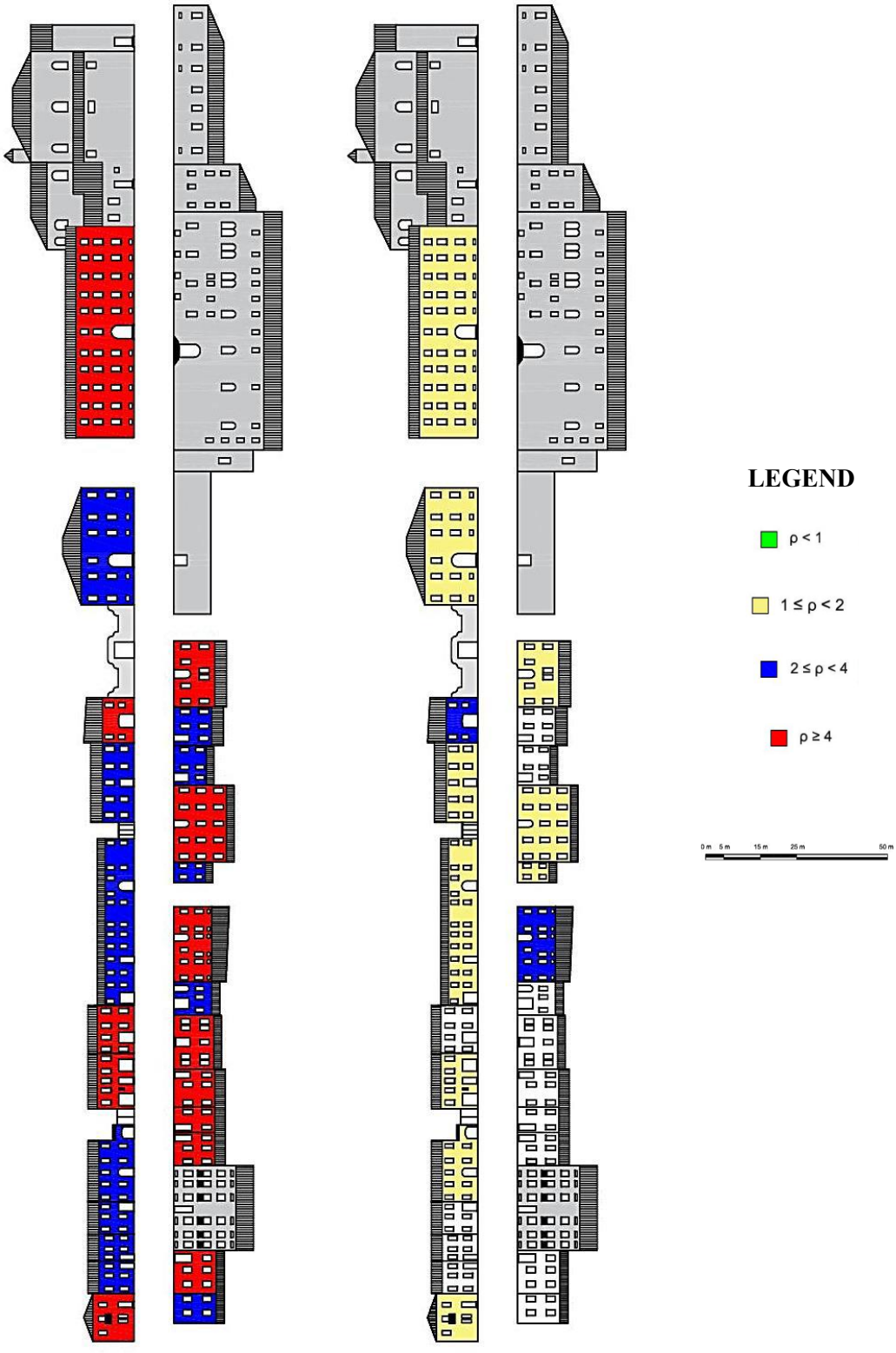

SIMPLE GLOBAL OVER-TURNING

GLOBAL OVERTURNING WITH TRANSVERSAL CON-NECTION

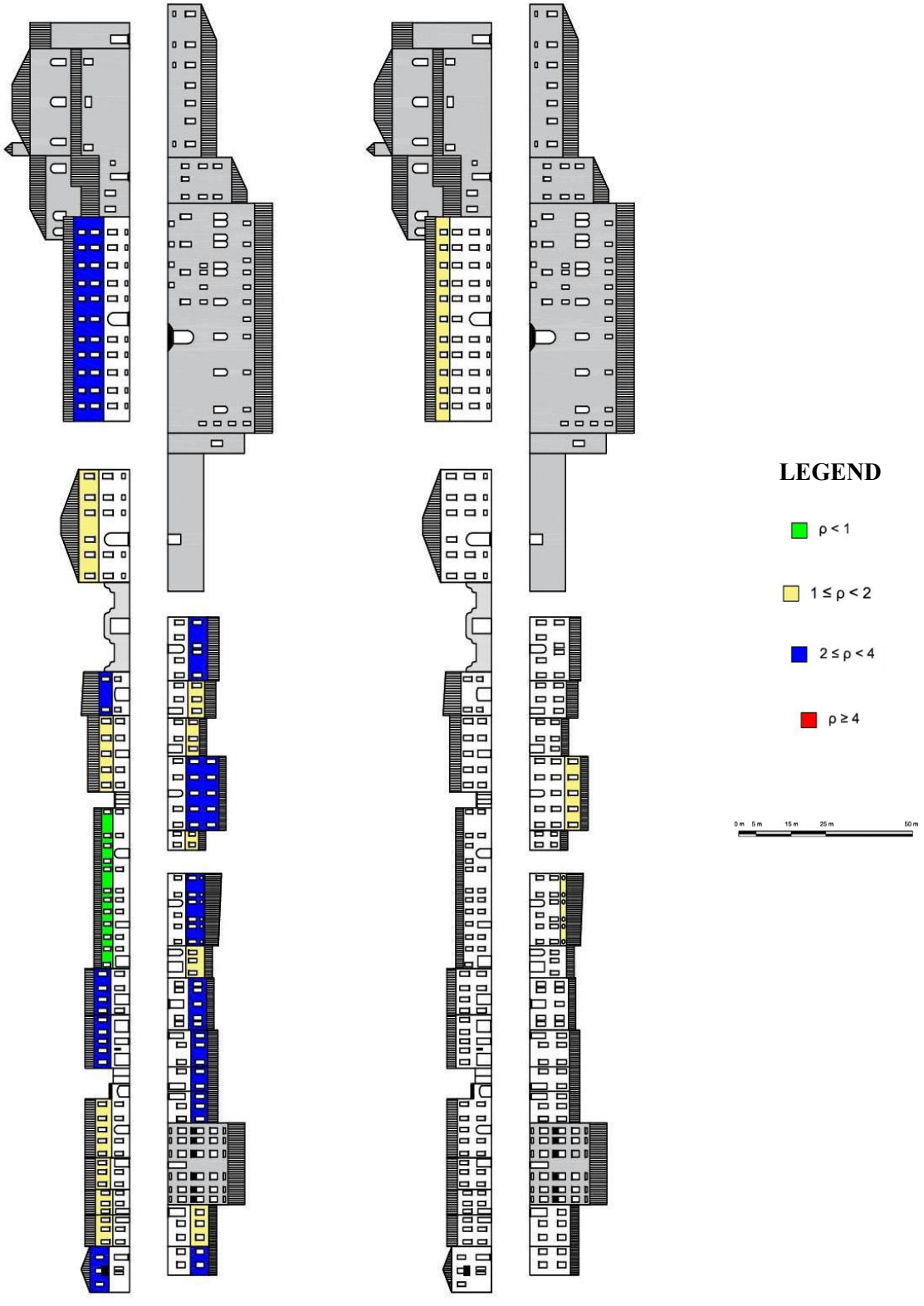

LOCAL SIMPLE GLOBAL OVER-TURNING AT 1ST LEVEL

LOCAL SIMPLE GLOBAL OVER-TURNING AT 2ND LEVEL

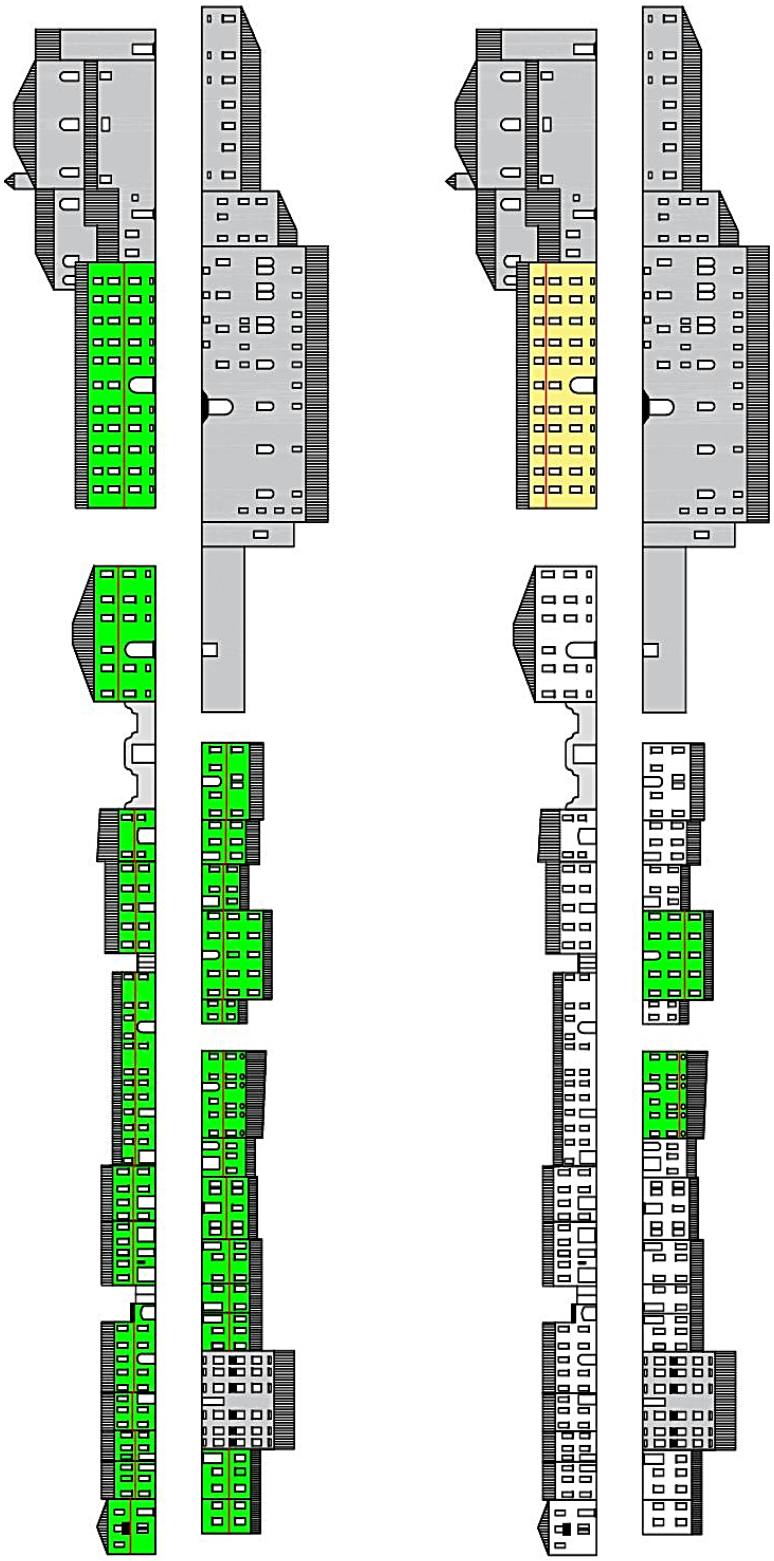

VERTICAL BENDING AT 1ST LEVEL

VERTICAL BENDING AT 2ND LEVEL

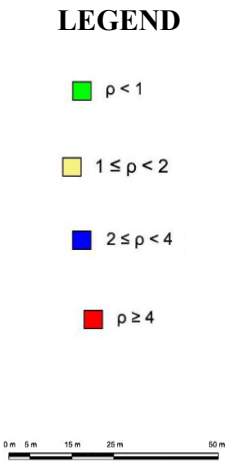

3.5.2.2 A historical aggregate in the center of Ferrara

We decided to survey a historical aggregate of buildings in the center of Ferrara (via Carlo Mayer) to improve the knowledge of masonry buildings with respect to the data provided by CARTIS database. For the selected compartment, there are two typologies of masonry buildings in the city center of Ferrara (MUR 1 and MUR 2) (Figure 3.1).

The MUR1 typology refers to buildings from two to four stories, belonging to the oldest part of the historic center (medieval area) but also to the Renaissance area up to the 1800s and early 1900s (Figure 3.13).

The MUR2 typology is more recent (from 1920 to 1945) and has a variable percentage of tie rods, even though it also has wooden floors and a wooden roof. The buildings of these types are for residential, commercial, tourist-accommodation, and office use (Figure 3.14).

a) b)

Figure 3.13: example of buildings MUR1 class.

a) b)

Figure 3.14: example of buildings MUR 2 class.

Table 3.4: buildings parameters from CARTIS Database.

Parameters	**MUR 1**	**MUR 2**
number of floors	2 - 4	2 - 4
average floor height [m]	2.5 – 3-5	2.5 – 3.5
average ground floor height [m]	3.5 – 5.0	2.5 – 3.5
average floor area [m^2]	100 – 230	70 – 170
age of building	before 1860 1861 – 1919	1919 - 1945
type of masonry	Clay brick wall	Clay brick wall
transversal connections	No information	No information
with tie rods or tie beams	70%	60%
average thickness of ground floor walls [cm]	30	30
average distance between walls parallel to the facade [m]	5.5	4.5
type of slab	wood	wood
type of roof	Wooden - not pushing	Wooden - not pushing

Table 3.4 shows the main parameters of the buildings in the historic center of Ferrara from CARTIS Database.

The parameter that most differentiates the two typologies are the age of construction, the average height of the ground floor and the different percentage of tie-rods.

The latter, understood as the percentage of buildings with chains compared to the total number of buildings, is useful information for defining the logic tree of possible collapse mechanisms and assigning a percentage for the fragility curves associated.

In fact, the presence of tie-rods at the level of all floors favors the occurrence of the expulsion mechanism and excludes overturning.

The structural behavior of URM buildings is directly dependent on the materials and constructive details and indirectly dependent on the usage and state of conservation. One of the main challenges when assessing existing buildings is the definition of the mechanical properties of the materials (e.g. quality of clay brick walls, see Figure 3.15).

In general, the weakest points of URM buildings are poor connections (between walls or between walls and floors or roof) and the limited stiffness of timber floors (Figure 3.16).

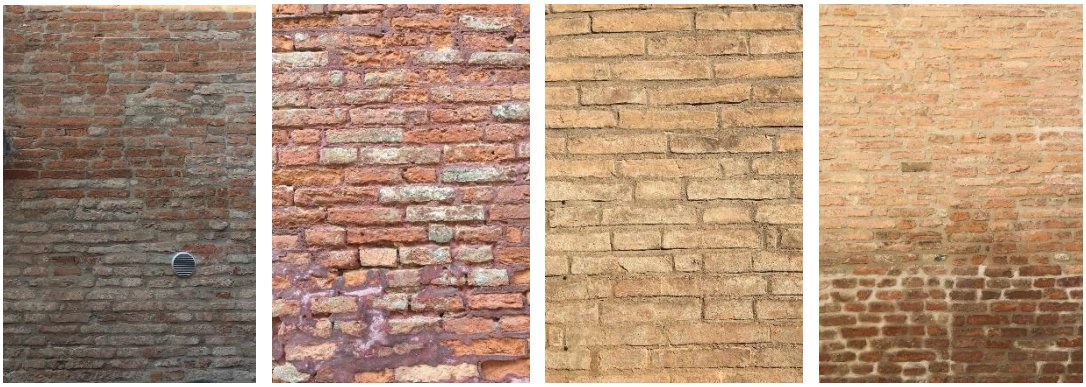

a) b) c) d)

Figure 3.15: types of clay brick walls in Ferrara for MUR1 and MUR2 class.

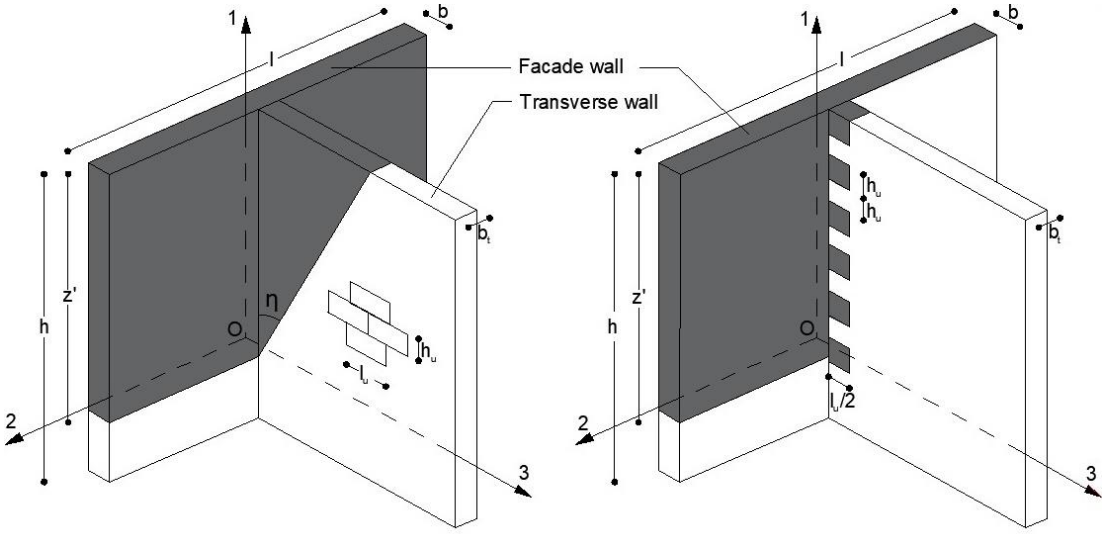

Figure 3.16: Out-of-plane collapse mechanisms taking into account connections with transversal walls (de Felice and Giannini, 2001).

For the aggregate considered, we conduct accurate analyzes for each structural unit belonging to the pathway, relating to the first mode most significant mechanisms.

In addition, an accurate visual analysis was carried out for each case study in order to characterize the individual facades and highlight the main critical issues.

In this study, all private buildings were considered, excluding historic buildings and churches. Buildings made of reinforced concrete were also excluded.

3.6 Evaluation of uncertainties

To assess the seismic behavior of buildings, the epistemic and aleatory uncertainties are briefly defined in the next sections to account for the possible variations within a given class of buildings. The geometry of the building is not considered an uncertainty

as the layout of the buildings is similar. Aleatory uncertainty is classified as irreducible uncertainty and refers to a property of the system associated with variability, whereas epistemic uncertainty can be reduced and is associated with a lack of knowledge by the analyst (Beer et al., 2013).

3.6.1 Epistemic uncertainties

The epistemic uncertainties for the analysis of the local behavior are related to the incomplete knowledge about the structure of the buildings. These features are treated by the logic-tree approach (Simões et al. 2020).

Figure 3.17 presents the logic tree for the URM buildings in Ferrara for different categories of buildings (MUR1 and MUR2). Each branch of the tree is given a weight based on expert judgment

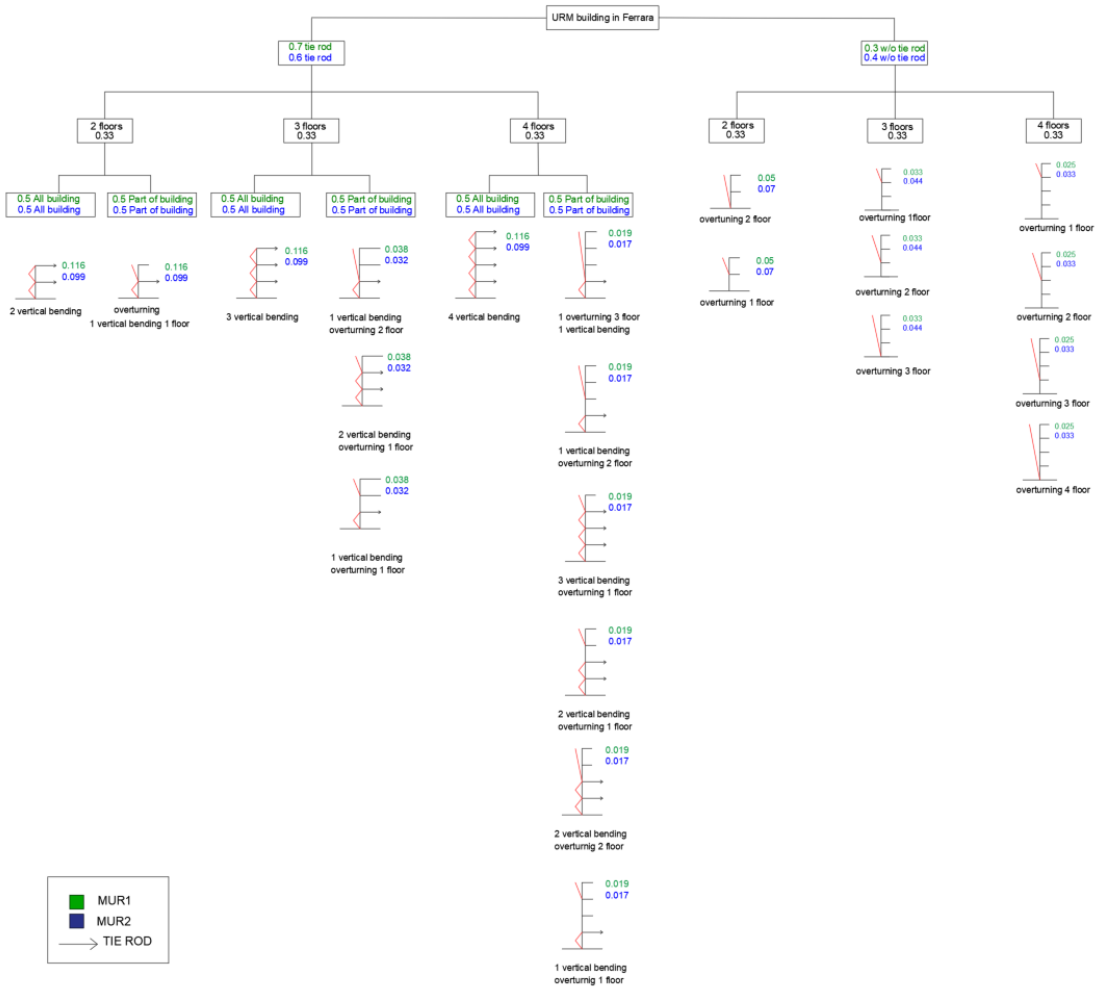

Figure 3.17: logic-tree for URM buildings in Ferrara of the possible local mechanisms with relative weights (green for the MUR 1 typology and blue for MUR2 typology).

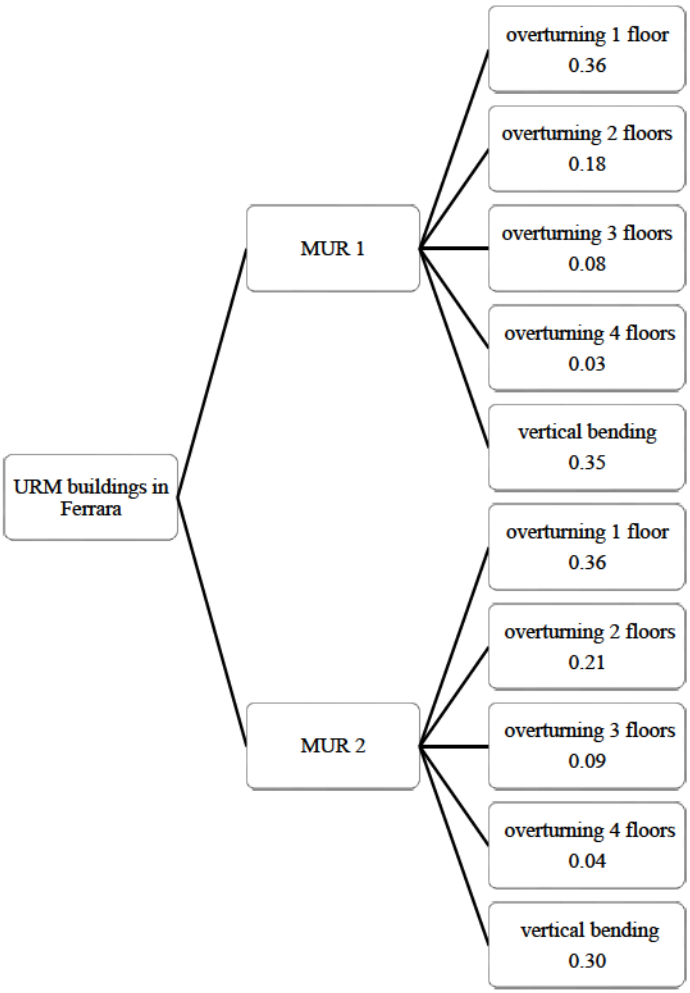

Figure 3.18: diagram of the relative weights for each type of collapse mechanism.

The end of a branch of the tree represents a class of possible mechanisms with specific features and the final weights.

The weight attributed to the class of mechanisms is determined by multiplying the weight of all the component branches of the tree. More in detail, from the first logic tree it is possible to obtain for the two main classes of masonry buildings with the relative associated weights for the various types of collapse mechanisms (Figure 3.18). The main mechanisms obtain from the logic tree are: overturning 1 floor, overturning 2 floor, overturning 3 floor, overturning 4 floor and vertical bending. With the expression overturning n floor, we mean a one-sided rocking with a height of the block corresponding to n floors. The relative mechanism is obtained for the sum of the weights that contain that mechanism. Only for the two-block mechanism, we consider a mechanism at the top floor of the building. The vertical bending in the lower floors have been exclude because the walls are more loaded than the top floor.

This increases the stability of the wall (Mauro et al. 2015). These weights will be used to create the typological curve for out-of-plane mechanisms.

3.6.2 Aleatory uncertainties

Aleatory uncertainties are related to the randomness of a certain phenomenon. For the analysis of the global behavior, the aleatory variables account for variations on the mechanical properties of masonry and geometrical properties of the wall. It is proposed to treat these aleatory variables by the Monte Carlo Method (Zio 2013) to define, in a random way, the properties to be assigned to the numerical models.

The parameter ranges were chosen using the ranges extrapolated from the CARTIS database and possible mechanisms. The random generation of the parameters was done considering an interval set described by a lower and higher value.

Generation occurs assuming a uniform distribution. This choice was made due to the fact that the information about the parameters was vague. The possible choice of a normal or lognormal probability distribution was not compliant because there were not enough tests for the relative parameters. The specific weight of the masonry is assumed constant to 18 kN/m^3. The facade walls vary with a height between 2.5 m and 12.50 m and a thickness between 0.28 and 0.43 m. The thickness was also defined considering causal values compatible with the possible combination of the bricks (i.e. single-leaf wall). Table 3.5 shows all parameters that are used to generate the samples.

A total of 1000 simulations are assumed to have a sufficient number of results to reach a good convergence in the estimation. In the random generation of the walls, the variability of the loads, the percentages of openings in the walls (Figure 3.19) and the presence of transverse connections were considered.

Openings in the walls are included as a variation of the center of mass for simple overturning. On the other hand, for vertical bending it is considered as a variation of the position of the hinge.

Table 3.5: categorization of aleatory variables.

Parameter	Lower bound	Upper bound
Number of floors	1	4
Inter-story height [m]	2.5	3.5
Ground – floor height [m]	2.5 (MUR 2) – 3.5 (MUR 1)	3.5 (MUR 2) - 5.0 (MUR 1)
Wall thickness [m]	0.28	0.43
Floor Span [m]	0	4.5 (MUR 1) - 5.5 (MUR -2)

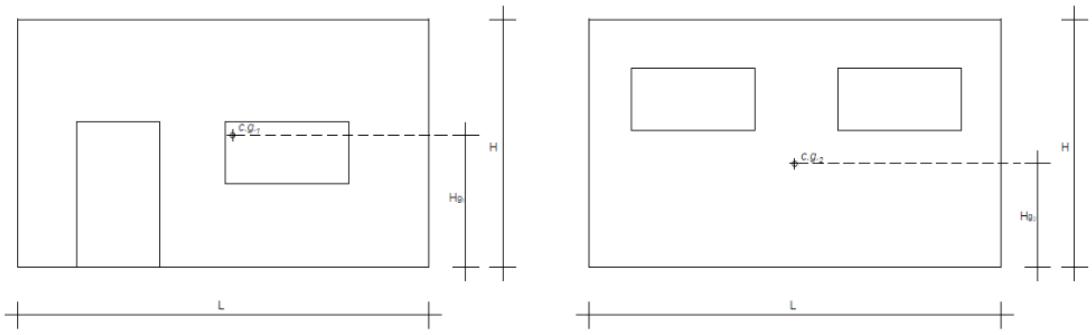

Figure 3.19: different possible combinations of wall with different types of openings.

3.7 Fragility analysis

3.7.1 General approach

A fragility function is defined as a lognormal cumulative distribution function:

$$P\left(C\middle|IM=x\right)=\Phi\left(\frac{\ln\left(x/\theta\right)}{\beta}\right) \tag{3.18}$$

where $P\left(C\middle|IM=x\right)$ is the probability that a ground motion with $IM=x$ will cause the collapse of the wall, $\Phi(\ )$ is the standard normal cumulative distribution function (CDF), θ is the mean of the fragility function and β is the standard deviation of $\ln IM$. To create a fragility curve, it is necessary to estimate the parameters that describe the curve, in particular the mean value and the standard deviation for a lognormal cumulative distribution function.

The parameters of the fragility curves can be estimated by various methods. The two most common are the incremental dynamic analysis (IDA) and multiple stripe analysis (MSA).

The first method consists in performing analyzes from a series of ground motions that are repeatedly incremented to find the IM causing the collapse (Vamvatsikos and Cornell, 2002).

The second method entails performing analyzes for each of the levels of IM from a ground motion set (Jalayer, 2003). A multi-stripe analysis (MSA) is used in this work.

3.7.2 Derivation of fragility curves

3.7.2.1 Selection of ground motions

In this chapter, we used ground motion records from the ESM and ITACA databases (Bindi et al., 2011). The 46 ground motion records used for this study have been derived from 22 different events, recorded in different regions of the Italian territory between 1972 and 2017 (Table 3.6). These ground motions are within a specified range: magnitude M_w between 5.0 and 7.0, Joyner-Boore distance R_{jb} between 0 and 30 km, EC8 soil classification from B to E, and strike-slip, reverse or reverse-oblique faults. The number of ground motions is in accordance with NEHRP Guidelines (Whittaker et al., 2011). The ground motions are mainly obtained by the Italian accelerometric network (Rete Accelerometrica Nazionale, RAN) managed by the Italian Civil Protection Department (DPC) and the national seismic network managed by Istituto Nazionale di Geofisica e Vulcanologia (INGV). The selected ground motions take into account a wide range of PGA as well as PGV (Suzuki and Iervolino, 2017).

3.7.2.2 Intensity Measure (IM)

The intensity measure is a parameter that quantifies the intensity of ground motion and serves as a connection between probabilistic seismic hazard analysis and probabilistic structural response analysis. The choice of this parameter has significant effects on structural response. In the Italian Building code (MIT, 2018), the use of Peak Ground Acceleration (PGA) is recommended for safety checks of mechanisms related with walls supported on ground. For mechanisms located at higher floors, Peak Spectral Acceleration (PSA) is more appropriate. It is well known that the use of PGA may lead to some inconsistencies (Housner, 1965). Other intensity measures such as Peak Ground Velocity (PGV) may sometimes result in more reliable fragility curves (Dimitrakopoulos and Paraskeva, 2015). However, PGA is the most used intensity measure in post-quake damage surveys, because its records are less sensitive than PSA to the scarcity of operating seismic stations. As a consequence, several empirical fragility functions are based on PGA (Buratti et al., 2017). Moreover, the use of PGA turns out to be useful when the global behavior of low-rise masonry buildings is of interest (Lagomarsino and Giovinazzi, 2006). For these reasons, the PGA is adopted as an intensity measure in this study.

Table 3.6: Italian ground motion records with important recorded PGA and PGV (†EC8 classification (CEN, 2004), *Epicentral distance, [I] = ITACA, [E]=ESM).

Year	Event	Event id	Station (Station code, Soil class†)	Focal mechanism	Magnitude M_w (M_L)	Distance* [km]	PGA [g]	PGV [cm/s]	Source
1972	Ancona	IT-1972-0005	Ancona, Rocca (ANR,B)	Unknown	(4,7)	7.7	0.55	9.9	[I]
1976	Friuli 1st shock	IT-1976-0002	Tolmezzo Centrale (TLM1,B)	Thrust	6.4	27.7	0.35	30.2	[I]
1976	Friuli after-shock	IT-1976-0027	Gemona (GMN, B)	Thrust	5.9	6.2	0.63	68.4	[I]
1976	Friuli 3rd shock	IT-1976-0030	Folgaria Cornino (FRC, B)	Thrust	6.0	16.2	0.34	23.7	[I]
1976	Friuli 3rd shock	IT-1976-0030	Gemona (GMN, B)	Thrust	6.0	4.0	0.25	30.5	[I]
1979	Norcia	IT-1979-0009	Cascia (CSC, B)	Normal	5.8	9.3	0.21	14.5	[I]
1980	Irpinia	IT-1980-0012	Sturno (STR, B)	Normal	6.9	33.3	0.32	70.4	[I]
1984	Lazio-Abruzzo	IT-1984-0004	Cassino-Sant'Elia (SCN0, C)	Normal	5.9	19.7	0.14	11.2	[I]
1990	Potenza	IT-1990-0001	Brienza (BRN, B)	Strike-slip	5.8	29	0.10	6.8	[I]
1997	Umbria Mar-che 2nd shock	IT-1997-0006	Nocera (NCR. E)	Normal	6.0	10.1	0.49	32.6	[I]
2002	Molise 1st shock	IT-2002-0045	S. Severo (SSV, B)	Strike-slip	5.7	38.1	0.57	2.1	[I]
2009	L'Aquila	IT-2009-0009	L'Aquila - Valterno - Centro Valle (AQV, B)	Normal	6.1	4.9	0.64	42.7	[I]
2009	L'Aquila	IT-2009-0010	L'Aquila - Valterno - Colle Grilli (AQG, B)	Normal	6.1	5	0.48	35.8	[I]
2009	L'Aquila	IT-2009-0011	L'Aquila - Valterno - F. Aterno (AQA, B)	Normal	6.1	5	0.43	31.9	[I]
2009	L'Aquila	IT-2009-0012	L'Aquila - Valterno - Aquil Park Ing. (AQK, B)	Normal	6.1	1.8	0.35	35.8	[I]

2009	L'Aquila after-shock	IT-2009-0102	S. Eusanio Forconese (MI05, B)	Normal	5.5	3.6	0.65	23.6	[I]
2012	Emilia 1st shock	IT-2012-0008	Mirandola (MRN, C)	Thrust	6.1	16.1	0.26	46.3	[I]
2012	Emilia 2nd shock	IT-2012-0011	Carpi (T0814, C)	Thrust	6.0	9.3	0.49	23.6	[I]
2012	Emilia 2nd shock	IT-2012-0011	Medolla (MIR01, C)	Thrust	6.0	0.5	0.41	52.4	[I]
2016	Central Italy	EMSC-20160824_0000006	Amatrice (AMT, B)	Normal	6.0	8.5	0.85	43.5	[ESM]
2016	Central Italy	EMSC-20160824_0000006	Nocera (NRC, B)	Normal	6.0	15.3	0.36	29.8	[ESM]
2016	Central Italy	EMSC-20161030_0000029	Rocchetta (MZ24, C)	Normal	6.5	24.5	1.00	14.3	[ESM]

3.7.2.3 Engineering Demand Parameter (EDP)

For the correct evaluation of the fragility curve, an appropriate engineering demand parameter (EDP) is necessary for association with the damage state. In this chapter, the damage state considered is the collapse damage state that corresponds to the complete overturn of the block.

The absolute peak rocking rotation $|\phi_{\max}|$ divided with the slenderness α is the EDP:

$$EDP = \frac{|\phi_{\max}|}{\alpha} \tag{3.19}$$

The choice of this dimensionless EDP is physically explained: the large value of EDP implies that the block starts rocking (EDP >0), high values (e.g. EDP > 1.0) show overturning as a consequence of rocking (Table 3.7). The parameter α for the vertical bending is assumed equal to the slenderness α_1 of lower block (Sorrentino et al., 2008). The collapse is considered with a EDP = 1.0 (Figure 3.20a). This choice is conventional. In fact, this value occurs when there is static instability. It is possible that the block-rocking without overturning with EDP>1 because the problem is strongly nonlinear (Dimitrakopoulos and Paraskeva, 2015).

Table 3.7: performance criteria for rocking behavior.

EDP	Damage state	Structural behavior	Mechanism
$\|\phi_{\max}\| / \alpha = 1.0$	Collapse	Overturning	One-sided rocking
$\|\phi_{\max}\| / \alpha_1 = 1.0$	Collapse	Overturning	Two-block mechanism

3.7.2.4 Multiple Stripe Analysis (MSA)

The parameter estimators were obtained using the maximum likelihood method (Baker, 2015). This method is widely used in literature as an alternative to the moments method to estimate the parameters because the estimators are asymptotically unbiased and efficient (Benjamin and Cornell, 1970). This method is briefly described hereinafter. The rocking analyses are performed for a level of intensity $IM = x_j$ which will give a number of collapses over the total number of the ground motions set. The probability of having z_j collapses in n_j ground motion per fixed intensity level is expressed as follows:

$$P\left(z_j \text{ collapses in } n_j \text{ ground motions}\right) = \binom{n_j}{z_j} p_j^{z_j} \left(1-p_j\right)^{n_j - z_j} \tag{3.20}$$

where the collapse of the block can be caused with a probability p_j for a certain level of intensity $IM = x_j$. The observations of non-collapse and collapse can be assumed as ground motion independent of each other.

The purpose of deriving the various collapse probabilities for different intensity levels is to derive a function with the highest probability from the collapse data observed by the rocking analysis. This is possible due to the likelihood method.

The likelihood for the entire set of data obtained from multiple levels of IM is expressed by the product of the binomial probabilities (Eq. (3.20) and is described as follows.

$$\text{Likelihood} = \prod_{j=1}^{m} \binom{n_j}{z_j} p_j^{z_j} \left(1-p_j\right)^{n_j - z_j} \tag{3.21}$$

where Π indicates the product of all m level of IM. The probability function is made explicit by substituting Eq. (3.21) for p_j

$$\text{Likelihood} = \prod_{j=1}^{m} \binom{n_j}{z_j} \Phi\left(\frac{\ln\left(x_j/\theta\right)}{\beta}\right)^{z_j} \left(1-\Phi\left(\frac{\ln\left(x_j/\theta\right)}{\beta}\right)\right)^{n_j - z_j} \tag{3.22}$$

Maximizing the likelihood function, it is possible to obtain the estimator parameters of the fragility curve that can be written:

$$\left\{\hat{\theta},\hat{\beta}\right\} = \arg\max_{\theta,\beta} \sum_{j=1}^{m} \left\{ \ln\binom{n_i}{z_j} + z_j \ln\Phi\left(\frac{\ln\left(x_j/\theta\right)}{\beta}\right) + \left(n_j - z_j\right) \ln\left(1-\Phi\left(\frac{\ln\left(x_j/\theta\right)}{\beta}\right)\right) \right\} \tag{3.23}$$

Figure 3.20 shows an example of a fragility curve obtained from the approach just described.

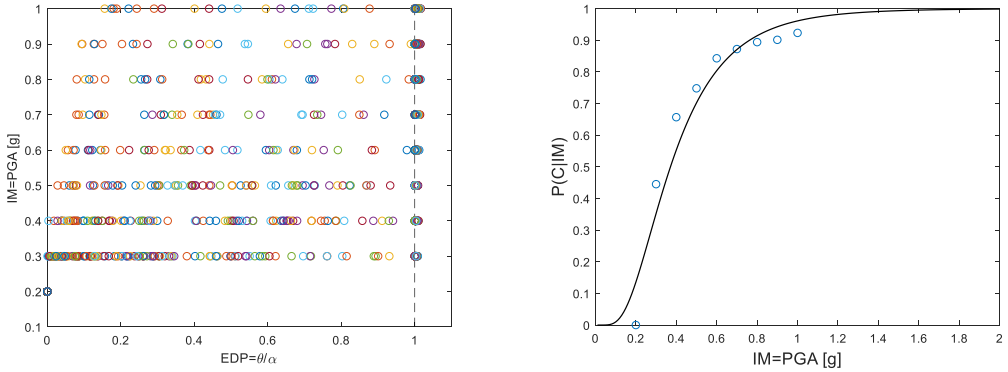

a) b)

Figure 3.20: example MSA analysis results; a) analyses causing collapse are plotted at a critical angle of greater than 1.0 and are offset from each other to aid in visualizing the number of collapses for IM levels. b) Observed fractions of collapse as a function of IM, and a fragility function estimated using Eq. (3.23).

3.7.2.5 Proposed typology fragility curves

The creation of typological fragility curves allows to include all uncertainties and describe a general behavior of the structure or element. Figure 3.21 shows the sensitivity analysis made for the mechanism of vertical bending. The parameters considered are the position of the formation of the hinge (Figure 3.21a) and the influence of the vertical force *N* (Figure 3.21b). In our case, we consider a wall 0.3×3.0m.

The position of the hinge has been changed considering the h_1 / h ratio which varies from 0.5 to 0.8 (ABK, 1981; Graziotti et al., 2016), which constitutes an input parameter for the nonlinear dynamic analyzes. This parameter has little influence on the variation of the fragility curve.

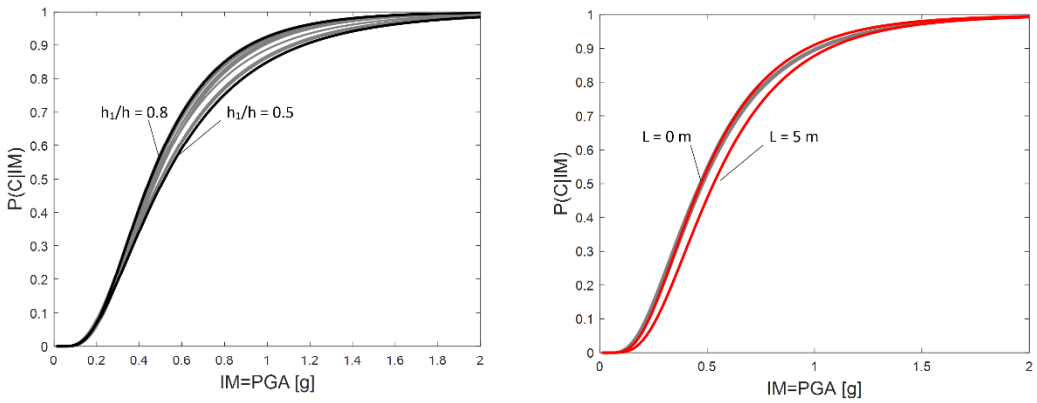

a) b)

Figure 3.21: sensitivity of the fragility parameters for vertical bending mechanism: a) variation of the position of the hinge (h_1/h from 0.5 to 0.8), b) variation of the vertical force N as effect of the span of the slab (L from 0 m to 5 m).

Instead, the vertical force affects the vulnerability of the wall. The vertical force was considered as the effect of the load due to the span of the slab. This force was applied in the center of the wall thickness. The type of floor chosen is a wooden slab at the roof of the structure (load of 2.5 kN/m^2). The span of the slab varies from 1.0 to 5.0 m, as found in Ferrara masonry structures (Table 3.4).

In Figure 3.21b, the span of the floor *L* varies from 0.0 m (where the floor does not discharge on the wall) to 5.0 m. It can be seen that the vertical force at the top is a stabilizing component for the wall and, therefore, lowers the vulnerability. This can also be seen with static and dynamic analyses (Mauro et al., 2015).

Subsequently, the fragility curves for the various mechanisms were created by varying the parameters. Each fragility curve was obtained by carrying out 44 nonlinear dynamic analyses for 9 different levels of intensity. For each curve, 396 nonlinear dynamic analyses were carried out for each wall considered. From the data extrapolated from CARTIS, we obtained intervals of parameters that were used as input for the analysis. The distributions could not be extrapolated due to the lack of information on the individual buildings. The database allows us to provide general data on a group of buildings. For each mechanism identified, a population of walls was created with randomly generated geometric parameters (Table 3.5).

This choice is the most reasonable given the availability of data. For the mechanisms, a Monte Carlo method was applied with a population of 1000 walls. The population is subdivided according to the various weights associated with the mechanisms (Figure 3.18) from which it is possible to obtain the relative fragility curves (Figure 3.22). Figure 3.22 shows the curves of the various mechanisms obtained from the population (gray curves) and their relative average curves (black curves). The fragility curves for the overturning mechanism of the first floor and the vertical bending mechanism are the same for both the MUR1 and MUR2 classes because the range of geometric parameters is the same. The curves are distinguished by a great variability of mean values and dispersions (Table 3.8). This is appreciable for simple overturning mechanisms (Figure 3.22c-h). In fact, the presence of loads, openings and wedges (it has been assumed 25% of the population with wedges), influences fragility curves. In particular, the position of the center of gravity changes and loads and wedges tend to make the block more stable, so that greater accelerations are required to induce collapse.

Table 3.8: lower and upper bound of mean (θ) and standard deviation (β) for fragility curves with Monte Carlo Simulation.

Mechanism	Lower bound		Upper bound	
	θ [g]	β [-]	θ [g]	β [-]
Top floor vertical bending	0.9728	0.8313	1.1343	0.6397
Overturning of the first floor	0.0688	1.3131	0.2731	1.0420
Overturning of two floors for MUR1 class	0.1717	1.2589	0.9166	0.8818
Overturning of two floors for MUR2 class	0.1717	1.2589	0.668	0.9120
Overturning of three floors for MUR1 class	0.4545	0.2353	2.0131	0.9131
Overturning of three floors for MUR2 class	0.4655	0.9252	2.0241	0.9131
Overturning of four floors for MUR1 class	0.4788	0.9086	2.0241	0.9131
Overturning of four floors for MUR2 class	0.4658	0.9076	2.0132	0.9221

The fragility curves for the mechanisms present in the survey (Figure 3.23) have been obtained from 98 possible mechanisms for the aggregate. Figure 3.23 shows the curves of the various mechanisms obtained from the population (gray curves) and their relative average curves (black curves). The average curves for the single mechanism are generated using the arithmetic mean of the means and variances of the single curve. The overall global typological curves for out-of-plane mechanisms are shown in Figure 3.24. All the curves are obtained by weighted arithmetic mean of the mean values and variances of fragility curves previously obtained from the individual class of mechanisms.

The curves of each class of mechanism are the mean curves of the mechanisms (Figure 3.23). These weights are obtained from the logical trees created from the possible collapse configurations (Figure 3.18). Each class of mechanism (e.g. vertical bending) is summarized by a mean fragility curve. This fragility curve is defined by two parameters: the mean value and the standard deviation. Each class of mechanism is also associated with its weight (e.g. 0.36 for vertical bending (Figure 3.18)). These parameters are obtained for all the mechanism classes and are aggregated to create the overall global typological curve using the weighted arithmetic mean.

The most significant comparison is between the average curve obtained from the population of the MUR1 class (this category constitutes 90% of the total of the buildings surveyed) with the curve obtained from the survey of the compartment. For completeness, the comparison between the curves of the MUR2 population is also reported. The typological fragility curves MUR1 and MUR2 are very similar despite the different age of construction which has little influence on the likelihood of overturning.

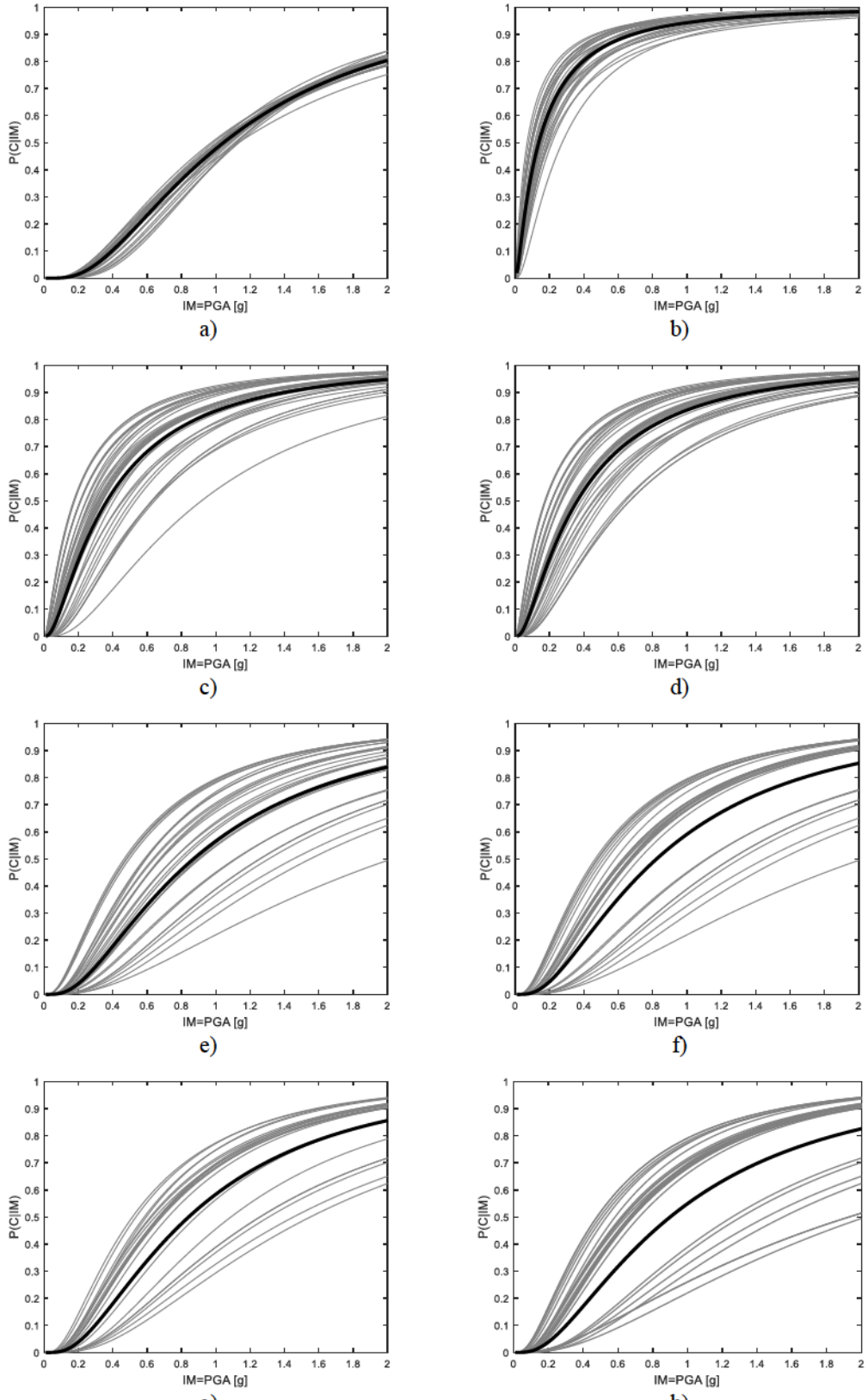

Figure 3.22: fragility curves from CARTIS database (average curve in black, sample curves in grey): a) top floor vertical bending, b) overturning of the first floor, c) overturning of two floors for MUR1 class, d) overturning of two floors for MUR2 class, e) overturning of three floors for MUR1 class f) overturning of three floors for MUR2 class, g) overturning of four floors for MUR1 class, h) overturning of four floors for MUR2 class.

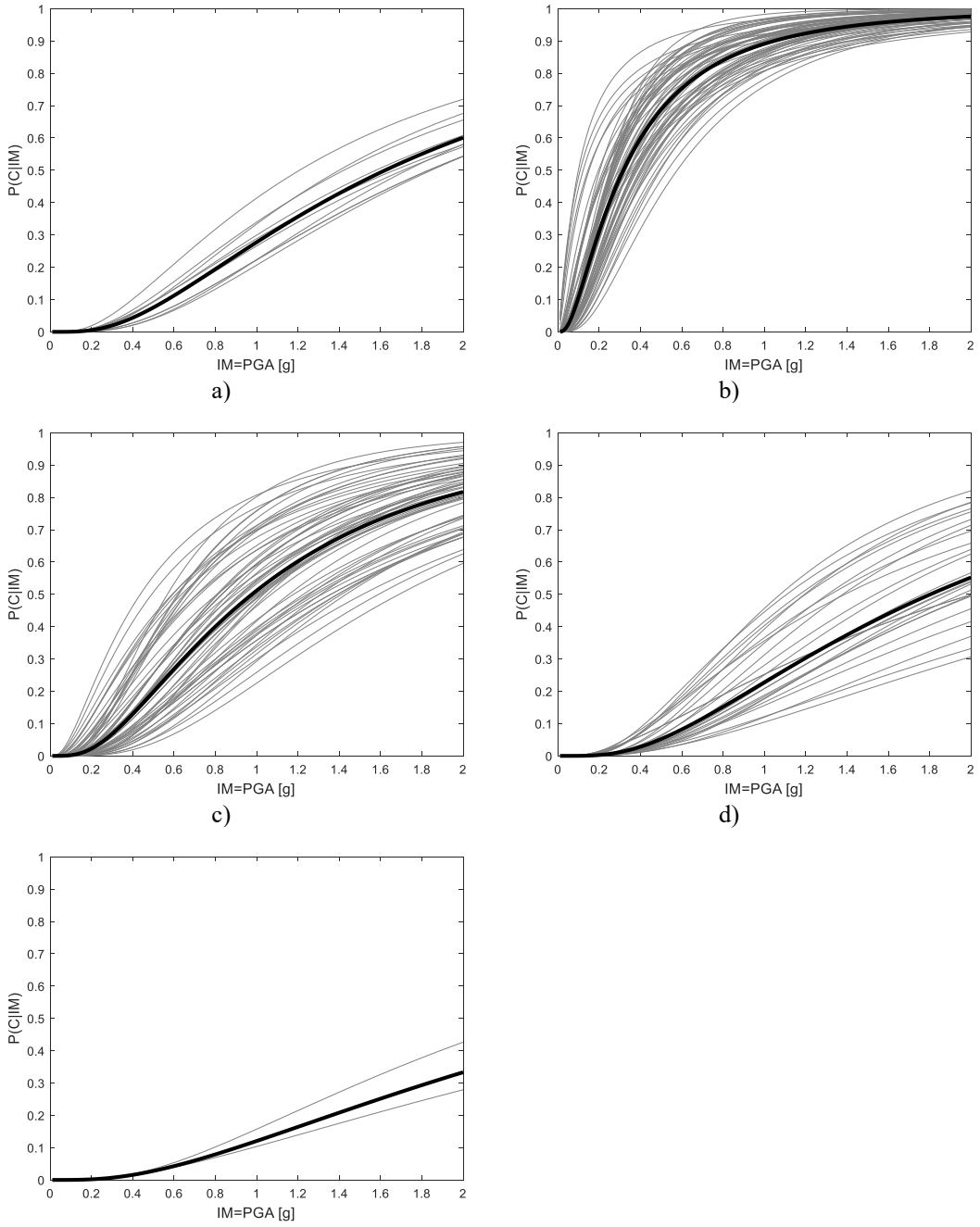

Figure 3.23: fragility curves from the survey of the historical aggregate in the center of Ferrara (black average curve, grey survey curves): a) vertical bending, b) overturning of the first floor, c) overturning of two floors, d) overturning of three floors, e) overturning of four floors.

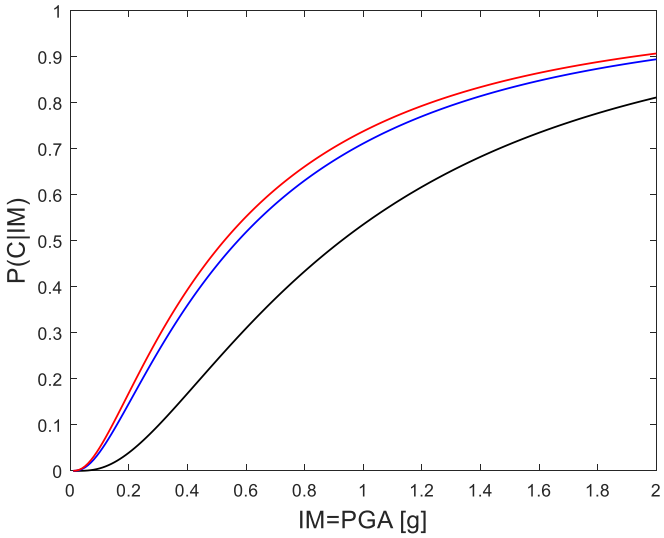

Figure 3.24: comparison between the average curves obtained from the population created from the CARTIS database and the average curves obtained from the survey of the historical aggregate: the typological curve MUR1 (blue line), the typological curve MUR2 (red line) and the typological survey curve (back line).

The quality of the connections, slenderness and mass of the walls, load and span of the floors influences the fragility curves. The variation of the parameters between the class MUR 1 and MUR 2 is small (Figure 3.24) therefore the obtained fragility curves are close. Also, the buildings have good masonry qualities and textures (Figure 3.15), good transversal connections, and the presence of tie rods or tie beams. Some indications on the masonry quality are reported in the CARTIS manual for the MUR1 and MUR2 typologies. Furthermore, supplementary assessments were made by evaluating the masonry quality in a qualitative way (e.g. visual inspection, expert judgement) through the survey. It is possible to say in general that under seismic action, buildings from different historical periods do not show great differences in our case study. It can be seen how the average population curves are more conservative than that obtained from the survey. This evidence is due to the greater number of walls analyzed for the various mechanisms obtained by the population than the number of walls obtained from the survey.

The difference between the obtained curves is due to the level of knowledge of the walls. The survey increases the level of knowledge about the walls therefore the curve reduces the uncertainty associated with the geometry of the wall and provides a more detailed description of the walls for the historic aggregate. Moreover, the curves obtained from the survey consider the good masonry quality of the walls and the connection with the transverse walls. The MUR1 and MUR2 classes obtained from CARTIS

have within themselves the variability of an entire type of building, while the aggregate has more homogeneous characteristics and less dispersed geometric and mechanical properties (e.g. buildings built in a specific period, similar masonry quality).
In this case, the most significant parameter is the connection of the wall with orthogonal walls. Indeed, transversal connections help to greater stability of the wall compared to its absence.
The transversal connections between walls detected in the survey are good in most of the buildings of the aggregate. Instead, these are present in lower rate in the building typologies provided by the CARTIS database. The higher data quality allows us to have curves more representative than the curves from CARTIS. Having a detailed description of the buildings provides more data on the geometry and loads applied on the walls. The approach used also shows how with less detailed information (CARTIS), it is possible to obtain good appreciable results in terms of probabilistic evaluation of the vulnerability of the typologies of masonry walls typical of the Po valley.

3.8 Conclusions

This chapter presents a procedure for the derivation of typological fragility functions for OOP local failure mechanisms in unreinforced masonry buildings. The proposed method starts with the data processing of the CARTIS database. A qualitative description of the building stock and associated relevant uncertainties (material, geometrical, loads) are initially considered. Epistemic uncertainties are included through the use of logical trees. Mechanical models, the validity of which is documented in the literature also from results of experimental campaigns, are introduced to analyze the OOP response of masonry walls. A dynamic approach is used, adopting a multiple stripe analysis method to derive fragility curves estimators. Finally, fragility functions are fitted to the computed fragilities.
The method is applied to historical aggregates of URM buildings. For the selected compartment in the city center of Ferrara, two building typologies (MUR 1 and MUR 2) are identified. MUR1 typology refers to buildings belonging to the oldest part of the historic center (medieval area) but also to the Renaissance area up to the 1800s and early 1900s, whereas MUR2 typology is more recent (from 1920 to 1945) and has a different percentage of tie rods on the total of the buildings.

The final fragility functions provide an overall assessment of the seismic vulnerability for these classes of buildings. The fragility curves for the MUR1 and MUR2 classes are not very different from each other although the buildings are of different construction periods. What distinguishes the two types is the presence of tie rods or tie beams and connections. The masonry quality is good for both classes. The fragility curves obtained by the two classes are different from the survey. The survey increases the level of knowledge about the walls therefore the curve reduces the uncertainty associated with the geometry of the wall and provides a more detailed description of the walls for the historic aggregate.

The results show the moderate quality of the building stock and the important role of the connections in the vulnerability of the aggregates of masonry buildings. Indeed, the introduction of effective tie rods, modifying the OOP failure mechanisms from rocking to vertical bending, can dramatically reduce the vulnerability of aggregates, keeping the streets of historic centers operational even after strong earthquakes. The proposed approach, due to its computational efficiency, may be useful for identifying the seismically most fragile typologies of the urban context. Therefore, it is a tool capable of orienting targeted retrofit strategies.

Typological fragility curves for these local mechanisms then provide a first step for the evaluation of damages and the assessment of economic losses on an urban scale. This can help to identify possible scenarios for civil protection.

In future researches, we would like to analyze other aggregates present in Italy, including building typologies similar to those of the Po Valley. This will also have to consider the uncertainties relating to the geometry of macro-elements and loads. The influence of the interaction between the floor effect of masonry structures and the local collapse mechanisms can be a further aspect to be explored. Finally, we will hopefully integrate these results into a comprehensive assessment method including the global behavior of masonry structures.

4 Uncertainty quantification for local failure mechanisms in existing URM buildings in seismic zones

This chapter aims to quantify the effect of the uncertainty of the parameters such as geometric data, mechanical characteristics and the entity and position of the loads for out-of-plane failure mechanisms in unreinforced masonry buildings (URM) in the city of Ferrara.

The chapter discusses the modeling of uncertainties by fuzzy methods for masonry walls. These walls are made of good quality masonry with fired clay bricks and lime mortar, as typical for the buildings in the Po Valley, such as those hit by the 2012 Emilia earthquake. In the frequent case of slender elements with good material properties, the wall response can be modeled as an assembly of rigid bodies and linear kinematic limit analyses, as defined in Italian code, or dynamic analyses for studying the rocking motion are utilized. These techniques are employed to provide the "fuzzy" fragility curves as a function of peak ground acceleration (PGA).

This is the first step for a probabilistic evaluation of the collapse loads under seismic actions, taking into account the actual variability of seismic input, and sensitivity analysis is also presented for the described procedures and different local collapse mechanisms.

4.1 Uncertainty modeling

The uncertain characteristics of the structural parameters can be modeled by fuzzy techniques. The most important aspect in the description of uncertain parameters is to specify the membership function according to the available information.

The data used have different origins: data from the CARTIS database, experimental data from technical literature (Bracchi et al., 2016; Savoia et al., 2016; Squassina, 2011), data collected directly by the authors and data obtained from experimental

laboratories of the city (i.e. Life s.r.l.) as we specify for each group of parameters.
Therefore, it is not easy to define belonging to a single class of information as described in Möller and Beer, (2004). Generally, this information which in our case are the structural parameters can be divided into four categories:

- information type I: a small number of elements contained in a sample;
- information type II: a linguistic assessment;
- information type III: the result of a single uncertainty measurement;
- information type IV: knowledge based on experience.

The creation of the membership function represents a subjective evaluation of the uncertainty that is generated from the basis of the information available. A simple membership function such as a linear or polygonal function is recommended, unlike more complicated descriptions which can be less robust with complicated models (Möller and Beer, 2004).

4.1.1 Material parameters

The mechanical parameters were deduced from the summary report with technical and operational indications drawn up by CIRI (Centro Interdipartimentale per la Ricerca Industriale) for the Emilia Romagna region. These indications are based on an experimental campaign in situ on the walls of masonry buildings affected by the 2012 earthquake. This experimental campaign was conducted on buildings in the Po valley between the provinces of Reggio Emilia, Modena and Ferrara.
These results give a good knowledge of the mechanical characteristics of the masonry characterized by fired clay bricks and poor quality of the mortars. The parameter used in these analyses is mainly the compressive strength of the masonry. Table 4.1 shows the average values proposed by the report with those required by the current code for compressive strength (f_k) and shear strength (τ_0).
Two cases are considered that can be found: masonry buildings made of solid bricks and lime mortar characterized by mortars of poor characteristics, joints that are not particularly thin and facing or badly connected, unconsolidated masonry and perfect wall texture and masonry buildings with effective transversal connections. The unit weight of the masonry was assumed to be 18 kN/m^3 without considering it uncertain.

This parameter is not sufficiently variable when considering a restricted study area (i.e. the lower Emilia area). As noted by the authors of the experimental campaign, the results are to be considered with extreme caution in particular for the compressive strength. In fact, in buildings with tests with double flat jacks, the resistance calculated with the Eurocode 6 appears significantly overestimated (formula 3.1 at §3.6.1 (CEN, 2005a)).

A further contribution to a better understanding of the estimate of the mechanical parameters of the masonry can be the masonry quality index (MQI) (Borri et al., 2015, 2020). This index provides the order of magnitude of the mechanical parameters based on a qualitative criteria evaluation that considers many factors such as the shape of the blocks, the volumetric ratios between the components and the masonry texture and finally the compressive and shear strength of the mortar and blocks.

But in this case, we are dealing with a class of information type II (Möller and Beer, 2004) that represents more a linguistic assessment than a set of experimental data.

Finally, a large series of experimental data collected through tests with pairs of flat jacks from a private laboratory in the city of Ferrara was taken into account (i.e. Life s.r.l.).

In the analyzes, the fuzzy number relating to the properties of the wall material was created considering the minimum defined value of the tests as the lower extreme, the highly plausible value equal to the average value and the upper value of the tests as the upper extreme. This is shown in Table 4.1, where also the values suggested by the current Italian building code are presented (MIT, 2018).

Table 4.1: resistance parameters for solid brick and lime mortar walls: values according to code and from experimental campaigns.

Type of masonry		f_k [N/cm^2]		τ_0 [N/cm^2]	
		MIT (2018)	Savoia et al. (2016)	MIT (2018)	Savoia et al. (2016)
solid brick masonry and lime mortar	lower bound	240	346	6.0	4.5
	mean value	320	396	7.6	9.8
	upper bound	400	439	9.2	10.9
solid brick and lime mortar masonry with transverse connection[1]	lower bound	312	450	7.8	5.8
	mean value	416	515	9.9	12.7
	upper bound	520	571	12.0	14.2

[1] parameters improved using coefficient 1.3, as per Table C8A.2.2 of the Italian code (MIT, 2018).

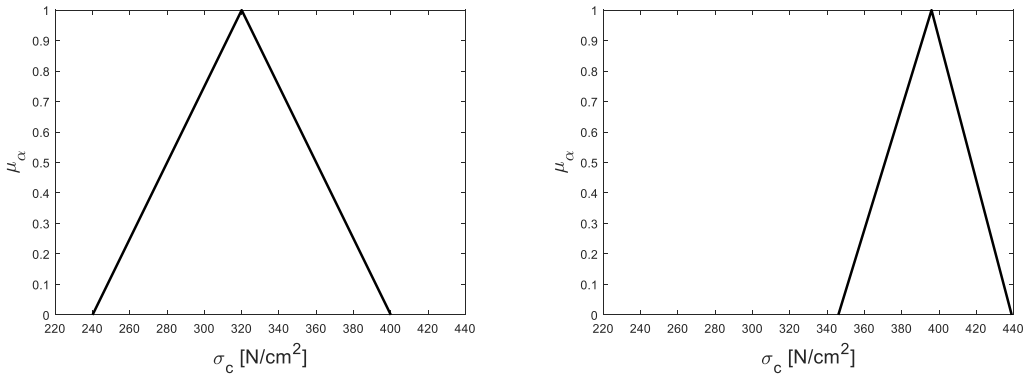

Figure 4.1: fuzzy number for compressive strength of masonry: a) limits from the Italian code b) limits from Savoia et al. 2016.

This can be summarized in this form:

$$\tilde{\sigma}_c = < \sigma_{c_{\min}}, \sigma_{c_{\text{mean}}}, \sigma_{c_{\max}} > \tag{4.1}$$

where $\sigma_{c_{\min}}$ is the minimum value of masonry compressive strength, $\sigma_{c_{\text{mean}}}$ is the mean value of masonry compressive strength and $\sigma_{c_{\max}}$ maximum value of masonry compressive strength.

Figure 4.1 reports the fuzzy numbers for masonry compressive strength with the limit of Italian code and the limits reported in Savoia et al., 2016.

The compressive strength of the masonry allows evaluating the response of the wall considering the material despite the hypothesis of rigid blocks. This can be done by retreating the pivot point defined based on the compression behavior of the interface and considering the crushing effects (Mehrotra and DeJong, 2018). There is also an alternative way to take into account the finished width of the support area through the cracks by introducing a thickness reduction factor (ratio between actual thickness and gross thickness) as a function of the compressive strength of the masonry (Vaculik and Griffith, 2017).

4.1.2 Load parameters

The loads and their application represent the uncertainty that at first sight is difficult to represent unlike the geometric parameters of the wall. The quantification of loads requires a level of knowledge that the Censis database does not capture. For this

reason, the CARTIS database is used (Zuccaro et al., 2016). Thanks to the compilation of sheets, the database can provide higher quality data on the building stock for a city (e.g. Ferrara). It provides information on the type of building, heights, dimensions of the walls and above all types of floors and their spans. It also gives information on the presence of curbs, cross-connections and chains. Having these data, it is possible to estimate loads of the floor and the span of the floor combined with the geometric and typological data of the floor. For a more detailed description see the previous chapter and Nale et al. (2021).

Figure 4.2 shows some of the fuzzy numbers considered to determine the uncertainty of the loads. The span of the floor is a datum obtained from CARTIS, while the load of the floor and the position of the unloading of this load is determined by integrating the information obtained from on-site inspections after the 2012 Emilia earthquake and from the survey carried out for the compartment analyzed in Chapter 3. Table 4.2 is summarized these data by fuzzy numbers

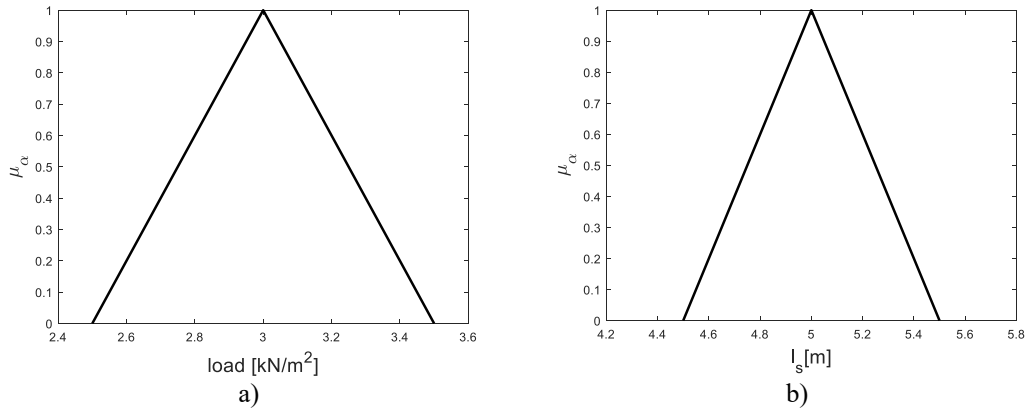

Figure 4.2: fuzzy numbers for describing load uncertainty: a) load fuzzy number, b) fuzzy number for the span of the wood slab.

Table 4.2: fuzzy numbers for the main load parameters.

Parameter	Fuzzy number
average distance between walls parallel to the facade [m]	<4.5, 5.0, 5.5>
floor load g_k [kN·m^2]	<2.5, 3.5, 4.0>
position of load application on the wall [m]	<0*t*, 0.3*t*, 0.50*t*>

[1] *t* is the thickness of the wall.

4.1.3 Geometric parameters

The essential geometric parameters that regulate the out-of-plane collapse and the related local mechanisms are the thickness of the wall (which in the case of walls with not well-connected facings must be considered distinctly between the internal wall on which the loads weigh on and the external) and the wall height. These two fuzzy numbers in Figure 4.3 define the slenderness of the wall.

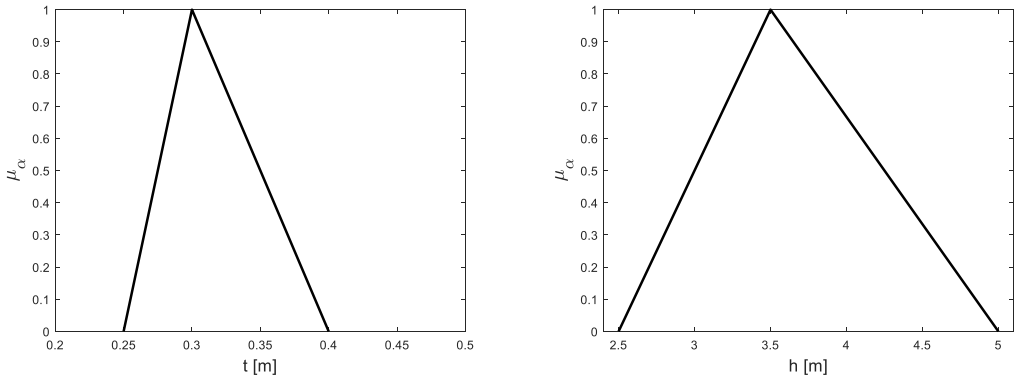

a) b)

Figure 4.3: fuzzy numbers of the geometric parameters of the walls: a) wall thickness, b) wall height.

Also in this case CARTIS data are used. For a more complete description, see the previous chapter (Table 3.4). Table 4.3 shows the main geometric parameters used for the creation of the fragility curves.

Table 4.3: fuzzy numbers for the main geometric parameters.

Parameter	Fuzzy number
average floor height [m]	<2.5, 3.0, 3.5>
average ground floor height [m]	<2.5, 3.5, 5.0>
average thickness of ground floor walls [m]	<0.25, 0.30, 0.40>

To compare the results with those shown in Zuccaro et al. (2016), the analysis was extended to data for walls of the same quality but obtained in other cities of the Po Valley, Venice (Squassina, 2011) and Pavia (Bracchi et al., 2016) as shown in Figure 4.3 and Table 4.3. As regards the thickness of the walls, large variability of thicknesses was found due to the different brick formats in the walls of the city. This is partly due to the lack of quality standards in the different construction periods and subsequent interventions in certain buildings. Figure 4.4 shows an example of different brick formats present in Venice in the period between the XII-XV centuries.

Figure 4.4: different brick formats present in the Po valley (image from Squassina (2011)).

4.2 Fragility curves with fuzzy input

In the last 20 years, the fragility curves are the most used tool for the assessment of seismic risk for structures. A lot of fragility curves from static and dynamic methods are available in the literature (Silva et al., 2019), see also the previous chapter and Nale et al. (2021). Given the inherent variability in the various structural parameters of the walls, we want to include the associated uncertainty using fuzzy techniques.

In this paragraph, we propose a method to create analytical fragility curves for local collapse mechanisms by incorporating the uncertainty (i.e. fuzziness) that is consistent and time-invariant. The approach is based on those present in the literature and adapted to the problem analyzed, see also (Colangelo, 2012, 2013).

The probability of exceeding a certain state of damage (i.e. collapse) conditioned to a certain level of intensity of a ground motion is described by the fragility curve (Cornell and Krawinkler 2000). The conditioned probability P_{ij} be represented as follows:

$$P_{ij} = \mathbb{P}\left\{R_i < S_i \middle| G = g_i\right\} \tag{4.2}$$

where S_i is the demand of the structure for a given intensity $G = g_i$ and R_i the capacity of the structure for the damage state i. Capacity is generally considered deterministic (it is calculated using computational models) and demand is considered a random variable. If instead the capacity is considered a random variable with uncertain parameters for the damage state i, the probability must be considered as a random

fuzzy event, (Zadeh, 1968), that can be described as follows:

$$P_{ij} = \mathbb{P}\left\{R_i < S_i \middle| G = g_i \middle\| \mu_i\right\} \tag{4.3}$$

wherein this case the measure of the intensity of the ground motion not only conditions the probability but is also conditioned by the membership function μ. When the value of μ is equal to 1, the fragility curve is brought back to that predicted by the classical theory of probability. Usually, this curve is described by a log-normal function:

$$P_i = \Phi\left(\frac{\ln(g/\theta)}{\beta}\right) \tag{4.4}$$

in which Φ is the standard normal distribution function and the parameters θ and β which are the mean and the standard deviation for the relative damage state i. They are estimated using fitting techniques which can be the least-squares method and the maximum likelihood method (Baker, 2015).

By applying fuzzies in the creation of the fragility curves, we will obtain a bundle of fragility curves characterized by two extremes corresponding to $\mu = 0$ and an internal curve corresponding to $\mu = 1$. In the following, as regards the dynamic approach, the procedure for calculating these curves is based on applying multiple stripe analysis (MSA) with the integration of fuzzy numbers. The MSA procedure was described in the previous chapter. What we do is create the fuzzy number for each nonlinear dynamic analysis of the block. Having a fuzzy number of output it is possible to evaluate if the block is overturned or not for the extremes and the most probable values. Having n simulations for the determined IM, in our case the peak ground acceleration, conditioned by the relative value of the membership function, it is possible to obtain the probability of overcoming for a given damage state.

Having the relative probability, it is possible to subsequently obtain the relative fragility curve using the principle of maximum likelihood for that given value of the membership function (Figure 4.5). To verify the robustness of the curves, the Kolmogorov-Smirnov test (Kolmogorov 1941, Smirnov 1939) and Chebyshev's inequality are applied (Papoulis 1991).

In the following, we present “fuzzy” fragility curves obtained as described for the mechanisms: single-leaf overturning wall, double-leaf overturning wall, overturning

of wall and part of the transversal connection, vertical bending of simple and double-leaf walls. The equation of the dynamic motion is reported in the previous chapter and Nale et al. (2021).

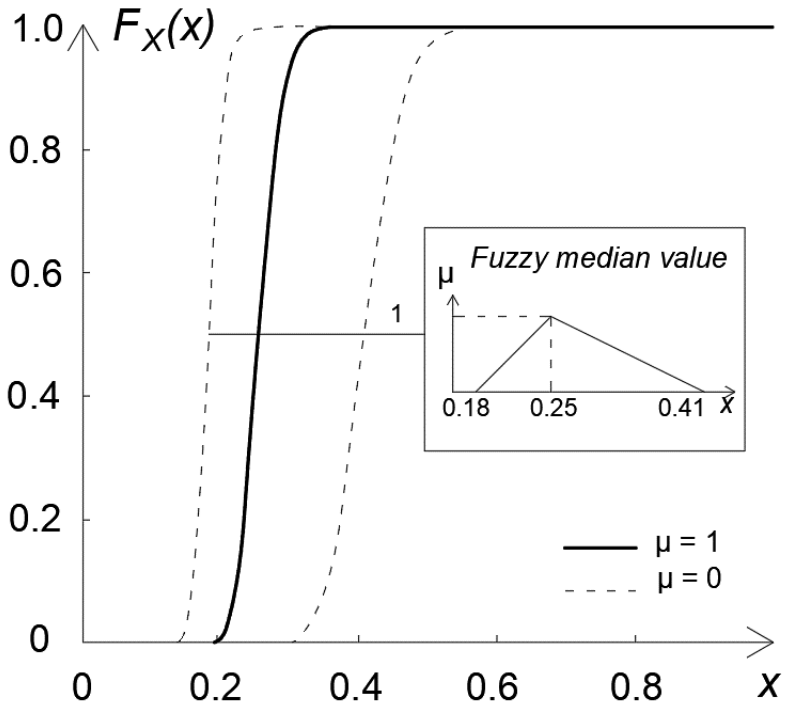

Figure 4.5: “fuzzy” fragility curve for a structure.

These fuzzy distribution curves can provide insight into some aspects of the uncertainty. They can be interpreted in two ways:

1) At a given fixed exceedance probability provide the fuzzy interval (Figure 4.5). Fixed for example a probability of 50% of the overcoming of a state of damage (e.g. collapse), it is possible to determine the fuzzy interval and the average value of the intensity measurement.
2) Evaluate the variation in the probability of exceeding fixed a measure of intensity and a level of the membership function α_k (Figure 4.6). Thus, it is possible to evaluate the probability intervals for which, given an intensity measure, the overcoming of the damage state occurs (e.g. collapse).

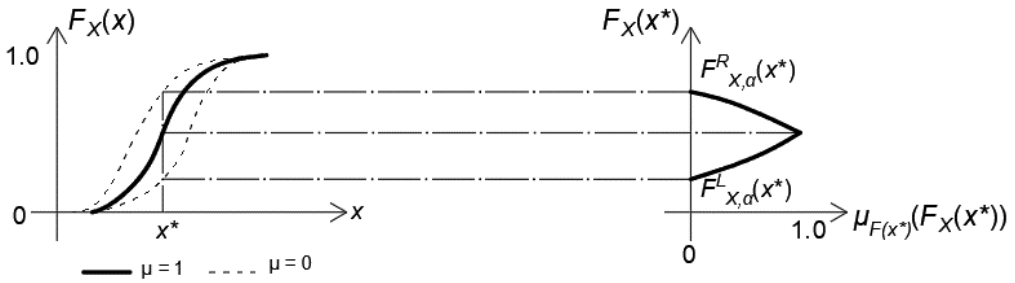

Figure 4.6: fuzzy probability distribution for a determinate value of x^* variable.

4.2.1 Fuzzy fragility analysis based on static approaches

The force-based approach is one of the most widely used techniques for the assessment of collapse in the technical literature (MIT, 2018; Sorrentino et al., 2016). For a complete description of the equations used see Section 3.3.2. In this paragraph, we propose fragility curves with fuzzy input using static analysis as a model for creating curves.

4.2.1.1 Local collapse mechanisms

Several local collapse mechanisms are used in this chapter for the derivation of fragility curves:

- single-leaf overturning wall:

  the mechanism consists of a rigid rotation for entire facades or portions of walls with respect to axes at the base of the wall. The wall structure is loaded by actions outside the plane. The overturning affects only the highest floor of the building or portions of the wall below the roof as a special case.

- double-leaf overturning wall:

  The mechanism consists of the rigid rotation of the external curtain of walls with disconnected facings, or even sack, with respect to mainly horizontal axes at the base. In such cases, the two geometric parameters can have almost independent behavior, as in the extreme case of the sack walls, or, in presence of connecting hangings, interact along the common surface. Under seismic action, it is possible that the internal facing transfers part of its inertia onto the external

one. The evaluation of the deformability that allows the transfer of horizontal actions across the contact surface between the two vestments, which would involve, among other things, the removal of the rigid block hypothesis, is problematic. In the following we assume the interaction between they are limited to the top of the wall only and consider a kinematics that affects both faces.

- overturning of wall and part of transversal connection:

  The mechanism consists of a rigid rotation of entire facades or portions of walls with respect to axes in prevalence horizontal accompanied by the dragging of parts of the masonry structures belonging to the bracing walls. The size of the triangular part that remains connected to the wall depends on the quality of the masonry (Borri et al., 2015) and its uncertainty is evaluated with the fuzzy shown in Figure 4.7.

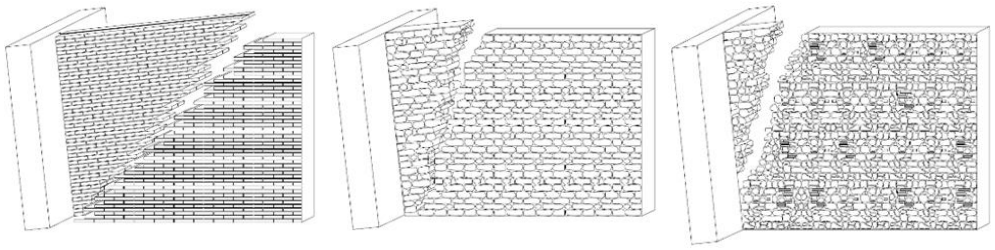

a) b) c)

Figure 4.7: different angle for different masonry quality for overturning of the wall with a part of transversal connection: a) good quality wall with an angle between 30 and 45 degrees, b) medium quality wall with an angle between 30 and 45 degrees, c) poor quality wall with an angle between 30 and 45 degrees (Borri, 2003).

- vertical bending of single-leaf wall:

  the vertical bending mechanism consists of the formation of a horizontal cylindrical hinge that divides the wall structure into two rigid blocks. The combination of the vertical and horizontal actions on the wall determines the establishment of a sort of vertical arc effect whereby the horizontal forces are discharged on the constraints at the ends of the wall. However, if the latter exceeds a certain value, the vertical actions are no longer sufficient to counteract the stabilizing effect of the bending moment and this establishes the kinematics.

- vertical bending of single leaf wall with a height of 2 floors:
  the mechanism provides a formation of a horizontal cylindrical hinge that divides the wall between two blocks and it is described by the reciprocal rotation of the same around this axis for actions outside the plan. It is frequent in buildings with supported floors and a tie beam on the roof.

- vertical bending of double-leaf wall:
  the mechanism presents a formation of a horizontal cylindrical hinge that divides the external curtain of a wall between into two blocks and it is described by the reciprocal rotation of the same around this axis for out-of-plane actions. In the case examined, the interaction between the two faces is considered, assuming the possibility that a small percentage of horizontal forces acting on the internal face, can be transmitted to the external one in relation to its stiffness characteristics and the connection methods on the common surface. A simplified heuristic evaluation is reported in Beolchini et al. (2005) where he suggests a corrective coefficient equal to 1.2 for the mass of the external facing.

4.2.1.2 An alternative method for generating "fuzzy" fragility curves

In this paragraph, the fuzzy fragility curves are estimated starting from a fuzzy number obtained from the linear or non-linear kinematic analyses following the Italian norms (MIT, 2018, 2019). By exploiting the theory of evidence, it is possible to obtain a distribution characterized by lower and upper bounds with uncertain data (Figure 4.8). This method has particular advantages on any computational applications where there is little information (Savoia, 2002).

Each input considered by us is represented by a variable defined by a fuzzy number $\tilde{X}_i$. Each fuzzy number is associated with a membership function $\mu_i(x_i)$ which represents the distribution of possibilities that is compatible with a probability according to the available information. It is possible to show that the membership function of a fuzzy number represents the distribution of possibilities that correspond to probability distributions compatible with the given information (Ferrari and Savoia, 1998). For the relative fuzzy algebra between fuzzy numbers, we remand to Dubois et al. (1994) and Kaufmann and Gupta (1991).

Starting from the definition of the various membership functions, it is possible, using the theory of evidence, to define the upper and lower bounds of the pdf (p_{iL}, p_{iR}) as a function of the number of inputs (i = 1, 2) described as follows:

$$p_{iL}(x_i)=\begin{cases}0 & x_i < x_{iL}\\ \dfrac{d\mu_i}{dx_i} & x_{iL} \le x_i \le x_{iC}\\ 0 & x_{iC} < x_i\end{cases} \qquad p_{iR}(x_i)=\begin{cases}0 & x_i < x_{iC}\\ -\dfrac{d\mu_i}{dx_i} & x_{iC} \le x_i \le x_{iR}\\ 0 & x_{iR} < x_i\end{cases} \tag{4.5}$$

Based on the rules between binary operations and exploiting the extension principle is the combined probability of the two fuzzy numbers:

$$p_{YH}(y)=p_{1J}(x_1)\,p_{2K}(x_2) \tag{4.6}$$

By integrating the previous equation it is possible to define the lower and upper CDFs of the output variable Y.

$$F_{YH}(y)=\int_{y_L}^{y} p_{YH}(y)\,\mathrm{d}y \tag{4.7}$$

So these curves have the following property:

$$\forall x_i \quad F_{iR}(x_i)\le F_i(x)\le F_{iL}(x_i) \;\Rightarrow\; \forall y \quad F_{YR}(y)\le F_Y(y)\le F_{YL}(y) \tag{4.8}$$

By exploiting binary operations it is possible to define asymptotic expressions for the CDFs as follows:

$$\begin{aligned} F_{YL}(y) &= \int_{x_{1U}}^{x_1}\int_{x_{2V}}^{x_2} \frac{\mathrm{d}\mu_1}{\mathrm{d}x_1}\frac{\mathrm{d}\mu_2}{\mathrm{d}x_2}\,\mathrm{d}x_1\mathrm{d}x_2 \\ F_{YL}(y) &= 1-\int_{x_{1\not\in}}^{x_1}\int_{x_{2\not\in}}^{x_2} \frac{\mathrm{d}\mu_1}{\mathrm{d}x_1}\frac{\mathrm{d}\mu_2}{\mathrm{d}x_2}\,\mathrm{d}x_1\mathrm{d}x_2 \end{aligned} \tag{4.9}$$

Figure 4.8 presents the comparison of the lower and upper range of CDFs (F_{YL}, F_{YR}) from probability theory (solid line). It is also possible to see the lower and upper limits of the probability (F_{y^*}, F_y^*) obtained as an extended fuzzy operation (dashed line).

Finally, the same figure shows the most probable curve F_Y obtained as two compatible pdfs for the fuzzy number $\tilde{X}_i$.

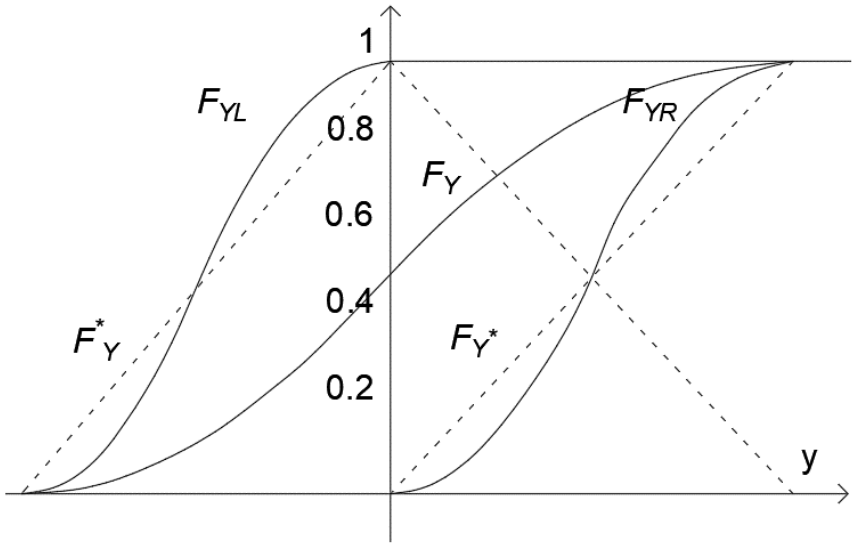

Figure 4.8: triangular fuzzy number F_{y*} and upper F_y^* bounds of fuzzy number, lower F_{YL} and upper F_{YR} CDFs and general CDF F_Y (Ferrari and Savoia, 1998).

4.2.1.3 General considerations

From the fragility curves, it is possible to derive some general considerations on the behavior of local collapse mechanisms. Double-leaf walls mechanisms are extremely vulnerable to seismic action.

In Figure 4.9, it is possible to see how collapse can occur for very low PGA values. In the case examined, the interaction between the two faces is neglected, assuming the possibility that a small percentage of horizontal forces acting on the internal face can be transmitted to the external one in relation to its stiffness characteristics and the connection methods on the common surface as previously discussed.

Moreover, for single leaf walls, the most vulnerable mechanism appears the simple overturning mechanism compared to the vertical bending one.

This confirms when it is already widely known in the literature. One significant aspect is how uncertainty varies in the various mechanisms. Uncertainty is greater for vertical bending mechanisms. This is mainly due to the role of the stabilizing effect of the normal force at the summit. This is visible in Section 4.4.1 where the sensitivity analysis will be carried out.

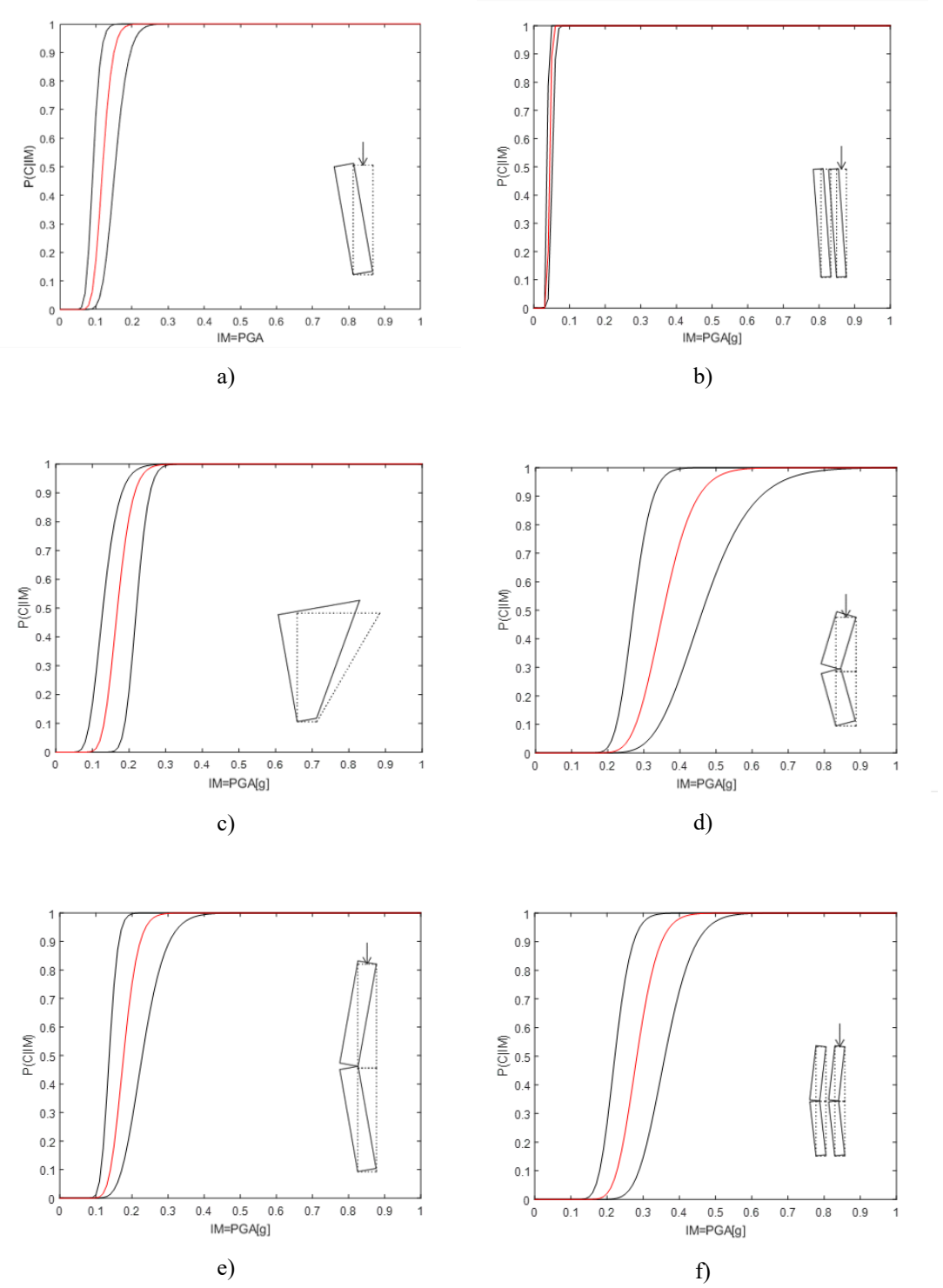

Figure 4.9: fuzzy fragility curves for different collapse mechanisms based on static methods (in red the fragility curve with μ = 1, in black with μ= 0): a) simple overturning of a single leaf wall, b) simple overturning of double-leaf wall, c) overturning of wall and part of connection wall, d) vertical bending of simple-leaf wall, e) vertical bending of simple-leaf wall of 2 floor height, f) vertical bending of double-leaf wall.

4.2.2 Fuzzy fragility analysis based on the dynamic approach

By applying the procedure described in Section 2.1.4, the fragility curves are obtained using fuzzy. As well known non-linear dynamic analyses of the wall were carried out assuming walls as rigid blocks. A ground motion set equal to the one used for the creation of the fragility curves in the previous chapter has been considered.

Figure 4.10 show fragility curves obtained assuming different local collapse mechanisms:

- single-leaf overturning wall (Figure 4.10a);
- double-leaf overturning wall (Figure 4.10b);
- overturning of wall and part of transversal connection (Figure 4.10c);
- vertical bending of single-leaf wall (Figure 4.10d-c);
- vertical bending of single leaf wall with height two floors and vertical bending of double-leaf wall (Figure 4.10f).

From the fragility curves, it is possible to derive some general considerations on the behavior of local collapse mechanisms. The vulnerability of local mechanisms is described by a fuzzy approach that develops cumulative distribution functions (CDF). In the dynamic field, many of the considerations made in the static field are confirmed. In this case, the curves are more vulnerable than the static method, i.e. with the same intensity (PGA), there are lower probabilities of overcoming (e.g. collapse) than the static approach. In fact, the rocking of the walls does not necessarily occur when became statically unstable ($|\theta_{max}| = 1$) because of its highly nonlinear nature but the overturning occurs when the wall becomes dynamically unstable. In this case the structure exhibit higher rotation than α. For this reason, the curve of fragility calculated with non-linear dynamic analysis is more vulnerable. An interesting aspect is the position of the curve with $\alpha = 1$ (most plausible curve) within the bundle. In the various cases discussed, this curve is never the average curve of the bundle of curves that are created. Indeed in some cases, the curve is close to the lower extremes (Figure 4.10d-f) in other cases it is close to the upper extreme (Figure 4.10b-e). This shows how uncertainty propagates in varying the input parameters and how the phenomenon that is strongly non-linear conditions the response. The vertical bending curve with a double-leaf wall (Figure 4.10f), shows as the uncertainties are such that to make a more vulnerable fragility curve plausible.

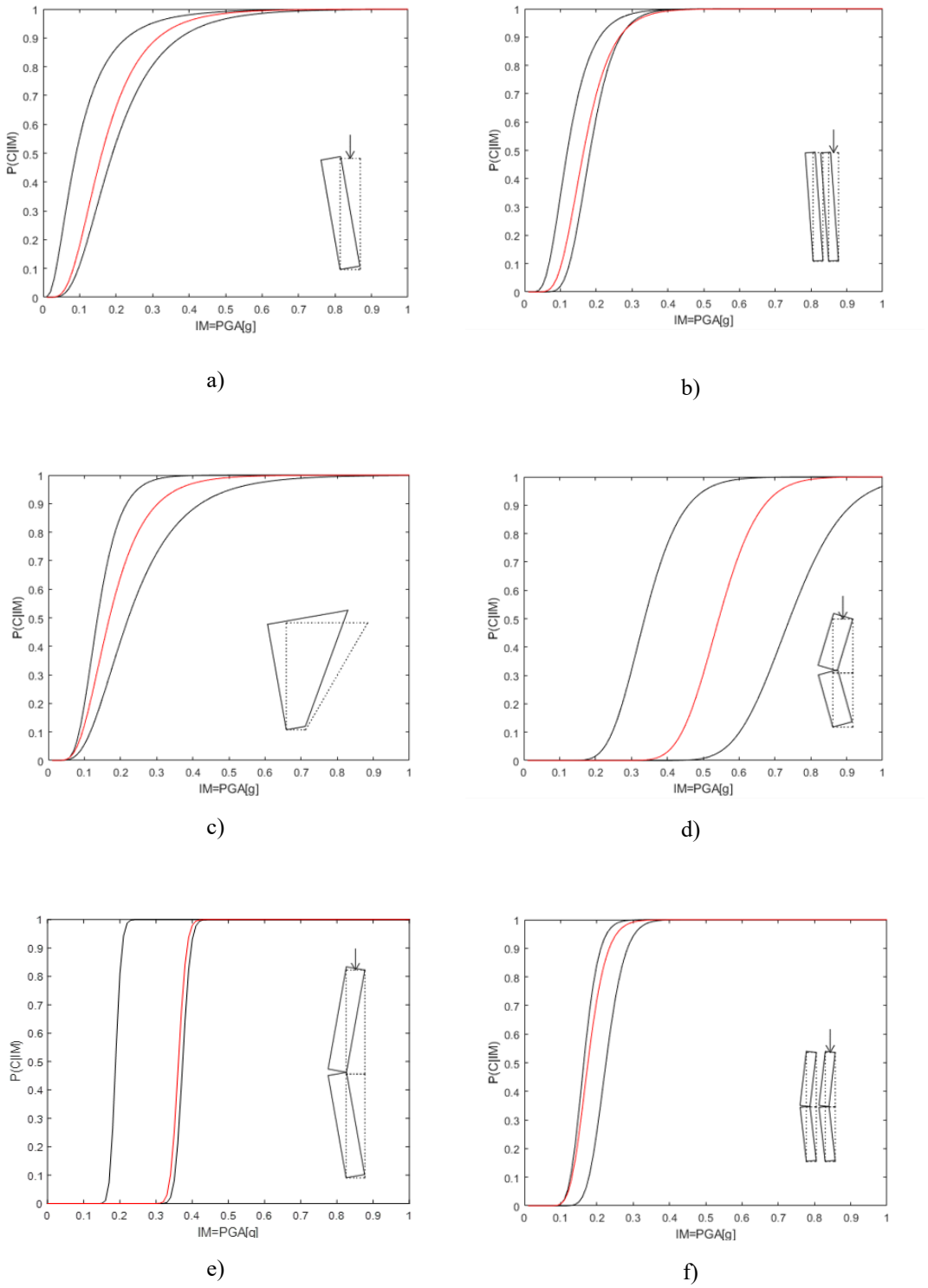

Figure 4.10: fuzzy fragility curves for different collapse mechanisms based on dynamic methods (in red the fragility curve with μ = 1, in black with μ = 0): a) simple overturning of a single leaf wall, b) simple overturning of double-leaf wall, c) overturning of wall and part of connection wall, d) vertical bending of simple-leaf wall, e) vertical bending of simple-leaf wall of 2-floor height, f) vertical bending of double-leaf wall.

4.2.3 Comparison with Monte Carlo simulation

The fragility curves obtained by fuzzy set theory were validated with a Monte Carlo simulation. The Monte Carlo simulation randomly generated input parameters that allow the calculation of the fragility curve.

This method presents some critical issues when increasing the inputs generated randomly. In fact, with an increase of inputs, it is also necessary to increase the number of samples. Therefore, if you want to analyze rare events (e.g. earthquakes, floods, explosions) characterized by *n* inputs, it is necessary to significantly increase the number of samples (e.g. for 6 inputs it is advisable to perform 10^6 samples). This is because we want to grasp the probability distribution without creating layers that can affect the response. By doing so, it is obvious that the computational time increases significantly. Adopting fuzzy set theories, it is possible to reduce the computational time by adopting simplified distributions that allow a more limited sampling than the general one envisaged by Monte Carlo simulations.

Figure 4.11 shows the Monte Carlo simulation results for the simple overturning and vertical bending mechanisms. The black lines represent the Monte Carlo simulations, while the red ones represent the most plausible value of the fuzzy fragility curve obtained from the previous analyzes. What we can see is that despite the randomness of the sampling the curves are within a confidence interval of the red curve. This shows the correctness of the method.

Application of fuzzy theories for these problems seems therefore acceptable to have a quantitative and rapid response of the vulnerabilities of the structural element.

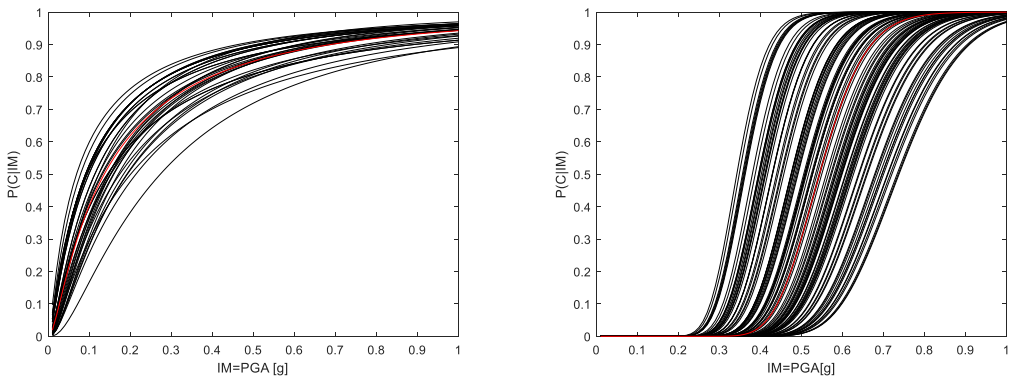

a) b)

Figure 4.11: a bundle of the curve from Monte Carlo simulation: a) simple overturning, b) vertical bending.

4.2.4 Comparison with current state of art

The fragility curves clearly show the reliability of a given structure as the intensity of the earthquake varies, generally represented by the PGA for masonry buildings. The fragility curve, if evaluated through numerical models, even the most correct and sophisticated, provides values relating to the single case where all the mechanical and geometric parameters are known with precision. In the case of existing masonry buildings, in particular, the ancient ones that represent a large part of our architectural heritage, the data are necessarily uncertain for the single building and are even more uncertain if estimates reliability and resilience on a territorial scale are desired, for example of a neighborhood or sector, if not even larger as is the aim of the CARTIS project. The purpose of this paragraph is whether the quantitative estimates of the uncertainties introduced by assuming the different parameters as fuzzies allow us to obtain "fuzzy" fragility curves that can be used in real cases and are reliable. As shown previously in this chapter, the fragility curves calculated using fuzzy intervals allow us to see how the vulnerability of a local collapse mechanism varies considering the uncertainties related to the parameters that affect a given collapse mechanism.

The "fuzzy" fragility curves are delimited by curves with $\mu = 0$ which represents the least plausible values and a curve with $\mu = 1$ which represents the most plausible value. We compare them with the fragility curves present in the technical literature (Zuccaro et al., 2017) in order to validate them and evaluate the sensibility to the uncertainties. The curves used for the comparison are based on a study on a regional scale of the local collapse mechanisms of 250000 buildings present on the national territory.

The data of 250000 buildings are generated randomly as a collection of different mechanical models where each case is described by the mechanical properties pertinent to the typological class provided by Zuccaro and Cacace (2012) for the vulnerability assessment. These curves are divided according to different collapse mechanisms and structural typologies that characterize masonry buildings in Italy. These curves are calculated using linear kinematic analysis with intensity measure the peak ground acceleration (PGA).

The procedure permits to compute of the failure probability of these mechanisms with their seismic response expressed through vulnerability curves for each typological class.

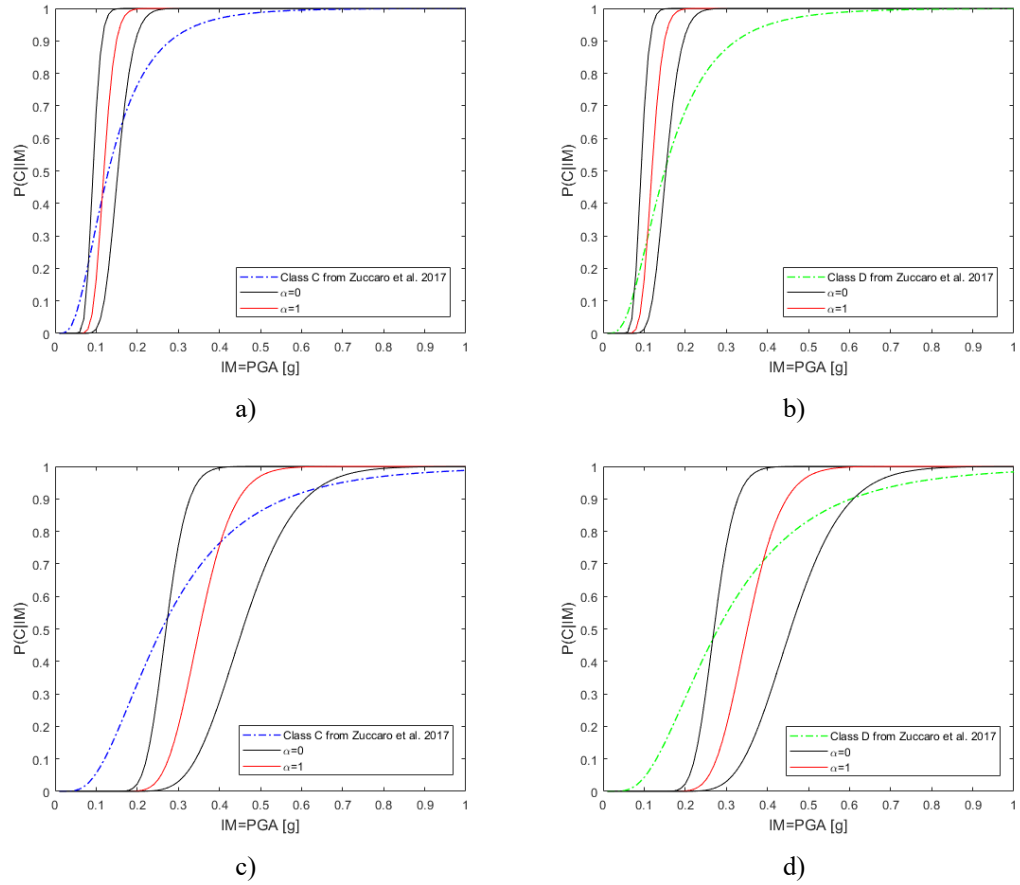

Figure 4.12: comparison between fuzzy fragility curves from static approach and curve obtained via a static approach from Zuccaro et al. (2017): a)-b) simple overturning for two vulnerability classes, c)-d) vertical bending for two vulnerability classes.

The vulnerability classification of buildings is based on the SAVE method (Zuccaro and Cacace, 2015) which groups four classes of vulnerability: A, B, C, D. The mechanisms instead are classified using the MEDEA methodology (Zuccaro and Papa, 2004). In the territory of the municipality of Ferrara, there are buildings with vulnerability classes C and D whose fragility curves will be compared with those obtained from fuzzy intervals.

In Figure 4.12a - b we compare the fragility curves obtained by fuzzy input, considering the uncertainties relative to masonry buildings of Ferrara, applying a static approach for the simple overturning mechanisms. The curves appear quite different from those contained in Zuccaro et al. (2017). The latter appears inside the bundle of the "fuzzy" curves for very low values of the PGA. The lower ability to withstand earthquakes with a higher PGA of the reference curves seems to be due to the great slenderness of the walls in Ferrara in comparison with the Zuccaro data. As we will see later the slenderness is the parameter to which the collapse is most sensitive in the

case of overturning. The curves are shown in Figure 4.12c - d, relative to vertical bending, are almost everywhere contained in the bundle of fuzzy curves. The discrepancy that in this case occurs for low values of the PGA is probably related to the fact that the minimum thickness of brick in Ferrara is 12 cm, while in other parts of the Po Valley there is a minimum thickness of 9 cm because they have a different format in the different locations.

It is worth noting that the fragility curves obtained by fuzzy input applying a dynamic approach give different results depending on the mechanism. For the simple overturning mechanism it is possible to see how the bundle of curves manages to contain the curve in the literature considering both buildings with vulnerability class C and D (Figure 4.13a-b). The case is different for the vertical bending mechanism for low PGA. In addition to the difference in the transversal thicknesses, this could be because the approach in the literature is more conservative than the dynamic one.

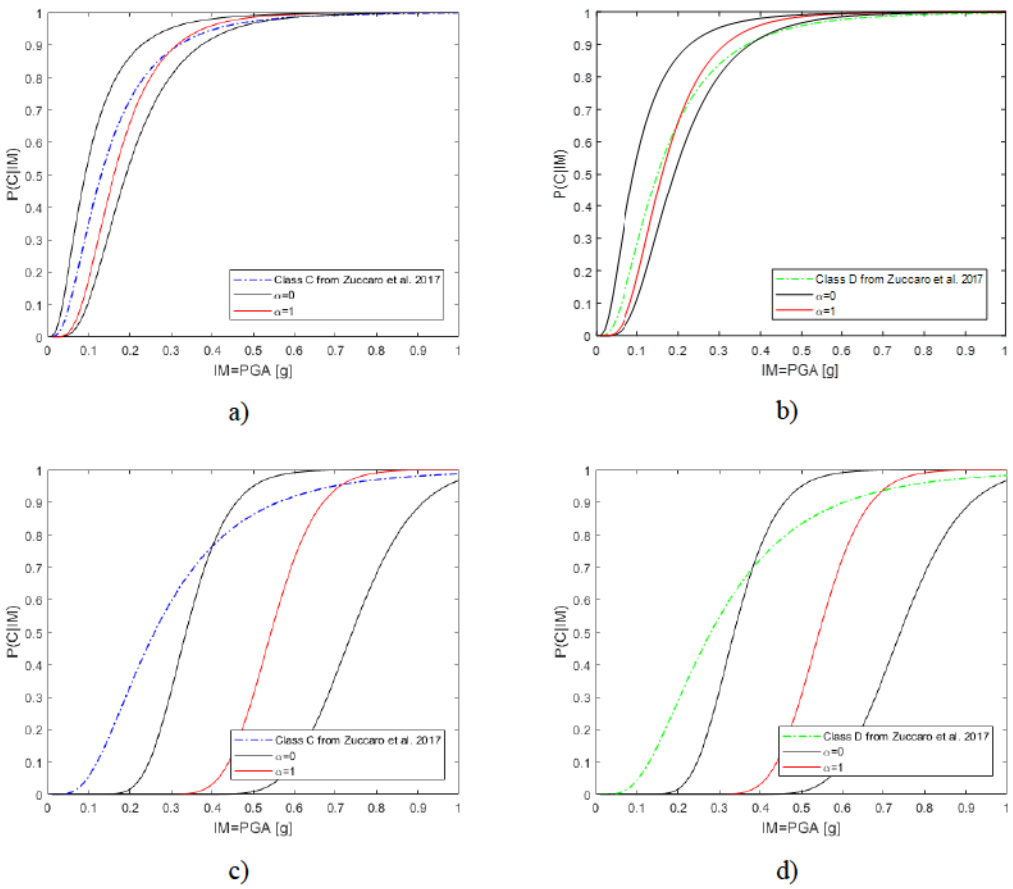

Figure 4.13: comparison between fuzzy fragility curves from dynamic approach and curve obtained via a static approach from Zuccaro et al. (2017): a)-b) simple overturning for two vulnerability classes, c)-d) vertical bending for two vulnerability classes.

Indeed, the linear kinematic analysis considers the collapse when the block starts rocking (the stabilizing moment is not balanced).

On the other hand, when considering the problem in dynamics, the block flips when the center of gravity leaves the block. This definition is purely conventional (static instability). In literature, it is possible to see that some blocks that reach this limit do not overturn but it happens only when an impulse collapses the block (dynamic instability). In fact, rocking is strongly influenced by the frequency content of the seismic and non-seismic input (e.g. in pulse or explosion).

From the fragility curves, it is possible to derive some general considerations on the behavior of local collapse mechanisms. The vulnerability of local mechanisms is described by a fuzzy approach that develops cumulative distribution functions (CDF). In the dynamic field, many of the considerations made in the static field are confirmed. In this case, the curves are less vulnerable than the static method, i.e. with the same intensity (PGA), there are lower probabilities of overturning (e.g. collapse) than the static approach. In fact, the rocking of the walls does not necessarily occur when became statically unstable ($|\theta_{max}| = 1$) because of its highly nonlinear nature but the overturning occurs when the wall becomes dynamically unstable. In this case the structure exhibit higher rotation than α. For this reason, the curve of fragility calculated with non-linear dynamic analysis is less vulnerable. An interesting aspect is the position of the curve with $\alpha = 1$ (most plausible curve) within the bundle. In the various cases discussed, this curve is never the average curve of the bundle of curves that are created. Indeed in some cases, the curve is close to the lower extremes (Figure 4.10d-f) in other cases it results close to the upper extreme (Figure 4.10b-e). This shows how uncertainty propagates in varying the input parameters and how the phenomenon that is strongly non-linear conditions the response.

4.3 Uncertainty quantification for seismic risk of local collapse mechanisms

The evaluation of the safety of a structure is one of the main objectives of earthquake engineering. The quantification of the collapse depends on several factors such as the seismic hazard of the site and the vulnerability of the structure. The quantification of the risk of collapse has become a robust procedure with the advent of performance-

based earthquake engineering (PBEE) which allows to include the uncertainties of seismic hazard and structural response with an excellent level of reliability (Deierlein et al., 2003; Krawinkler and Miranda, 2004).

4.3.1 Collapse risk metrics

The fragility curves represent the conditional probability of collapse of a structure in the function of the ground motion intensity *P(C|IM)*, that is, it represents a measure of the vulnerability of the structure regardless of the seismic hazard of the site. However, as is well known, the risk must nevertheless take into account not only the vulnerability but also the hazard defined as a product of seismicity and site effects. This paragraph discusses some recent proposals to define the risk of collapse in structural elements, generally defined in the literature as "risk metrics".

4.3.1.1 Probability of collapse at a specific ground motion intensity

Even assuming the PGA as seismic intensity (IM) according to the definition of Italian code, many problems remain about which IM to assume since it depends not only on the site but on the return time to be taken. In Haselton and Deierlein (2007), it is proposed, for reinforced concrete structures, to assume a conventional IM associated with a 2% probability of excess over 50 years. This partially combines the site hazard information (hazard level) with vulnerability (fragility curve), but this only provides the intensity measure of a single ground motion. This method does not incorporate the change in the probability of collapse with the inherent change of ground motion. This implies that the risk of collapse depends on the location of the structure and therefore there is no uniform risk parameter for the structures (Luco and Cornell, 2007). Therefore in the USA, recent regulations for instance the ASCE 7-10 (ASCE, 2010, Commentary C1), use a risk-targeted spectral ordinate instead of a hazard-targeted spectral ordinate in order to have a more uniform description of collapse risk between the structures**.** Recently, this method has been proposed also in Italy through the RINTC project (Iervolino et al., 2018; Iervolino and Dolce, 2018). The RINTC (The Implicit Seismic Risk of Code-Conforming Structures) project was funded by the Italian Civil Protection with the goal to apply the risk-targeted ground motion to evaluate the seismic structural reliability. Different structural typologies are evaluated including unreinforced masonry structures (Cattari et al., 2018; Manzini et al., 2018). The

unreinforced masonry (URM) buildings designed in accordance with the Italian building code provided very different levels of safety and it is linear static analysis largely over-conservative with respect to the nonlinear static approach. Lastly, the assessment made with advanced models and nonlinear dynamic analyses show that the vulnerability of modern URM buildings resemble to be overestimated their real behavior (Rosin et al., 2018).

4.3.1.2 Median collapse intensity

The median collapse intensity is a collapse metric that identifies the ground motion intensity when the probability of collapse is 50%. This metric is mainly used when you want to roughly estimate the risk of collapse for different structures, with similar dispersions, with the same intensity measure, but in the same site.

4.3.1.3 Mean annual frequency of collapse

One of the best metrics to evaluate the risk of collapse is the mean annual frequency of collapse. This method has as its main features a greater accuracy and less computational effort (Eads, 2013; Eads et al., 2013). To calculate the mean annual frequency of collapse, two components are needed which are the hazard curve and the fragility curve. The hazard curve describes the annual probability of exceeding an intensity measure obtained from a ground motion for a given site. The curves are obtained through the probabilistic seismic hazard analysis (PSHA) (Cornell, 1968; McGuire, 2004). As mentioned several times, the intensity measure adopted in this study is the peak ground acceleration (PGA). This value varies for each site and is defined for the Italian territory by Istituto Nazionale di Geofisica e Vulcanologia (Stucchi et al., 2011). The hazard estimates are freely available online (http://esse1-gis.mi.ingv.it/). The second component used is the fragility curve. In this way the vulnerability is described by a lognormal distribution that for a given earthquake with intensity measure *im* a relative probability of exceeding a damage state (e.g. collapse).

$$\lambda_c = \int_0^\infty P\left(C|IM\right) \cdot \left| \frac{d\lambda_{IM}\left(im\right)}{d\left(im\right)} \right| d\left(im\right) \tag{4.10}$$

where $P(C|IM)$ is the collapse fragility curve and $d\lambda_{IM}(im)/d(im)$ is the numerical derivative of the seismic hazard curve at the site. The equation (4.10) is solved by

numerical integration as there is no closed-form solution. Then the equation is solved as follows:

$$\lambda_c = \sum_{i=1}^{\infty} P\left(C|im_i\right) \cdot \left|\frac{d\lambda_{IM}\left(im_i\right)}{d\left(im\right)}\right| \delta\left(im_i\right) \tag{4.11}$$

where δim is the increment of IM, $P(C|im_i)$ is the probability of collapse at IM and the $d\lambda_{IM}(im)/d(im)$ is the slope of the seismic hazard curve at discrete IMs. All this adding for all IMs.

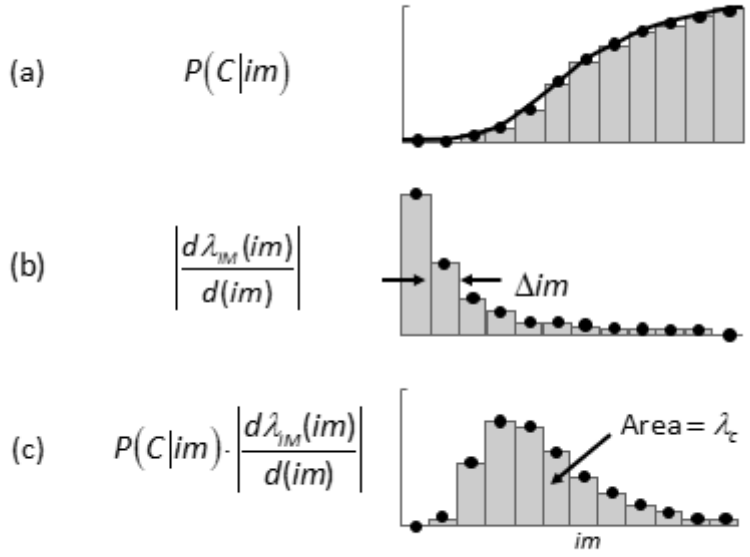

Figure 4.14: diagram of λ_C deaggregation: a) collapse fragility curve, b) slope of seismic hazard curve, c) λ_C deaggregation (Eads et al., 2013).

The probability of collapse provides general information on the reliability (this is closely related to the probability of collapse) and the risk of the wall under seismic action. This parameter does not provide any information on which intensities contribute most to the collapse. A useful tool to get more information is the deaggregation of the collapse (Figure 4.14). This tool is similar to what occurs when we want to understand in the probabilistic hazard analysis (PSHA) which seismic source contributes most to the hazard (Bazzurro and Cornell, 1999). In the figure, it is possible to see how the greatest contribution to the probability of collapse is provided

by the ground motion intensities which have the highest ordinates of the deaggregation curve.

The probability of collapse is the area under the deaggregation curve. A further indication provided by the curve is that most of the contribution to the collapse is provided by the low intensities of the ground motion. In these intensities, the slope of the seismic hazard curve is typically more important in these intensities than in the upper part of the fragility curve. Therefore, most of the collapse contribution necessarily does not come from higher ground motion intensities but in the lower part of the fragility curve.

4.3.1.4 Probability of collapse for a given time period

The mean annual frequency of collapse is described by λ_C. If the occurrence of earthquakes is assumed as a Poisson process (a frequent hypothesis in earthquake engineering following Cornell (1968)) the probability of one collapse P_C over t years can be written as follows:

$$P_C\left(\text{in } t \text{ years}\right) = 1 - \exp\left(-\lambda_C t\right) \tag{4.12}$$

The probability of collapse in one year can be approximated as the average annual frequency of collapse as follows:

$$P_C\left(\text{in } t \text{ years}\right) \cong \lambda_C \tag{4.13}$$

In general, designers and stakeholders are interested in understanding the probability of collapse of structures over a 50-year period (nominal life span). ASCE 7-10 (ASCE, 2010) target the probability of collapse for a structure to be less than 1% in 50 years which corresponds to the probability of collapse λ_c of $2.0 \cdot 10^{-4}$.

4.3.2 Fuzzy mean annual frequency of collapse for local mechanism

The procedure described above provides the mean annual frequency for a structure or a structural element where all the data are described by the classical theory of probability. The aim of the present section is to show as is possible to take into account the uncertainties presents on mechanical parameters, geometry and so on. The uncertainties are described by fuzzy variables as previously shown in Section 4.1.

These analyses allow determining a probability of collapse defined as a fuzzy number. The procedure for the evaluation of the collapse fuzzy number consists of:

1. fuzzy description of the site seismic hazard curve (Section 4.3.2.1)
2. fragility curve with fuzzy input (Section 4.2);
3. application of the α-level optimization for the evaluation of the fuzzy probability of collapse (Section 4.3.2.2);

4.3.2.1 Seismic hazard curve with fuzzy

The possibility of a potential earthquake occurring in a certain location is described by the seismic hazard curve using the Probabilistic Seismic Hazard Analysis (PSHA) (McGuire, 2004). An example of a hazard curve is shown in Ferrara, Italy (Figure 4.15).

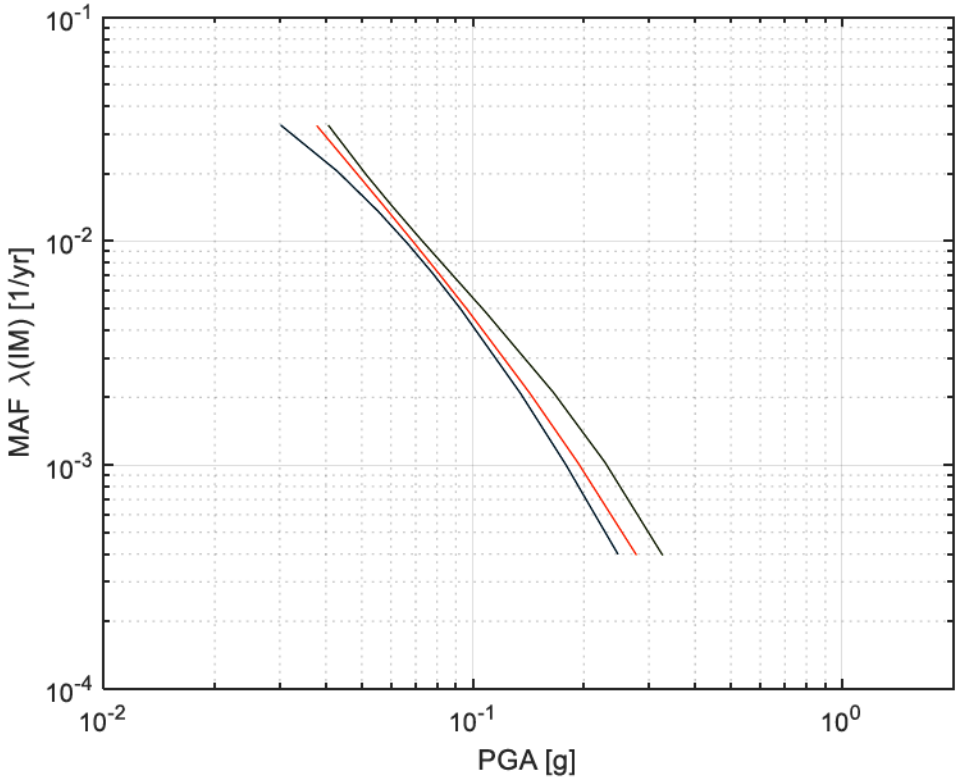

Figure 4.15: fuzzy hazard curve for the city of Ferrara.

These curves are characterized by aleatory and epistemic uncertainties. Generally, PSHA takes into account aleatory and epistemic uncertainty using logic trees (Abrahamson and Bommer, 2005).

In the case under study, the epistemic uncertainty was considered using a different approach than that conventionally defined using fuzzy sets. The choice to approach fuzzy is dictated by the development of the fragility curves using fuzzy and by the desire to standardize the methodology for calculating the probability of collapse. The site hazard curves used in this section are taken from the database of Istituto Nazionale di Geofisica e Vulcanologia (Stucchi et al., 2011). They are defined by three curves: the mean curve and the curve that corresponds to the 16th and 84th percentile respectively. The fuzzy transformation of this curve consists in considering the average curve as the vertex of a fuzzy number with a membership function that seems to be 1 ($\mu = 1$). The remaining two curves (that of the 16th and 84th percentile) are defined as the extremes of the range of the fuzzy number with the value of the membership function $\mu = 0.32$ (Buratti et al., 2012).

4.3.2.2 Fuzzy probability of collapse

Having defined the hazard curve in fuzzy numbers as well as the fragility curve, it is possible to evaluate the probability of collapse of the wall by considering the relative procedures described in Sections 2.1.4.1 and 4.3.1.3.

In particular, the α-cut consists in calculating for each defined value of the membership function the relative output value considering the relative input data for the considered α-value. This is combined by creating *n* samples with the formula for calculating the probability of collapse. In doing so, it is possible to construct the relative fuzzy number corresponding to the probability of collapse.

In Figure 4.16 it is possible to see how in the simple overturning mechanism the greatest contribution in terms of annual probability of collapse is given by earthquakes with PGA between 0.01g and 0.3g. These accelerations are easily found in Italian earthquakes. The interesting thing is to see what happens when a curb or chain is inserted into a wall. In this case, the simple overturning mechanism becomes a vertical bending mechanism. For this mechanism, it is possible to see that the greatest contribution in terms of annual probability of collapse is provided by earthquakes with PGA between 0.3g and 0.7g (Figure 4.16). This shows how this mechanism is less vulnerable than simple overturning. This is also confirmed by the lower probability of collapse of vertical bending compared to simple overturning. Table 4.4 shows the values of the fuzzy number of the annual probability of collapse.

Figure 4.17 illustrates the relative fuzzy numbers for simple overturning and vertical bending mechanism. For this area, the simple overturning mechanism is more vulnerable than vertical bending.

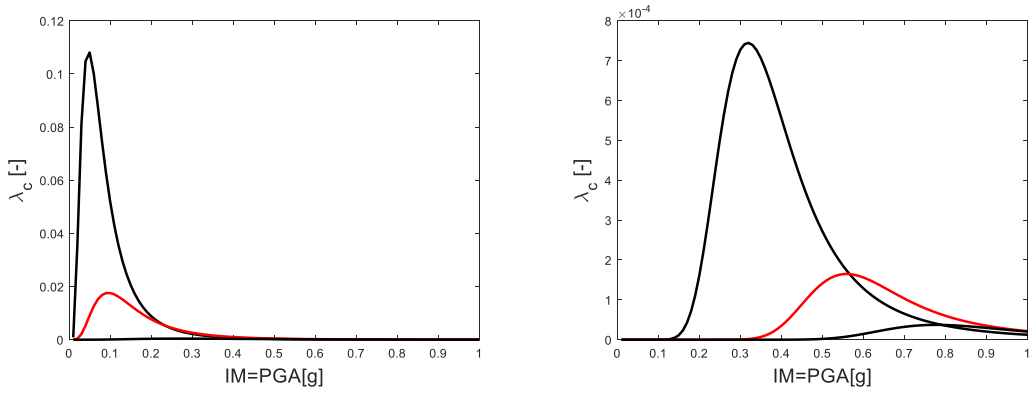

a) b)

Figure 4.16: fuzzy deaggregation of the probability of collapse, a) simple overturning, b) vertical bending.

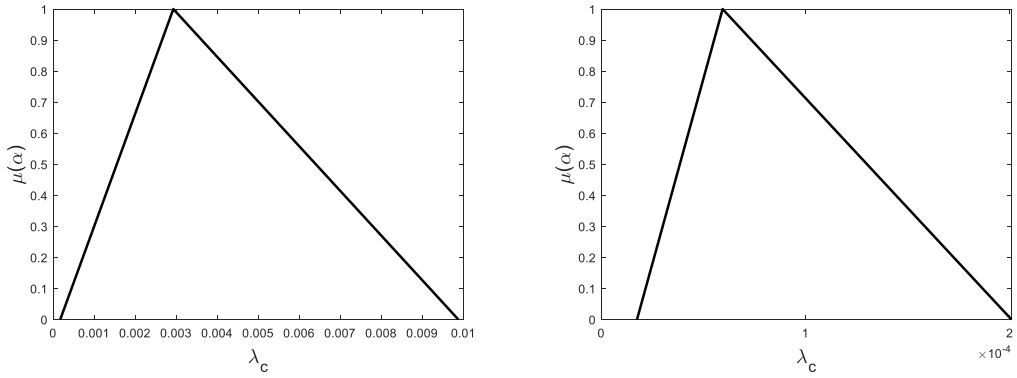

a) b)

Figure 4.17: fuzzy annual probability of collapse λ_C : a) simple overturning, b) vertical bending.

4.3.3 Safety Verification

The aim of this section is to quantify the reliability of a possible local mechanism in function of the seismic risk through the mean annual frequency of collapse taking also account the uncertainties on mechanical and geometrical parameters and vertical loads. According to Cornell (1969), the probability of failure (P_f) can be evaluated by use of the normal distribution function Φ as a function of the reliability index β.

$$P_f = \Phi(-\beta) \tag{4.14}$$

To define the safety of the structures it is necessary to compare the reliability index (β) or the probability of collapse (P_f) with the prescribed values allowed or required. Figure 4.17 presents the fuzzy number of the mean annual frequency of collapse (λ_c) that corresponds to the probability of failure (P_f). In this figure, two main mechanisms of collapse are used as a test: simple overturning and vertical bending.

The existing safety level in a fuzzy probabilistic safety assessment is described by a fuzzy probability of collapse value $\tilde{P}_f$ and a fuzzy reliability index value $\tilde{\beta}$.

$$\tilde{P}_f \leq P_{f_{perm}} \tag{4.15}$$

$$\tilde{\beta} \geq \beta_{req} \tag{4.16}$$

Having defined the probability of collapse and the reliability index as a fuzzy number, the inequalities cannot be defined as completely satisfied or not, but it will be necessary to divide into three main cases:

1. the verification is satisfied if all the elements of the fuzzy ($\tilde{\beta}$) are greater than the value of the required reliability index (β_{req})

$$\beta_{\alpha=0,l} \geq \beta_{req} \tag{4.17}$$

2. the verification is not satisfied if all the elements of the fuzzy ($\tilde{\beta}$) are smaller than the value of the required reliability index (β_{req})

$$\beta_{\alpha=0,r} < \beta_{req} \tag{4.18}$$

3. the verification is not fully satisfied when the required reliability index value (β_{req}) is an element of the fuzzy ($\tilde{\beta}$)

$$\beta_{req} \in \tilde{\beta} \wedge \beta_{\alpha=0,l} \neq \beta_{req} \tag{4.19}$$

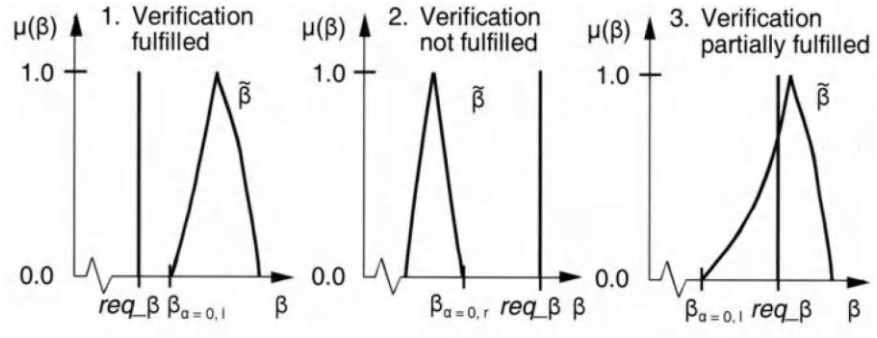

Figure 4.18: safety verification (Möller and Beer, 2004)

If the verification is partially satisfied, the fuzzy set is divided by two subsets $\tilde{\beta}_1$ and $\tilde{\beta}_2$ with a straight line β_{req}. The first subset $\tilde{\beta}_1$ is defined as follows:

$$\tilde{\beta}_1 = \left\{ \left(\beta, \mu(\beta) \right) \middle| \beta \in \tilde{\beta}; \beta \geq \beta_{req} \right\} \tag{4.20}$$

whose right part of the fuzzy set is verified while a second fuzzy subset $\tilde{\beta}_2$ is defined

$$\tilde{\beta}_2 = \left\{ \left(\beta, \mu(\beta) \right) \middle| \beta \in \tilde{\beta}; \beta < \beta_{req} \right\} \tag{4.21}$$

where the left part of the fuzzy set is the unverified part. The degree to which the values of β_1 and β_2 belong to the membership function $\mu(\beta)$ are evaluated by applying the maximum operator. The maximum value of the membership function is defined as follows (Möller et al., 2003):

$$\mu_1 = \sup_{\beta \in \tilde{\beta}_1} \left[\mu(\beta) \right] \tag{4.22}$$

$$\mu_2 = \sup_{\beta \in \tilde{\beta}_2} \left[\mu(\beta) \right] \tag{4.23}$$

The safety check is satisfied when it is evaluated by the μ_1 value while the safety check will not be satisfied by the μ_2 value. These values of the membership function can be interpreted as the degree of possibility that the verification is verified or not, respectively. With a value of $\mu_2 = 0$, the verification is not fully satisfied, while with $\mu_1 = 0$ the safety verification is fully satisfied.

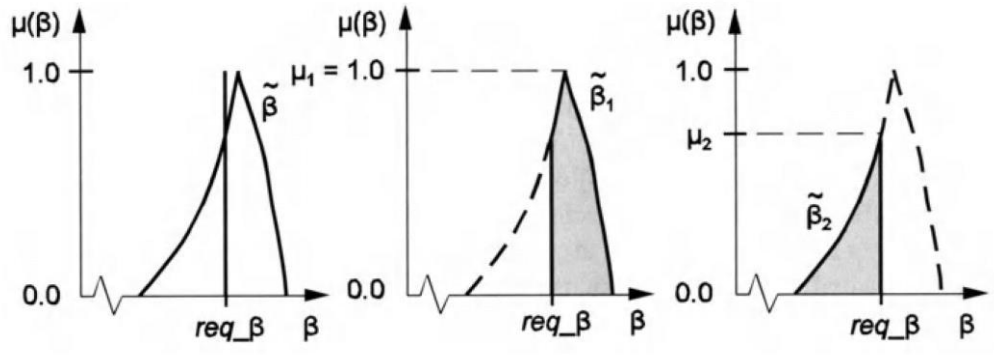

Figure 4.19: assessment of fuzzy safety level with subsets $\tilde{\beta}_1$ and $\tilde{\beta}_2$ (Möller and Beer, 2004).

The procedure described above has been applied for two recurrent local collapse mechanisms: simple overturning and vertical bending. The simple overturning is, as known, triggered by extremely low horizontal actions, and it is enough for example to insert a chain at the head of the wall to trigger the second mechanism which however requires a horizontal action about four times greater. Table 4.4 shows the value of the probability of collapse and the reliability index for masonry walls for the two mechanisms for the set of mechanical parameters reliable in the territory of the municipality of Ferrara. Figure 4.20 shows that for simple overturning, the check is not completely satisfied for typical values of masonry buildings and the hazard curve in Ferrara. It should be noted that in this case the wall is of good quality from the masonry point of view but has no transversal connection with the other walls. If we consider the role of the connections or the presence of chains (vertical bending), the reliability indexes increase and the probability of collapse decrease. If the walls were on upper floors or parapets at the top of the buildings these would be less safe given an increased probability of collapse due to the amplification effect of the structure on the site hazard curve.

Table 4.4: probability of collapse $\tilde{P}_C$ and reliability index $\tilde{\beta}$ for simple overturning and vertical bending mechanism.

	Mechanism	
	simple overturning	vertical bending
$\tilde{P}_C$	$<1.73\cdot10^{-3},2.90\cdot10^{-3},9.90\cdot10^{-4}>$	$<1.73\cdot10^{-5},5.94\cdot10^{-5},2.01\cdot10^{-4}>$
$\tilde{\beta}$	$<2.33,2.76,3.58>$	$<3.54,3.99,4.14>$

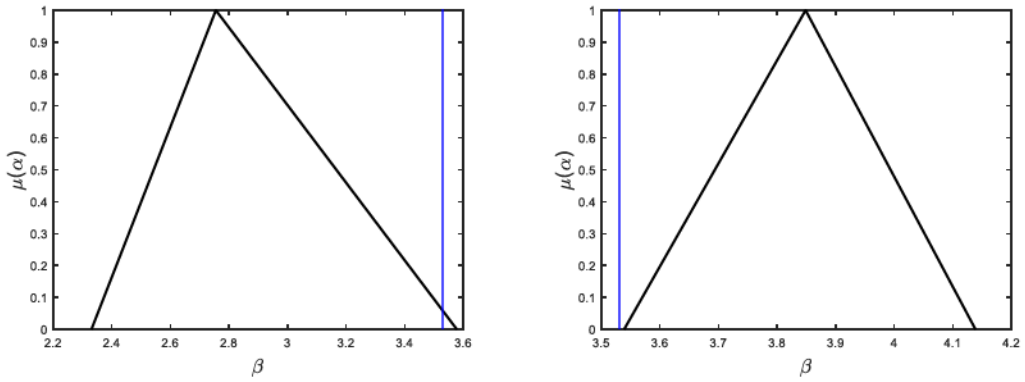

Figure 4.20: fuzzy reliability index $\tilde{\beta}$: a) simple overturning, b) vertical bending.

Let us remark that there is no commonly accepted definition of the values for reliability indices both in the technical literature and in the various technical standards. In the examples, we have reported what is defined by ASCE 7-10 (ASCE, 2010) that sets the probability of collapse for a structure at 1% in 50 years.

4.4 Sensitivity analysis

The sensitivity analysis allows you to evaluate in the presence of several uncertain parameters which ones have the most significant effect on the structural system or to quantify the influence of input uncertainties on the output parameters. The sensitivity index reported in this chapter has two components like a fuzzy number. These values correspond to their degree of plausibility. The first value is the result of the stochastic nature of the input parameter while the second derives from the degree of plausibility of the input. These sensitivity indices are between 0 and 1 and show the minimum and maximum impact that the input parameters have on the output variable. The degree of plausibility of the sensitivity index depends on the membership function. The fuzzy approach allows you to provide important information to encourage an informed decision-making process. This methodology is necessarily limited due to the high computational cost for non-linear analyzes combined with stochastic methods. This is partly an obstacle for practical applications. Computational times can be reduced by using sophisticated Monte Carlo simulations that allow for a significant reduction (Dubourg and Sudret, 2014; Lu et al., 2008; Wei et al., 2014; Zio, 2013).In this chapter, the High Dimensional Model Representations technique (HDMR) (Li et al., 2001) is

used for the evaluation of the indices and this allowed a considerable reduction in calculation times. Naturally, through advanced machine learning techniques, it is possible to further reduce these calculation times (Dubourg and Sudret, 2014; Wang et al., 2013; Wu, 1994). The formulation of even faster sensitivity analyzes is still being researched.

4.4.1 Sensitivity Analysis based on static approaches

Static analysis is the most widely used method for verifying the stability of the wall under seismic action (MIT, 2018, 2019). The linear kinematic limit analysis method consists in solving a simple equation between the stabilizing moment and the overturning moment which allows to derive the collapse load multiplier.

The purpose of the stability analysis, which includes the uncertainties of the structural parameters, is to understand which input parameters influence the collapse load multiplier which is the output variable. Understanding which input parameters affect simple mechanisms is relatively easy for most mechanisms. This Section aims to propose a robust and general method to evaluate the sensitivity of the parameters. For this purpose, the Sobol indices were used to evaluate the sensitivity to the parameters. Both the first order and the global index were used. A brief discussion from the mathematical point of view is treated in Section 2.5 as the relative bibliographic references.

Two different mechanisms were considered for the sensitivity analysis: single-leaf wall overturning, single-leaf wall vertical bending. The input parameters considered are:

- the compressive strength of the masonry (σ_c);
- geometric parameters of the wall such as base (B), height (H), depth (L);
- load parameters like floor load (g_k), floor span (l_s);
- position of the application of the load onto wall (d).

Figure 4.21 shows the results of the sensitivity analysis for the two mechanisms analyzed. As you can see, the parameters that most influence the structural response of the mechanisms are the geometric properties, in particular, the base and the height and the depth of the wall.

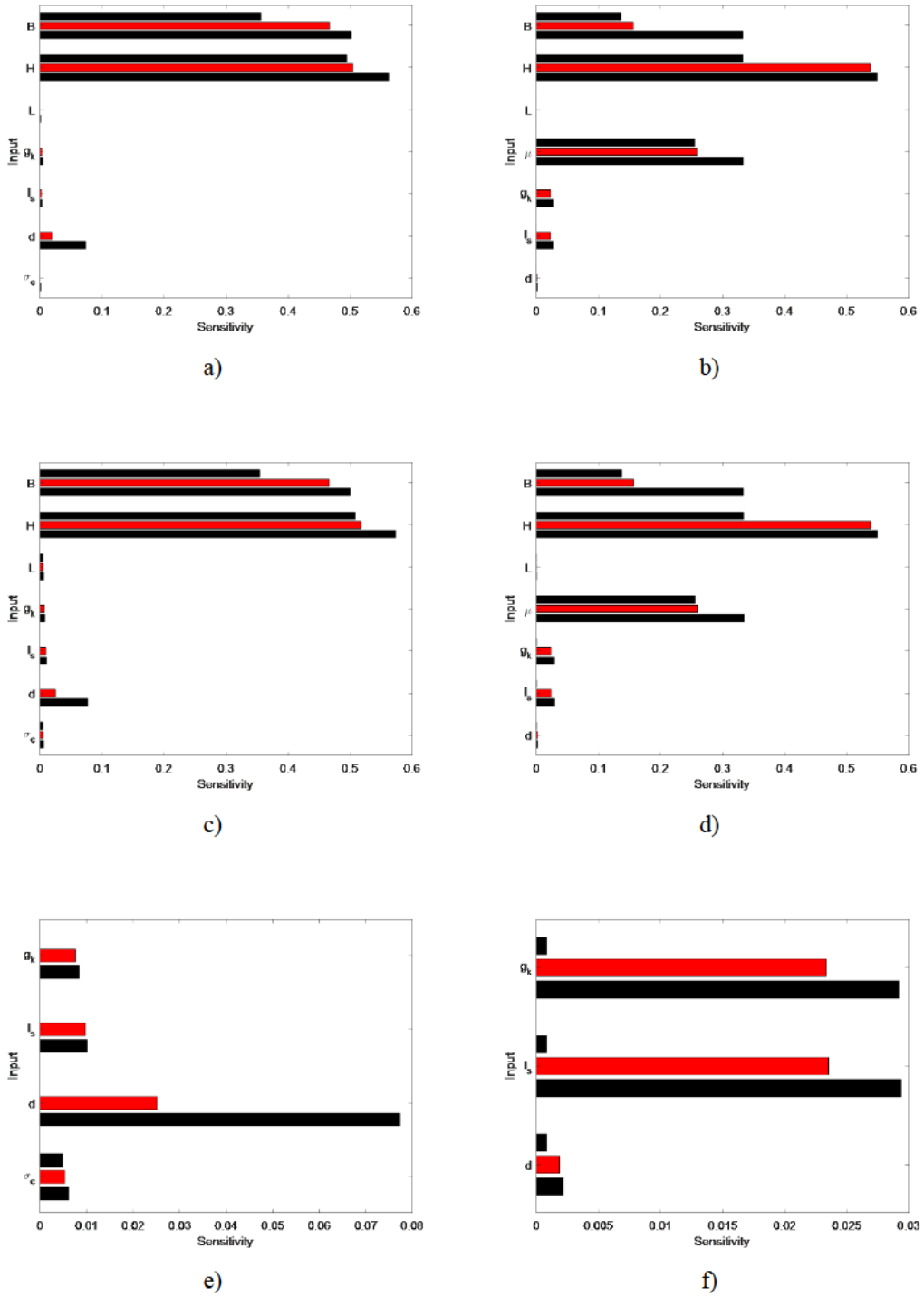

Figure 4.21: fuzzy sensitivity indices for one-sided rocking (left column) and two blocks rocking (right column): a) - b) first-order sensitivities; c)-d) total effect sensitivities; e)-f) total effect sensitivities with attention to the load inputs and its application.

Another parameter that influences the structural response is the point of application of the force obtained as a floor relief.

Indeed, if you investigate the role of loads on the collapse load multiplier, you can see how the application plays an important role with respect to the span and load of the floor. These results are well known in the literature and extensively investigated (see Chapter 3). An innovative aspect is that starting from the CARTIS data with the relative uncertainties associated with the parameters, it is possible to quantify which parameters influence the response in a robust mathematically and relatively quickly without detecting the aggregates in detail. In fact, this information can provide confidence intervals for the fragility curves in order to clarify the possible vulnerability intervals of the structures to the decision-maker.

4.4.2 Sensitivity Analysis based on dynamic approach

In this section, we carry out the sensitivity analysis for the local collapse mechanisms of simple overturning and vertical bending employing dynamic non-linear analysis. There are two aspects that we want to consider. First of all, as in the previous paragraph, quantify which uncertain parameters influence the output the most. Furthermore, we want to quantify how sensitive the result is to varying the seismic intensity or the PGA of the site.

4.4.2.1 Sensitivity Analysis in presence of local variation of PGA

The certainty of the seismic input is a phenomenon that has always characterized seismology. In fact, the uncertainty in the recording of the input (the precision is of the order of 0.01g) and the local effects present in the affected area make the parameters that can be calculated uncertain (e.g. PGA, pseudo-acceleration). This affects not only the non-linear dynamic analysis that takes place but also the fragility curves (Di Ludovico et al., 2020). The 2012 earthquake that hit Emilia was for instance characterized by local amplification and liquefaction phenomena (Fioravante et al., 2013; Lai et al., 2015; Papathanassiou et al., 2015). In addition, a relevant uncertainty has occurred on the PGA of the Shake Maps.

As you can see in Figure 4.22, the uncertainty of the PGA is different for the two events. In fact, between the first and the second shock, additional temporary stations were installed for the recording of the ground motons which greatly reduced the

uncertainty of the PGA. For further information on this topic see (Cultrera et al., 2014). Moreover, in the historical center sector of the city of Ferrara, it is possible to see how there are local phenomena (Figure 4.23). Indeed, there are areas where the liquefaction risk index is higher ($IL>5$) others where it is medium ($2<IL<5$). There are also phenomena of local amplification.

When a seismic event occurs in the presence of local effects, three situations can occur: absence of liquefaction and liquefaction in different steps. In fact, damage to structures can occur both in the absence of liquefaction and when liquefaction is present with lower PGA. In the absence of liquefaction, local mechanisms or diagonal in-plane cracks occur. In the presence of liquefaction, the damage caused by inertial forces is mostly absent because liquefaction works as a natural insulator.

The main damages that can be encountered are rigid rotations of buildings with significant loss of functionality of the structure, such as diagonal cracks due to the subsidence of the foundation. Damage from the combined effects of inertial forces and liquefaction-induced damage can also occur. The main difficulty is to predict when liquefaction occurs due to the characteristics of the soil.

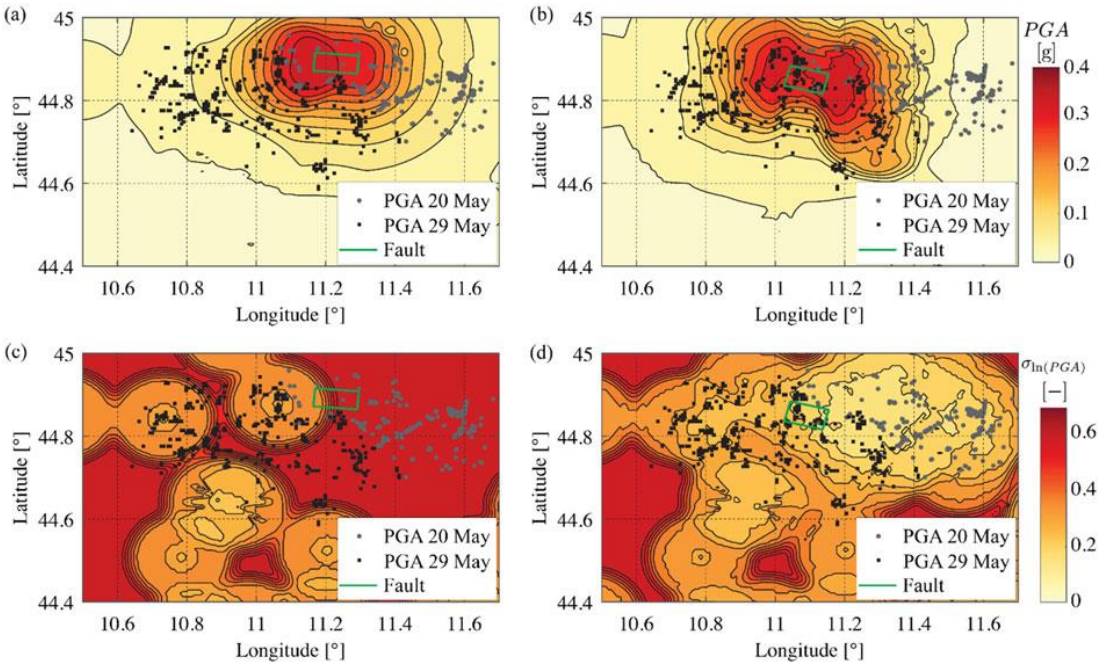

Figure 4.22: elaboration of Shake Maps for the 20 May (a-c) and 29 May (b-d) earthquakes with median PGA (50th percentile) and logarithm standard deviation of PGA (image from (Buratti et al., 2017)).

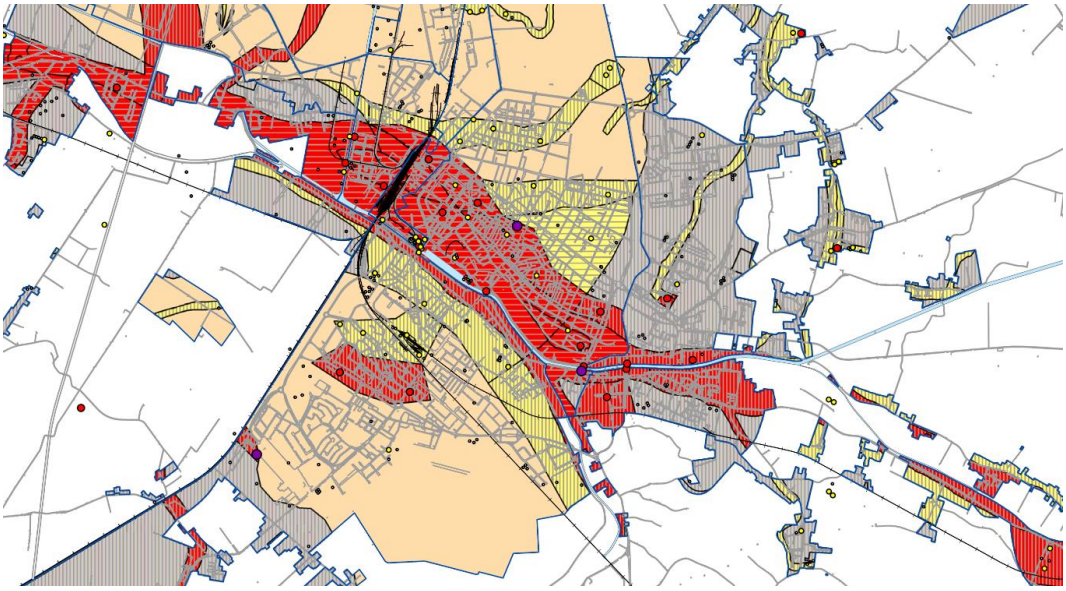

Figure 4.23. seismic microzonation map at level 3 for the city of Ferrara: in red the areas susceptible to high risk of liquefaction (IL>5), in yellow the areas at moderate risk of liquefaction (2<IL<5) and in gray the areas at low risk of liquefaction (IL<2). In orange, the areas susceptible to local amplification (Fa_{PGA} = 1.5:1.6) (image from (Fioravante and Giretti, 2013)).

Considering these phenomena, a sensitivity analysis was carried out for the simple overturning and vertical bending mechanisms. The input parameters considered in the analyses are:

- geometric parameters of the wall such as base (B), height (H), depth (L);
- position of plastic hinge (μ) only for vertical bending;
- load parameters like floor load (g_k), floor span (l_s);
- position of the application of the load onto wall (d);
- peak ground acceleration (PGA).

By introducing the intensity of the earthquake due to instrumental errors or local effects as an uncertain parameter, it is possible to see in Figure 4.24 how this uncertainty plays a decisive role in the structural response of the wall. It has greater relevance in the case of the simple overturning mechanism than in the vertical bending. The result is qualitatively intuitive because the fragility curves in the case of overturning are steeper (the sensibility represents in a certain sense the derivative of the output with respect to a parameter) and more dense. However, it seems the first time that this sensitivity has been quantitatively evaluated. In general, what emerged in the other sensitivity analyzes is highlighted: the geometric parameters play an

important role in the structural response. As regards the loads and their application, it is possible to see how the span of the floor influences the response more with respect to the point of application of the floor load on the wall and of the load itself.

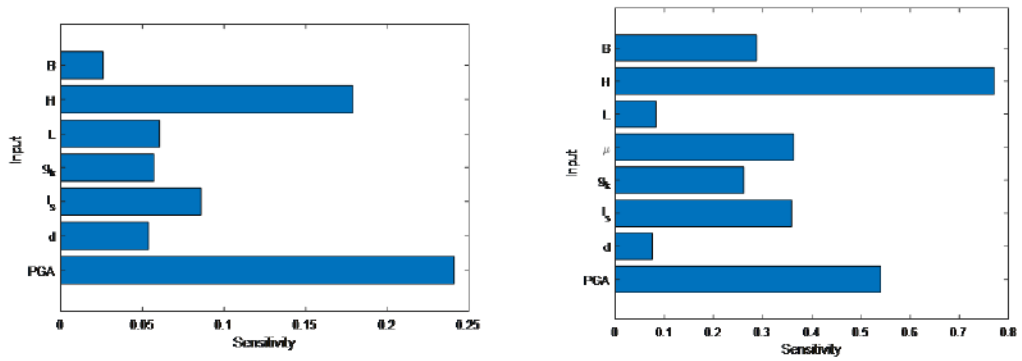

a) b)

Figure 4.24 first-order sensitivity indices: a) one-sided rocking, b)two-block mechanism

5 Reliability assessment of masonry columns of the Cathedral of Saint George the Martyr in Ferrara

This chapter focuses on the safety assessment of the masonry columns of the Cathedral of Saint George the Martyr in Ferrara, Italy. The current state of the column is detailed with the relative information on the mechanical properties of the materials, on the loads taking into account the variability of the intensity and the application points.
Particular attention is given to the creation of simplified mechanical models useful to obtain a fair compromise between computational times and the robustness of the results. These simplified models are validated with analytical solutions and numerical models usually applied (i.e., FEM models).

5.1 Heritage masonry building and structural reliability

As discussed in the first chapter the reliability assessment of existing structures requires appropriate assumptions and good levels of knowledge therefore, the evaluation process results always uncertain.
Obviously, when studying old buildings with important historical and/or artistic value (heritage buildings), the uncertainties increase (Augusti and Ciampoli, 2000). However, reliability analyzes for masonry structures constitute a research area that appears not yet fully investigated. This is due to the uncertainty not only associated with the material but also with loads and its boundary conditions. Several studies have been carried out analyzing the uncertainty of the masonry material (Asteris et al., 2019; Casciati and Faravelli, 2008; Ellingwood, 1981; Saloustros et al., 2019) but these papers do not achieve a suitable definition of the reliability index.
However, a first significant attempt is a work of Baratta (1991). The Author, without significant applications, proposes an estimate of a reliability index assuming masonry

as no-tension material and making the reliability index conditional on the age and fracture speed of the material.

Finally remember that in historic structures, long-term effects such as creep and material degradation play a fundamental role in the safety of the structures as shown with extensive experimental research by the collapse of the Civic Tower in Pavia (Figure 5.1a) (Binda, Anzani, and Saisi, 2008). Papa and Taliercio (2005) presented a numerical model for taking into account the action of cyclic and persistent loads on masonry, while Binda, Anzani, and Garavaglia (2008) proposed a probabilistic model for the study of the long-term behavior of masonry specimens subjected in laboratory to creep and pseudo-creep.

The failure of the Noto Cathedral (Figure 5.1b) serves as a warning of the interplay between weight and geometry, furthermore highlights that the no-tension assumption can provide a reliable behavior for masonry structures. In his book, Como (2013) provides a distinction between structures intrinsically stable and intrinsically unstable. This distinction helps to simplify an extremely complex problem such as that of monumental masonry structures.

By intrinsically stable structure we mean a structure that under given geometry and load distribution within the assumptions of no-tension behavior, satisfies equilibrium and admissibility of compression stresses. By intrinsically unstable structure we mean that the structure is not capable to sustain given loads under the no-tension material assumption.

Figure 5.1: some examples of the collapse of heritage masonry building: a) the ruin of Civic Tower of Pavia in 1989 after the collapse (image from Binda, Anzani, and Saisi (2008)), b) a damaged pillar of the Noto Cathedral (image from Saisi et al. (2008)).

Finally, let us remark that, given the complexity of the monumental structures, the verification of their safety must be done by integrating as much as possible all the information that can be obtained from the experimental tests in situ, from the numerical models and from the monitoring of the structures.

5.2 The Cathedral of Saint George the Martyr

The Cathedral of Saint George the Martyr is the seat of the Archbishop of Ferrara and it is dedicated to Saint George the patron saint of Ferrara and its construction represented the new role of the city of Ferrara. Namely, Ferrara is no longer a secondary center, but a city of increasing commercial and political importance in the 12th century.

In 1132, Pope Innocent II signed the breve (*litterae apostolicae*) for the concession of construction for the new cathedral. On the initiative of bishop Landolfo and Guglielmo degli Adelardi, de facto ruler of the city, the works began immediately when the city was being extended towards the left bank of the Po River. Certainly, 1135 constitutes a reference point in the dating of the first structure because this is engraved in the Latin inscription placed in the lunette of the main portal of the Cathedral and Pope Alexander III consecrated the main altar in 1177.

The current state of the cathedral is the result of a series of additions, modifications and restorations over the centuries that have changed its external appearance and completely changed its layout. Overall, the most significant changes were in the fifteenth century due to the intervention of Biagio Rossetti in the apse area and in the seventeenth century, made by Luca Danesi, in the transept. Finally, the total restructuring in baroque style was carried out by Francesco Mazzarelli on order of the archbishop cardinal Dal Verme in 1712-1728. These works completely changed the static structure which was transformed from a five naves structure with a wooden roof with a light weight, to a three naves structure with a complex system of vaulted masonry roofs that are very heavy (Figure 5.2).

The façade of the Cathedral is a clear example of a Romanesque style façade (Figure 5.3). Above the central door, you can see Saint George and the scenes from the New Testament by the sculptor Nicholaus (1135).

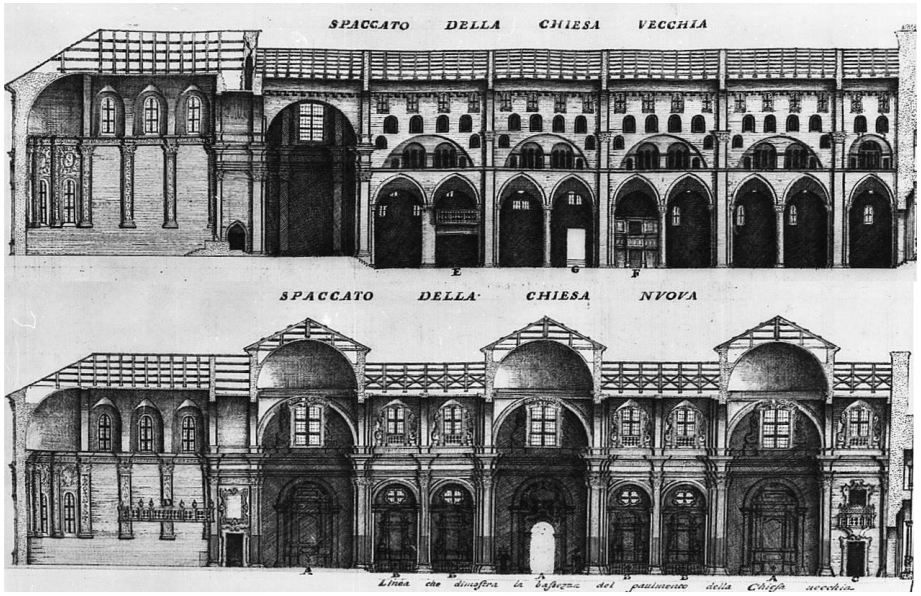

a)

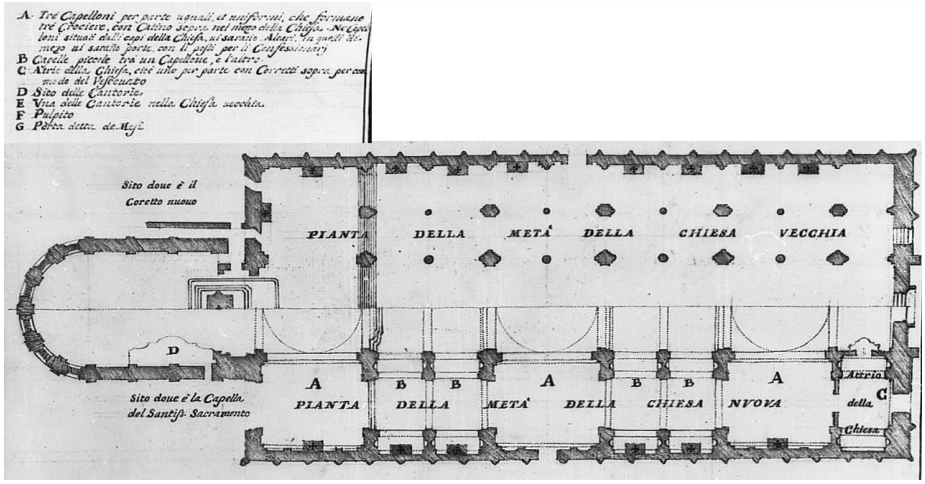

b)

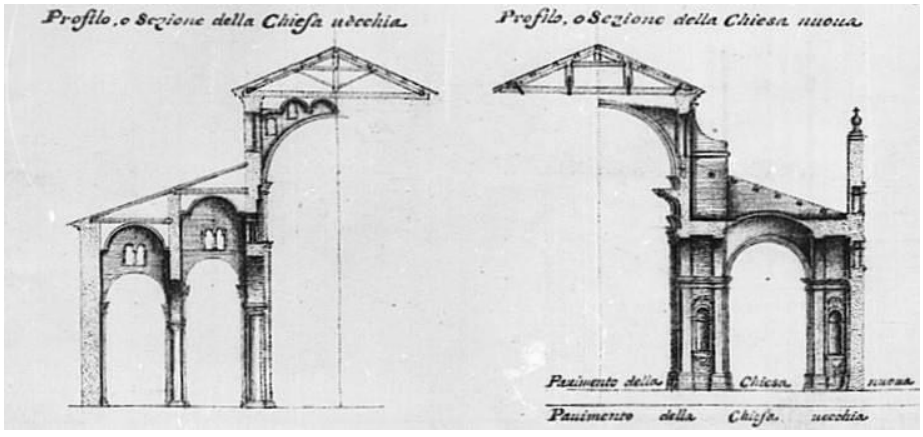

c)

Figure 5.2: comparison between the medieval and eighteenth-century cathedral: a) longitudinal sections, b) maps c) cross sections (Carbonara, 2015).

Figure 5.3: cathedral west front and façade.

A few decades later, the upper part was built in the Gothic style, it presents an extraordinary *Last Judgment* by an unknown sculptor above the central loggia. Two galleries and columns of various shapes decorate the side facing of the building. The *Loggia dei Mercanti* located on the ground floor has been occupied by shops since the Middle Ages. In the middle of the south side, it is possible to see what remains of the *Porta dei Mesi*, which takes its name from the magnificent carved panels depicting the months, demolished in the 18th century but some sculptures are still visible in the Cathedral Museum. Near the cathedral is the imposing Renaissance bell tower, in pink and white marble, an unfinished work attributed to Leon Battista Alberti. The brick apse, decorated with terracotta arches and marble capitals, is the work of the greatest Renaissance architect and urban planner of Ferrara, Biagio Rossetti.

As mentioned above, the interior of the cathedral was completely renovated in the 18th century in a grandiose Baroque style. To support the weight of the roof, Mazzarelli introduced new large masonry pillars (about 2.30 m by 4.20m) between the two lateral naves and the central one, with a greater span, which partially incorporate the previous medieval pillars. The eighteenth-century column does not appear to be perfectly connected to the medieval one. Moreover, inside the columns, there are sometimes iron rings. In fact, these pillars were the subject of restoration work in the 1930s by the Superintendence for Architectural Heritage of Bologna and then the diocesan chancery

intervened.

The pillars are cracked and the plasters seriously damaged, also due to the poor quality of the plasters and mortars used in those restorations, so much so that a new intervention is necessary. Following the seismic events of May 2012, the commissioner for the reconstruction of the Emilia-Romagna Region decided to finance new restorations.

5.3 The case of the pillars of the Cathedral

The pillars of the cathedral have been the subject of interventions and investigations since the phases immediately following the renovation works of the 30s of the last century due to the crack pattern and the detachment of portions of plaster. A main problem encountered is the capillary rise of the typical humidity of the Ferrara area. For the humidity, remedies of dubious efficacy were adopted (Nunziante, 2021).

On geometry, it seems relatively easy to identify, working on the current relief and bearing in mind Mazzarelli's drawing in Figure 5.2, the axes of the major pillars and minor of the secondary aisles. Instead, it is necessary to reflect carefully on Mazzarelli's plan to obtain the exact position of the medieval pillars on these axes.

The old medieval pillars are in an eccentric position, that is to say more moved towards the great nave, as shown by the essays carried out and only covered, on the front that looks at it, from a light wall lining, sufficient to are outline the classical forms of the orders that today characterize the great baroque pillars. Two columns can therefore be seen side by side: a medieval one, which is incorporated into the eighteenth-century one (Figure 5.4).

We assume pillar B4 as a reference for the investigation (Figure 5.5). For this pillar, analyzes were carried out for the mechanical characterization of the masonry by means of laboratory tests on the components i.e., compression tests on brick cubes and double punching on the mortars, taking appropriate samples of eighteenth-century and medieval mortars. Tests were carried out with single flat jacks, aimed at an indicative verification of the entity of the average stresses.

From the wall texture, it is possible to distinguish the eighteenth-century masonry from the medieval one (Figure 5.6). The thickness of the brick block is the simplest parameter from which it is possible to distinguish the two wall textures. In fact, the thickness of the medieval brick block is 65 mm while the eighteenth-century one is 55 mm.

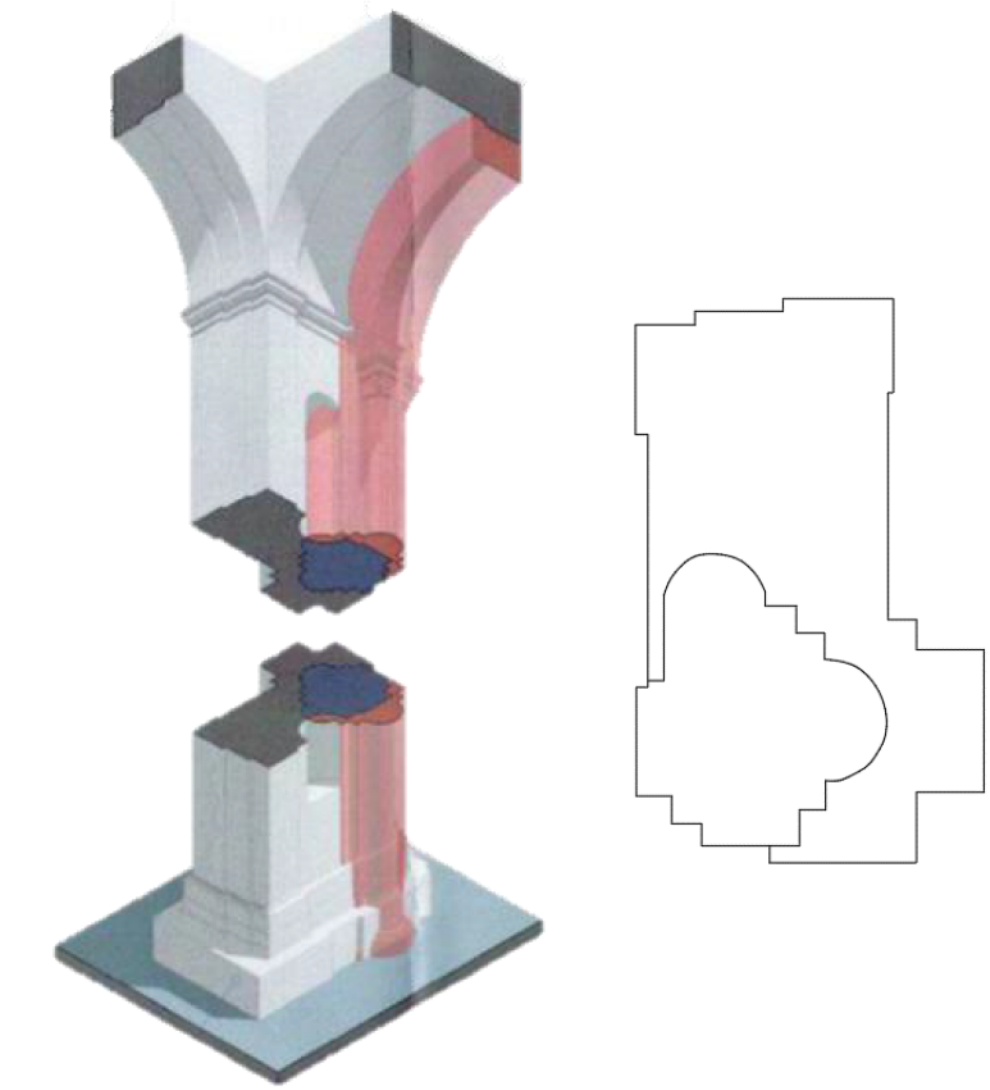

Figure 5.4: axonometric view of the medieval parts (in red) and the cross-section of the pillar.

However, the various alterations that took place over the centuries are such that on a superficial level the medieval part has been reconstructed for some sections. This condition is evident for the portion next to the base of the column where it is entirely rebuilt with bricks similar to those of the eighteenth century.

The structural critical issues of the pillars emerged in the 1930s and already with the local interventions of the 1800s. In the 1930s the first interventions were carried out aimed at reducing the structural criticalities that emerged from the cracking pattern carried out at the time. The intervention plan carried out at the time was performed without a uniform approach. Figure 5.7 shows a reconstruction of the metal interventions carried out in the 1930s.

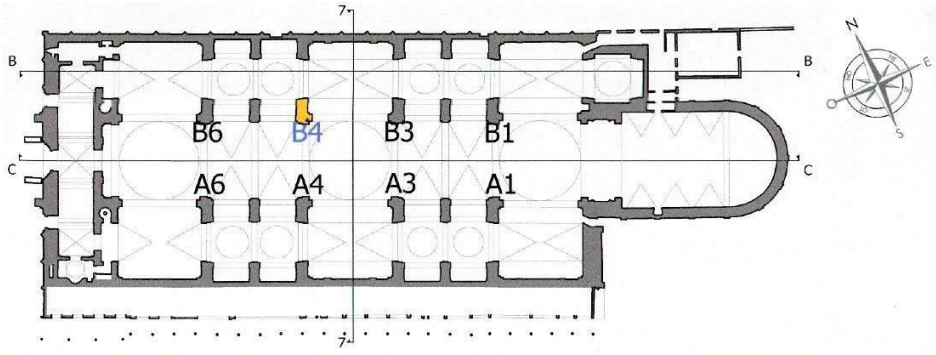

a)

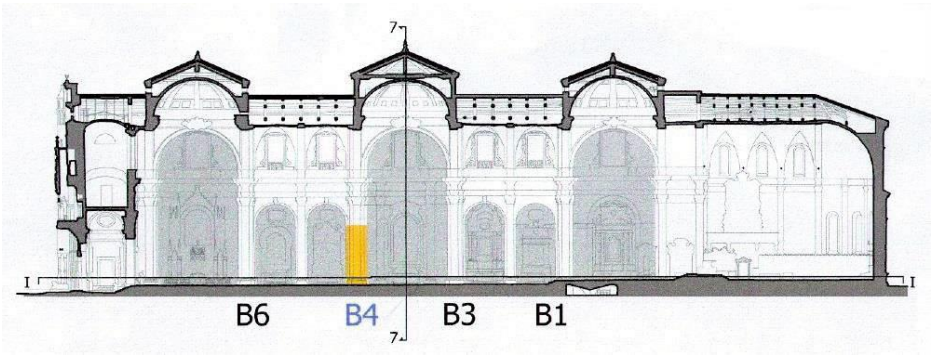

b)

c)

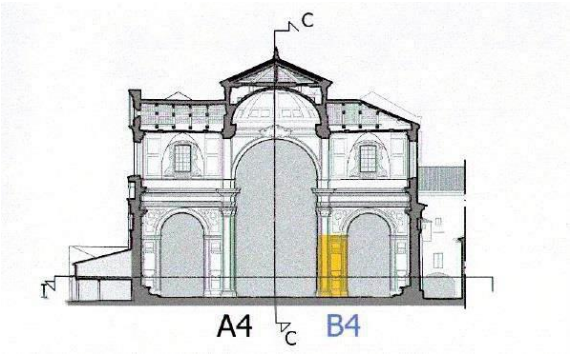

d)

Figure 5.5: plan and section of the cathedral with column B4 highlighted a) plan of the cathedral, b) section C-C, c) section B-B, d) section 7-7.

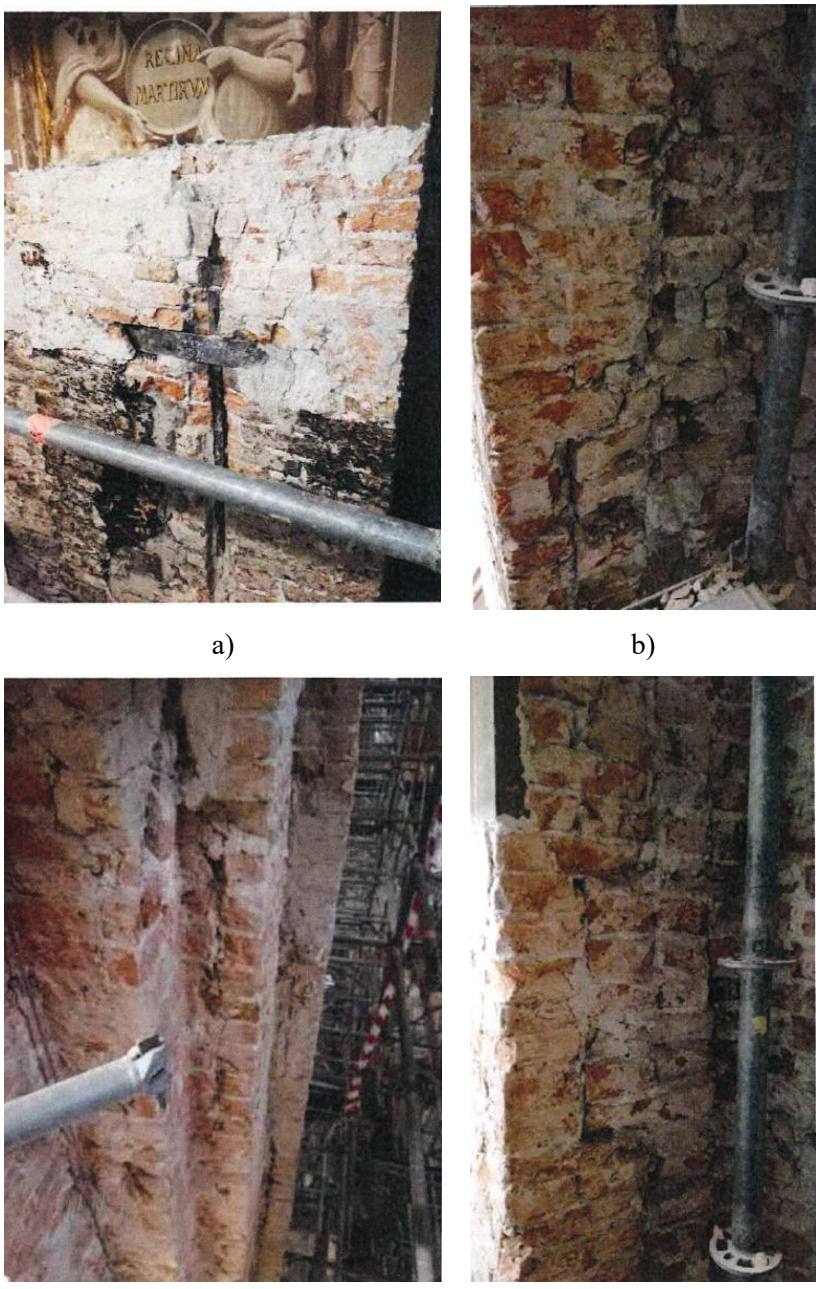

a) b)

c) d)

Figure 5.6: a) injuries in the presence of metal elements, b) vertical cracks in the wall face, c) lack of clamping of the masonry, d) irregular texture of the wall face.

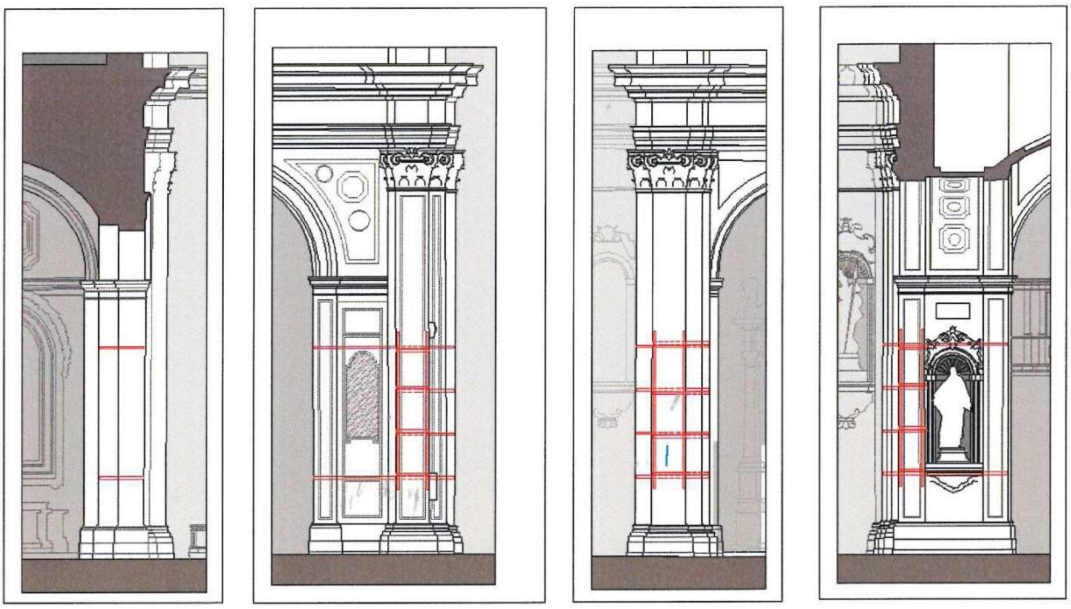

Figure 5.7: reconstruction of the metal elements presents in the masonry column.

From the tests and analyzes carried out, numerical evaluations reported below could be affected by errors due to the numerous unknowns and calculation limitations. The test with the flat jack for measuring the operating pressures can be considered a rough reference of the state of average stress, when suitably validated, as an error linked to edge effects, to local conditions of the masonry of both state of conservation and weaving, to tolerances instrumental.

The theoretical analysis of the stress distribution cannot take into account the load history of the structure, which remains uncertain. In fact, the succession of construction phases should be considered, the conservation of part of the medieval structures, including a portion of the ancient column could have retained a relevant load share. Furthermore, being non-contemporary structures, differential settlements may have occurred that cannot be quantified but such as to influence the distribution of stresses. In addition to the column, in the eighteenth-century reorganization of the cathedral a part of the clerestory of the medieval church was conserved, with annexed structures, including large unloading arches that are still visible today. One hypothesis is that these structures are still pushing.

The first simplifying hypothesis on the column behavior is to assume that medieval and baroque can be considered made of, eventually distinct, homogeneous masonry material. Investigations show a weak level of clamping, moreover the distribution of the metal insertions cannot be considered such as to guarantee collaboration between

the two portions of the masonry volume.

5.3.1 Material

The stripping of the B4 pillar made it possible to evaluate the masonry texture and mechanically characterize the material by means of on-site tests.

The simple jack test allowed the measurement of the operating pressures. These values are indicative of the average stress state. Although for the case study, this methodology can be considered reliable i.e. the loads are high; the stress measures are however affected by an intrinsic error due to edge effects, local conditions of both loading and weaving and also instrumental tolerances. From the mechanical characterization of the mortar and brick blocks, it emerged that medieval mortars are on average better than those of the eighteenth century. Figure 5.8 shows the wall textures present in the cathedral.

a) b) c) d)

Figure 5.8: details of the wall texture.

5.3.1.1 Characteristic compressive strength of masonry

The characteristic compressive strength of masonry f_k, can be determined from results of tests on masonry specimens using the formula reported in Eurocode 6 (CEN, 2005a):

$$f_k = K \cdot f_b^{\alpha} \cdot f_m^{\beta} \tag{5.1}$$

where:

- f_k is the characteristic compressive strength of the masonry, in N/mm^2;
- K is a constant and, where relevant, modified according to 3.6.1.2(3) and or

3.6.1.2(6);

- α, β are constants;
- f_b is the normalized mean compressive strength of the units, in the direction of the applied action effect, in N/mm^2;
- f_m is the compressive strength of the mortar, in N/mm^2.

Applying the formula for eighteenth-century masonry, the compressive strength of the masonry is equal to 4.34 MPa. The compressive strength of medieval masonry is instead equal to 4.76 MPa. These results are based on 20 compression tests on brick cubes to determine the compressive strength for the blocks, while for the determination of the compressive strength of the mortars they are determined by 10 tests for medieval mortars and 30 tests for eighteenth-century mortars. The results of all tests are available in Appendix A. Table 5.1 shows the average values and the relative standard deviations.

Table 5.1: results value experimental tests.

Parameter	Mean value μ [MPa]	Standard deviation σ
f_b	17.61	5.64
f_{m1000}	2.98	0.72
f_{m1700}	4.06	0.56

5.3.1.2 Modulus of elasticity

In the absence of a value determined by tests in accordance with EN 1052-1, the short-term secant modulus of elasticity of masonry E, for the use in structural analysis, may be taken:

$$E = K_E f_k = 1000 \cdot f_k \tag{5.2}$$

where K_E is equal to 1000 and f_k is the compressive strength of the masonry.

The long-term modulus $E_{long\ term}$ is reduced to allow for creep effects such that:

$$E_{\text{long term}} = \frac{E}{1+\phi_\infty} \tag{5.3}$$

In our case, a value of the creep coefficient ϕ_∞ equal to 1.0 has been assumed. Therefore, the value of the elastic modulus in the long term corresponds to half of the elastic modulus in the short term.

5.3.2 Load

Table 5.2 and Figure 5.9 show the value of the actions transferred to the pillar by the individual arches and which are included in a single assessment and added to the horizontal and vertical loads, which for simplicity we consider applied at the barycenter of the arch sections.

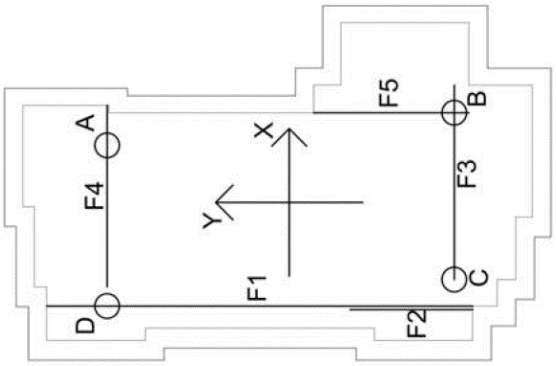

Figure 5.9: example of section and position of the applied loads.

Table 5.2: value of loads, heights and distances from the axes of their application.

Load	[kN]	Z [m]	E_y [m]	E_x [m]	Note
A	150	17	1.4861	0.5238	weight vault
B	320	17	1.3477	0.8192	weight dome and plumes
C	87.12	17	1.3477	0.8096	weight vault
D	92.5	9	1.4861	0.8436	weight vault
F1 horizontal	159	9			from arch
F1 vertical	304	9	0	0.8436	from arch
F2 horizontal	927	11.5			from arch
F2 vertical	1375	11.5	1	0.8721	from arch
F3 horizontal	511	17			from arch
F3 vertical	1217	17	1.3477	0	from arch
F4 horizontal	500	9			from arch
F4 vertical	920	9	1.4861	0	from arch
F5 horizontal	511	17			from arch
F5 vertical	1217	17	0.8336	0.8192	from arch

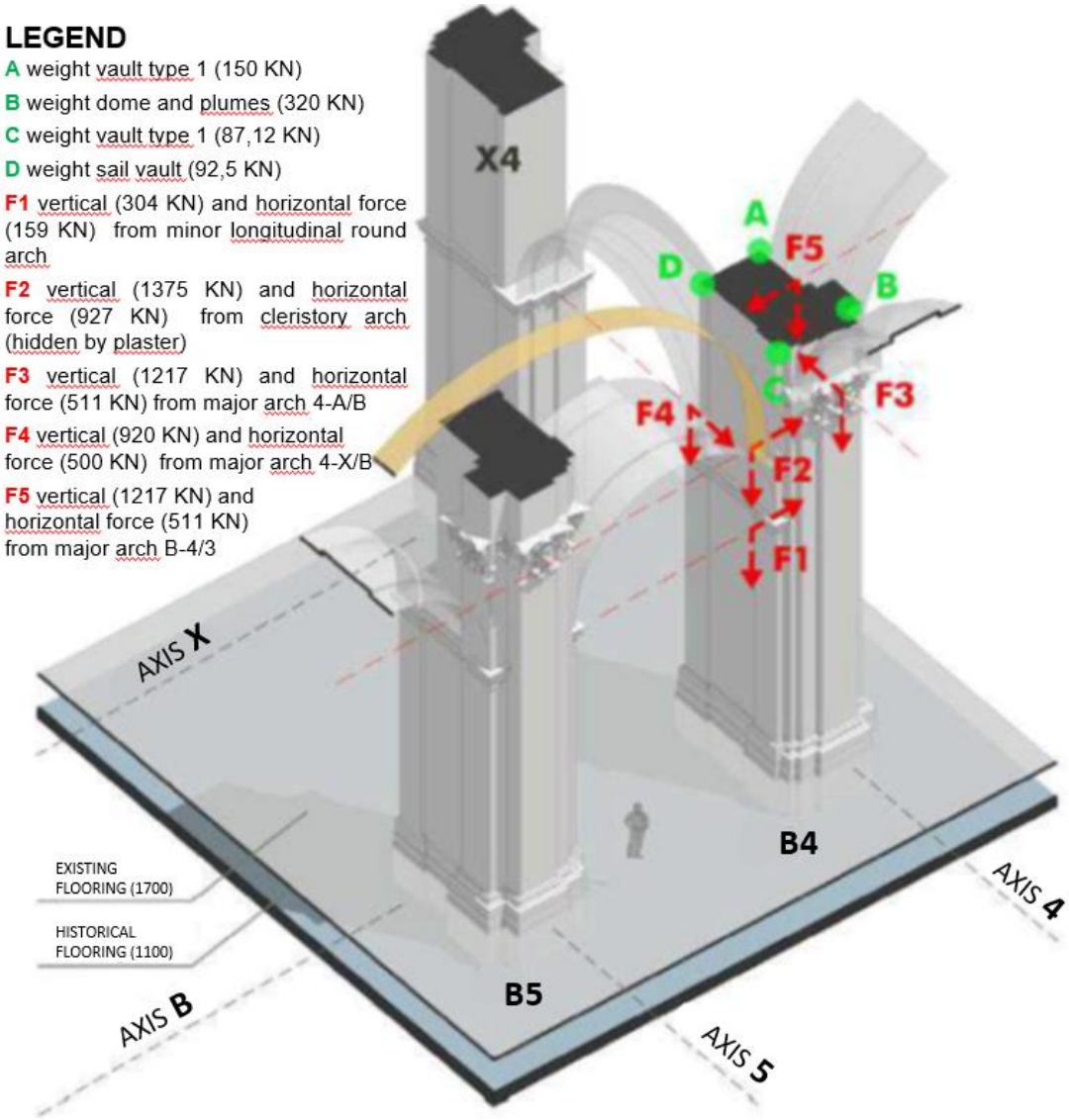

Figure 5.10: diagram of the loads insisting on pillar B4.

The evaluation of the thrust of the circular (o round) arches is obtained by identifying the curve of the arch pressure. The loads estimated through the volumes at the bary-centric curve and by calculating the thrust curve. Figure 5.10 report the overall picture of the forces acting on the column and their application.

In the following paragraph, the horizontal stresses acting on the pillar by the arches and the weights that the domes always exert on it are critically discussed.

5.3.3 The thrust of the arches

The values reported in the previous paragraph are evaluated considering the elastic material with secant modulus and fixed constraints. However, the horizontal thrust of the arches and more generally of all curved masonry structures changes in the centuries

due to the viscosity of the material (humidity, and other eventual damages of the material) and possible subsidence of the impost over time. This topic is dealt with extensively in Como (2013). The possible variations of the horizontal thrust are presented below.

For instance, an arch or a dome is inserted into a more complex structural system on which they unload their thrust. The impost of the arch or the supporting drum of the dome, under the actions transmitted to them and undergoing a small deformation, are sufficient to determine the slight yield to imposts.

In the columns of historic masonry buildings and generally in complex buildings we are in the presence of uncertain conditions on the loads that can influence our judgment on the stability of the column even more than the uncertainty on the mechanical parameters of the masonry. Therefore, it is important to quantify the possible variation in the extent of the horizontal thrust and to estimate the possible variation of the points of application of the loads.

In his book, Como (2013) indicates how, due to the effect of viscous deformations and the relaxation of the constraints, the value at the limit state of the horizontal thrust tends to a minimum value. The main aspects of the Como treatment justify the following reliability analysis of column B4 are presented in a concise manner below.

5.3.3.1 The limits of the arch thrust: minimum and maximum

The thrust exerted by the masonry arch under assigned distributions of forces is an essential feature of the arch mechanics. If the arch reaches a state of admissible equilibrium, there will certainly be at least one pressure curve placed inside the arch and funicular of the loads acting.

In general, the position of the pressure curve is uniquely defined as soon as three points are set through which the curve must pass: two at the imposts and one in the keystone of the arch. In general, there are infinite curves of possible pressures. Among all these curves there is the pressure curve that corresponds to the minimum thrust of the arc and that corresponds to the maximum.

For the arch in Figure 5.11, the dotted curve is the minimum thrust one, the continuous line is the maximum thrust one. Here, it is noted that the pressure curve relating to the minimum thrust creates an axis curve inside the bow that has the minimum light and the maximum deflection, while the axis curve relating to the maximum thrust has

maximum light and minimum deflection. All these possible thrusts include the thrust actually exerted by the bow.

The evaluation of this thrust constitutes a complex problem with no simple solution. On the other hand, this evaluation is necessary, as it allows to verify the structures on which this thrust is unloaded. In general, according to Como (2013), it is the minimum thrust that, as a rule, can best approximate the thrust actually present.

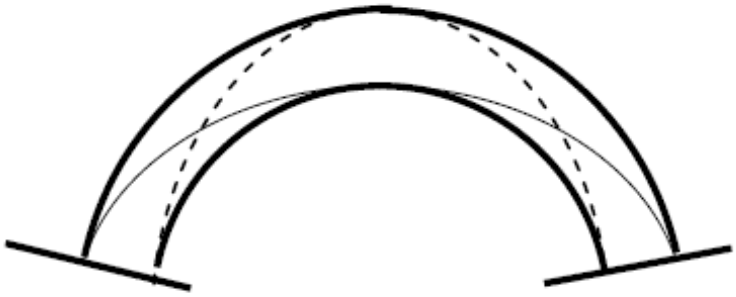

Figure 5.11: pressure curve corresponding to the maximum and minimum thrust.

5.3.3.2 Possible causes of the variation of the thrust

5.3.3.2.1 The effect of elastic deformation on the thrust of the arch

Various aspects affect the thrust of the masonry arch and it may be useful to examine the evolution of stress during the construction process. The arch is first built on the rib. At the end of construction, before dismantling, the bow is unloaded, as all the weight of the bow rests on the rib. When the bow is disarmed, the arch goes into compression and pushes against the springers. Immediately after dismantling, the arch is subject to uniform compression: the funicular of the loads coincides with the axis of the arch.

The corresponding thrust exerted by the bow is then simply evaluated. In fact, if L is the arc span measured on its axis, f is the corresponding arrow and M_c indicates the bending moment at the middle section of the corresponding supported beam, with the same span of the arch and the same distribution of loads, the thrust H of the arch is:

$$H = \frac{M_C}{f} \tag{5.4}$$

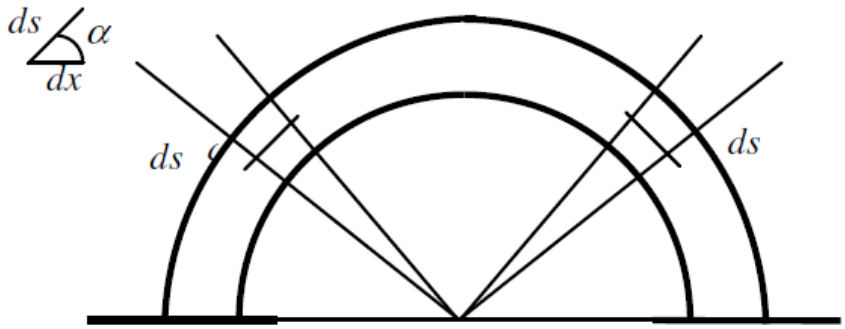

Figure 5.12: elastic contraction of two symmetrically voussoirs.

In particular, if the load p is constant and the arch is parabolic, it can:

$$H = \frac{pL^2}{8f} \tag{5.5}$$

Since the arch goes into compression, all its segments undergo elastic shortening of all voussoirs (Figure 5.12). There is therefore an immediate drop in thrust and the pressure curve rises in the key section. The calculation of this thrust drop can be carried out by referring to the elastic diagram of the arch. Due to the magnitude of the stresses involved, the occurrence of the thrust fall ΔH does not determine the state of traction in the sections. The thrust fall ΔH is then determined by imposing that it must be such as to produce an elastic distance between the springers of the arch equal and opposite to the approach that occurs between them due to the elastic shortening of the arch under the loads acting on the disarming, as shown in Figure 5.13.

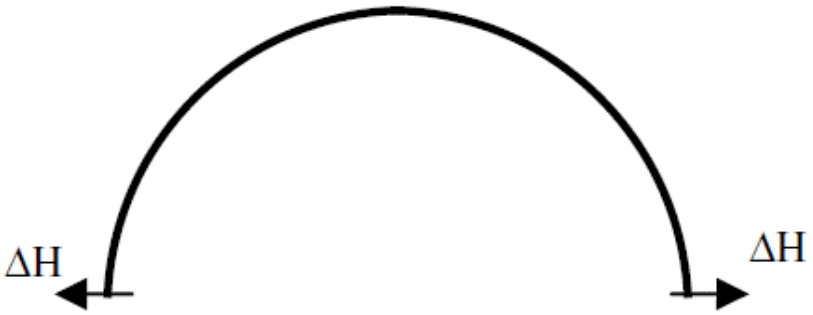

Figure 5.13: extension of the springers due to the thrust drop ΔH.

The presence of mortar joints, also due to their viscous deformability, produces over time a further shortening of the arch axis, greater than would occur in the absence of joints, due to the elastic deformability of the segments in stone. The presence of mortar joints therefore produces a greater drop in thrust and ultimately a more reduced thrust at the springers.

5.3.3.2.2 Cracking of the arch

A masonry arch usually has a presence of a crack characterized by the presence of a lesion on the intrados, near the key section. This behavior will be defined as physiological. A more accurate inspection shows the presence of similar lesions on the extrados, near the haunches. This cracking can be motivated by the thrust drop that occurs in the arch when it is disarmed. The assessment carried out of the extent of this drop in thrust, however, makes it possible to exclude that this is responsible for this cracking.

It is almost inevitable in a masonry arch, and particularly in a historical arch, to find lesions in the intrados between the joints, near the key section. If this happens, unless the arch does not have initial construction defects, it must be assumed that a springer failure has actually occurred due to the thrust of the arch. The case of the arch that is grafted between two piers or between two side walls is still very frequent. In this case, a very slight rotation of the foundation of the piers involves a slight widening of the springers of the arch or of the vault responsible for the crack in key. In an arch of a historic building, therefore, if a slight crack appears in the intrados in the key, it is almost certain that small subsidence has occurred with consequent slight enlargement of the springers.

5.3.3.3 Interpretation of the minimum thrust within the limit analysis of arches in no-tension material

The development of slight subsidence in the imposts of an arch is a practically certain event during the time. In this case, the masonry arch follows the subsidence that occurs at the imposts and it deforms according to a mechanism, adapting its pressure curve to the kinematics. This involves the development of a hinging on the extrados in keystone and two symmetrical hinges on the intrados depending on the geometry of the arch itself. The pressure curve is then arranged according to the precise geometry regulated

by the condition of the minimum thrust. The behavior of the arch in the presence of subsidence can be interpreted in the context of the rigid masonry model that does not react to traction. In these conditions, the thrust of the arch is the minimum among all those statically admissible. The determination of the minimum arc thrust can therefore develop according to the static method. The kinematic method can be used to obtain summary information both on the location of the hinges on the intrados and on the extent of the thrust. In the case of a parabolic arch (Figure 5.12), the minimum thrust is obtained with a mechanism characterized by the presence of hinges to the imposts on the intrados. The procedure described in the following is developed in Como (2013) and is apparently more precise, however let us remark that the arches of the cathedral of Saint George appear far from a collapse incipient.

Figure 5.14 describes the pressure curve in conditions of minimum thrust of the semi-circular round arch subject to its own weight. In the right half of the arc the curve of pressures is drawn. The angle $\bar{\alpha}$ identifies the position of the hinge of the failure mechanism.

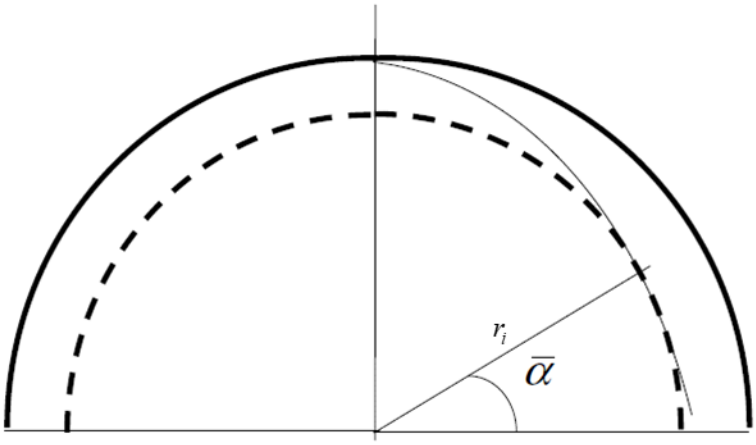

Figure 5.14: The pressure curve for the arch of minimum thrust with the indication of the position of the internal hinge.

5.4 Stability of masonry piers

The stability of the piers has been extensively studied starting with Leonhard Euler in 1744. In the last thirty years, the stability of the masonry pillars under the effect of the load eccentricity has been analyzed. The masonry material consists of brick and mortar, which has a certain tensile strength. This property is a key element in evaluating the load-bearing capacity. One of the frequent assumptions for this material is that the

solid does not resist tensile strength therefore assuming a no-tension material. This assumption for masonry rectangular columns is widespread in structural mechanics and is taken up by the pioneering works of Sahlin (1971), Yokel (1971) and Frisch-Fay (1975), which analyzes the stability of masonry pillars with a single eccentric load. A beam model is assumed for the column and the Authors consider the constitutive model to determine the axis displacement using a second-order differential equation. Subsequently, the problem was analyzed considering a limited compressive strength (De Falco and Lucchesi, 2002, 2003) and extended to circular columns (Broseghini et al., 2018; Gurel, 2016). The effects of viscosity on the stability of the columns is presented in Cecchi and Tralli (2012)

Helpful design tips are also provided through correlations for the ultimate load and initial eccentricity for rectangular and circular sections. These models have also been extended to non-linear constitutive models (La Mendola, 1997; Romano et al., 1993). Finally, models with discretization of the elements with algebraic formulations have also been proposed (La Mendola and Papia, 1993). These models have also been extended to non-linear constitutive models. Finally, models with discretization of the elements with algebraic formulations have also been proposed. An experimental campaign was recently conducted which compared the analytical results for eccentrically loaded dry-stone rectangular pillars (polymethylmethacrylate brickwork pillars) (Gei and Misseroni, 2018). The instability of the pillars and masonry walls due to eccentricity of the load have been extensively investigated also through experimental campaigns (Adam et al., 2010; Brencich and de Felice, 2009; Cavaleri et al., 2005; Drysdale and Hamid, 1983; Hatzinikolas et al., 1980; Sandoval et al., 2011).

5.4.1 Analytical method

This paragraph reports for completeness the analytical treatment for masonry pillars subject to an eccentricity of the load. The main passages useful for dealing with the problem are reported. A more detailed exposition is reported in Como (2013).

The analytical study is linked to what happens with the cracking where the effective depth D of the section decreases while the cracked length of the column increases with the deformations. For this reason, the column can appear as a bar with variable moment of inertia with the significant condition that the variation in inertia is unknown and that it is not symmetrically arranged around the material axis. When the column has zero

tensile strength, cracks will occur at the slightest tendency for traction, the relative stress distributions are trapezoidal in the non-traced area and triangular in the cracked portion.

On the other hand, when the column has a small amount of tensile strength, this will accumulate on the convex face in some sections of the untracked zone, but once the tensile limit has been exceeded and the crack crosses the cross section, it is assumed that the stress concentration will exclude all shapes except the triangular stress distribution (Figure 5.15).

In Figure 5.15, an example of a beam subject to eccentric load is shown. The cross section is sketched on the right-hand side where *b* is and *D* are the width and depth of the cross section, *e* is the eccentricity of load applied *P*, *n* indicates the neutral axis, $\beta = 3w(0)/2$ the height of the compressed part of the cross section at $x = 0$, *x* the coordinate taken along the axis of pillar, *y* is the coordinate taken from the neutral axis, *v(x)* the displacement function of the longitudinal axis and γ the vertical displacement of the load *P*.

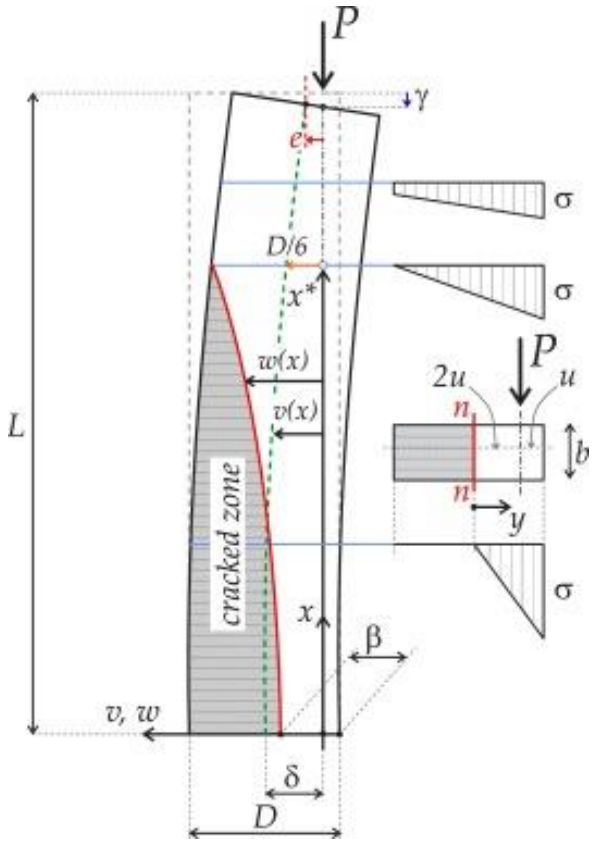

Figure 5.15: geometry and notation used in the analytical solutions in the case of the piers is partially damaged (Gei and Misseroni, 2018).

The parameters that govern the displacement load relations are now reported.

$$L\sqrt{\frac{P}{EJ}} = f\left(\frac{e}{d}, \frac{\delta}{d}, \frac{P}{bd}, \sigma_t\right) \tag{5.6}$$

This phenomenon is governed by various parameters, the main ones of which are: the eccentricity of the load, the dimensions of the section, the load and finally the tensile strength of the masonry.

The instability problem of the masonry pillar can be solved as follows:

A. the load-displacement $P(\delta)$ of the pillar when it is compressed everywhere can be expressed as follows:

$$L\sqrt{\frac{P}{EJ}} = \cos^{-1}\left(\bar{e}/\bar{\delta}\right) \tag{5.7}$$

B. the load-displacement $P(\delta)$ of the pillar when each cross section of the structure is partially damaged can be written as follows

$$L\sqrt{\frac{P}{EJ}} = q\sqrt{1-2\bar{\delta}}\,T\left(\bar{e};\bar{\delta}\right) \tag{5.8}$$

where $q = 3\sqrt{3}/2\sqrt{2}$ and

$$T\left(z;\bar{\delta}\right) = \sqrt{2(1-2z)\left(\bar{\delta}-z\right)} + \left(1-2\bar{\delta}\right)\tanh^{-1}\left(\sqrt{2}\sqrt{\frac{\bar{\delta}-z}{1-2z}}\right) \tag{5.9}$$

the following formula represents the deformed shape:

$$x(v) = L\frac{T\left(\bar{v};\bar{\delta}\right)}{T\left(\bar{e};\bar{\delta}\right)} \tag{5.10}$$

that the space of points in the plane *(x,w)* correspondent to the neutral axes that can be identified analytically as

$$x(w) = L\frac{T\left((1-\bar{w})/2;\bar{\delta}\right)}{T\left(\bar{e};\bar{\delta}\right)} \tag{5.11}$$

C. the pillar is fully compressed in the top part along the longitudinal axis and cracked in the remaining.

$$L\sqrt{\frac{P}{EJ}} = S\left(1/6;\bar{\delta}\right) - S\left(\bar{e};\bar{\delta}\right) + q\sqrt{1-2\bar{\delta}}\,T\left(\bar{e};\bar{\delta}\right) \tag{5.12}$$

where

$$S\left(z;\bar{\delta}\right) = \tanh^{-1}\left\{z\left[\frac{1}{12}\left(\frac{8}{9\left(1-2\bar{\delta}\right)}-1\right)-z^2\right]^{-1/2}\right\} \tag{5.13}$$

The deformed shape of the axis in the cracked part of the pillar can be represented implicitly as

$$x(v) = L\frac{q\sqrt{1-2\bar{\delta}}\,T\left(\bar{v};\bar{\delta}\right)}{S\left(1/6;\bar{\delta}\right) - S\left(\bar{e};\bar{\delta}\right) + q\sqrt{1-2\bar{\delta}}\,T\left(1/6;\bar{\delta}\right)} \tag{5.14}$$

while in the undamaged part, it is

$$x(v) = L\frac{S\left(1/6;\bar{\delta}\right) - S\left(\bar{v};\bar{\delta}\right) + q\sqrt{1-2\bar{\delta}}\,T\left(1/6;\bar{\delta}\right)}{S\left(1/6;\bar{\delta}\right) - S\left(\bar{e};\bar{\delta}\right) + q\sqrt{1-2\bar{\delta}}\,T\left(1/6;\bar{\delta}\right)} \tag{5.15}$$

and the interface is located at

$$x^* = x\left(D/6\right) = L\frac{q\sqrt{1-2\bar{\delta}}\,T\left(1/6;\bar{\delta}\right)}{S\left(1/6;\bar{\delta}\right) - S\left(\bar{e};\bar{\delta}\right) + q\sqrt{1-2\bar{\delta}}\,T\left(1/6;\bar{\delta}\right)} \tag{5.16}$$

In the damaged part, the place of neutral axes is

$$x(w) = L\frac{q\sqrt{1-2\bar{\delta}}T\left(\left(1-\bar{w}\right)/2;\bar{\delta}\right)}{S\left(1/6;\bar{\delta}\right)-S\left(\bar{e};\bar{\delta}\right)+q\sqrt{1-2\bar{\delta}}T\left(1/6;\bar{\delta}\right)} \tag{5.17}$$

Figure 5.16 shows how the displacement load curve varies as a function of eccentricity by means of incremental analysis. As it is possible to observe, an increase in the eccentricity of the load leads to a lowering of the peak of the critical load, resulting in instability of the masonry pillar.

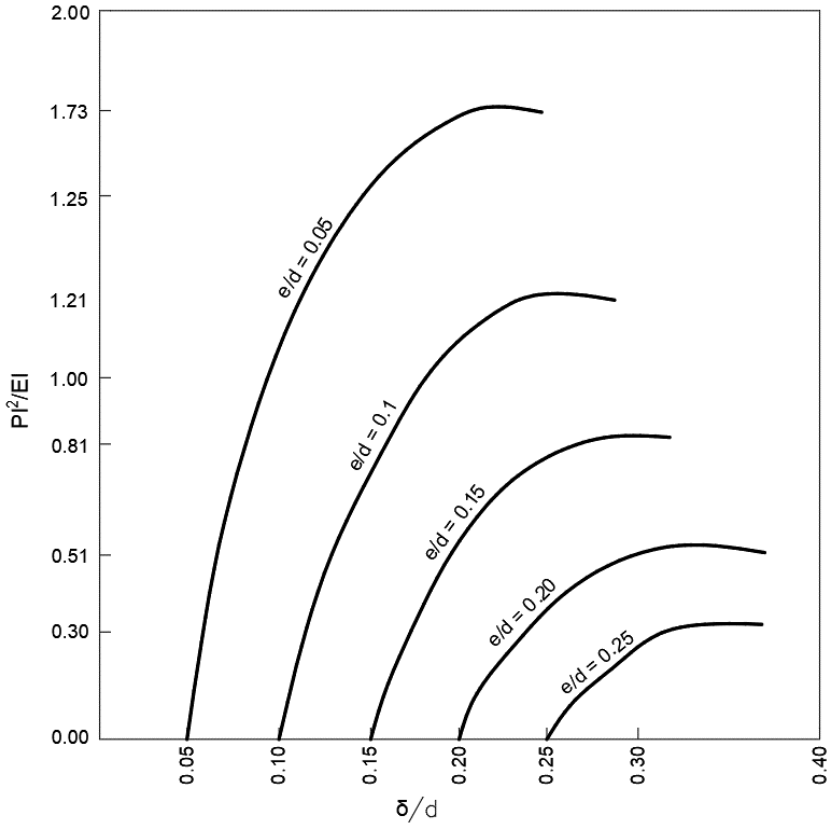

Figure 5.16: load-displacement relation with different load eccentricities (Frisch-Fay, 1975).

5.4.2 International Codes

In addition to the various analytical methods described in the previous paragraph, it is interesting to analyze what is proposed by international standards. In particular, in this paragraph, the Italian and European standards are examined. These methods use a reduction coefficient. This coefficient reduces the load bearing capacity of the wall strictly depends on the geometric parameters, the eccentricity of the load at the top and

the properties of the materials. Furthermore, the coefficient wants to take into account the non-linearity of the material, conditioned mainly by the low tension of the masonry and the geometric non-linearity caused by the lateral deviation of the wall. These approaches are widely used to evaluate the bearing capacity of walls and present some limits for the columns.

5.4.2.1 Italian building construction code (NTC 2018)

The Italian standard provides a compressive and bending stress check for the stability of masonry walls in the case of the Ultimate Limit States (ULS) through a simplified method (§ 4.5.6.2, MIT, 2018). This is allowed in the hypothesis of articulation.
The reduced design unit strength ($f_{d,rid}$) for the structural member is defined as follows:

$$f_{d,rid} = \Phi \cdot f_d \tag{5.18}$$

where Φ is the coefficient of reduction obtained using Table 5.3 and f_d is the design resistance obtained as the ratio between the characteristic compressive strength of the masonry f_k and the partial safety factor γ_M. In the case of existing buildings, the partial safety factor ($\gamma_M = 3$) must be multiplied by the knowledge factor *FC* (MIT, 2019).

$$f_d = f_k / (\gamma_M \cdot FC) \tag{5.19}$$

The reduction coefficient Φ is a function of the conventional slenderness λ and the eccentricity coefficient *m*. The latter coefficient is defined as a function of the eccentricity of the load *e* and the thickness of the wall *t*. Linear interpolation is used for values not present in Table 5.3.

Table 5.3. coefficient of reduction Φ.

	Coefficient of eccentricity m = 6 e/t				
Slenderness λ	**0**	**0.5**	**1.0**	**1.5**	**2.0**
0	1.00	0.74	0.59	0.44	0.27
5	0.97	0.71	0.55	0.39	0.27
10	0.86	0.61	0.45	0.27	0.16
15	0.69	0.48	0.32	0.17	
20	0.53	0.36	0.23		

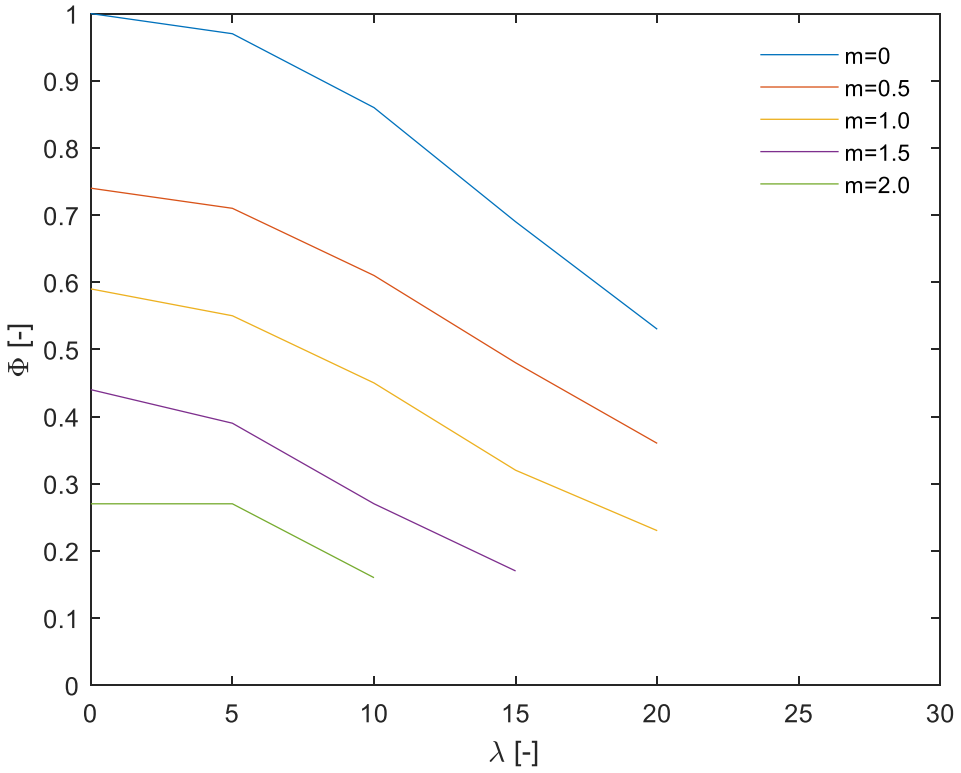

Figure 5.17: capacity reduction Φ as a function of slenderness λ and coefficient of eccentricity *m* in NTC 2018 (MIT, 2018).

Figure 5.3 shows the trend of the reduction coefficient as a function of slenderness and eccentricity. With an increase in slenderness, it is possible to see a decrease in the reduction factor. Similarly, the same thing is found when the coefficient of eccentricity increases.

The same relations developed for the stability of walls are commonly also used to verify the stability of the columns. However, NTC2018 makes reference for the stability of the columns only for the compressive strength of the masonry, that it is drastically reduced. Furthermore, it assumes a rectangular geometry, constraint and load conditions that are not realistic for the problem at hand.

However, the code suggests in this situation to refer to more accurate analyses and standards of proven validity, which are consistent with the principles that are the basis of the Italian standard.

5.4.2.2 European code (EC6)

The EC6 presents a more detailed approach for evaluate the load capacity bearing of masonry elements. The same considerations regarding geometry, load conditions and

constraints of NTC2018 are valid for the Eurocodes as well. These conditions turn out to be unrealistic for piers.

$$f_{d,rid} = \Phi \cdot f_d \tag{5.20}$$

where Φ is the capacity reduction coefficient and f_d is the compressive strength of masonry. The Eurocode 6 provides a formula for the calculation of the reduction coefficient which is:

$$\Phi = \left[\left(1 - 2\frac{e}{t} \right) e^{-\frac{u^2}{2}} \right] \tag{5.21}$$

where e is the eccentricity of applied load and t is the thickness of wall and u a numerical factor described as follows:

$$u = \frac{\lambda - \alpha}{\beta - \rho \frac{e}{t}} \tag{5.22}$$

with α, β, ρ are 0.0063, 0.73 and 1.17 respectively. The parameter is defined as $\lambda = \frac{h}{t}\sqrt{\frac{f_k}{E}}$, where, h is the height of the element, t is the thickness of the element, E is the elastic modulus and f_k is the characteristic compressive strength of masonry.

Figure 5.18 shows how the reduction coefficient varies as a function of slenderness and as a function of the eccentricity of the load. It is possible to see how an increase in slenderness results in a reduction in the coefficient. The same thing is visible as the eccentricity of the load increases.

In recent works (Sandoval et al., 2011), the parameters that characterize the previous formulation are modified to obtain a better approximation of the experimental results reported in the technical literature, without substantially modifying the formulation.

De Falco and Lucchesi (2003) always under the hypothesis of rectangular geometry, constant load and eccentricity, present solutions in the closed form assuming the masonry is not resistant to traction, with perfectly plastic behavior and deformation limited compression. In presence of modest eccentricities, the results coincide with EC6.

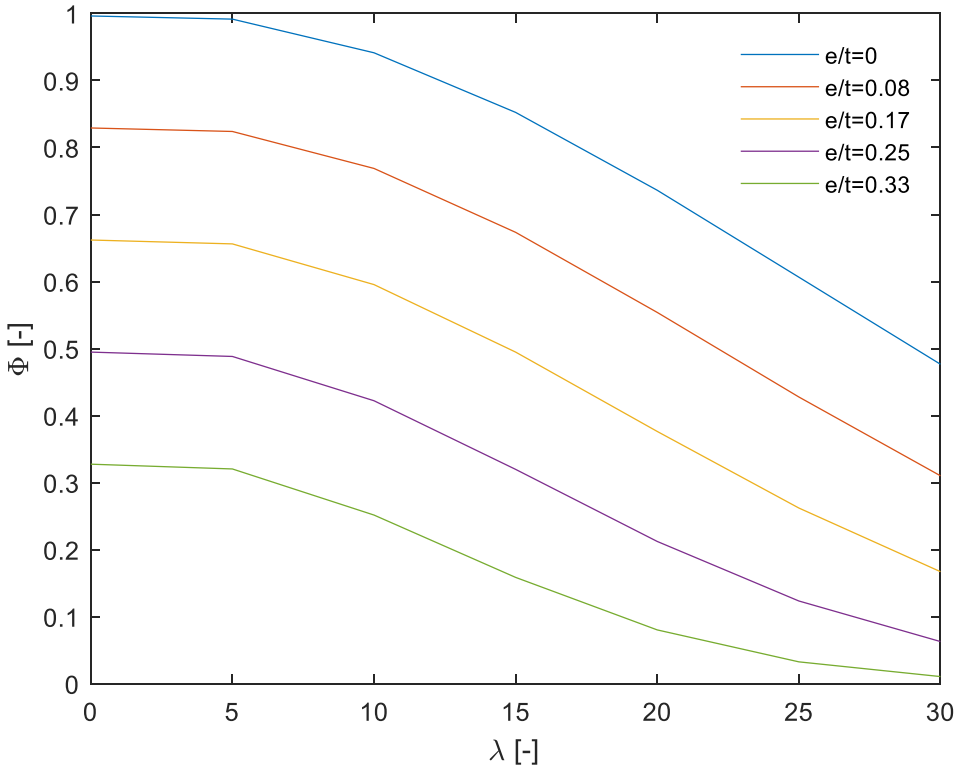

Figure 5.18: capacity reduction Φ as a function of slenderness λ in EC6 (CEN, 2005a).

5.5 Column modeling

The application of both NTC2018 and EC6 appear unrealistic. The column under study has a complex geometry compared to those observed in the literature (Gurel, 2016). Furthermore, in the present case, the cross-section is composed of two elements from different historical periods (medieval and baroque) which are subjected to different loads at different heights. To verify this element and take into account the presence of several different loads and with different eccentricities, irregular geometry and discontinuity of the walls, the only solution would seem to be to resort to 3D modeling of the column using computational techniques such as Finite Element Method (FEM) or Discrete Element Method (DEM). In the case of large and irregularly shaped columns, the analysis in the non-linear field requires a high computational burden; thousands of degrees of freedom are required, compared to a not simple interpretation of the results and an only apparent quality given the uncertainties on the internal conformation of the column and the loads applied.

Therefore, this chapter proposes a verification method that is certainly approximate but able to take into account in a simple, easy to interpret and computationally inexpensive way of the specific characteristics of the columns under examination.

5.5.1.1 Finite Element Method Model

Fort the case study of a masonry column, a finite element model of the column was developed in which the design loads provided by the designers were applied.

The numerical model of the column and the mechanical analysis were performed using the ABAQUS FEM package (SIMULIA, 2006).

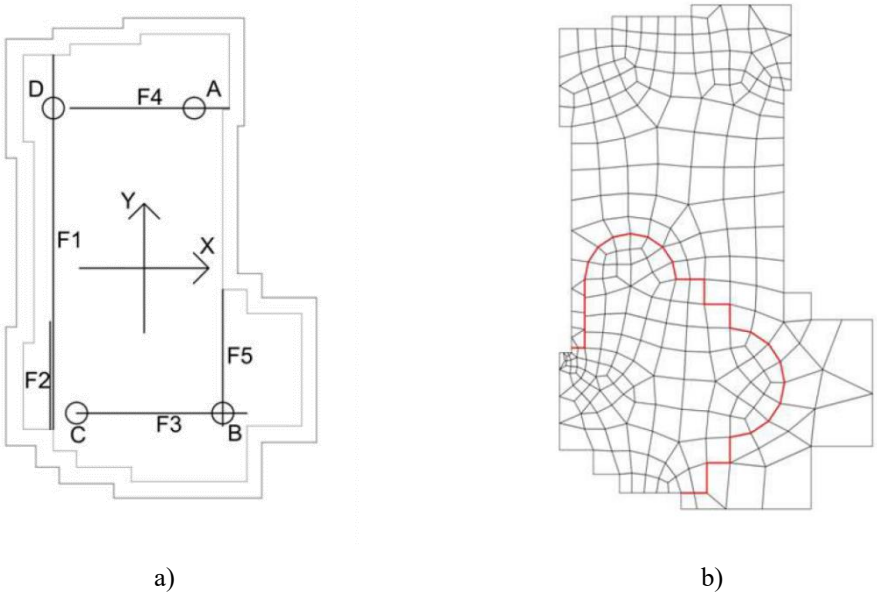

a) b)

Figure 5.19: load distribution and mesh in the section used for the FEM model.

5.5.1.2 Constitutive law

The stress-strain relationship of masonry in compression is non-linear and may be taken as linear, parabolic, parabolic rectangular or as rectangular, for the purposes of designing a masonry section. This is proposed by EC6 (CEN, 2005a).

The nonlinear behavior of the material is examined through the Concrete Damage Plasticity (CDP) constitutive model. This model is extensively employed to describe the nonlinear properties of masonry and concrete structures. This model was first suggested for the analysis of reinforced concrete (RC) structures (Alfarah et al., 2017; Lubliner et al., 1989). CDP is described by a multi-dimensional elastoplastic yield surface, where its change depends on the uniaxial damage failure model under tension and compression. The failure surface coincides with the Drucker-Prager yield

function, which can be switched to Mohr-Coulomb criteria through a parameter K_c (Figure 5.20).

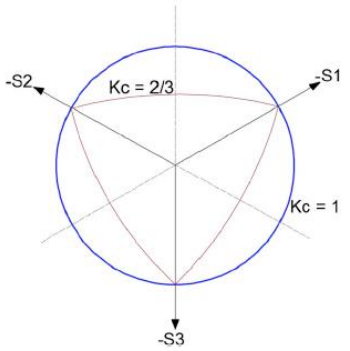

Figure 5.20: Drucker-Prager and Mohr-Coulomb failure surfaces in Abaqus

A parameter called “eccentricity” regularizes the surface to avoid numerical instabilities. The different behavior under compression and tension is provided by a parabolic softening in compression and an exponential or linear softening in tension (Figure 5.21).

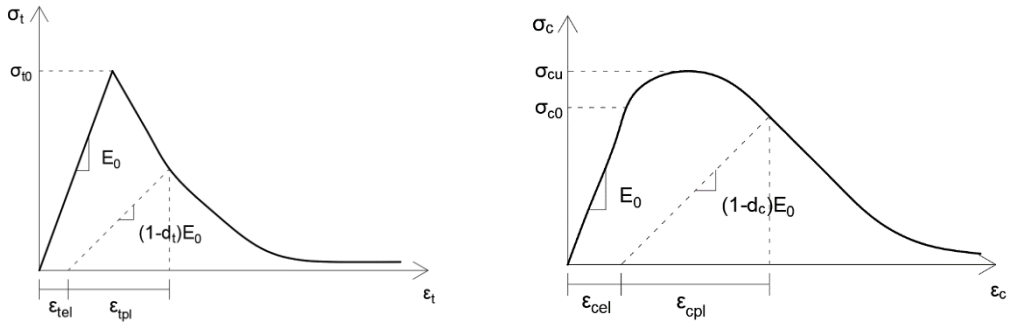

a) b)

Figure 5.21: constitutive law: a) traction and b) compression.

The corresponding degradation of the elastic stiffness is regulated by two parameters d_t and d_c, which are correlated with the plastic strain. The damage variables range in the interval from 0.0 to 1.0 which corresponds to an undamaged material to a total loss of strength. This approach permits a linear softening in tension and it is used in these analyses. (Figure 5.21).

The parameter of viscosity is usually assumed in a range of 0.0001–0.0005. In these analyses, a value of 0.0003 is assumed in order to obtain a fair compromise to ensure reliable results and to have a good convergence. The values used in the analyses to define the yield surface are reported in Table 5.4.

Table 5.4: parameter for the Concrete Damage Plasticity constitutive model.

Parameter	Value
dilatation angle ψ	10°
flow potential eccentricity *e*	0.1
K_e	0.667
viscosity parameter	0.0003

5.5.1.3 Limitations

The FEM gives results that are compatible with the analytical and numerical model. Given the complexity of the fem model adopted, the use of this model in the stochastic analysis is complicated and burdensome from a computational point of view. The use of emf in stochastic areas does not always manage to correctly grasp and characterize the uncertainties due to the large number of variables involved. In fact, as shown in Babuška and Motamed (2016) for composite materials, stochastic multiscale models such as stationary random fields, which are based on precise probability theory, are not capable of correctly characterizing uncertainty in fiber composites.

Advanced stochastic models based on imprecise uncertainty theory and used by fuzzy stochastic models would be able to accurately describe this problem. In the case of masonry, given the complexity of the constitutive laws, the robustness of the method is difficult to control as careful calibration is required. It is precisely for this reason that the simplification adopted of the beam model allows having an easily controllable model combined with an acceptable computational time.

5.5.1.4 Comparison of FEM model with Italian and European standard

The masonry material is considered a module for long-term loads based on the short-term secant module ($E = 1000f_k$), reduced by a coefficient that takes into account the creep effects as provided by Eurocode 6 (CEN, 2005b; § 3.7.2).

$$E_{long-term} = \frac{E}{1+\phi_\infty} \tag{5.23}$$

Where $\phi_\infty = 1$ is the final creep coefficient and $E_{long\text{-}term} = 500f_k$ is the long-term modulus. In literature for masonry columns and walls, the long-term behavior has been analyzed considering the creep phenomena under high levels of stress (Como, 2013;

Verstrynge, Schueremans, and Van Gemert, 2011; Verstrynge, Schueremans, Van Gemert, et al., 2011).

Many models developed to analyze the long-term behavior of masonry were considered by calibrating the models with empirical and semi-empirical methods (Choi et al., 2007). These models have as a critical aspect the lack of generality that derives from specific situations (Papa and Taliercio, 2005; Saisi et al., 2008). Some works try to give a rigorous model for the behavior of masonry walls over time by means of viscoelastic models. Cecchi and Tralli (2012) develop a viscoelastic model in analytical form for the masonry walls together with homogenization procedures.

In order to evaluate the stability of the masonry column, it was decided to carry out an incremental analysis of the column considering the actual section. The mechanical properties of the masonry have been reduced by their safety factor. In this way, by increasing the loads, the multiply found corresponds to the reduction coefficient defined by the various codes.

In Figure 5.22 it is possible to see the trend of the displacement multiplier curve. The multiplied result at break is equal to 0.89 for the column under study. In carrying out the analyzes, a non-linear constitutive law for the material was assumed and the geometric non-linearity was considered. The non-linear nature of the material can be grasped by evaluating the relative deformations and tension for the various increments as shown in Figure 5.23.

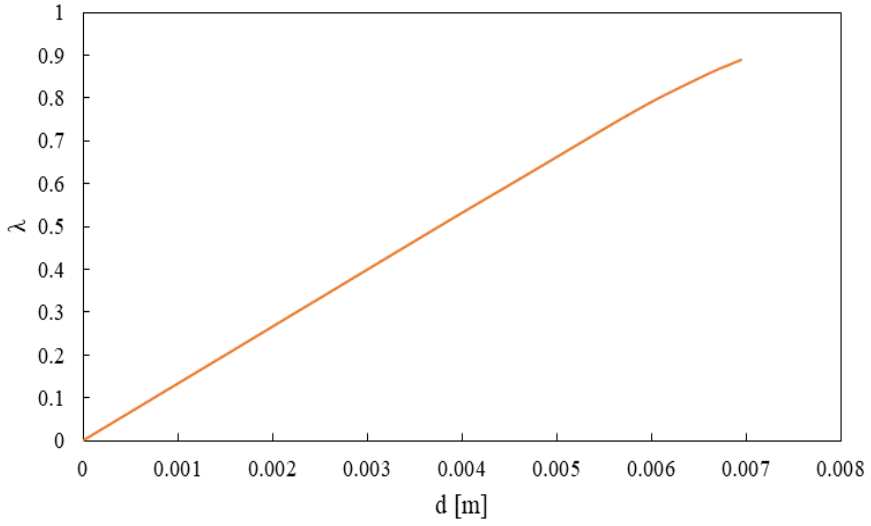

Figure 5.22: multiplier – displacement relationship for the column.

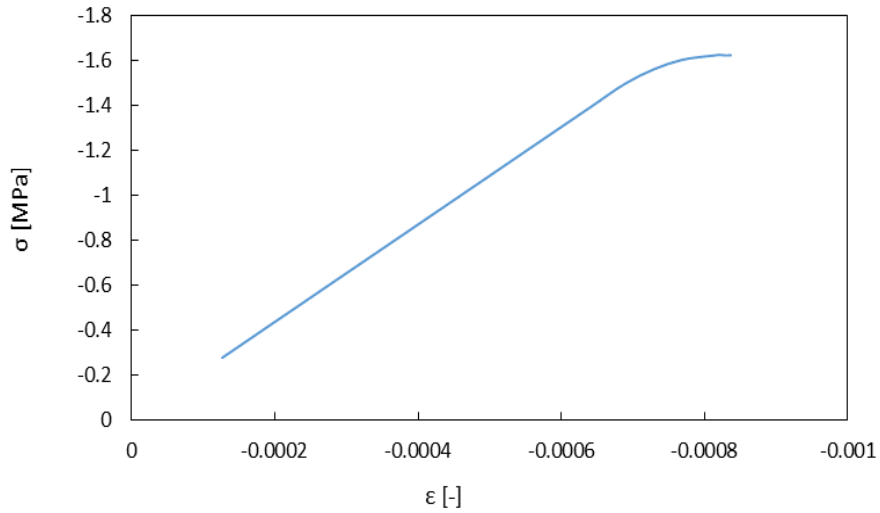

Figure 5.23: tension – deformation relationship of the most stressed element.

The formula suggested by Italian and European legislation considers only a load at the top for a masonry wall, However, the actual case of S. George pillars appears quite different.

Table 5.5 shows the results obtained considering the different codes (NTC 2018, EC6, CTS Toscana Region Advice). For the sake of completeness, the CTS is the regional technical-scientific committee on seismic risk. The purpose of this committee is to provide advisory advice on legislation and design. It is possible to see how the Italian legislation for the case under study is the most conservative of the methods adopted.

Table 5.5: capacity reduction factor for different standard and numerical simulations.

	NTC 2018	EC6	CTS Advice	FEM Results
Φ	0.82	0.87	0.87	0.89

5.5.2 The Beam Model proposed

In this section, we propose a simplified model to evaluate the structural response of the column. The choice of this model is driven by reducing computational times for analyzes in the stochastic context.

5.5.2.1 Approximation of the thrust curve

It is assumed that the masonry columns have load and restraint conditions such that the characteristics of the stress due to the external vertical and horizontal loads and to their own weight are known in all sections. In other words, the thrust curve is assigned,

which, in the absence of distributed loads, will be straight and in the presence of distributed actions, will be curvilinear (Figure 5.24).

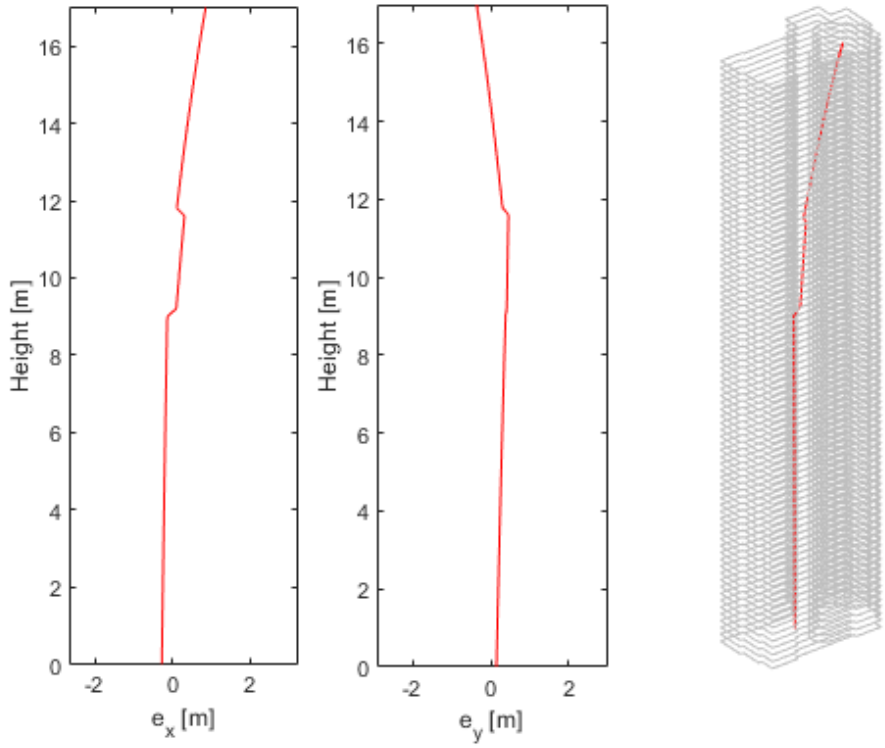

Figure 5.24: thrust curve along *x*-axis, *y*-axis and in axonometric view.

N control sections are introduced to check the admissibility of the stress state, these sections contain all the sections where concentrated actions are applied, both vertical and horizontal, due to the discharges of the arches and vaults that weigh on the column. Flexural moments (i.e. vertical loads and eccentricities) are assumed constant between two successive control sections so only normal vertical stresses are considered. Obviously, as *N* increases the pressure curve thus approximated converges to the exact one.

5.5.2.2 Masonry constitutive law

Given the simplicity of the model, the assumption of no tension behavior for the masonry can be easily introduced. This simplification is compatible with the small and often difficult value to estimate tensile strength.

The uniaxial behavior of masonry can be idealized with three simplified models (Angelillo et al., 2014): zero, one and two. The definition of these models comes from the

number of parameters used to define them (Figure 5.25).

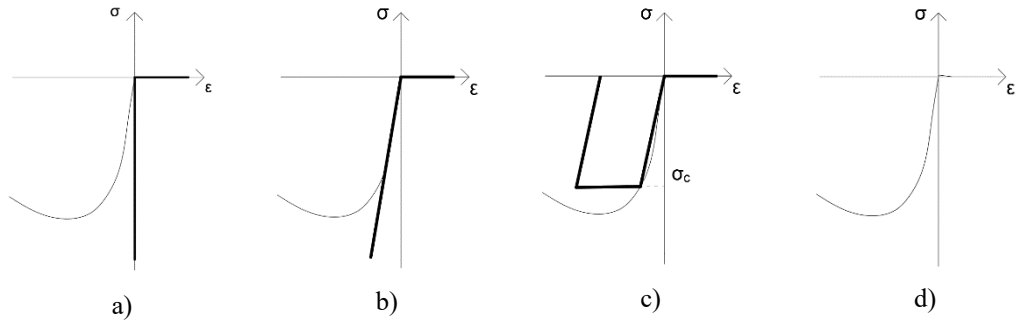

Figure 5.25: masonry constitutive law in the case of uniaxial behavior: (a) model zero, (b) model one, (c) model two and d) real constitutive law (Angelillo et al., 2014).

Model one assumes a linear ratio between stress and strain in compression. This constitutive law needs only one parameter: the elastic modulus E. Model two assumes an elastic perfectly plastic law with limited strength σ_c in compression.

These models appear quite rudimentary and very simple, however, according to (Como, 2013; Heyman, 1995; Huerta, 2006), this option represents a correct choice for old masonry structures given the difficulty of defining some parameters of the structure due to the uncertainties associated with loads, constraint conditions and material properties.

In our case in question, having to do a stochastic analysis of the column, the most efficient computational strategy to evaluate the reliability of the column is through this simplified constitutive model. In the structural beam model, linear elastic model and elastic perfectly plastic model were used. The simplest solution is to consider the Heyman hypothesis of infinite shear strength valid, that is to verify only at normal stresses. However, it seems possible, once the tangential tensions are known, to assume, for the crisis function, a crisis function with the associated flow as shown in Figure 5.26.

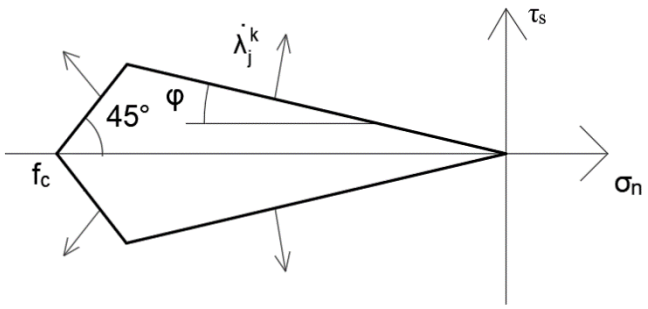

Figure 5.26: interface failure surface.

5.5.2.3 Hypothesis on the stress state

In analogy with the classic hypotheses of de Saint Venant theory, only the following components of the stress tensor are assumed to be different from zero: σ_z, σ_{xz}, σ_{yz}.
Based on the assumption in Section 5.5.2.1, which approximates the thrust curve with bending moments constant in each interval, in the *N*-1 sections only the normal stresses σ_z assumed to be non-positive will be different from zero.

5.5.2.4 Conservation of the cross-sections

The hypothesis of conservation of flat sections is usually accepted for one-dimensional elements even in the presence of non-linear behavior of the material, e.g. the fiber model used for columns in reinforced concrete (Frangopol et al., 1996; Lee and Mosalam, 2004). With reference to Figure 5.19 denoted by *w* the axial component of the displacement, *w*° its value at the arbitrary origin of the axes and ϕ_x and ϕ_y the rotations around the coordinate axes (generic as long as orthogonal) we have:

$$w(z) = w^0(z) + \phi_x(z)\,y - \phi_y(z)\,x \tag{5.24}$$

By virtue of the assumption of Section 5.5.2.1, the axial displacement varies linearly in each of the *N*-1 or

$$w^0(z) = w^{0'}z\,,\ \phi_x(z) = \phi_x'(z)\,,\ \phi_y(z) = \phi_y'(z) \tag{5.25}$$

Therefore, also the deformations ε_z in each section are linear in *x* and *y*, that is, they lie in a plane

$$\varepsilon_z = w^{0'} + \phi_x' y - \phi_y' x \tag{5.26}$$

In the elastic field also the σ_z is linear in *x* and *y*, while for no tension or elastic-plastic material this assumption is not consistent.

5.5.2.5 Principle of stationary Potential Energy

In the presence of uniaxial problems, it is possible to obtain in the case defined in Section 5.5.2.2 the state function of deformation energy $\phi(\varepsilon)$ represented in the case of no-tension and elastic-perfectly plastic material in compression.

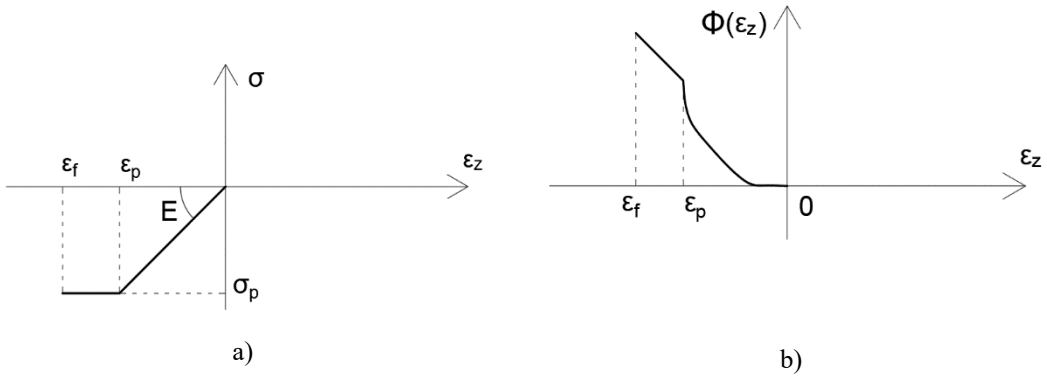

a) b)

Figure 5.27: constitutive law (σ-ε) and deformation energy ϕ.

The potential energy for the generic trait *n* of height h_n can be written as follows:

$$\Pi\left(w^0,\varphi_x,\varphi_y\right)=\int_0^{h_b}\int_A\phi(\varepsilon_z)dA-\int_A\left(Nw^{0'}+M_x\varphi'_x+M_y\varphi'_y\right)dA \qquad (5.27)$$

The stationarity of Π, Π=0, gives the three equations of equivalence between the stress characteristics *N*, M_x, M_y and the normal stresses (σ_z).

$$\begin{aligned} N &= \int_A \sigma_z(\varepsilon_z)\,\mathrm{dA} \\ M_x &= \int_A \sigma_z(\varepsilon_z)\cdot y dA \\ M_y &= -\int_A \sigma_z(\varepsilon_z)\cdot x dA \end{aligned} \qquad (5.28)$$

In the case of linear elastic material, the three equations are linear and their solution, in the case of a barycentric and principal reference system, provides the classic Navier formula.

5.5.2.6 Single beam model

In this paragraph, the model of the single beam is shown. This model describes the behavior of the column under the action of loads. This approach can be extended to any type of column section. Figure 5.28 shows the section of the column present in the cathedral.

The calculation of the stress state can be traced back to the solution of *N* (or *N+1*) systems of 3 algebraic equations, generally non-linear 5, in the 3 unknowns w'^{o}, ϕ_x', ϕ_y', and in the calculation of σ_z, therefore in the stress calculation directly from the relations σ_z (ε_z).

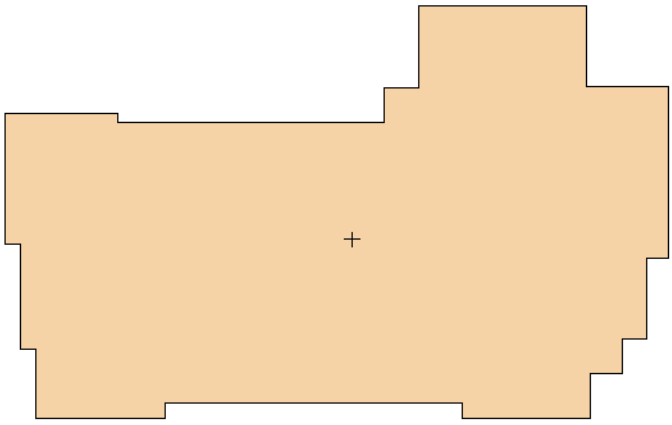

Figure 5.28: section of the column.

The section can then be written as follows:

$$\begin{bmatrix} A & S_y & S_x \\ S_x & I_{xy} & I_x \\ S_y & I_y & I_{xy} \end{bmatrix} \cdot \begin{bmatrix} w'_0 \cdot E \\ \varphi'_x \cdot E \\ \varphi'_y \cdot E \end{bmatrix} = \begin{bmatrix} N \\ M_x \\ M_y \end{bmatrix} \tag{5.29}$$

where A is the area of the section, S_x is the first moment of area in the x-direction, S_y is the first moment of area in the direction y, I_x denotes the moment of inertia around the x-axis, I_y denotes the moment of inertia around the y-axis, I_{xy} is the moment of inertia around the y-axis when the objects are rotated around the x-axis, N is axial force, M_x is the bending moment along x, M_y is the bending moment along y.

Given the system, it is possible to subsequently calculate the quantities useful for evaluating the behavior under the loads of the column.

A. Stresses and strains

The solution is sought according to the following scheme:

1. Checking the position of the pressure center and entering the values of N, M_x and M_y.
2. Solution in the hypothesis of linear elastic material. It is about calculating the Area, the static moments and the moments of inertia of a figure generally known as a polygon.
3. The ε_z calculated in the previous iteration can be greater than 0, and the

intersection line with the initial figure can be expressed by the area A_0, which identified the area with zero stresses. A new area is identified in which the inertial areas and quantities will be calculated in order to solve the system.

4. Calculate the ε_z and σ_z and fix a convergence check. If it is violated you go back to Step 2.

In the case of the non-linear behavior of the masonry that includes an elastic-plastic section, the relative area is identified and the necessary quantities are recalculated.

B. Displacement

Starting from the base of the column where null displacements are assumed for each section, w is known that varies linearly and the constant curvatures ϕ' in a fixed reference. Neglecting the contribution to the displacement due to the Poisson's ratio, we calculate for each segment a displacement u, according to x, and v, according to y, piecewise parabolic. It is trivial to proceed by successive sections to reconstruct the displacement in z. (It will be a continuous function with discontinuous second derivatives or even more brutally a broken one if we start from rotations)

C. Nonlinear geometric effects

Once the deformation is known, the position of the vertical loads and their eccentricities are updated and a second-order analysis is carried out with the above procedure and then recalculating the displacements. Obviously, a convergence parameter is introduced and if necessary, it is repeated.

The following paragraphs report the results of the analyzes defined by a linear elastic constitutive law and with a no tension material.

5.5.2.6.1 Linear elastic material

The trend of deformations and tensions in the column is shown in Figure 5.35, assuming a linear elastic material. In this figure, it is possible to see the maximum and minimum values in the various sections along the height. A part of the column is in traction in particular between 4 and 11 meters. As far as the displacements are concerned, they are compatible with those obtained for the FEM analyzes. In particular, the displacements in the y-direction are more relevant than the x-axis (Figure 5.30).

LINEAR ELASTIC

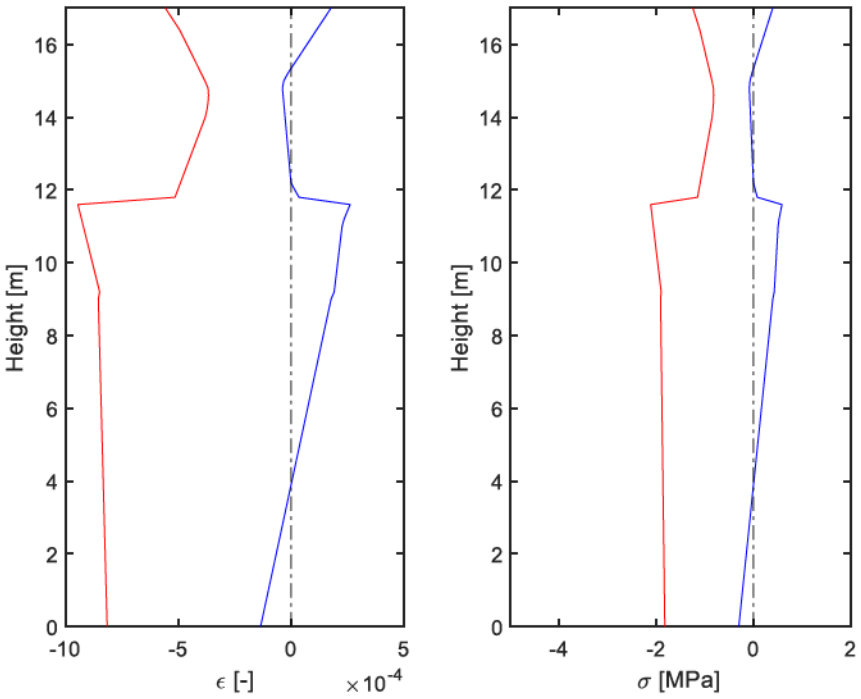

Figure 5.29: trend of maximum and minimum deformations (left); trend of the maximum and minimum stresses (right) in the various sections of the column.

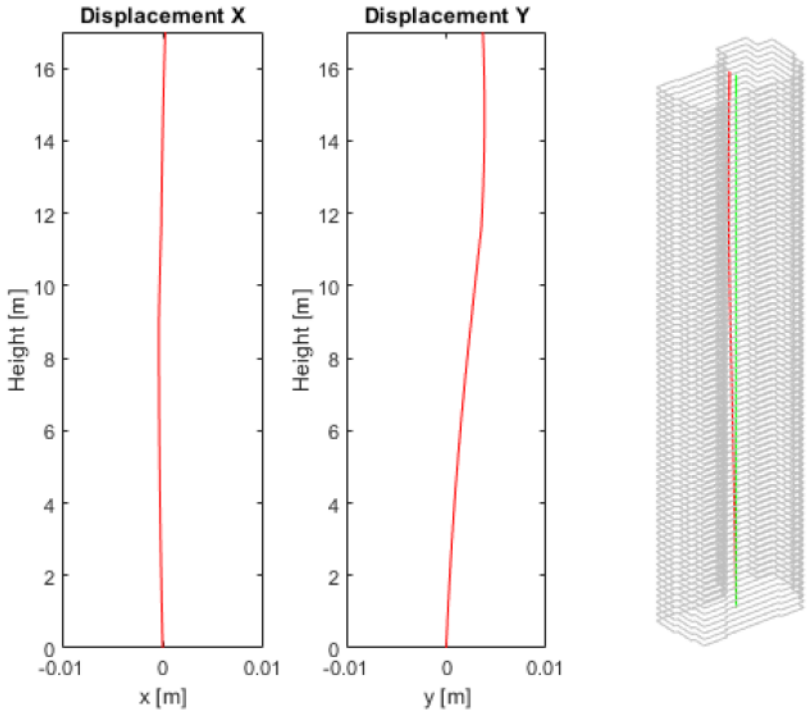

Figure 5.30: displacement diagram along the x-axis and the y-axis of the column.

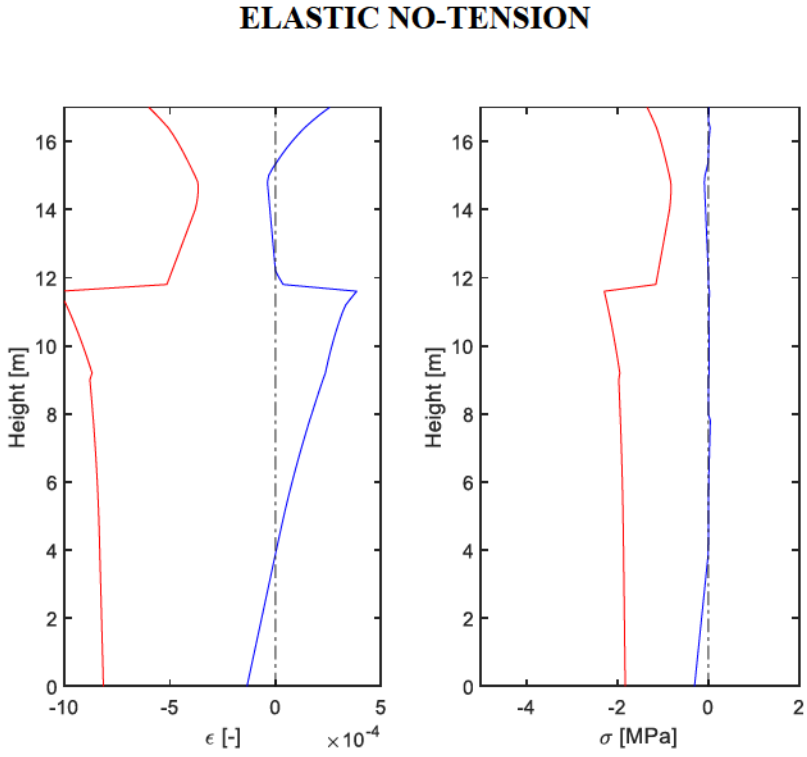

Figure 5.31: trend of maximum and minimum deformations (left); trend of the maximum and minimum stresses (right) in the various sections of the column.

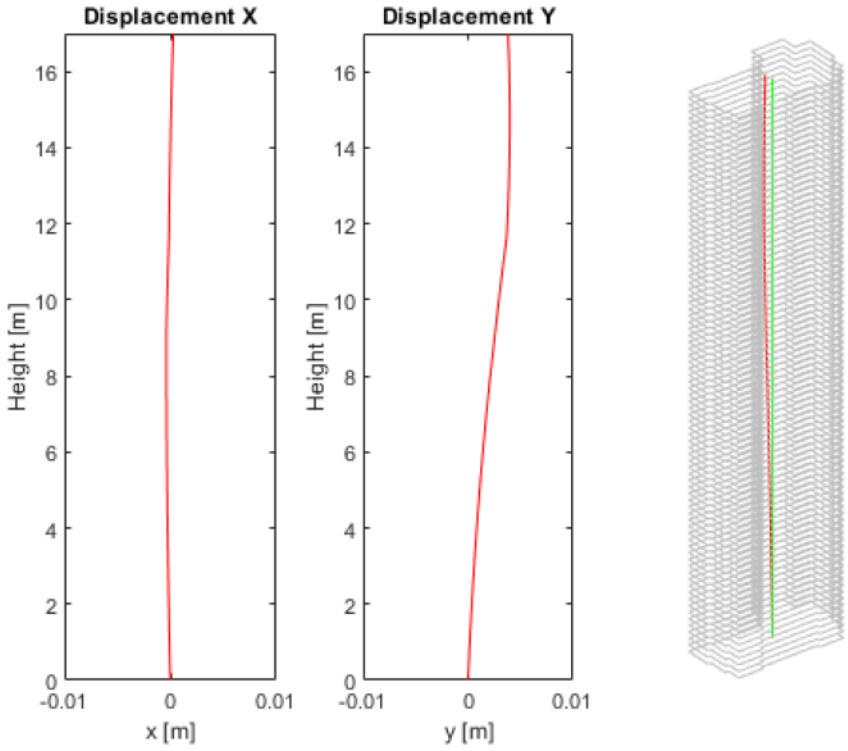

Figure 5.32: displacement diagram along the x-axis and the y axis of the column.

5.5.2.6.2 Elastic no-tension constitutive law

A further next step is to analyze the behavior of the structure considering a no-tension law for the masonry material. Figure 5.31 shows the trend of the maximum and minimum deformations along the height of the column.

The significant thing is the part where the tensile stresses are zeroed thanks to the constitutive model adopted. In particular, this occurs between 4 and 11 meters.

5.5.2.7 Two beams model

For taking into account that the medieval and baroque columns do not appear connected a second model is used. This adopted structural scheme has some similarities with what is proposed for braced frames (Pozzati, 1977). In particular with the walls that are connected to each other by means of uprights (Chitty, 1947).

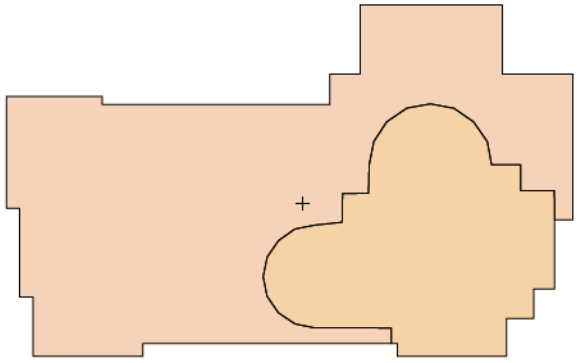

Figure 5.33: section of the two connected column: medieval section (clearer), eighteenth-century section (lighter).

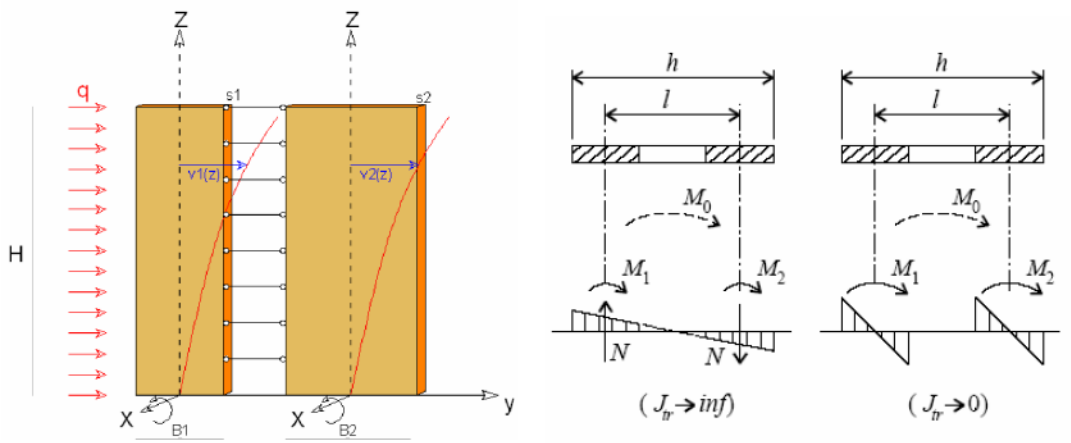

a) b)

Figure 5.34: model proposed by Rosman-Beck (Pozzati, 1977).

If the columns are completely distinct, the three equilibrium equations for each column Eq. (5.29) are written separately and there are 6 equations with 6 variables.

Since the horizontal displacements (v_1 and v_2) are equal along z i.e., the deformation of the axis lines is affine, the two columns have the same curvatures ϕ'_x and ϕ'_y. The equilibrium equations from 6 are reduced to 4. The equilibrium equations for rotation are reduced to 2, the integrals are extended to the entire compound section and the moments M_x and M_y are the overall external ones. There are 2 distinct equations to the translation in z, where the integrals are extended to a column as the known term represents the normal stress applied to the medieval or eighteenth-century column.

Figure 5.34 shows the comparison between the case of the integral section and the one under examination where, being the rotation and the curvature of 1 and 2 equal, the displacement diagrams and the deformation diagrams have the same inclination.

The system of equations that allows you to evaluate the variables is shown below:

$$\begin{bmatrix} A_1 & S_{y_1} & S_{x_1} & 0 & 0 & 0 \\ S_{x_1} & I_{xy_1} & I_{x_1} & 0 & 0 & 0 \\ S_{y_1} & I_{y_1} & I_{xy_1} & 0 & 0 & 0 \\ 0 & 0 & 0 & A_2 & S_{y_2} & S_{x_2} \\ 0 & 0 & 0 & S_{x_2} & I_{xy_2} & I_{x_2} \\ 0 & 0 & 0 & S_{y_2} & I_{y_2} & I_{xy_2} \end{bmatrix} \cdot \begin{bmatrix} w'_{0_1} \cdot E_1 \\ \varphi'_{x_1} \cdot E_1 \\ \varphi'_{y_1} \cdot E_1 \\ w'_{0_2} \cdot E_2 \\ \varphi'_{x_2} \cdot E_2 \\ \varphi'_{y_2} \cdot E_2 \end{bmatrix} = \begin{bmatrix} N_1 \\ M_{x_1} \\ M_{y_1} \\ N_2 \\ M_{x_2} \\ M_{y_2} \end{bmatrix} \tag{5.30}$$

where subscript 1 indicates the eighteenth-century section while subscript 2 indicates the medieval section. A_1 and A_2 are the area of sections, S_{x_1} and S_{x_2} are the first moment of area in the x-direction, S_{y_1} and S_{y_2} are the first moment of area in the direction y, I_{x_1} and I_{x_2} denote the moment of inertia around the x-axis, I_{y_1} and I_{y_2} denote the moment of inertia around the y-axis, I_{xy_1} and I_{xy_2} are the moment of inertia around the y-axis when the objects are rotated around the x-axis, N_1 and N_2 are axial force, M_{x_1} are M_{x_2} the bending moment along x, M_{y_1} and M_{y_2} is the bending moment along y.

These axial forces and bending moments are distributed according to the areas and moments of inertia of the sections (Pozzati, 1977). They are defined as follows:

$$N_1 = N\frac{A_1}{A_1 + A_2} \qquad N_2 = N\frac{A_2}{A_1 + A_2}$$

$$M_{x_1} = M_x\frac{J_{x_1}}{J_{x_1} + J_{x_2}} \qquad M_{x_1} = M_x\frac{J_{x_1}}{J_{x_1} + J_{x_2}} \tag{5.31}$$

$$M_{y_1} = M_y\frac{J_{y_1}}{J_{y_1} + J_{y_2}} \qquad M_{y_2} = M_y\frac{J_{y_1}}{J_{y_1} + J_{y_2}}$$

where N, M_x and M_y are quantities already calculated for the single beam.

The following paragraphs report the results of the analyzes defined by a linear elastic constitutive law and with a no tension material.

5.5.2.7.1 Linear elastic material

Figure 5.35 shows the maximum and minimum trend of stresses and strains for the composite column. The section of the eighteenth-century column between 6 and 11 meters is in traction while the medieval section is in traction only between 9 and 11 meters. Therefore, when the hypothesis of no-tension is considered, these areas will have a partialization of the sections.

Figure 5.36 shows the displacements for the columns made up of the medieval one and the eighteenth-century one. The same shape can be seen in both deformations in both x and y directions. Of course, given the nature of the loads, the displacements are greater along the y-direction.

5.5.2.7.2 Elastic no-tension constitutive behavior

Once the elastic analysis was carried out, the case with the no tension elastic material was analyzed. As in the previous analysis, the column is made up of two columns to which the curvatures in their directions are considered equal.

As for the elastic case, the maximum and minimum values of the deformations are equal. The tensions change, especially the traction ones due to the different constitutive law. In fact, in this case the tensile stresses are zeroed (Figure 5.37). Having calculated the deformations, it is possible to obtain the displacements relative to the two sections.

LINEAR ELASTIC

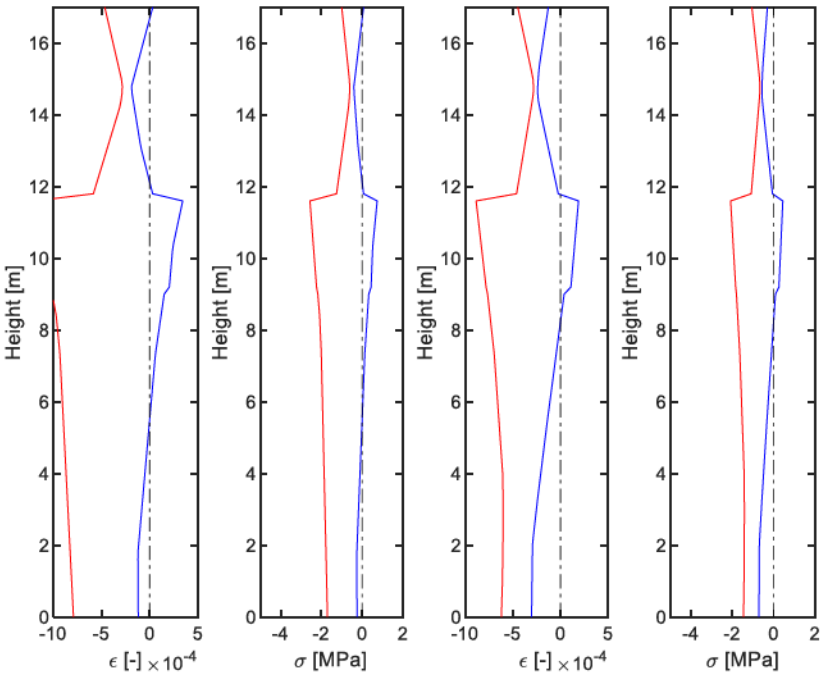

Figure 5.35: trend of the maximum and minimum stresses and the relative deformations for the composite column (left, the results of the eighteenth-century column, right, the results of the medieval column).

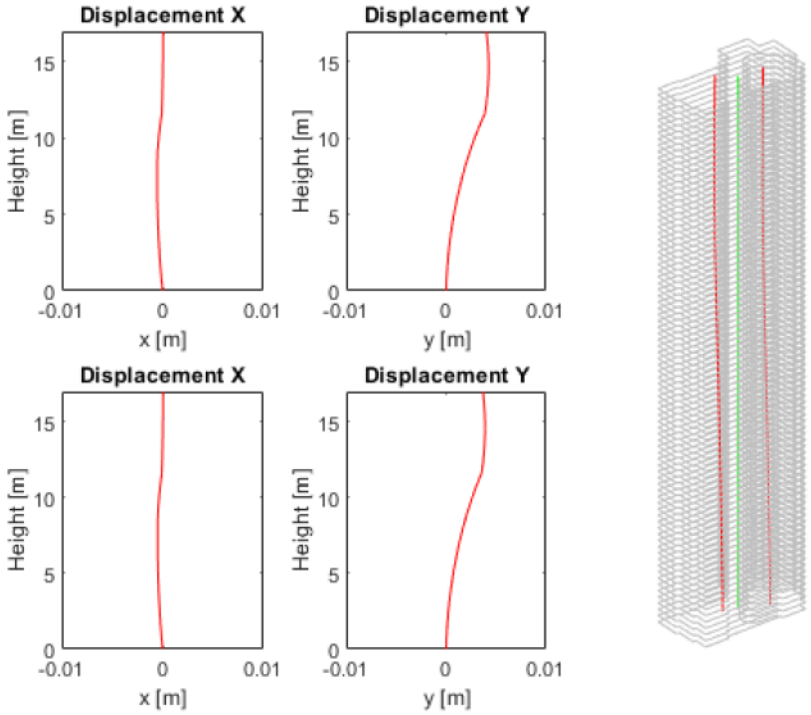

Figure 5.36: displacements along x and y for the composite column (above the displacements of the eighteenth-century column, under the displacements of the medieval column).

ELASTIC NO TENSION

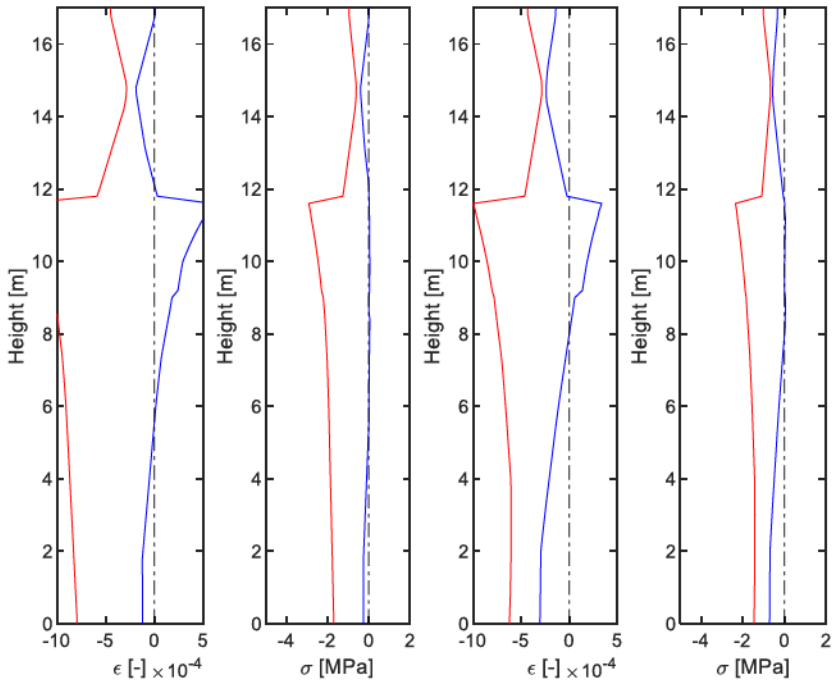

Figure 5.37: trend of the maximum and minimum stresses and the relative deformations for the composite column (left, the results of the eighteenth-century column, right, the results of the medieval column).

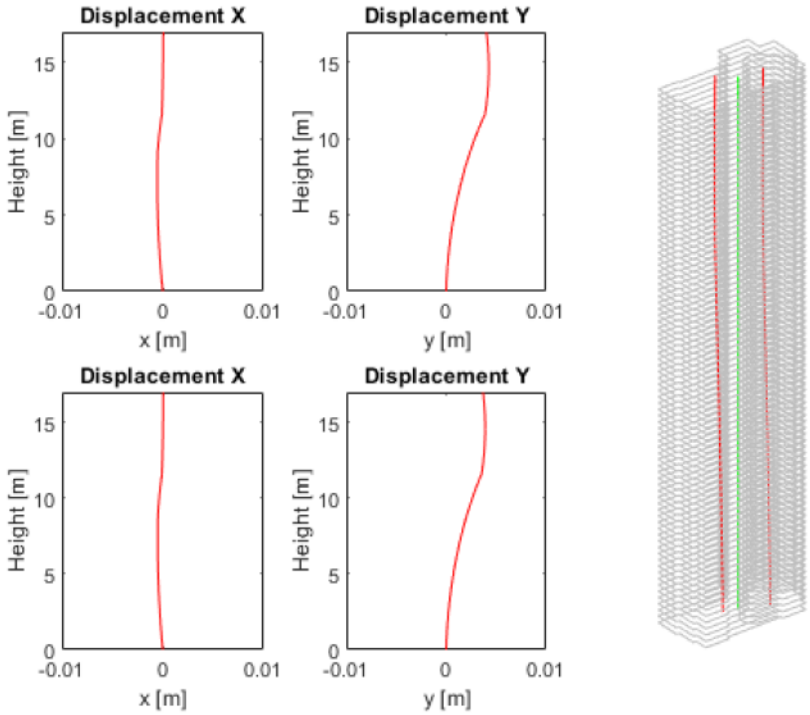

Figure 5.38: displacements along x and y for the composite column (above the displacements of the eighteenth-century column, under the displacements of the medieval column).

As can be seen in Figure 5.38, the deformed columns (i.e. medieval and eighteenth century) have the same shape. This is related to the model adopted. The displacements along *y*, that is, along the short side of the section, prove to be more important than those in the *x*-axis. Compared to the model with the single section, the shape of the deformation is different.

5.5.3 Validation

This section reports the validation for the beam model previously introduced. The beam model is, namely, adopted as a numerical model to be used in subsequent analyzes in the stochastic field (Chapter 6). This model compared to the FEM model has a considerable advantage in terms of computational burdens both with linear analyzes and especially when non-linear analyzes are performed. In the following the beam model provides well approximate results comparing the model with the analytical formulations proposed by Frisch-Fay (1975), under the assumption of no tension material and taking into account nonlinear geometric effects. Analogously the beam model well approximates FEM results, these comparisons performed in the linear field are useful to evaluate the effect of the complex geometry of the section and of the lack of connection between medieval and baroque columns.

5.5.3.1 Comparison of beam model with analytical solution

The comparison with the analytical solution was made by considering a homogeneous rectangular section with a section having dimensions of 3.97 x 2.24 m and a height of 17.00 m. Section analyzes were performed at 0.2 m pitch for a total of 85 sections.

The response of the displacement of the column was evaluated with an incremental analysis. The dimensionless force ($L\sqrt{P/EJ}$) has been increased with a step of 0.01.

A no-tension constitutive law was considered for the material. In general, each section analyzed that has its part in tension is subjected to 10 iterations with a tolerance of 0.001 MPa.

Figure 5.39 displays the incremental analysis with the force-displacement relationship. The force and displacement relationship has been dimensionless. In the figure, we compare the results obtained from the numerical beam model previously described with the analytical solution (see Section 5.4.1). It is possible to see how the beam model captures the results of the analytical solution well.

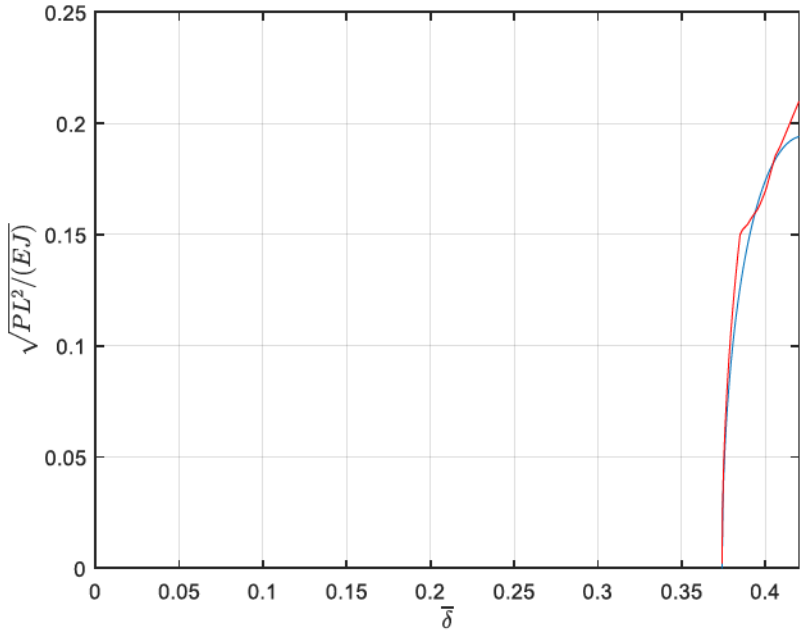

Figure 5.39: dimensionless load $L\sqrt{P/EJ}$ as function of the dimensionless displacement $\bar{\delta}$: comparison between analytical solution (blue curve) and numerical solution employing numerical model (red curve).

The results are practically coincident with the first part of the curve where we have a linear behavior. When the behavior is non-linear, the first discrepancies, due to discretization and approximation effects, appear but the numerical curve is always very close to the analytic one. The good approximation of the force-displacement relationship allows us to say that the beam model represents well the structural behavior under loads.

5.5.3.2 Comparison between the beam model and the FEM model

In this paragraph, the comparison between the FEM model and the beam model is presented. This comparison is important because the results obtained justify the use of the beam model for subsequent stochastic analyzes. The results summarized in Table 5.6 - 5.7 and the following pages (Table 5.8 – 5.12) show how the results obtained with the beam model approximate in a satisfactory way those obtained with the finite element program (i.e. Abaqus).

In our case study, the choice of a beam model rather than a FEM model is dictated by the desire to significantly reduce computational times and costs and on the other hand to have a simple model to verify the column. In fact, considering the large number of elements and the related problems of brick elements, it is difficult to manage any

anomalies due to the elements in a stochastic environment. The beam model with a few degrees of freedom allows for greater control. Finally, it is worth noting to underline as the use FEM for the problem at hand is questionable given the non-regularity of the texture of the masonry inside the column.

In the following figures (Table 5.8 – 5.12) it is possible to see how the tensions trend in the various sections is very similar. Only for the distribution of tensions at 7.50 m can be found a slight difference.

Table 5.6: comparison of the stresses obtained between the FEM model and Beam model for a single column.

Height [cm]	Minimum stress value FEM model [MPa]	Minimum stress value Beam Model [MPa]
142	-1.82	-1.85
372	-1.27	-1.30
490	-0.61	-0.63
520	-1.26	-1.30
750	-0.99	-0.95

Table 5.7: comparison of the stresses obtained between the FEM model and Beam model for the double connected column.

Height [cm]	Minimum stress value FEM model[1] [MPa]	Minimum stress value double beam section model [MPa]
142	-1.9640	-1.90
372	-1.0293	-1.05
490	-0.8015	-0.84
520	-1.6503	-1.61
750	-1.0319	-1.01

[1] sections connected with rigid links

Section at 149 cm

Table 5.8: stress distribution for the various FEM and beam models.

	Single section	Composite section
FEM Model	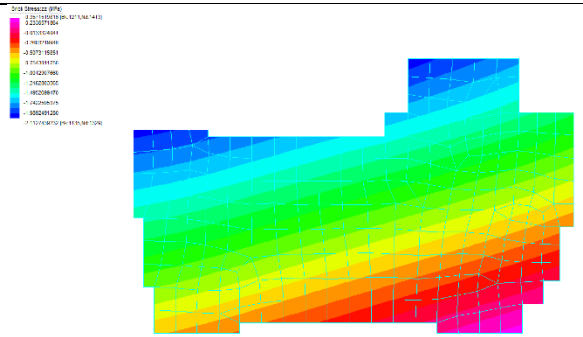	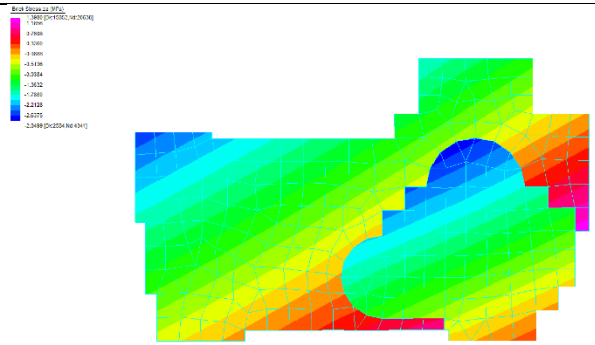
	σ_z [MPa]	σ_z [MPa]
Beam Model	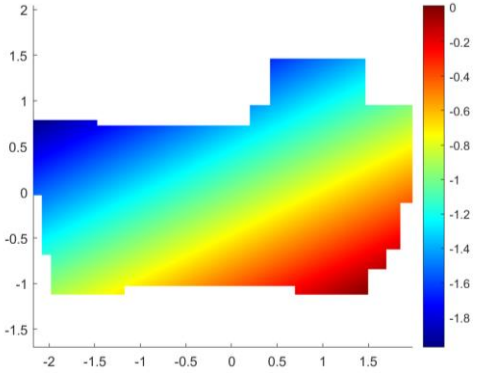	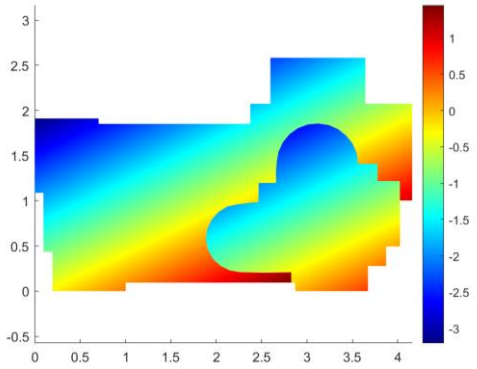
	σ_z [MPa]	σ_z [MPa]

Section at 372 cm

Table 5.9: stress distribution for the various FEM and beam models.

	Single section	Composite section
FEM Model	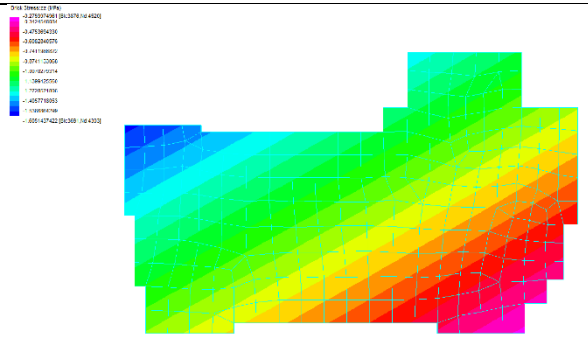	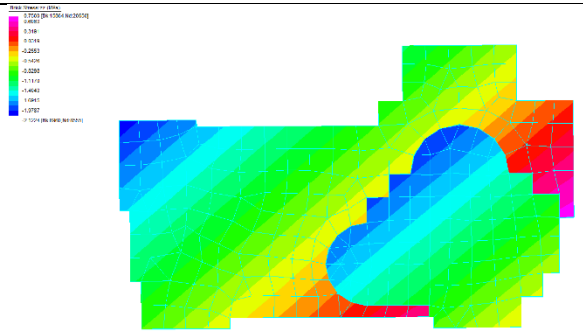
	σ_z [MPa]	σ_z [MPa]
Beam Model	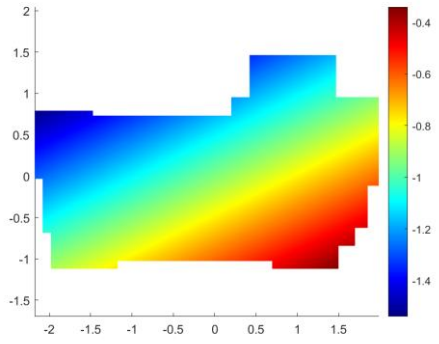	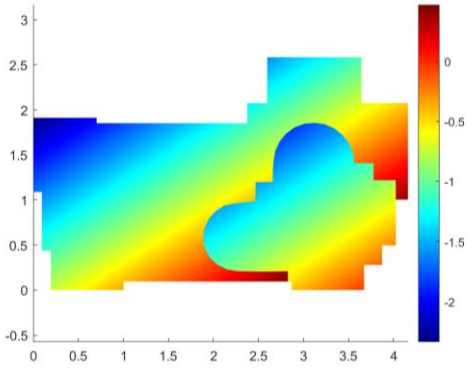
	σ_z [MPa]	σ_z [MPa]

Section at 490 cm

Table 5.10: stress distribution for the various FEM and beam models.

	Single section	Composite section
FEM Model	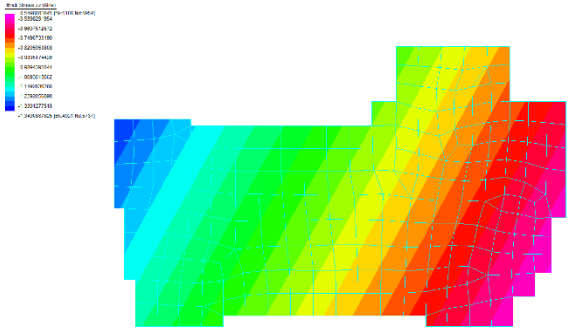	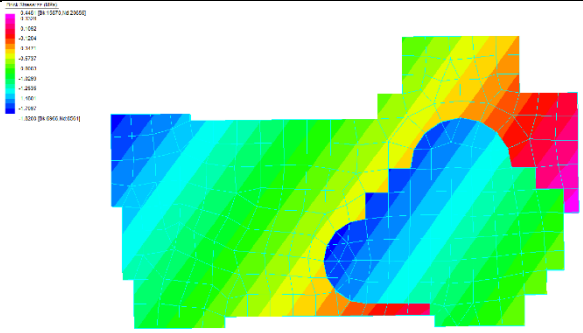
	σ_z [MPa]	σ_z [MPa]
Beam Model	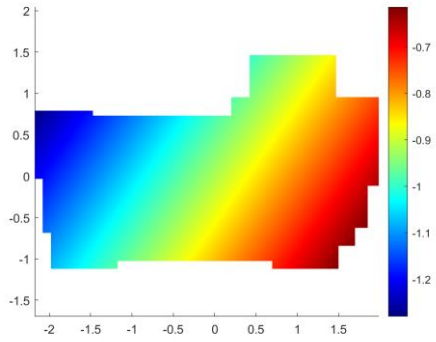	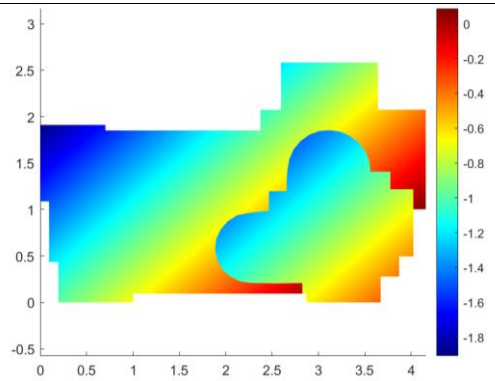
	σ_z [MPa]	σ_z [MPa]

Section at 520 cm

Table 5.11: stress distribution for the various FEM and beam models.

	Single section	Composite section
FEM Model	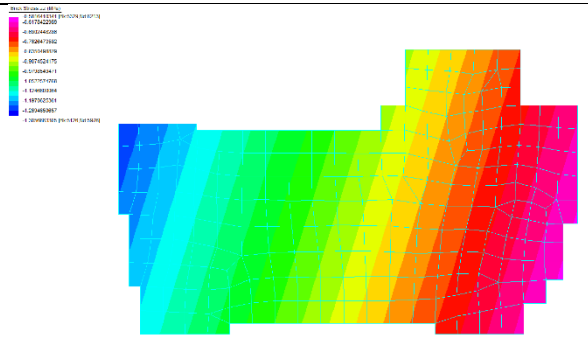	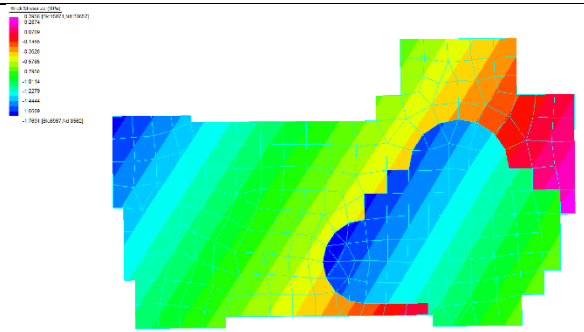
	σ_z [MPa]	σ_z [MPa]
Beam Model	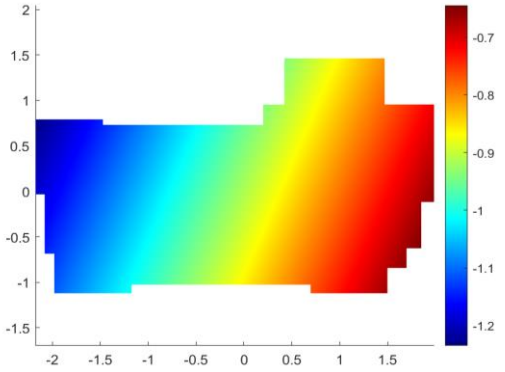	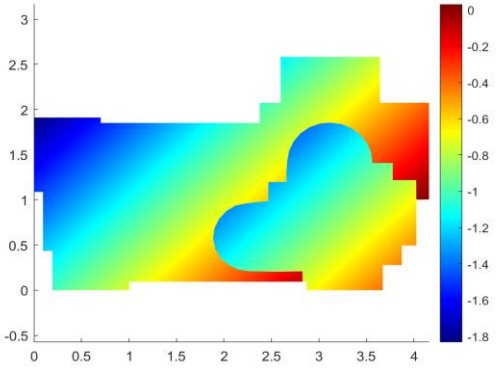
	σ_z [MPa]	σ_z [MPa]

Section at 750 cm

Table 5.12: stress distribution for the various FEM and beam models.

	Single section	Composite section
FEM Model	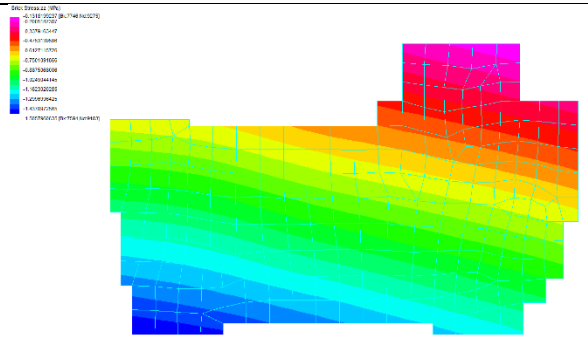	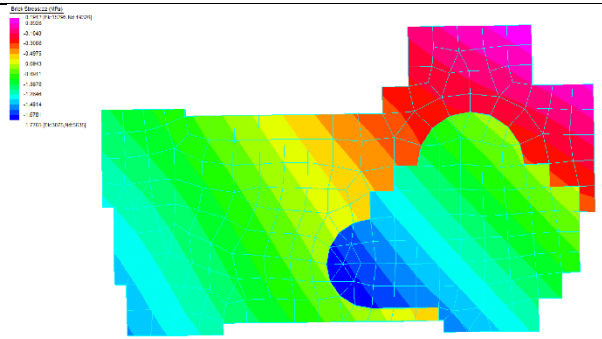
	σ_z [MPa]	σ_z [MPa]
Beam Model	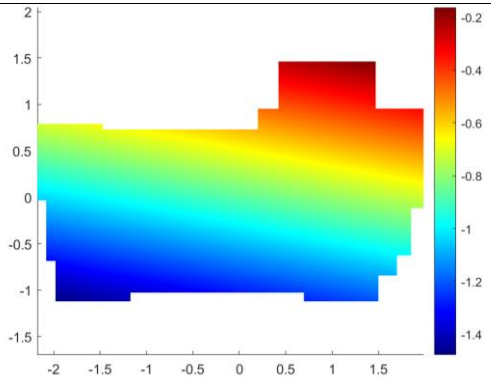	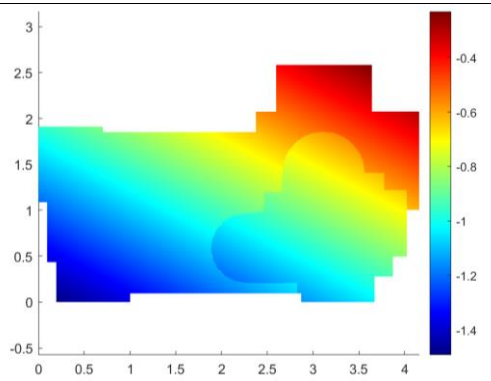
	σ_z [MPa]	σ_z [MPa]

5.5.4 Comparison of numerical models with experimental test values

The results reported in this section show how the FEM and the beam model are able to capture the stresses in points of the cross-sections identified by the experimental tests rather accurately. Furthermore, the model connected with rigid connections is able to capture the structural behavior of the column considering the complexity of the element. In fact, the connection of the medieval and eighteenth-century sections was one of the unknown factors of the problem.

Figure 5.40 shows the points where the tensions are analyzed in the column by means of experimental tests. In particular, tests were carried out with a simple jack and tests with a double jack for the column.

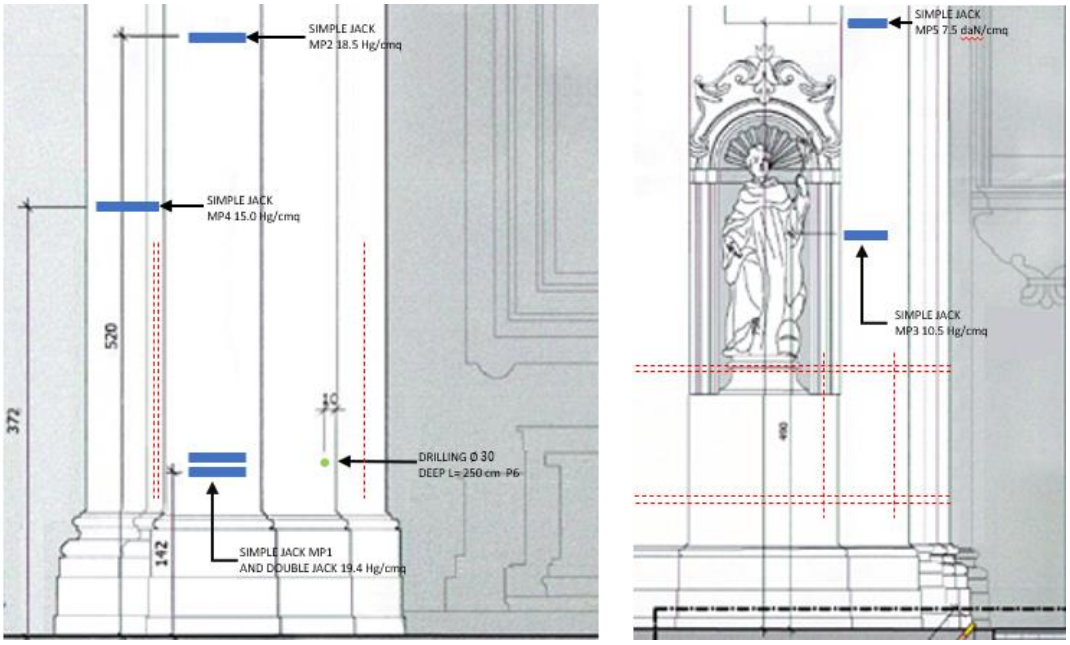

a) b)

Figure 5.40: view of the pillar and the relative points where the on-site tests were carried out.

Table 5.13: comparison of the stresses obtained between the FEM model and the tests.

Height [cm]	Tension tests [MPa]	Single section tension [MPa]	Tension connected sections with rigid links [MPa]
142	-1.94	-1.82	-1.9640
372	-1.50	-1.27	-1.0293
490	-1.05	-0.61	-0.8015
520	-1.85	-1.26	-1.6503
750	-0.75	-0.99	-1.0319

Table 5.14: comparison of the stresses obtained between the beam model and the tests.

Height [cm]	Tension tests [MPa]	Single section tension [MPa]	Tension connected sections [MPa]
142	-1.94	-1.85	-1.90
372	-1.50	-1.30	-1.05
490	-1.05	-0.63	-0.84
520	-1.85	-1.30	-1.61
750	-0.75	-0.95	-1.01

Both FEM and beam models approximate the experimental results in an acceptable way even simply by assuming an elastic linear behavior for the masonry and as a load condition hypothesized by the designers and reported previously in Table 5.13 and Table 5.14.

6 Uncertainty quantification of masonry piers

This chapter presents a procedure for quantifying the uncertainties encountered in the structural analysis of masonry pillars of the cathedral of Ferrara. This method can be applied where the main sources of uncertainties are vague and imprecise information such as the characterization of the material; both the size and location of the loads are not precisely known.

The purpose of quantifying uncertainties is to evaluate the presence of adequate safety margins. In this chapter, the uncertainties are quantified through fuzzy theories that allow deriving the interval bounds and the mean structural response.

6.1 Modeling of uncertainties

The cathedral columns represent a case where the uncertainties of the material, loads and their location influence the structural response.

The quantification of uncertainties is difficult with standard techniques i.e., classical probability analysis. Indeed, if you want to apply this approach, you need a robust set of data that in this case, it is not available. Therefore, a rigorous assessment of the uncertainty of the material cannot be applied in this case (Sun et al., 2020). A Bayesian type update cannot be applied due to the small number of experimental tests performed. Based on the available data, the most robust approach that can be applied appears fuzzy set theory. These theories are also functional to better describe the possible variation of the actions transmitted by the arcs that push on the column and their eccentricity.

6.1.1 Uncertainties on the mechanical properties of materials

The modeling of the uncertainties of the materials was done by processing the data of the experimental tests. Experimental tests such as compression tests on brick and double punching tests on mortar made it possible to obtain the characteristic value of the compressive strength of the masonry. For more details on the material of the columns see Section 5.3.1 and Appendix A.

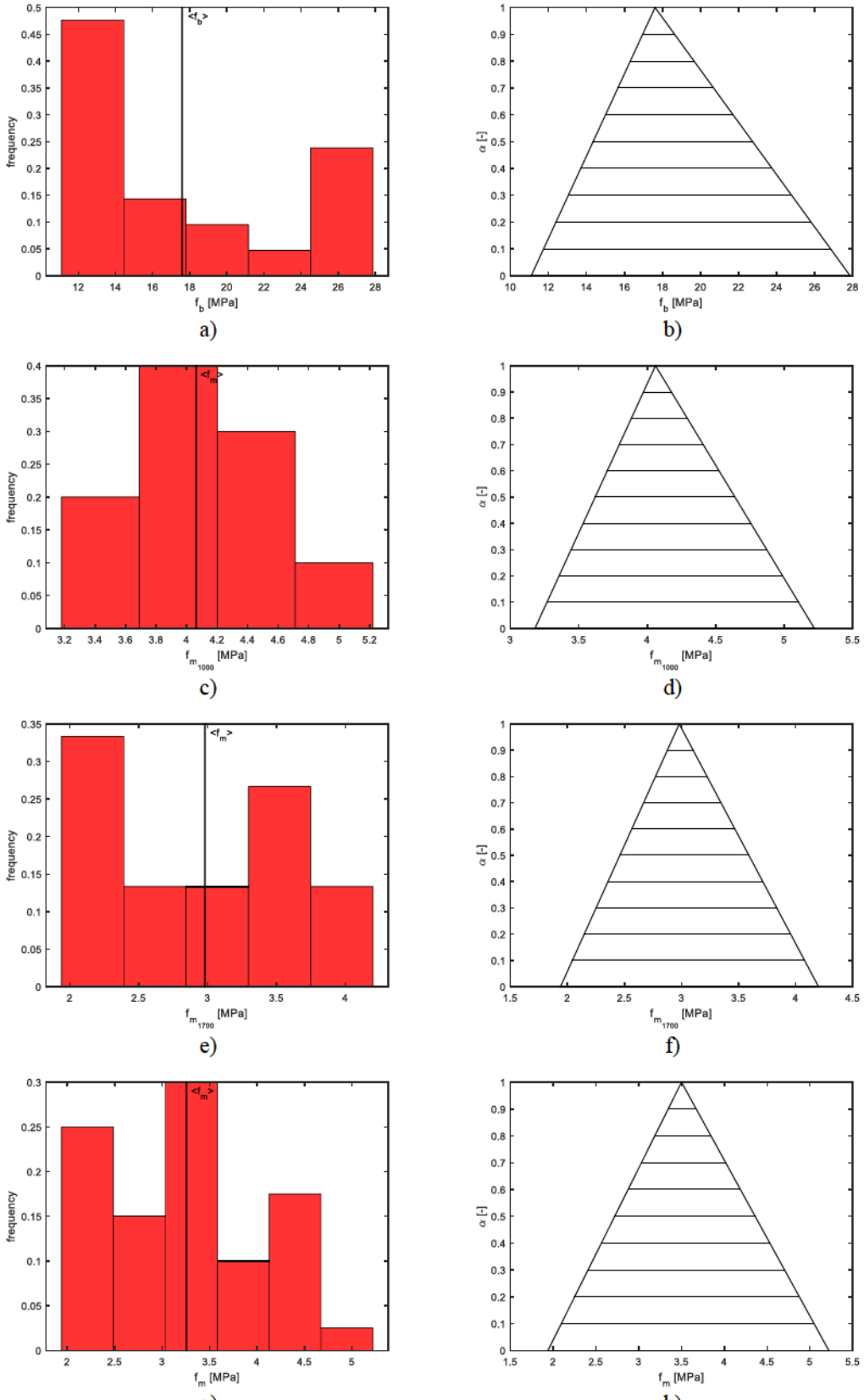

Figure 6.1: sample (left) and relative fuzzy (right) of mechanical properties: a) – b) resistance of brick cubes, c) – d) resistance of medieval mortar, e) – f) resistance of the eighteenth-century mortar, g) – h) average resistance of mortar.

Table 6.1: fuzzy numbers of the mechanical properties of masonry.

Parameter	Value [MPa]
Compressive strength of brick (f_b)	<15.1,17.6,21.3>
Compressive strength of medieval mortar (f_{m1000})	<3.67,4.1 4.6>
Compressive strength of eighteenth-century mortar (f_{m1700})	<2.69,2.98,3.3>
Compressive strength of mortar (f_m)	<2.69,4.06,4.58>
Compressive strength of medieval masonry (f_{c1000})	<4.14,4.77,5.64>
Compressive strength of eighteenth-century masonry (f_{c1700})	<3.77,4.34,5.14>
Compressive strength of masonry (f_c)	<3.89,4.48,5.30>
Secant modulus of elasticity for medieval masonry (E_{m1000})	<4137,4767,5641>
Secant modulus of elasticity for eighteenth-century masonry (E_{m1700})	<3771,4345,5137>
Secant modulus of elasticity for masonry (E_m)	<3888,4479,5298>

The experimental campaign showed how the average resistance of eighteenth-century mortar has lower values than the medieval one. This is due to the different mineralogical compositions.

Figure 6.1c-e shows the values of the compressive strength due to double punching of the mortars according to a histogram. In Figure 6.1g the compressive strength of the block is always shown with a histogram. Each histogram is associated with the relative fuzzy numbers (Table 6.1).

The compressive strength values of the masonry were obtained by following the formula in Eurocode 6 (CEN, 2005a) (Section 5.3.1.1).

A triangular shape was chosen for the fuzzy. This choice is due to the fact that allows to evaluate the fuzzy successes and respond quickly and expeditiously (Möller and Beer, 2004). Furthermore, the form is compatible with the form of the lognormal distribution hypothesized by Savoia et al. (2016).

6.1.2 Uncertainties on loads and their application

The modeling of loads and their application play a key role in the structural response and also in their reliability in probabilistic terms. The magnitude of most loads changes as a function of time and their application. This can be due to natural phenomena (e.g., wind, earthquake) or human-induced effects (e.g., dead loads, live loads).

Furthermore, there are time-induced phenomena such as the deterioration of materials or their viscosity. This means that loads have to be represented as stochastic processes.

However, the assessment of their reliability is not so trivial.

Very often, indeed, it is not possible to create perfect probabilistic models for loads and their application due to insufficient data and imprecision in their evaluation. Therefore, the creation of probabilistic models for loads and their application is one of the most uncertain factors in reliability analyzes.

Over the past 35 years, the Joint Committee on Structural Safety (JCSS) has established through guidelines the basic principles for assessing the risk and reliability of structures (JCSS, 2001). This standardized procedure cannot be applied in the present case. Actually, analysis with classical probability methods is not strictly applicable for monumental structures due to the impossibility of comparing with other similar buildings. For this reason, a non-frequentist approach to probability is fundamental in order to be able to cross-reference the available information. Fuzzy theories appear useful for our case.

As explained in Section 5.3.3, the arch thrust varies over time due to viscous effects as actually happens in the present case: the horizontal force is considered uncertain by making it vary while the vertical can be assumed constant. Figure 6.2 shows the variation of the horizontal forces as a function of the maximum and minimum thrust of the arch. To define the fuzzy number, the minimum and maximum values of the arch thrust are considered as extremes of the number, while the vertex of the fuzzy number corresponding to the most plausible value was considered that defined by the designers (Table 6.2).

Table 6.2: range of arc thrust values.

Arch Force	Minimum thrust [kN]	Maximum thrust [kN]	Thrust by the designer [kN]
F1	127	167	159
F2	529	973	927
F3	488	537	511
F4	331	525	500
F5	488	537	511

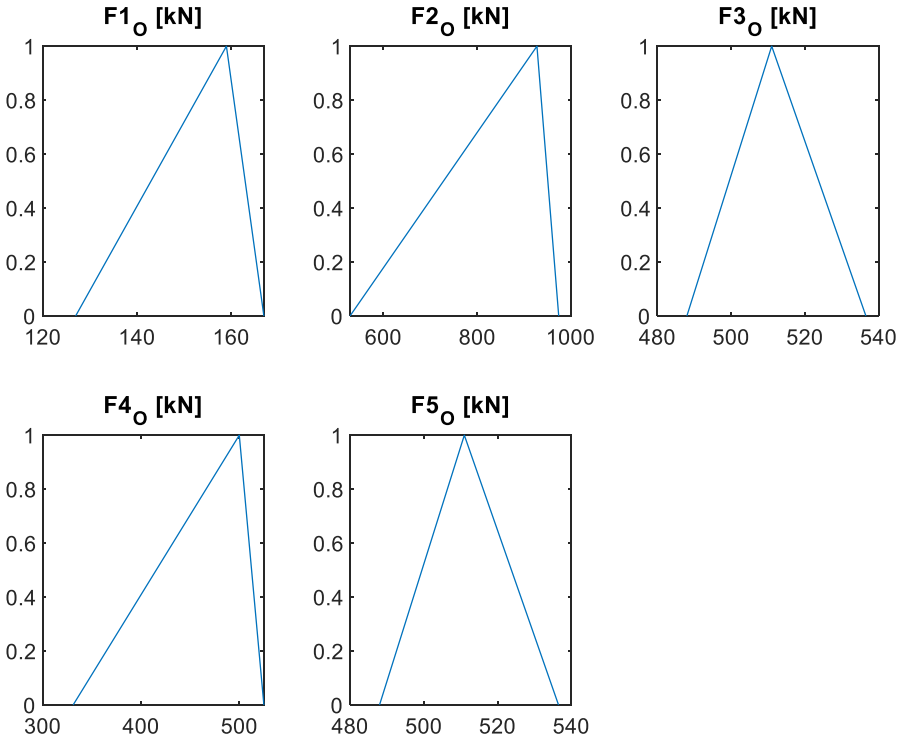

Figure 6.2: fuzzy number of the horizontal component of loads.

In addition to this variation, the position of the vertical forces with an eccentricity of 0.10 m from the most probable value was considered uncertain. The variation of all the eccentricities allows representing the unknown loading position. This uncertainty is a very important variable in the variation of deformations and displacements. Naturally, the assumption made was assumed considering a plausible range with the dimensions of the arch. This evaluation from experimental tests and structural identification is extremely complex.

Figure 6.3 shows the relative fuzzy numbers for the various eccentricities of the forces along the *x*-axis. Figure 6.4 shows the relative fuzzy numbers for the various eccentricities of the forces along the *y*-axis. The values of the eccentricities are defined considering the distance from the center of gravity of the section.

Figure 6.5 shows the areas for the membership function equal to zero of the various points of application of the forces. As it is easy to guess, a variation of the point of application of these forces involves a variation of the relative pressure curve and therefore of the relative distribution of the stresses and deformations inside the column. Of course, this also implies a variation of the displacement.

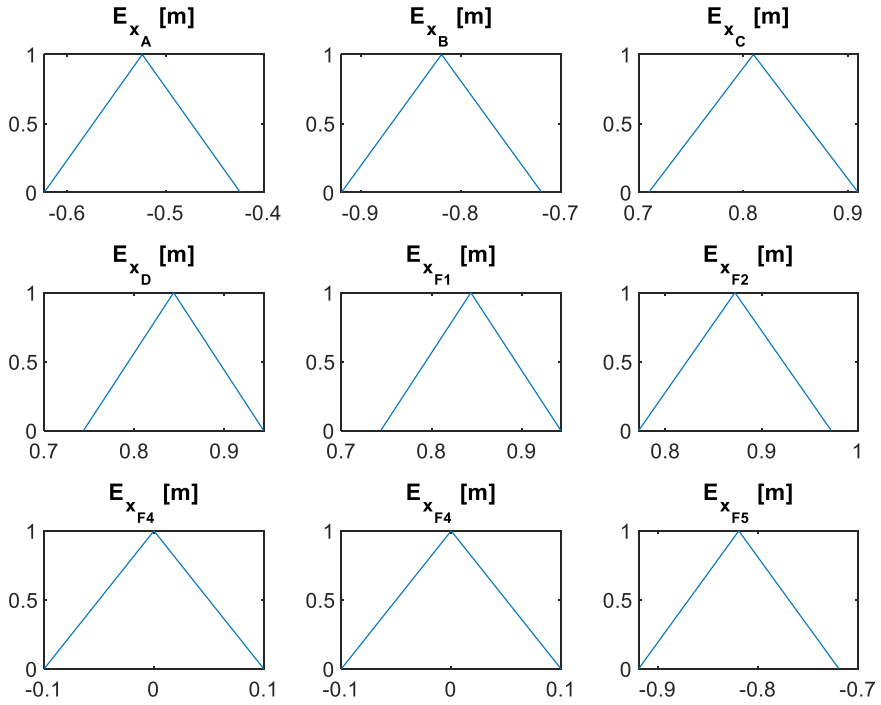

Figure 6.3: fuzzy number of the eccentricity of the vertical loads along the *x*-axis.

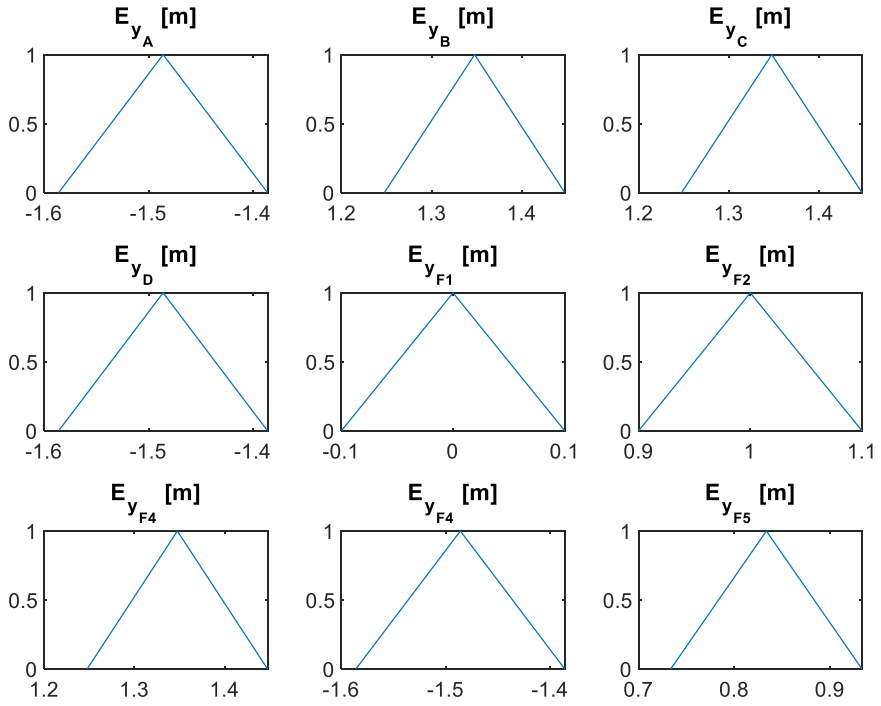

Figure 6.4: fuzzy number of the eccentricity of the vertical loads along the *y*-axis.

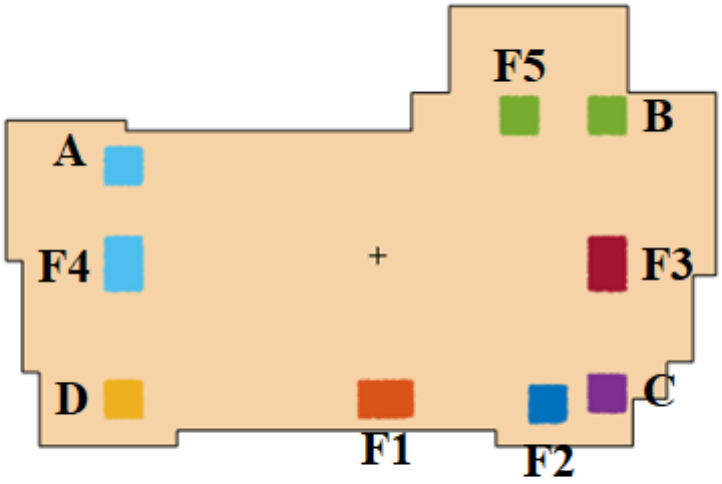

Figure 6.5: eccentricity variation area for vertical loads on the section (i.e., with α = 0).

6.2 UQ-Analyses

The analysis for quantifying uncertainties for column B4 considered consists of two parts (see Section 5.3):

- the computation of interval bounds;
- the computation of the mean performance.

These two indicators provide evidences on the uncertainty of the structural response and how the input parameters propagate their uncertainties in the response.

6.2.1 Computation of mean response

The calculation of the mean value of the interval corresponds to the interval of the fuzzy number whose membership function is equal to 1 (α = 1). This average value can be an interval if the response fuzzy is a trapezoidal fuzzy. In the case in which we are in the presence of a fuzzy triangular number, this interval corresponds to a value. In the following figures, the average value is represented by the red curve.

6.2.2 Computation of interval bounds

The computation of interval bounds corresponds to the extremes of the fuzzy. These represent the values of the membership function equal to 0 (α = 0). In the following figures, this interval is represented by black curves. The calculation of the interval bounds is done by applying the α-set optimization. For more details on the procedure see Section 2.1.4.1 and Möller et al. (2000).

A brief description of the results obtained using the beam model is now reported. We considered both cases where the column is modeled as a single beam and two coupled beams. Figure 6.6 shows the fuzzy number relative to the thrust curve for the column. It is possible to see how the variation of the thrust curves is not so significant for the uncertainties considered. Both curves remain within the section indicating that the stability of the column is possible.

Starting from the top of the column it is possible to see how the thrust curve is outside the core of inertia. This indicates how, if the material is linearly elastic, the sections are partially in traction.

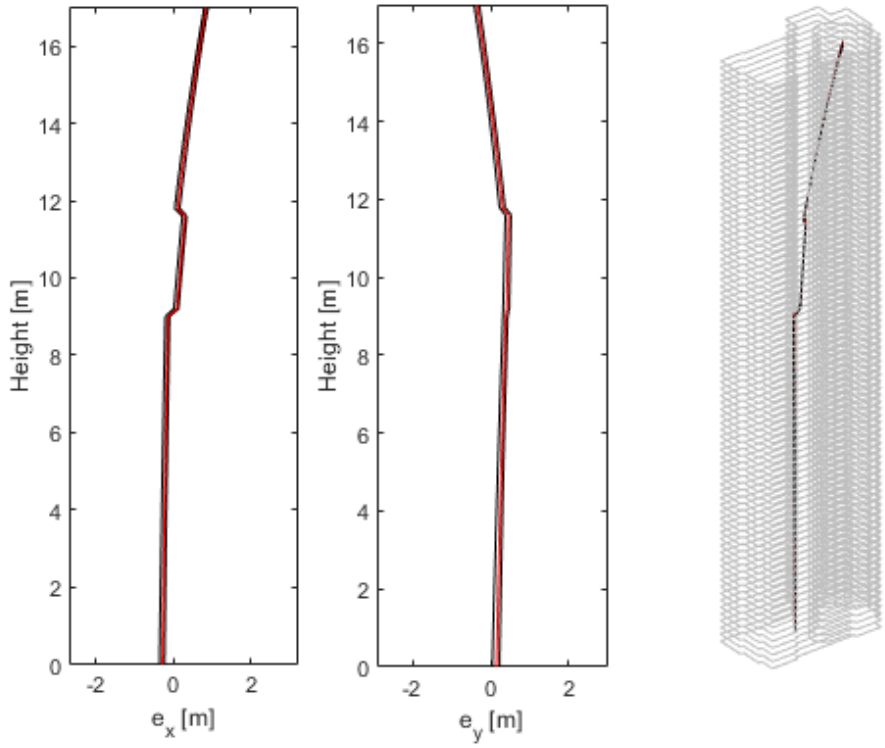

Figure 6.6: column line of thrust column (red line with α = 1, black line with α = 0).

Moreover, as the height decreases, the fuzzy pressure curves fall almost completely within the core of inertia. In this case, the section is completely compressed. This bundle shift of the thrust curves is obviously due to the stabilizing effect of the column's dead load.

Figure 6.7 shows how the contour of the thrust curves (membership function value with $\alpha = 0$) are outside the core of inertia calculated in an approximate way considering an equivalent rectangular section.

The variation of the forces does not imply a repositioning of the neutral axis but an increase in the tensions. The repositioning of the neutral axis occurs following the variation of the eccentricity. In fact, the whole section can remain in compression as much as remains inside the core, while when it comes out of the core a part of the section goes into traction. When considering an elastic material this does not involve important considerations in the mechanical field except when it reaches the breaking stress. If, on the other hand, we consider a no-tension material, as in our case masonry, when the material is in traction, cracks are created in the part that was in traction in the elastic range.

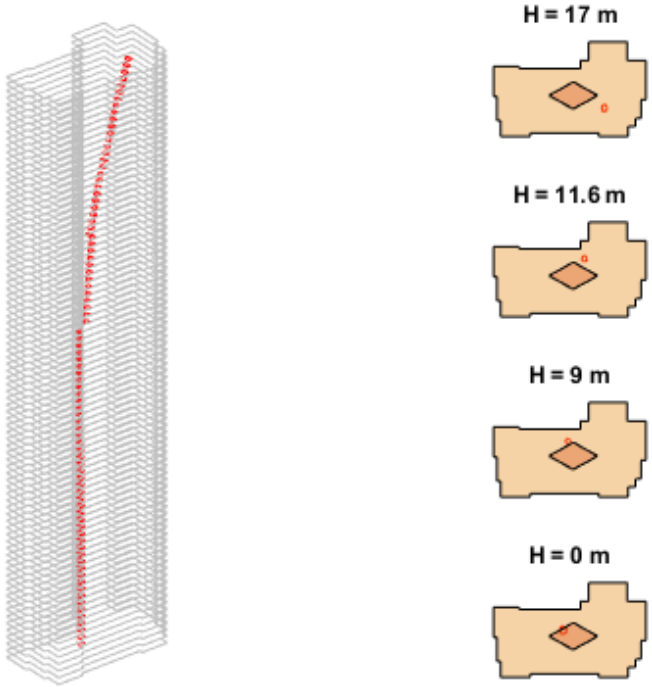

Figure 6.7: fuzzy thrust curve with $\alpha = 0$ and sections with the relative simplified central core of inertia.

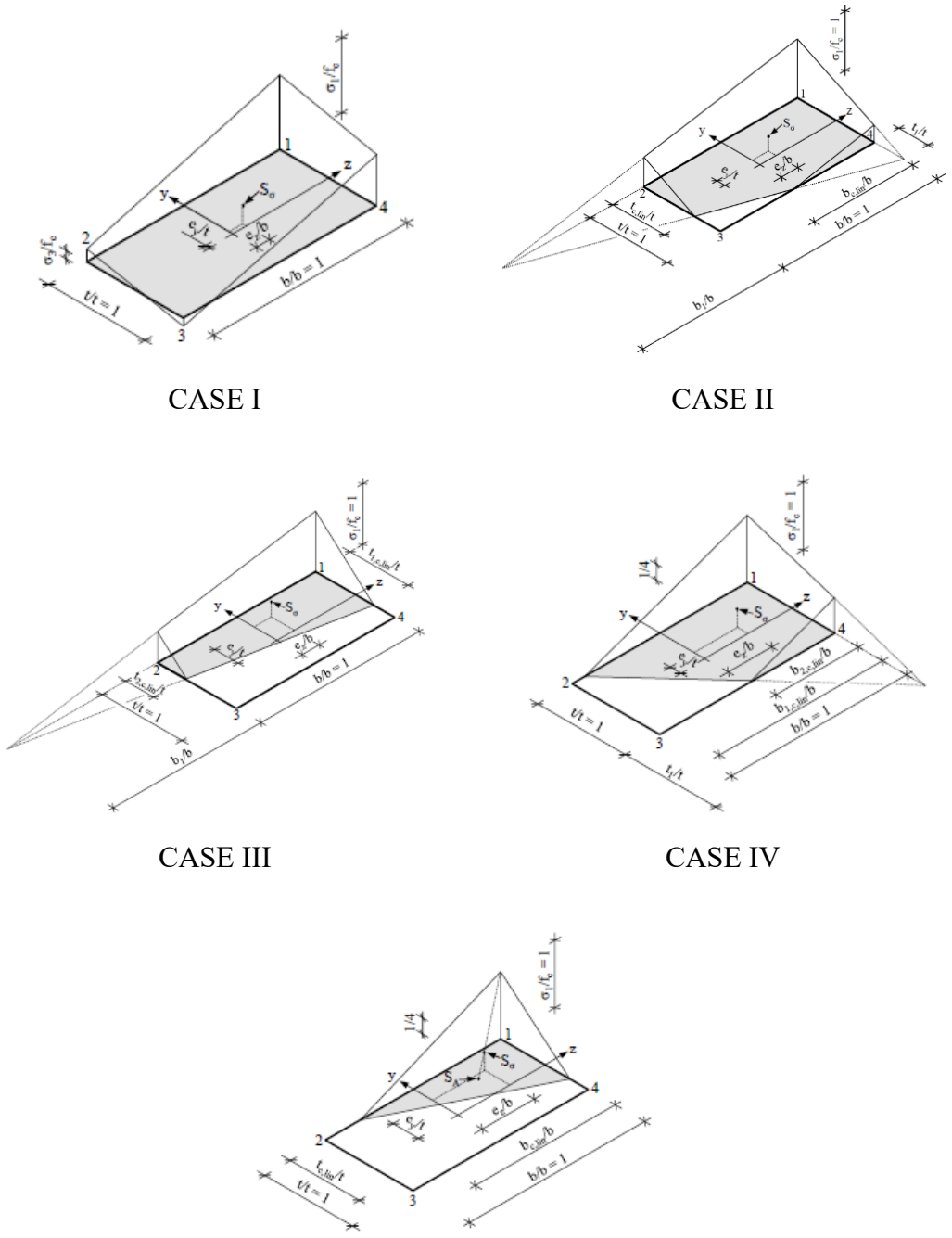

Figure 6.8: stress distribution of the rectangular cross-section for different load cases (Förster, 2018).

Figure 6.8 shows the different tension distribution in the simple case of rectangular sections.

Figure 6.9 shows the areas in which we can have a significant variation of the neutral axis and of the tensile stresses that lead to cracking of the material. Enßlin (1941) divides the variation in the distribution of tensions into five cases.

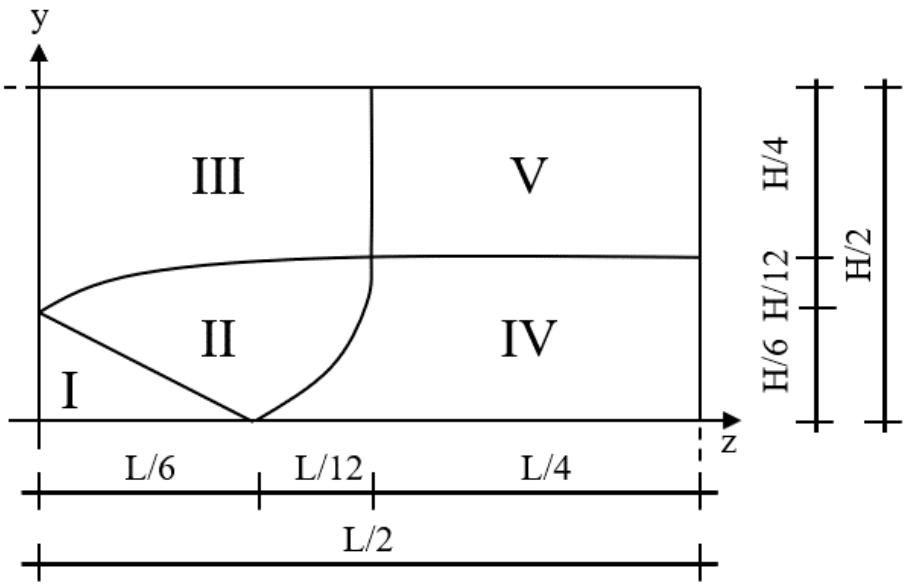

Figure 6.9: Cross-sectional quarter to differentiate between cases depending on the eccentricities for linear-elastic material behavior without flexural strength according to Enßlin (1941).

Finally, Figure 6.10 shows the various areas as they vary depending on a variation in eccentricity; for simplicity, everything is depicted for a rectangular section. The considerations can be extended to the actual section of the column. Along with the height of the column, the section remains mainly in compression (case I) and some cases in traction. For cases in traction, it is possible to see how the pressure curve is slightly outside the core of inertia. This implies that for our case study the distribution of stresses falls into case II.

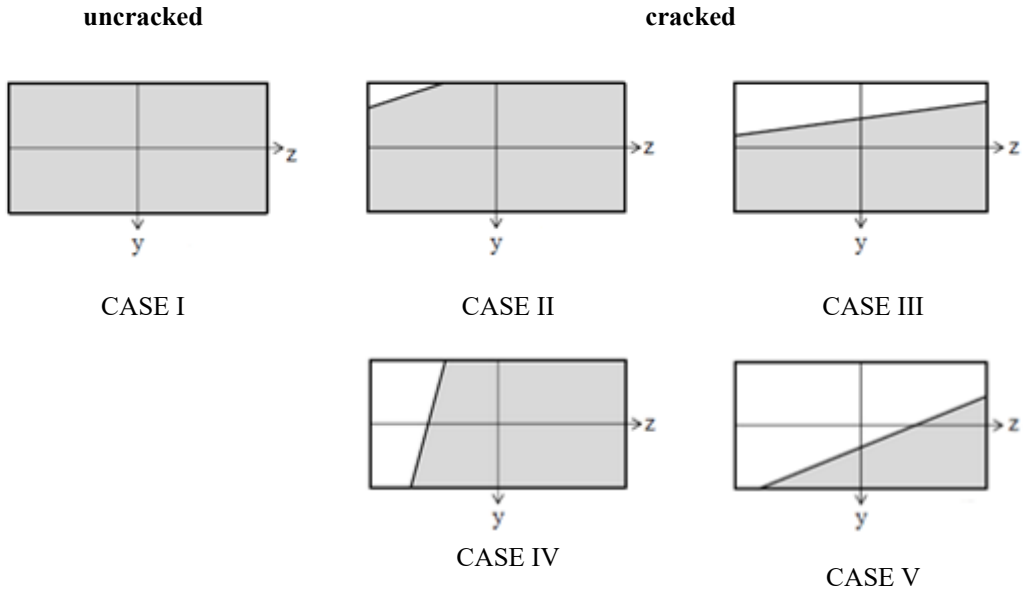

Figure 6.10: compressed areas for different cases (Förster, 2018).

6.2.2.1 Single beam model

This section shows the fuzzy structural analysis results for the column modeled as a single beam. For more details about this structural model, see Section 5.5.2.6.

6.2.2.1.1 Linear elastic material

As a first case study, the structural response of the column is analyzed, assuming that the masonry has a linear elastic constitutive behavior. This assumption is made in the first instance to validate the stochastic model with Monte Carlo simulation. The comparison results are reported in Section 6.2.2.3. The fuzzy structural analysis allows obtaining useful information on the uncertainty of the material and the load.

Traction stresses are present at the top of the column (Figure 6.11) in particular from 6 to 11 meters and from 15 to 17 meters. Naturally, the tractions decrease with the stabilizing contribution due to the own weight. From 11 to 17 meters, you can see how the uncertainties in the tensions are not so important. In fact, the relative fuzzy is very narrow compared to what can be extrapolated from zero to 11 meters. This is due to a greater role of horizontal forces and their eccentricity. A significant aspect of this analysis is that it shows how uncertain inputs can influence the response making the section in some cases completely compressed or in other cases partially in traction.

Figure 6.12 shows the displacements along X and Y of the column by means of fuzzy numbers. The interval bounds are in black and the average value is in red.

6.2.2.1.2 Elastic no-tension constitutive behavior

As seen in Section 5.5.1.2 and widely discussed in the literature, the no-tension constitutive model is particularly suitable for evaluating the structural response of masonry elements. As discussed above, indeed, the pillar is composed of a Medieval column incorporated into the Baroque column, made of different bricks and mortar. In addition, the masonry is uneven and variable inside the pillar (Figure 5.6). The tensile strength is low and very uncertain while experimental tests show that the compressive strength is discrete. The fuzzy structural analysis allows obtaining useful information on the uncertainty of the material and the load.

Figure 6.13 shows the values of the maximum and minimum deformations of the various sections of the column. Furthermore, the maximum and minimum normal stress in the various sections of the column are shown.

LINEAR ELASTIC

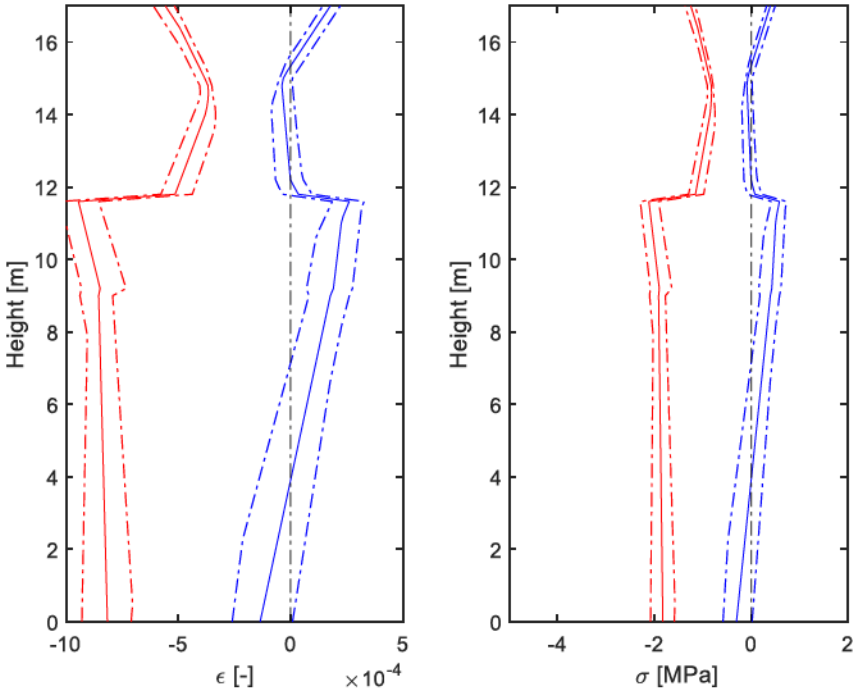

Figure 6.11: fuzzy numbers of the maximum and minimum deformations and tensions in the section along the height considering the no-tension material (dotted line with α = 0, solid line with α = 1).

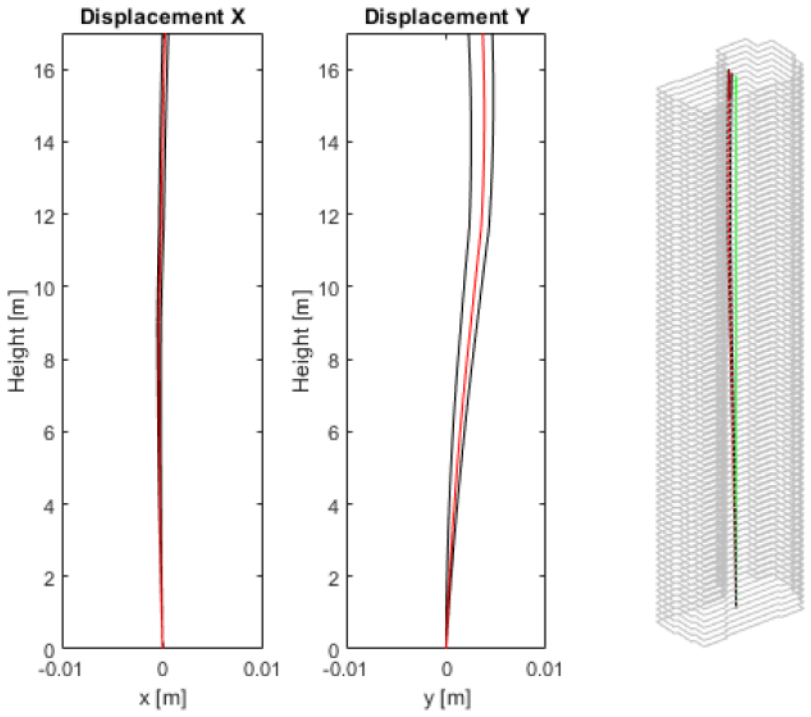

Figure 6.12: fuzzy numbers of the maximum displacement of the section along the height of the column (black line with α = 0, red line with α = 1).

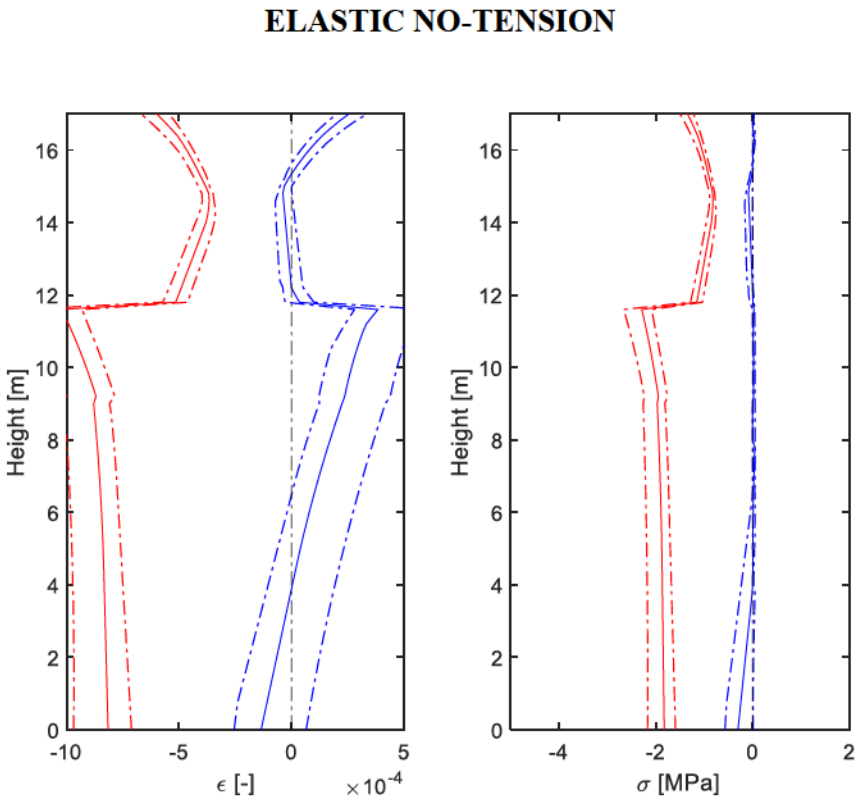

Figure 6.13: fuzzy numbers of the maximum and minimum deformations and tensions in the section along the height considering the no-tension material (dotted line with α = 0, solid line with α = 1).

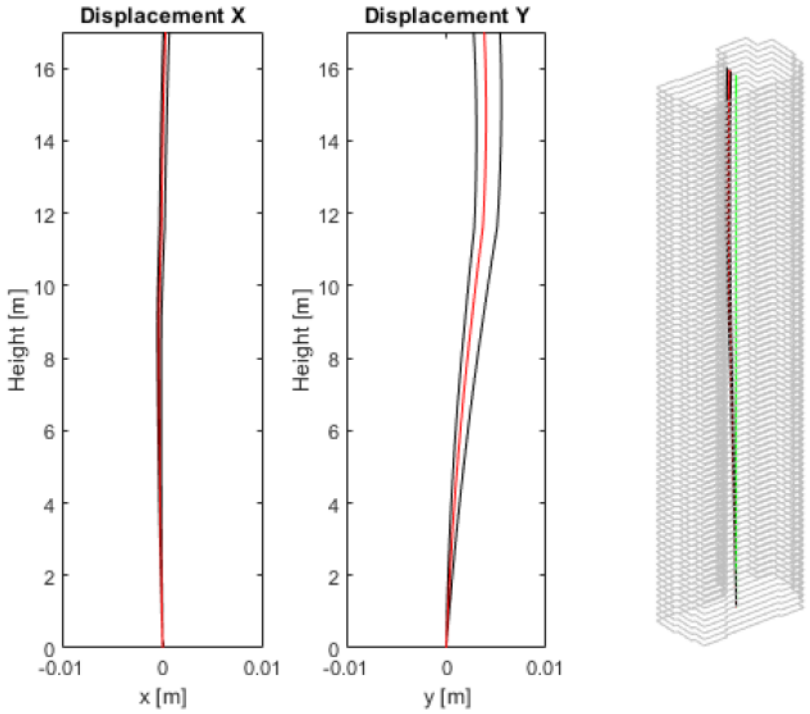

Figure 6.14: fuzzy numbers of the maximum displacement of the section along the height of the column (black line with α = 0, red line with α = 1).

Because the tensile stresses are not present the variability induced by the fuzzy variables is strongly reduced in correspondence with those sections where the linear elastic model gives consistent traction.
Figure 6.14 shows the displacements along *x* and *y* of the column by fuzzy for each section. The displacement fuzzies numbers are characterized by the most probable value not centered between the extremes of the fuzzy. This shows the propagation of uncertainties.

6.2.2.2 Two beam model

This section shows the fuzzy structural analysis results for the column modeled as two sections having the same horizontal displacements but different vertical ones; the so-called two-beam model. For more details see Section 5.5.2.7.

6.2.2.2.1 Linear Elastic material

As a first case study, the structural response of the column, assuming that the masonry has a linear elastic constitutive behavior, equal to all pillars, is presented. This assumption is made in the first instance to validate the stochastic model with Monte Carlo simulation (see Section 6.2.2.3).
This model allows obtaining the deformations and tensions of the two columns (the medieval and eighteenth-century ones) by distributing the moments and axial forces appropriately.
Having connected the two sections with connecting links, these allow an equal displacement having both curvatures equal.
The fuzzy structural analysis allows obtaining interesting information on the uncertainty of the material and the load.
From the results of the elastic analyzes, it emerged that in both sections from 6 to 12 meters they are partially in traction (Figure 6.15). It also emerges that the eighteenth-century section has greater tensions than the medieval one.
Figure 6.16 shows the displacements of the two columns. As you can see, the deformations are the same in terms of curvature. This is in accordance with the adopted model.

LINEAR ELASTIC

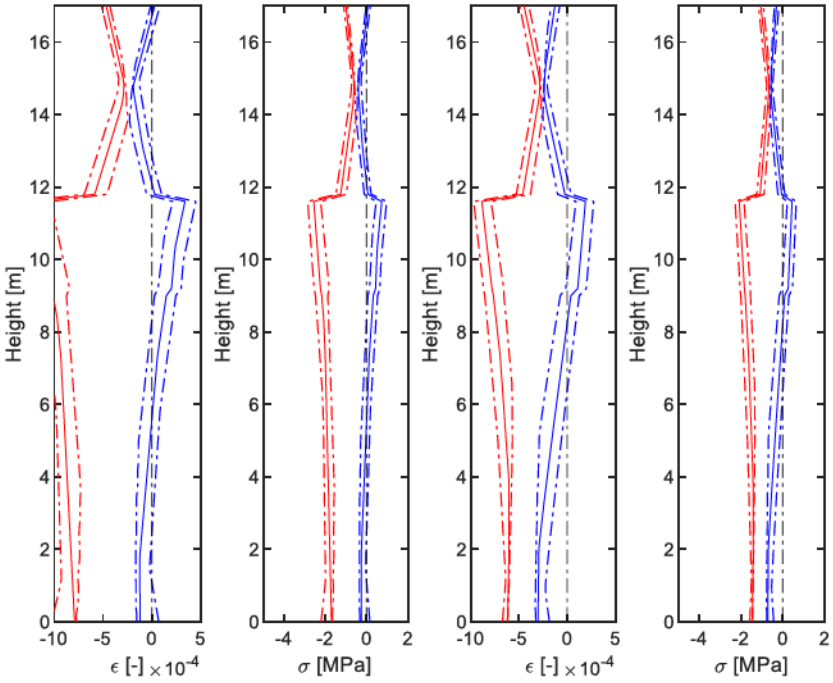

Figure 6.15: fuzzy numbers of the maximum and minimum deformations and tensions in the coupled sections along the height considering the no-tension material (dotted line with $\alpha = 0$, solid line with $\alpha = 1$).

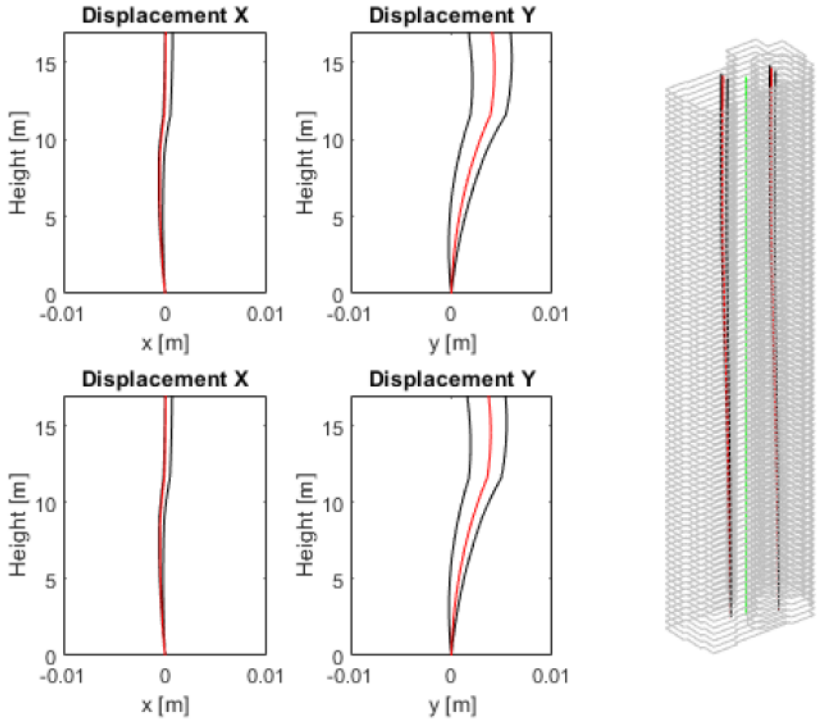

Figure 6.16: fuzzy numbers of the maximum displacement of the section along the height of the column (black line with $\alpha = 0$, red line with $\alpha = 1$).

ELASTIC NO-TENSION

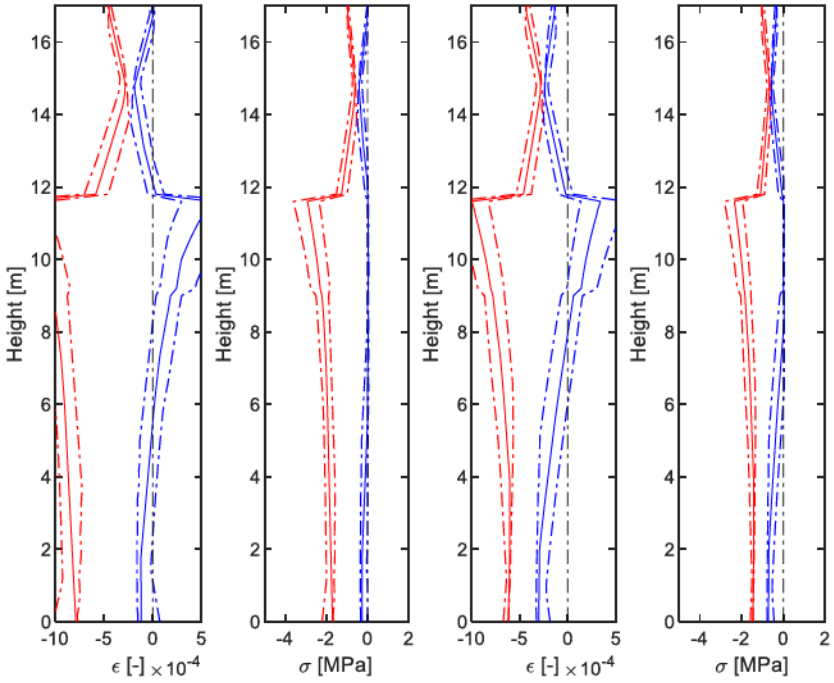

Figure 6.17: fuzzy numbers of the maximum and minimum deformations and tensions in the coupled sections along the height considering the no-tension material (dotted line with α = 0, solid line with α = 1).

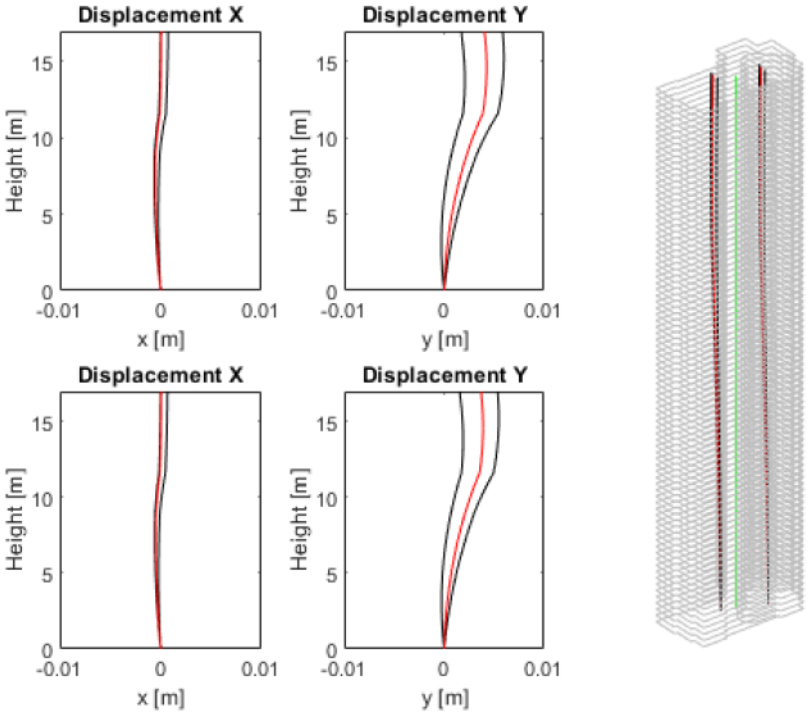

Figure 6.18: fuzzy numbers of the maximum displacements of the two coupled sections along the height of the column (black line with α = 0, red line with α = 1).

6.2.2.2.2 Elastic no-tension constitutive behavior

After having validated the model with the linear elastic constitutive bond, a second structural model is adopted considering a no-tension elastic constitutive relationship constant in all the pillar.

The fuzzy structural analysis allows obtaining interesting information on the uncertainty of the material and the loads.

Figure 6.17 shows the values of the maximum and minimum deformations of the various sections of the column. Furthermore, the maximum and minimum tensions of the various sections of the column are shown.

Because the tensile stresses are not present the variability induced by the fuzzy variables is strongly reduced in correspondence with those sections where the linear elastic model gives consistent traction.

Figure 6.18 shows the displacements along x and y of the column by fuzzy for each section. The displacement fuzzies created are characterized by the most probable value not centered between the extremes of the fuzzy. This shows the propagation of uncertainties.

6.2.2.3 Validation with Monte Carlo simulation

As known, fuzzy numbers are used to define an equivalence class of probability distributions compatible with the available data.

Starting from the description with the fuzzy number of the uncertainties involved, it is possible to evaluate the structural response for certain fractiles (small or large) compared to the Monte Carlo simulation that is widely used in literature. Response variables estimated by fuzzy numbers are generally more conservative than classical probability (Savoia, 2002).

Results tend towards classical probability when the number of tests is large enough to stabilize the mean value. In fact, to assess the probability of failure in rare events, it is necessary to increase the number of samples significantly to capture such events.

Figure 6.19 – 6.20 shows the result of the Monte Carlo simulation for the evaluation of the membership function with $\alpha = 0$ using α-cut (for more details see Section 2.1.4.1) for the two-beam models considered. We see how the variability of the various inputs creates different responses in terms of structural response.

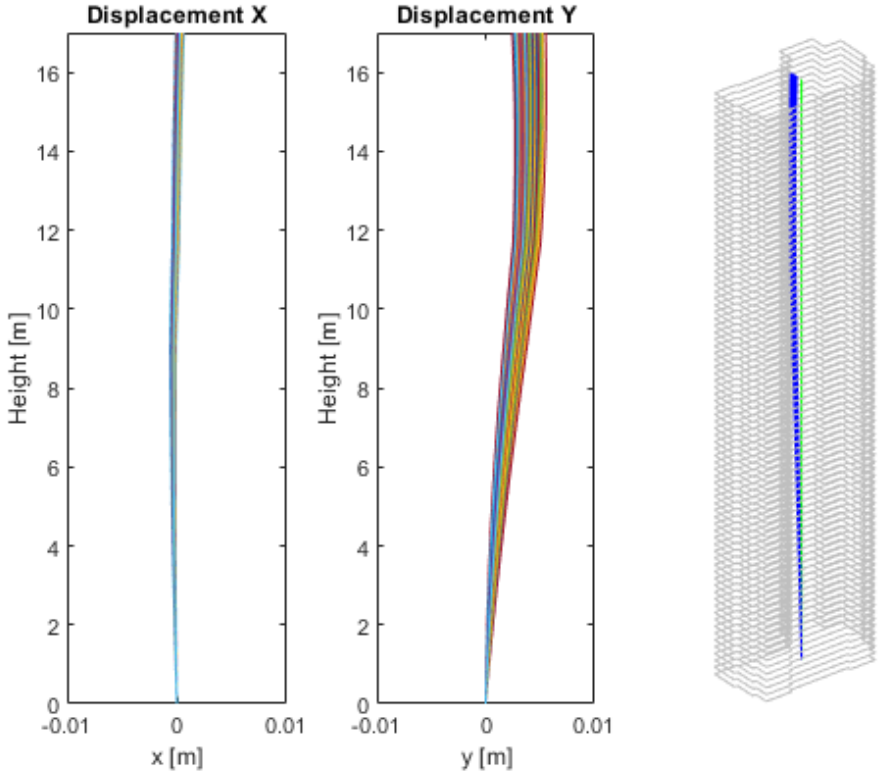

Figure 6.19: displacement of the section along the height of the column thought Monte Carlo simulation.

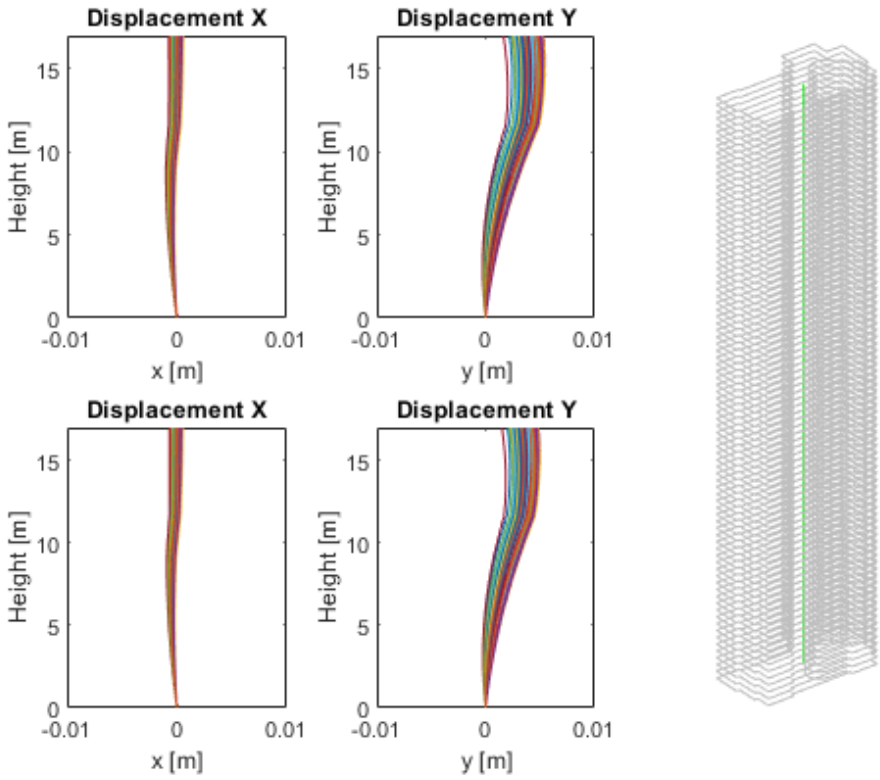

Figure 6.20: displacement of the composite section along the height of the column through Monte Carlo simulation.

For the test, MATLAB on a computer with Intel(R) Core(TM) i5-6200U CPU @ 2.30GHz and 8 GB of RAM was used. The times for a model beam were 290.81s for Monte Carlo Simulation while 154.62s for the fuzzy approach. Both algorithms used for the analyzes were parallelized to reduce computational times. Furthermore, to obtain good results in terms of convergence, Monte Carlo simulations have higher sample numbers than those of fuzzy ones (e.g. $n_{MSC} = 1000$, $n_{Fuzzy} = 100$).

This is due to the fact of a large number of variables present and the desire to minimize the criticalities of the MCS method which, in the presence of insufficiently large tests, can create bias.

It is worth noting that calculating the response using the classic Monte Carlo simulation would be more expensive from a computational point of view.

6.2.3 Performance rating

From the results shown it emerges that the uncertainty of the loads and their relative application significantly affects, for the problem at hand, the structural response compared to the uncertainty of the material alone. In fact, the uncertainty of the horizontal thrusts of the arches and the point of application of the resultant of vertical loads affects the pressure curve and subsequently the stresses and strains distribution. The uncertainty of the material, which is more widely considered in literature, appears less significant and affects above all and only the deformations.

This aspect is not secondary if we consider complex structures whose exact definition of the loads is not certain. In most cases, the average value corresponds to the value normally assumed in deterministic analyzes, therefore the most plausible value.

An important aspect of uncertainty analysis is the interval bounds. The values of the interval bounds show how introducing an uncertainty changes the structural response. Quantifying uncertainties aims to be a tool in the evaluation phase of the structural response of a component and not to be used in the design phase. In fact, anyone we must deal not only with the average value that generally a structural analysis reports but also with the intervals bounds in order to make a correct decision. The correct interpretation of this interval also allows eventually being able to integrate the information with further data provided by experimental tests.

Therefore, the level of knowledge appears important in a structural analysis of monumental buildings.

7 Conclusions

7.1 Overview

The prevention of collapse and damage to structures is one of the most important objectives of earthquake engineering. Advances in computational power and more accurate models allow today to predict structural behavior, making risk assessment possible.

The risk assessment should nowadays be accompanied by the quantification of the uncertainty of the parameters. This allows the analyst to provide, in addition to the quantitative risk assessment, also the margins of the assessment by providing the degree of knowledge of the decisions that will then be made based on the information available.

Various aspects of the uncertainty quantification for unreinforced masonry building were discussed in this dissertation. The thesis aims to achieve the following main objectives:

1. to develop a stochastic methodology upon which can be quantified seismic structural response in presence of vague and imprecise information using simplified mechanical models;
2. to identify, investigate and evaluate the various uncertainties in structural masonry elements in existing and historic structures;
3. to evaluate through sensitivity analysis, the parameters that influence the structural response and the collapse of these elements under seismic actions.

7.2 Summary of findings and conclusions

The present section summarizes the main conclusions of this work and is organized by topic. Some limitations and suggestions for future work associated with specific findings are discussed in the next section.

7.2.1 Uncertainty in fragility curve for local mechanism on regional scale

In recent years, the evaluation of structures on a regional scale has generated significant attention from researchers and stakeholders. Simplified models have been developed for the assessment of the seismic risk of structures in urban areas in order to provide assessments for economic losses of an urban area. This dissertation analyzes the local collapse mechanisms of masonry structures in the territorial context by basing its data on the CARTIS database. The choice of evaluating the local mechanisms is centered on evaluating those masonry structures present in the territory of the city of Ferrara which, due to the lack of connections, are vulnerable and do not have a global behavior.

Chapter 3 presents a methodology for the evaluation of fragility curves for local collapse mechanisms, i.e. simple overturning and vertical bending, for a compartment of the historic center of Ferrara. These mechanisms, which are the most common, are evaluated by including aleatory and epistemic uncertainty. Fragility curves were created for the various mechanisms and finally summarized in a typological curve. The final fragility functions provide an overall assessment of the seismic vulnerability for these classes of buildings. The fragility curves for the MUR1 and MUR2 classes are not very different from each other although the buildings are of different construction periods. What distinguishes the two types is the presence of tie rods or tie beams and connections. The masonry quality is good for both classes. The fragility curves obtained by the two classes are different from the survey. The survey increases the level of knowledge about the walls therefore the curve reduces the uncertainty associated with the geometry of the wall and provides a more detailed description of the walls for the historic aggregate.

The results show the moderate quality of the building stock and the important role of the connections in the vulnerability of the aggregates of masonry buildings. Indeed, the introduction of effective tie rods, modifying the OOP failure mechanisms from rocking to vertical bending, can dramatically reduce the vulnerability of aggregates, keeping the streets of historic centers operational even after strong earthquakes. The proposed approach, due to its computational efficiency, may be useful for identifying

the seismically most fragile typologies of the urban context. Therefore, it is a tool capable of orienting targeted retrofit strategies.

The second part of the study instead investigates the quantification of uncertainties in a rigorous way using the fuzzy set theory (Chapter 4). This approach allows thanks to the available information to provide a probabilistic assessment of the vulnerability of the mechanisms including not only the uncertainty associated with the earthquake but above all the uncertainty associated with geometric data, materials and loads for out-of-plane failure mechanisms in unreinforced masonry buildings (URM) in the city of Ferrara. In particular, we focus on the modeling of uncertainties by fuzzy methods for masonry walls. These walls are made of good quality masonry with fired clay bricks and lime mortar, as typical for the buildings in the Po Valley, such as those hit by the 2012 Emilia earthquake. In the frequent case of slender elements with good material properties, the wall response can be modeled as an assembly of rigid bodies and linear kinematic limit analyses, as defined in NTC2018, or dynamic analyses for studying the rocking motion are utilized. These techniques are employed to provide the "fuzzy" fragility curves as a function of peak ground acceleration (PGA). This is the first step for a probabilistic evaluation of the collapse loads under seismic actions, taking into account the actual variability of seismic input, and sensitivity analysis allows to understand which parameters influence the structural response. As has been shown, seismic input and acting loads play an important role in the behavior of the walls. In general, typological fragility curves for these local mechanisms then provide a first step for the evaluation of damages and the assessment of economic losses on an urban scale. This can help to identify possible scenarios for civil protection.

7.2.2 Uncertainty in stability of masonry columns

The second part of the thesis analyzes the stability and safety of masonry columns. These structural elements are particularly common in historic and monumental buildings. In Chapters 5-6 the masonry columns of the Cathedral of Saint George the Martyr in Ferrara are analyzed.

Chapter 5 is evaluated the current state of column B4 with the relative information on the mechanical properties of the materials, on the loads taking into account the variability of the intensity and of the application points. Particular attention is given to the creation of simplified mechanical models useful to obtain a fair compromise between

computational times and the robustness of the results. These simplified models are validated with analytical solutions and numerical models usually applied (i.e., FEM models). The simplified models created have shown that with a reduced computational effort it is possible to have results similar to those obtained with FEM techniques in terms of strains and stresses. It also shows how the formulas provided for by the codes (NTC 2018, EC6) are conservative with respect to the numerical methods adopted. The reliability of these structural elements is also analyzed considering the role of mechanical properties, loads and their application modes through a Monte Carlo Simulation.

Finally, Chapter 6 presents a procedure for quantifying the uncertainties encountered in the structural analysis of masonry pillars of the cathedral of Ferrara. This method can be applied where the main sources of uncertainties are vague and imprecise information such as the characterization of the material, the loads, and their location. The purpose of quantifying uncertainties is to evaluate the presence of adequate safety margins. These uncertainties are quantified through the fuzzy set theory that allows deriving the interval bounds and the mean structural response.

The results show that the uncertainty of the loads and their relative application significantly affects the structural response compared to the uncertainty of the material alone. In fact, the uncertainty of the horizontal thrusts of the arches and the point of application of the resultant of vertical loads affects the pressure curve and subsequently the stresses and strains distribution. The uncertainty of the material, which is more widely considered in literature, appears less significant and affects the deformations. This aspect is not secondary if we consider complex structures whose exact definition of the loads is not certain. In most cases, the average value corresponds to the value normally assumed in deterministic analyzes, therefore the most plausible value.

An important aspect of uncertainty analysis is the interval bounds. The values of the interval bounds show how introducing an uncertainty changes the structural response. Quantifying uncertainties aims to be a tool in the evaluation phase of the structural response of a component and not to be used in the design phase. Indeed, it is necessary to deal not only with the average value that generally a structural analysis reports but also with the intervals bounds in order to make a correct decision. The correct interpretation of this interval also allows eventually being able to integrate the information

with further data provided by experimental tests. Therefore, the level of knowledge appears really important in a structural analysis of monumental buildings.

7.3 Limitations and suggestions for future work

This dissertation has limitations that require future research developments.
Regarding the local collapse mechanisms for masonry walls, future works will analyze the uncertainty of the various masonry typologies using recent numerical techniques that would be very useful (e.g. p-box, Bayesian updating). In future research, we would like to analyze other aggregates present in Italy, including building typologies similar to those of the Po Valley. This will also have to consider the uncertainties relating to the geometry of macro-elements and loads. The influence of the interaction between the floor effect of masonry structures and the local collapse mechanisms can be a further aspect to be explored. Finally, we will hopefully integrate these results into a comprehensive assessment method including the global behavior of masonry structures.
The study conducted on the columns of the cathedral represents a first step in assessing the safety of the structural elements in a quantitative manner. This was done using the fuzzy set theory which allows a first evaluation of the structural behavior based on the available information. Future research would like to extend the investigation of the quantification of uncertainties by means of sensitivity analyzes that would allow defining in greater detail which parameters influence the structural behavior. A further step would be to define a safety index correlated to the reliability index for this type of structure which is difficult to investigate as a whole due to the considerable variability of the data.
The extension of this methodology would then allow, if properly calibrated, to be applied to monitoring problems of the structures. In fact, by collecting data from experimental tests and simulations, it could be possible to have a more defined picture of the problems and criticalities of the analyzed structures.

7.4 Concluding remarks

This dissertation contributes to improve the role of uncertainties in assessing the reliability and vulnerability of masonry structures by proposing a methodology that evaluates the uncertainty with a probabilistic model based on fuzzy set theory.

The results of this thesis should be interpreted considering the limitation of the studies. It is the hope that assessing the safety of the structural elements in a quantitative manner will be used by researchers and stakeholders to understand the uncertainty to which the risk analysis is subjected and therefore the consequent decision-making process.

List of Symbols

The next list describes several symbols that will be later used within the body of the document.

Probabilistic Methods and procedures

Symbol	Description
~	Fuzziness
α	Membership function value and basis of α-cuts
θ	Vector of epistemic parameters
$\Xi(\cdot)$	Membership function of a fuzzy variable
$\Phi(\cdot)$	Cumulative distribution function (CDF) of a standard normal variable
Ω	Event space
ω	Elementary event

Symbol	Description
$\mathrm{Bel}(\cdot)$	Belief function
$\mathcal{D}$	Domain
$\mathcal{E}$	Event, subset of Ω
$\mathcal{E}^C$	Complementary event to $\mathcal{E}$
$\mathcal{F}$	Collection of events in Ω $(\sigma-\text{algebra})$
$\underline{F}$	Lower bound of a p-box, belief
$\overline{F}$	Upper bound of a p-box, plausibility
$\mathcal{J}$	Event subset of Ω
$\mathbb{E}(\cdot)$	Expected value operator

$\mathbb{I}(\cdot)$	Indicator function
m	Probability mass, basic probability assignment
n_{MCS}	number of samples in Montecarlo Simulation
$\mathbb{P}(\cdot)$	Probability measure
$\mathbb{R}$	Space of real numbers
S_i	First order of Sobol ’indices
S_{T_i}	Total order of Sobol ’indices
$\mathrm{Pls}(\cdot)$	Plausibility function
$\mathrm{Var}(\cdot)$	Variance

List of Acronyms

The next list describes several acronyms that will be later used within the body of the document.

Probabilistic models

BPA	Basic probability assignment
CDF	Cumulative distribution function
DS	Dempster-Shafer
eCDF	Empirical cumulative distribution function
FORM	First order reliability method
MC	Monte Carlo
MCS	Monte Carlo Simulation
PDF	Probability density function
SA	Sensitivity Analysis
UP	Uncertainty propagation
UQ	Uncertainty quantification

Risk assessment

JCSS	Joint Committee on Structural Safety
PRA	Probabilistic Risk Assessment
PSA	Probabilistic Safety Assessment
QRA	Quantitative Risk Assessment

Other acronyms

CDP	Concrete Damage Plasticity
DEM	Discrete Element Method
DMEM	Discrete Macro-Element Modeling
FEM	Finite Element Method
IM	Intensity measure
MAF	Mean Annual Frequency

MQI	Masonry Quality Index
MSA	Multiple Stripe Analysis
MUR 1	Masonry type 1
MUR 2	Masonry type 2
NSCD	Non-Smooth Contact dynamics
OOP	Out-of-plane
PBEE	Probabilistic based earthquake engineering
PEER	Pacific Earthquake Engineering Research
PGA	Peak ground acceleration
PSHA	Probabilistic seismic hazard analysis
SDOF	Single degree of freedom
TSC	Total strain-based crack
ULS	Ultimate Limit State
URM	Unreinforced masonry

Appendix A Experimental tests

The average values of the tests on brick-and-mortar samples carried out by the LIFE s.r.l. laboratory is shown below for the masonry of the cathedral of Ferrara, considering the first and second investigation campaigns. We thank the engineers of the cathedral's intervention works for the data provided (Mezzadringegneria s.r.l.).

Table 0.1: results of compression tests on brick cubes.

Period	ID TEST	Strength [MPa]
2015-2017	1	14.2
	2	14.6
	3	14.2
	4	12.9
	5	12.9
	6	13.9
	7	11.5
	8	13.5
	9	11.1
2019	10	27.86
	11	26.65
	12	25.53
	13	23.95
	14	24.56
	15	25.58
	16	18.13
	17	17.62
	18	19.61
	19	14.48
	20	14.20
	21	12.82

Table 0.2: double punching tests on eighteenth-century mortar.

Period	ID TEST	Strength [MPa]
2015-2017	1	4.2
	2	2.8
	3	4.2
	4	3.44
	5	3.57
	6	3.5
	7	3.57
	8	3.5
	9	2.8
	10	4.2
	11	2.39
	12	1.94
	13	2.32
	14	2.07
	15	2.17
	16	2.1
	17	2.23
	18	2.17
	19	2.17
	20	2.1
2019	21	3.57
	22	3.31
	23	3.06
	24	4.20
	25	2.93
	26	2.80
	27	3.06
	28	3.44
	29	2.93
	30	2.67

Table 0.3: double punching tests on medieval mortar.

Period	ID TEST	Strength [MPa]
2015-2017	1	5.22
	2	4.58
	3	4.2
	4	3.57
	5	4.07
	6	3.95
	7	3.69
	8	3.18
	9	4.2
	10	3.95

Results of double jack test

LABORATORI INGEGNERIA FERRARA

committente: LEONARDO SRL
indirizzo: -
cantiere: DUOMO CATTEDRALE DI FERRARA
commessa: 1651
documento: doc14 Rev.00 del 30/05/2019
data prove: 15/05/2019

parte d'opera:	COLONNA B4	
spessore muratura:	--	cm
tipologia muratura:	MATTONI PIENI - MALTA di CALCE	
tensione di esercizio misurata con martinetto singolo:	1,94	MPa
tensione di uscita dal campo elastico lineare:	4,21	MPa
tensione di rottura:	4,70	MPa
modulo Young verticale:	4156	MPa
modulo di Poisson:	0,38	-
modulo di elaticità tangenziale:	1510	MPa

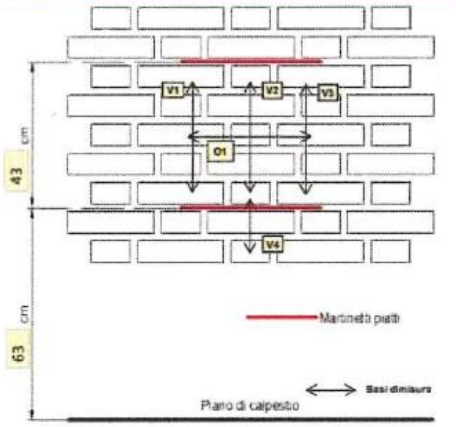

La figura illustra schematicamente la disposizione e la codifica delle basi di misura rispetto ai martinetti piatti.
La tipologia e la tessitura della muratura disegnata sono da considerarsi come puramente esemplificative.

ALLEGATO NUMERICO

ID MP1	MARTINETTO PIATTO DOPPIO - ASTM C 1197						
tensione di compressione	base deformometrica millesimale (lunghezza iniziale 250mm)						Modulo Poisson
	εV1	εV2	εV3	εV4	ηO1	ηO2	
[MPa]	[micron/m]	[micron/m]	[micron/m]	[micron/m]	[micron/m]	[micron/m]	-
0,00	0	0	0		0		
0,32	140	224	20		-4		
0,65	260	-44	-288		-120		
0,97	380	104	-204		-124		
1,30	480	204	-164		-144		
0,65	376	72	-280		-192		
0,00	128	-192	-456		-20		
0,65	332	48	-252		-84		
1,30	512	240	-112		-68		0,32
1,62	576	248	-48		-112		0,43
1,94	628	376	-104		-300		
1,30	508	232	-236		-196		
0,65	356	104	-212		-128		
0,00	108	-148	-408		-16		
0,65	372	88	-296		-64		

Bibliography

ABK, 1981. *Methodology for mitigation of seismic hazards in existing unreinforced masonry building: wall testing, out plane*. El Segundo, California.

Abrahamson, N. A., and Bommer, J. J., 2005. Probability and Uncertainty in Seismic Hazard Analysis. *Earthquake Spectra*, **21**(2), 603–607. SAGE Publications Ltd STM. DOI: 10.1193/1.1899158

Adam, J. M., Brencich, A., Hughes, T. G., and Jefferson, T., 2010. Micromodelling of eccentrically loaded brickwork: Study of masonry wallettes. *Engineering Structures*, **32**(5), 1244–1251. DOI: 10.1016/j.engstruct.2009.12.050

Alfarah, B., López-Almansa, F., and Oller, S., 2017. New methodology for calculating damage variables evolution in Plastic Damage Model for RC structures. *Engineering Structures*, **132**, 70–86. DOI: 10.1016/j.engstruct.2016.11.022

Amster, H. J., and Djomehri, M. J., 1976. Prediction of Statistical Error in Monte Carlo Transport Calculations. *Nuclear Science and Engineering*, **60**(2), 131–142. Taylor & Francis. DOI: 10.13182/NSE76-A26869

Ang, A. H.-S., and Tang, W. H., 2007. *Probability concepts in engineering: emphasis on applications in civil & environmental engineering* (2nd ed.). New York: Wiley.

Angelillo, M., Lourenço, P. B., and Milani, G., 2014. Masonry behaviour and modelling. In M. Angelillo (Ed.), *Mechanics of Masonry Structures*, CISM International Centre for Mechanical Sciences (Vol. 551, pp. 1–26). Vienna: Springer Vienna. DOI: 10.1007/978-3-7091-1774-3_1

de Angelis, M., Patelli, E., and Beer, M., 2017. Forced Monte Carlo Simulation Strategy for the Design of Maintenance Plans with Multiple Inspections. *ASCE-ASME Journal of Risk and Uncertainty in Engineering Systems, Part A: Civil Engineering*, **3**(2). DOI: 10.1061/AJRUA6.0000868

ASCE, 2010. *Minimum design loads for buildings and other structures (ASCE/SEI 7-*

10). Reston, VA, USA: American Society of Civil Engineers (ASCE).

Asteris, P. G., Moropoulou, A., Skentou, A. D., Apostolopoulou, M., Mohebkhah, A., Cavaleri, L., Rodrigues, H., et al., 2019. Stochastic Vulnerability Assessment of Masonry Structures: Concepts, Modeling and Restoration Aspects. *Applied Sciences*, **9**(2), 243. DOI: 10.3390/app9020243

Augusti, G., Baratta, A., and Casciati, F., 1984. *Probabilistic Methods in Structural Engineering*. CRC Press.

Augusti, G., and Ciampoli, M., 2000. Heritage buildings and seismic reliability. *Progress in Structural Engineering and Materials*, **2**(2), 225–237. John Wiley & Sons, Ltd. DOI: 10.1002/1528-2716(200004/06)2:2<225::AID-PSE28>3.0.CO;2-5

Aven, T., and Renn, O., 2010. Risk Management. *Risk Management and Governance* (pp. 121–158). Berlin, Heidelberg: Springer Berlin Heidelberg. DOI: 10.1007/978-3-642-13926-0_8

Ayyub, B. M., 2014. *Risk analysis in engineering and economics* (Second edition.). Boca Raton: CRC Press, Taylor & Francis Group.

Babuška, I., and Motamed, M., 2016. A fuzzy-stochastic multiscale model for fiber composites: A one-dimensional study. *Computer Methods in Applied Mechanics and Engineering*, **302**, 109–130. DOI: 10.1016/j.cma.2015.12.016

Baker, J. W., 2015. Efficient Analytical Fragility Function Fitting Using Dynamic Structural Analysis. *Earthquake Spectra*, **31**(1), 579–599. DOI: 10.1193/021113EQS025M

Baratta, A., 1991. Statics and Reliability of Masonry Structures. In F. Casciati and J. B. Roberts (Eds.), *Reliability Problems: General Principles and Applications in Mechanics of Solids and Structures* (pp. 205–235). Vienna: Springer Vienna. DOI: 10.1007/978-3-7091-2616-5_6

Barthe, D., Deraemaeker, A., Ladevèze, P., and Guillaume, P., 2003. On a Theory of the Quantification of the Lack of Knowledge (LOK) in Structural Computation. *IMAC XXI - 21st International Modal Analysis Conference*. Kissimmee, United States.

Bazzurro, P., and Cornell, C. A., 1999. Disaggregation of seismic hazard. *Bulletin of*

the Seismological Society of America, **89**(2), 501–520.

Beer, M., Ferson, S., and Kreinovich, V., 2013. Imprecise probabilities in engineering analyses. *Mechanical Systems and Signal Processing*, **37**(1), 4–29. DOI: 10.1016/j.ymssp.2013.01.024

Ben-Haim, Y., 2006. *Info-gap decision theory: decisions under severe uncertainty* (2. ed.). Amsterdam: Academic Press.

Benjamin, J., and Cornell, C. A., 1970. *Probability, Statistics, and Decisions for Civil Engineers*. New York: Dover Publications, Inc.

Beolchini, G., Milano, L., and Antonacci, E., 2005. *Repertorio dei meccanismi di danno, delle tecniche di intervento e dei relativi costi negli edifici in muratura - Definizione di modelli per l'analisi strutturale degli edifici in muratura* (No. Volume II-Parte I). Convenzione di Ricerca con la Regione Marche; Consiglio Nazionale delle Ricerche - Istituto per la Tecnologia delle Costruzioni - Sede di L'Aquila; Dipartimento di Ingegneria delle Strutture, delle Acque e del Terreno (DISAT) - Università degli Studi di L'Aquila (p. 93). L'Aquila: Regione Molise.

Bi, S., Broggi, M., Wei, P., and Beer, M., 2019. The Bhattacharyya distance: Enriching the P-box in stochastic sensitivity analysis. *Mechanical Systems and Signal Processing*, **129**, 265–281. DOI: 10.1016/j.ymssp.2019.04.035

Bi, S., Ouisse, M., and Foltête, E., 2018. Probabilistic Approach for Damping Identification Considering Uncertainty in Experimental Modal Analysis. *AIAA Journal*, **56**(12), 4953–4964. American Institute of Aeronautics and Astronautics. DOI: 10.2514/1.J057432

Binda, L., Anzani, A., and Garavaglia, E., 2008. Simple checks to prevent the collapse of heavy historical structures and residual life prevision through a probabilistic model. In L. Binda (Ed.), *Learning from Failure Long-term Behaviour of Heavy Masonry Structures*, International Series on Advances in Architecture (pp. 205–223). Southampton, Boston: WIT Press.

Binda, L., Anzani, A., and Saisi, A., 2008. Failures due to long-term behaviour of heavy structures. *Learning from Failure Long-term Behaviour of Heavy Masonry Structures*, International Series on Advances in Architecture (pp. 1–28). WIT Press.

Bindi, D., Pacor, F., Luzi, L., Puglia, R., Massa, M., Ameri, G., and Paolucci, R., 2011. Ground motion prediction equations derived from the Italian strong motion database. *Bulletin of Earthquake Engineering*, **9**(6), 1899–1920. DOI: 10.1007/s10518-011-9313-z

Booth, T. E., and Amster, H. J., 1978. Prediction of Monte Carlo Errors by a Theory Generalized to Treat Track-Length Estimators. *Nuclear Science and Engineering*, **65**(2), 273–281. Taylor & Francis. DOI: 10.13182/NSE78-A27156

Borri, A., 2003. *La nuova normativa antisismica per gli edifici esistenti in muratura*. Caltagirone.

Borri, A., Corradi, M., Castori, G., and De Maria, A., 2015. A method for the analysis and classification of historic masonry. *Bulletin of Earthquake Engineering*, **13**(9), 2647–2665. DOI: 10.1007/s10518-015-9731-4

Borri, A., Corradi, M., and De Maria, A., 2020. The Failure of Masonry Walls by Disaggregation and the Masonry Quality Index. *Heritage*, **3**(4). DOI: 10.3390/heritage3040065

Boscato, G., Pizzolato, M., Russo, S., and Tralli, A., 2014. Seismic Behavior of a Complex Historical Church in L'Aquila. *International Journal of Architectural Heritage*, **8**(5), 718–757. DOI: 10.1080/15583058.2012.736013

Bracchi, S., Rota, M., Magenes, G., and Penna, A., 2016. Seismic assessment of masonry buildings accounting for limited knowledge on materials by Bayesian updating. *Bulletin of Earthquake Engineering*, **14**(8), 2273–2297. DOI: 10.1007/s10518-016-9905-8

Brencich, A., and de Felice, G., 2009. Brickwork under eccentric compression: Experimental results and macroscopic models. *Compatibility of Plasters and Renders on Salt Loaded Substrates*, **23**(5), 1935–1946. DOI: 10.1016/j.conbuildmat.2008.09.004

Broseghini, M., Zanetti, P., Jefferson, A. D., and Gei, M., 2018. Progressive instability in circular masonry columns. *Engineering Structures*, **157**, 96–104. DOI: 10.1016/j.engstruct.2017.11.044

Bruneau, M., and Reinhorn, A., 2007. Exploring the Concept of Seismic Resilience for Acute Care Facilities. *Earthquake Spectra*, **23**(1), 41–62. SAGE Publications Ltd

STM. DOI: 10.1193/1.2431396

Buratti, N., Ferracuti, B., Savoia, M., Antonioni, G., and Cozzani, V., 2012. A Fuzzy-Sets Based Approach for Modelling Uncertainties in Quantitative Risk Assessment of Industrial Plants Under Seismic Actions. *Chemical Engineering Transactions*, **26**, 105–110. DOI: 10.3303/CET1226018

Buratti, N., Minghini, F., Ongaretto, E., Savoia, M., and Tullini, N., 2017. Empirical seismic fragility for the precast RC industrial buildings damaged by the 2012 Emilia (Italy) earthquakes. *Earthquake Engineering & Structural Dynamics*, **46**(14), 2317–2335. John Wiley & Sons, Ltd. DOI: 10.1002/eqe.2906

Caddemi, S., Ricciardi, G., and Saccà, C., 2002. Limit Analysis of Structures with Stochastic Strengths by a Static Approach. *Meccanica*, **37**(6), 527–544. DOI: 10.1023/A:1020939103140

Carbonara, G., 2015. Lavori di riparazione e miglioramento sismico della Cattedrale di Ferrara.

Carocci, C. F., 2012. Small centres damaged by 2009 L'Aquila earthquake: on site analyses of historical masonry aggregates. *Bulletin of Earthquake Engineering*, **10**(1), 45–71. DOI: 10.1007/s10518-011-9284-0

Casciati, F., and Faravelli, L., 2008. A Knowledge-Based System for Seismic Vulnerability Assessment of Masonry Buildings. *Computer-Aided Civil and Infrastructure Engineering*, **6**(4), 291–301. DOI: 10.1111/j.1467-8667.1991.tb00260.x

Cattari, S., Camilletti, D., Lagomarsino, S., Bracchi, S., Rota, M., and Penna, A., 2018. Masonry Italian Code-Conforming Buildings. Part 2: Nonlinear Modelling and Time-History Analysis. *Journal of Earthquake Engineering*, **22**(sup2), 2010–2040. DOI: 10.1080/13632469.2018.1541030

Cattari, S., Degli Abbati, S., Ferretti, D., Lagomarsino, S., Ottonelli, D., Rossi, M., and Tralli, A., 2012. The seismic behaviour of ancient masonry buildings after the earthquake in Emilia (Italy) on May 20th and 29th, 2012. *Ingegneria Sismica*, **29**(2–3), 87–119.

Cavaleri, L., Failla, A., La Mendola, L., and Papia, M., 2005. Experimental and analytical response of masonry elements under eccentric vertical loads. *Engineering*

Structures, **27**(8), 1175–1184. DOI: 10.1016/j.engstruct.2005.02.012

Cecchi, A., and Tralli, A., 2012. A homogenized viscoelastic model for masonry structures. *International Journal of Solids and Structures*, **49**(13), 1485–1496. DOI: 10.1016/j.ijsolstr.2012.02.034

CEN, 2004. *Eurocode 8: Design of structures for earthquake resistance of structures, Part 1-1: General rules, seismic actions and rules for buildings*. *EN 1998-1:2004*.

CEN, 2005a. *Eurocode 6 - Design of masonry structures - Part 1-1: General rules for reinforced and unreinforced masonry structures*.

CEN, 2005b. *Eurocode 8 - Design of structures for earthquake resistance - Part 3: Assessment and retrofitting of buildings.*

Chácara, C., Cannizzaro, F., Pantò, B., Caliò, I., and Lourenço, P. B., 2019. Seismic vulnerability of URM structures based on a Discrete Macro-Element Modeling (DMEM) approach. *Engineering Structures*, **201**, 109715. DOI: 10.1016/j.engstruct.2019.109715

Chioccarelli, E., De Luca, F., and Iervolino, I., 2012a. *Preliminary study of Emilia (May 20th 2012) earthquake ground motion records V2.11*. Terremoto Emilia 2012 (p. 110). Naples, Italy: ReLUIS.

Chioccarelli, E., De Luca, F., and Iervolino, I., 2012b. *Preliminary study of Emilia (May 29th 2012) earthquake ground motion records V1.0*. Terremoto Emilia 2012 (p. 64). Naples, Italy: ReLUIS.

Chiozzi, A., and Miranda, E., 2017. Fragility functions for masonry infill walls with in-plane loading. *Earthquake Engineering & Structural Dynamics*, **46**(15), 2831–2850. DOI: 10.1002/eqe.2934

Chiozzi, A., Nale, M., and Tralli, A., 2017. Fragility assessment of non-structural components undergoing earthquake induced rocking motion. *Atti del XVII Convegno ANIDIS L'ingegneria Sismica in Italia : Pistoia, 17-21 settembre 2017*. Pisa: Pisa University Press. Retrieved from http://digital.casalini.it/9788867418541

Chitty, L., 1947. LXXVIII. On the cantilever composed of a number of parallel beams interconnected by cross bars. *The London, Edinburgh, and Dublin Philosophical*

Magazine and Journal of Science, 7, **38**(285), 685–699. Taylor & Francis. DOI: 10.1080/14786444708521646

Choi, K.-K., Lissel, S. L., and Reda Taha, M. M., 2007. Rheological modelling of masonry creep. *Canadian Journal of Civil Engineering*, **34**(11), 1506–1517. NRC Research Press. DOI: 10.1139/L07-062

Clementi, F., 2021. Failure Analysis of Apennine Masonry Churches Severely Damaged during the 2016 Central Italy Seismic Sequence. *Buildings*, **11**(58). DOI: https://doi.org/10.3390/buildings 11020058

Clementi, F., Milani, G., Ferrante, A., Valente, M., and Lenci, S., 2019. Crumbling of Amatrice clock tower during 2016 Central Italy seismic sequence: Advanced numerical insights. *Frattura ed Integrità Strutturale*, **14**(51), 313–335. DOI: 10.3221/IGF-ESIS.51.24

Colangelo, F., 2012. A simple model to include fuzziness in the seismic fragility curve and relevant effect compared with randomness: A model to include fuzziness in the fragility curve. *Earthquake Engineering & Structural Dynamics*, **41**(5), 969–986. DOI: 10.1002/eqe.1169

Colangelo, F., 2013. Probabilistic characterisation of an analytical fuzzy-random model for seismic fragility computation. *Structural Safety*, **40**, 68–77. DOI: 10.1016/j.strusafe.2012.09.008

Como, M., 2013. *Statics of Historic Masonry Constructions*. Springer Series in Solid and Structural Mechanics (1st ed.). Springer-Verlag Berlin Heidelberg.

de Cooman, G., Ruan, D., and Kerre, E. E., 1995. *Foundations and Applications of Possibility Theory*. Advances in Fuzzy Systems? Applications and Theory (Vol. 8). World Scientific. DOI: 10.1142/2775

Cornell, C. A., 1968. Engineering seismic risk analysis. *Bulletin of the Seismological Society of America*, **58**(5), 1583–1606.

Cornell, C. A., 1969. A Probability-Based Structural Code. *ACI Journal Proceedings*, **66**(12), 974–985. DOI: 10.14359/7446

Cultrera, G., Faenza, L., Meletti, C., D'Amico, V., Michelini, A., and Amato, A., 2014.

Shakemaps uncertainties and their effects in the post-seismic actions for the 2012 Emilia (Italy) earthquakes. *Bulletin of Earthquake Engineering*, **12**(5), 2147–2164. DOI: 10.1007/s10518-013-9577-6

D'Altri, A. M., Sarhosis, V., Milani, G., Rots, J., Cattari, S., Lagomarsino, S., Sacco, E., et al., 2020. Modeling Strategies for the Computational Analysis of Unreinforced Masonry Structures: Review and Classification. *Archives of Computational Methods in Engineering*, **27**(4), 1153–1185. DOI: 10.1007/s11831-019-09351-x

D'Ayala, D., 2005. Force and Displacement Based Vulnerability Assessment for Traditional Buildings. *Bulletin of Earthquake Engineering*, **3**(3), 235–265. DOI: 10.1007/s10518-005-1239-x

D'Ayala, D., 2013. Assessing the seismic vulnerability of masonry buildings. In K. Goda and S. Tesfamariam (Eds.), *Handbook of Seismic Risk Analysis and Management of Civil Infrastructure Systems* (pp. 334–365). Woodhead Publishing. DOI: 10.1533/9780857098986.3.334

D'Ayala, D., and Speranza, E., 2003. Definition of Collapse Mechanisms and Seismic Vulnerability of Historic Masonry Buildings. *Earthquake Spectra*, **19**(3), 479–509. DOI: 10.1193/1.1599896

De Falco, A., and Lucchesi, M., 2002. Stability of columns with no tension strength and bounded compressive strength and deformability. Part I: large eccentricity. *International Journal of Solids and Structures*, **39**(25), 6191–6210. DOI: 10.1016/S0020-7683(02)00467-5

De Falco, A., and Lucchesi, M., 2003. Explicit Solutions for the Stability of No-Tension Beam-Columns. *International Journal of Structural Stability and Dynamics*, **03**(02), 195–213. World Scientific Publishing Co. DOI: 10.1142/S0219455403000823

Decanini, L., De Sortis, A., Goretti, A., Langenbach, R., Mollaioli, F., and Rasulo, A., 2004. Performance of Masonry Buildings during the 2002 Molise, Italy, Earthquake. *Earthquake Spectra*, **20**(1_suppl), 191–220. DOI: 10.1193/1.1765106

Deierlein, G. G., Krawinkler, H., and Cornell, C. A., 2003. A framework for performance-based earthquake engineering. *Pacific Conference on Earthquake Engineering* (pp. 140–148). DOI: 10.1061/9780784412121.173

DeJong, M. J., and Dimitrakopoulos, E. G., 2014. Dynamically equivalent rocking structures. *Earthquake Engineering & Structural Dynamics*, **43**(10), 1543–1563. DOI: 10.1002/eqe.2410

Dempster, A. P., 1967. Upper and Lower Probabilities Induced by a Multivalued Mapping. *The Annals of Mathematical Statistics*, **38**(2), 325–339. DOI: 10.1214/aoms/1177698950

Di Ludovico, M., Chiaradonna, A., Bilotta, E., Flora, A., and Prota, A., 2020. Empirical damage and liquefaction fragility curves from 2012 Emilia earthquake data. *Earthquake Spectra*, **36**(2), 507–536. SAGE Publications Ltd STM. DOI: 10.1177/8755293019891713

Dimitrakopoulos, E. G., and Paraskeva, T. S., 2015. Dimensionless fragility curves for rocking response to near-fault excitations. *Earthquake Engineering & Structural Dynamics*, **44**(12), 2015–2033. John Wiley & Sons, Ltd. DOI: 10.1002/eqe.2571

Doherty, K., Griffith, M. C., Lam, N., and Wilson, J., 2002. Displacement-based seismic analysis for out-of-plane bending of unreinforced masonry walls. *Earthquake Engineering and Structural Dynamics*. DOI: 10.1002/eqe.126

Dolce, M., Speranza, E., Dalla Negra, R., Zuppiroli, M., and Bocchi, F., 2015. Constructive Features and Seismic Vulnerability of Historic Centres Through the Rapid Assessment of Historic Building Stocks. The Experience of Ferrara, Italy (pp. 165–175). DOI: 10.1007/978-3-319-08533-3_14

Drysdale, R. G., and Hamid, A. A., 1983. Capacity of Concrete Block Masonry Prisms under Eccentric Compressive Loading. *ACI Journal Proceedings*, **80**(2). DOI: 10.14359/10465

Dubois, D., and Prade, H., 1988. *Possibility Theory*. Boston, MA: Springer US. DOI: 10.1007/978-1-4684-5287-7

Dubois, D., Prade, H. M., and Dubois, D. J., 1994. *Fuzzy sets and systems: theory and applications*. Mathematics in science and engineering (6. [print.].). New York, NY: Academic Press.

Dubourg, V., and Sudret, B., 2014. Meta-model-based importance sampling for reliability sensitivity analysis. *Special Issue In Honor of Professor Wilson H. Tang*, **49**, 27–

36. DOI: 10.1016/j.strusafe.2013.08.010

Eads, L., 2013, October. *Seismic collapse risk assessment of buildings: effects of intensity measure selection and computational approach* (PhD Dissertation). Stanford, CA, USA: Stanford University.

Eads, L., Miranda, E., Krawinkler, H., and Lignos, D. G., 2013. An efficient method for estimating the collapse risk of structures in seismic regions. *Earthquake Engineering & Structural Dynamics*, **42**(1), 25–41. John Wiley & Sons, Ltd. DOI: 10.1002/eqe.2191

Eldred, M. S., Swiler, L. P., and Tang, G., 2011. Mixed aleatory-epistemic uncertainty quantification with stochastic expansions and optimization-based interval estimation. *Reliability Engineering & System Safety*, Quantification of Margins and Uncertainties, **96**(9), 1092–1113. DOI: 10.1016/j.ress.2010.11.010

ElGawady, M. A., Ma, Q., Butterworth, J. W., and Ingham, J., 2011. Effects of interface material on the performance of free rocking blocks. *Earthquake Engineering & Structural Dynamics*, **40**(4), 375–392. DOI: 10.1002/eqe.1025

Ellingwood, B., 1981. Analysis of Reliability for Masonry Structures. *Journal of the Structural Division*, **107**(5), 757–773. DOI: 10.1061/JSDEAG.0005703

Ellingwood, B. R., and Kinali, K., 2009. Quantifying and communicating uncertainty in seismic risk assessment. *Structural Safety*, Risk Acceptance and Risk Communication, **31**(2), 179–187. DOI: 10.1016/j.strusafe.2008.06.001

Enßlin, M., 1941. *Hütte - Des Ingenieurs Taschenbuch* (27th ed., Vol. 1). Berlin: Akademischer Verein Hütte.

Faes, M. G. R., Daub, M., Marelli, S., Patelli, E., and Beer, M., 2021. Engineering analysis with probability boxes: A review on computational methods. *Structural Safety*, **93**, 102092. DOI: 10.1016/j.strusafe.2021.102092

de Felice, G., and Giannini, R., 2001. Out-of-plane seismic resistance of masonry walls. *Journal of Earthquake Engineering*, **5**(2), 253–271. DOI: 10.1080/13632460109350394

Ferrante, A., Loverdos, D., Clementi, F., Milani, G., Formisano, A., Lenci, S., and

Sarhosis, V., 2021. Discontinuous approaches for nonlinear dynamic analyses of an ancient masonry tower. *Engineering Structures*, **230**, 111626. DOI: 10.1016/j.engstruct.2020.111626

Ferrari, P., and Savoia, M., 1998. Fuzzy number theory to obtain conservative results with respect to probability. *Computer Methods in Applied Mechanics and Engineering*, **160**(3–4), 205–222. DOI: 10.1016/S0045-7825(97)00301-0

Ferreira, T. M., Maio, R., Costa, A. A., and Vicente, R., 2017. Seismic vulnerability assessment of stone masonry façade walls: Calibration using fragility-based results and observed damage. *Soil Dynamics and Earthquake Engineering*, **103**, 21–37. DOI: 10.1016/j.soildyn.2017.09.006

Ferretti, D., and Tralli, A., 2013, February 1. Edifici in Muratura - Danneggiamento sisma Emilia 2012.

Ferson, S., and Ginzburg, L. R., 1996. Different methods are needed to propagate ignorance and variability. *Reliability Engineering & System Safety*, Treatment of Aleatory and Epistemic Uncertainty, **54**(2), 133–144. DOI: 10.1016/S0951-8320(96)00071-3

Fioravante, V., and Giretti, D., 2013. *Comune di Ferrara Studio di Microzonazione Sismica di Terzo Livello Attuazione dell'Articolo 11 della Legge 2 giugno 2009 n.77, dell'O.P.C.M 4007/2012 e della Delibera della Giunta Regionale dell'Emilia-Romagna, 1302-2012*. Ferrara: Università degli Studi di Ferrara - Dipartimento di Ingegneria.

Fioravante, V., Giretti, D., Abate, G., Aversa, S., Boldini, D., Capilleri, P. P., Cavallaro, A., et al., 2013. Earthquake Geotechnical Engineering Aspects of the 2012 Emilia-Romagna Earthquake (Italy). *International Conference on Case Histories in Geotechnical Engineering* (pp. 1–34). Presented at the 7th Conference of the International Conference on Case Histories in Geotechnical Engineering, Chicago, IL, USA: Missouri University of Science and Technology.

Flage, R., and Aven, T., 2015. Emerging risk – Conceptual definition and a relation to black swan type of events. *Reliability Engineering & System Safety*, **144**, 61–67. DOI: 10.1016/j.ress.2015.07.008

Förster, V., 2018. *Tragfähigkeit unbewehrter Beton-und Mauerwerksdruckglieder bei zweiachsig exzentrischer Beanspruchung* (PhD Dissertation). Darmstadt: Technische Universität Darmstadt.

Frangopol, D. M., Ide, Y., Spacone, E., and Iwaki, I., 1996. A new look at reliability of reinforced concrete columns. *Structural Safety*, **18**(2), 123–150. DOI: 10.1016/0167-4730(96)00015-X

Frisch-Fay, R., 1975. Stability of masonry piers. *International Journal of Solids and Structures*, **11**(2), 187–198. DOI: 10.1016/0020-7683(75)90052-9

Gei, M., and Misseroni, D., 2018. Experimental investigation of progressive instability and collapse of no-tension brickwork pillars. *International Journal of Solids and Structures*, **155**, 81–88. DOI: 10.1016/j.ijsolstr.2018.07.010

Giresini, L., Fragiacomo, M., and Lourenço, P. B., 2015. Comparison between rocking analysis and kinematic analysis for the dynamic out-of-plane behavior of masonry walls. *Earthquake Engineering & Structural Dynamics*, **44**(13), 2359–2376. DOI: 10.1002/eqe.2592

Giuffré, A., 1996. A Mechanical Model for Statics and Dynamics of Historical Masonry Buildings. *Protection of the Architectural Heritage Against Earthquakes* (pp. 71–152). Vienna: Springer Vienna. DOI: 10.1007/978-3-7091-2656-1_4

Graziotti, F., Tomassetti, U., Penna, A., and Magenes, G., 2016. Out-of-plane shaking table tests on URM single leaf and cavity walls. *Engineering Structures*, **125**, 455–470. DOI: 10.1016/j.engstruct.2016.07.011

Gurel, M. A., 2016. Stability of Slender Masonry Columns with Circular Cross-Section under Their Own Weight and Eccentric Vertical Load. *International Journal of Architectural Heritage*, **10**(8), 1008–1024. Taylor & Francis. DOI: 10.1080/15583058.2016.1177748

Hall, J. W., Rubio, E., and Anderson, M. G., 2004. Random sets of probability measures in slope hydrology and stability analysis. *Zeitschrift für Angewandte Mathematik und Mechanik*, **84**(10–11), 710–720. DOI: 10.1002/zamm.200410146

Haselton, C., and Deierlein, G., 2007. *Assessing seismic collapse safety of modern reinforced concrete moment frame buildings* (No. Report 156). Stanford University,

CA, USA: The John A. Blume Earthquake Engineering Center.

Hatzinikolas, M., Longworth, J., and Warwaruk, J., 1980. Failure Modes for Eccentrically Loaded Concrete Block Masonry Walls. *ACI Journal Proceedings*, **77**(4). DOI: 10.14359/7003

Helton, J. C., and Burmaster, D. E., 1996. Guest editorial: treatment of aleatory and epistemic uncertainty in performance assessments for complex systems. *Reliability Engineering & System Safety*, Treatment of Aleatory and Epistemic Uncertainty, **54**(2), 91–94. DOI: 10.1016/S0951-8320(96)00066-X

Helton, J. C., Johnson, J. D., and Oberkampf, W. L., 2004. An exploration of alternative approaches to the representation of uncertainty in model predictions. *Reliability Engineering & System Safety*, Alternative Representations of Epistemic Uncertainty, **85**(1), 39–71. DOI: 10.1016/j.ress.2004.03.025

Helton, J. C., Johnson, J. D., Oberkampf, W. L., and Sallaberry, C. J., 2006. Sensitivity analysis in conjunction with evidence theory representations of epistemic uncertainty. *The Fourth International Conference on Sensitivity Analysis of Model Output (SAMO 2004)*, **91**(10), 1414–1434. DOI: 10.1016/j.ress.2005.11.055

Helton, J. C., and Oberkampf, W. L., 2004. Alternative representations of epistemic uncertainty. *Reliability Engineering & System Safety*, **85**(1), 1–10. DOI: 10.1016/j.ress.2004.03.001

Heyman, J., 1995. *The stone skeleton: structural engineering of masonry architecture*. Cambridge, UK: Cambridge University Press.

Housner, G. W., 1963. The behavior of inverted pendulum structures during earthquakes. *Bulletin of the Seismological Society of America*, **53**(2), 403–417.

Housner, G. W., 1965. Intensity of Earthquake Ground Shaking Near the Causative Fault. *3rd World Conference on Earthquake Engineering* (pp. 94–115).

Huerta, S., 2006. Galileo was Wrong: The Geometrical Design of Masonry Arches. *Nexus Network Journal*, **8**(2), 25–52. DOI: 10.1007/s00004-006-0016-8

Iervolino, I., and Dolce, M., 2018. Foreword to the Special Issue for the RINTC (The Implicit Seismic Risk of Code-Conforming Structures) Project. *Journal of Earthquake*

Engineering, **22**(sup2), 1–4. DOI: 10.1080/13632469.2018.1543697

Iervolino, I., Spillatura, A., and Bazzurro, P., 2018. Seismic Reliability of Code-Conforming Italian Buildings. *Journal of Earthquake Engineering*, **22**(sup2), 5–27. Taylor & Francis. DOI: 10.1080/13632469.2018.1540372

Indirli, M., S. Kouris, L. A., Formisano, A., Borg, R. P., and Mazzolani, F. M., 2013. Seismic Damage Assessment of Unreinforced Masonry Structures After The Abruzzo 2009 Earthquake: The Case Study of the Historical Centers of L'Aquila and Castelvecchio Subequo. *International Journal of Architectural Heritage*, **7**(5), 536–578. DOI: 10.1080/15583058.2011.654050

International Council on Monuments and Site, 2011. *Guidance on Heritage Impact Assessments for Cultural World Heritage Propertie*. Paris, France: ICONOS.

Jalayer, F., 2003. *Direct probabilistic seismic analysis: implementing non-linear dynamic assessments*. (PhD Dissertation). Stanford, CA, USA: Stanford University.

JCSS, 2001. *Probabilistic Model Code*. The Joint Committee on Structural Safety.

Jia, G., Taflanidis, A. A., and Beck, J. L., 2017. A New Adaptive Rejection Sampling Method Using Kernel Density Approximations and Its Application to Subset Simulation. *ASCE-ASME Journal of Risk and Uncertainty in Engineering Systems, Part A: Civil Engineering*, **3**(2). DOI: 10.1061/AJRUA6.0000841

Karlsson, A., Johansson, R., and Andler, S. F., 2010. An Empirical Comparison of Bayesian and Credal Set Theory for Discrete State Estimation. In E. Hüllermeier, R. Kruse, and F. Hoffmann (Eds.), *Information Processing and Management of Uncertainty in Knowledge-Based Systems. Theory and Methods*, Communications in Computer and Information Science (Vol. 80, pp. 80–89). Berlin, Heidelberg: Springer Berlin Heidelberg. DOI: 10.1007/978-3-642-14055-6_9

Kaufmann, A., and Gupta, M. M., 1991. *Introduction to fuzzy arithmetic: theory and applications* (2. [print.].). New York: Van Nostrand Reinhold.

Kelly, D. L., and Smith, C. L., 2009. Bayesian inference in probabilistic risk assessment—The current state of the art. *Reliability Engineering & System Safety*, **94**(2), 628–643. DOI: 10.1016/j.ress.2008.07.002

Kelly, D., and Smith, C., 2011. *Bayesian Inference for Probabilistic Risk Assessment*. Springer Series in Reliability Engineering. London: Springer London. DOI: 10.1007/978-1-84996-187-5

Kiureghian, A. D., and Ditlevsen, O., 2009. Aleatory or epistemic? Does it matter? *Structural Safety*, Risk Acceptance and Risk Communication, **31**(2), 105–112. DOI: 10.1016/j.strusafe.2008.06.020

Klir, G. J., 2006. *Uncertainty and information: foundations of generalized information theory*. Hoboken, N.J: Wiley-Interscience.

Krawinkler, H., and Miranda, E., 2004. Performance-Based Earthquake Engineering. In Y. Bozorgnia and V. V. Bertero (Eds.), *Earthquake Engineering from Engineering Seismology to Performance-Based Engineering* (p. 976). CRC press. DOI: 10.1193/1.1896960

La Mendola, L., 1997. Influence of Nonlinear Constitutive Law on Masonry Pier Stability. *Journal of Structural Engineering*, **123**(10), 1303–1311. American Society of Civil Engineers. DOI: 10.1061/(ASCE)0733-9445(1997)123:10(1303)

La Mendola, L., and Papia, M., 1993. Stability of Masonry Piers under Their Own Weight and Eccentric Load. *Journal of Structural Engineering*, **119**(6), 1678–1693. American Society of Civil Engineers. DOI: 10.1061/(ASCE)0733-9445(1993)119:6(1678)

Ladevèze, P., Puel, G., and Romeuf, T., 2006. Lack of knowledge in structural model validation. *Computer Methods in Applied Mechanics and Engineering*, John H. Argyris Memorial Issue. Part I, **195**(37), 4697–4710. DOI: 10.1016/j.cma.2005.10.017

Lagomarsino, S., 2015. Seismic assessment of rocking masonry structures. *Bulletin of Earthquake Engineering*, **13**(1), 97–128. DOI: 10.1007/s10518-014-9609-x

Lagomarsino, S., and Giovinazzi, S., 2006. Macroseismic and mechanical models for the vulnerability and damage assessment of current buildings. *Bulletin of Earthquake Engineering*, **4**(4), 415–443. DOI: 10.1007/s10518-006-9024-z

Lagomarsino, S., and Resemini, S., 2009. The Assessment of Damage Limitation State in the Seismic Analysis of Monumental Buildings. *Earthquake Spectra*, **25**(2), 323–346. DOI: 10.1193/1.3110242

Lai, C. G., Bozzoni, F., Mangriotis, M.-D., and Martinelli, M., 2015. Soil Liquefaction during the 20 May 2012 M5.9 Emilia Earthquake, Northern Italy: Field Reconnaissance and Post-Event Assessment. *Earthquake Spectra*, **31**(4), 2351–2373. SAGE Publications Ltd STM. DOI: 10.1193/011313EQS002M

Lee, T.-H., and Mosalam, K. M., 2004. Probabilistic fiber element modeling of reinforced concrete structures. *Computers & Structures*, **82**(27), 2285–2299. DOI: 10.1016/j.compstruc.2004.05.013

Li, G., Rosenthal, C., and Rabitz, H., 2001. High Dimensional Model Representations. *The Journal of Physical Chemistry A*, **105**(33), 7765–7777. DOI: 10.1021/jp010450t

Liberatore, D., and Spera, G., 2001. Oscillazioni di blocchi snelli: valutazione sperimentale della dissipazione di energia durante gli urti. *10º Convegno Nazionale "L'ingegneria Sismica in Italia."* Potenza-Matera.

Lu, Z., Song, S., Yue, Z., and Wang, J., 2008. Reliability sensitivity method by line sampling. *Structural Safety*, **30**(6), 517–532. DOI: 10.1016/j.strusafe.2007.10.001

Lubliner, J., Oliver, J., Oller, S., and Oñate, E., 1989. A plastic-damage model for concrete. *International Journal of Solids and Structures*, **25**(3), 299–326. DOI: 10.1016/0020-7683(89)90050-4

Luco, N., and Cornell, C. A., 2007. Structure-Specific Scalar Intensity Measures for Near-Source and Ordinary Earthquake Ground Motions. *Earthquake Spectra*, **23**(2), 357–392. SAGE Publications Ltd STM. DOI: 10.1193/1.2723158

Magenes, G., and Penna, A., 2011. Seismic design and assessment of masonry buildings in Europe: recent research and code development issues. *Proceedings of the 9th Australasian Masonry Conference*. Presented at the 9th Australasian Masonry Conference, Queenstown, New Zealand: Jason Ingham, Manicka Dhanasekar, & Mark Masia.

Maio, R., Ferreira, T. M., Vicente, R., and Estêvão, J., 2016. Seismic vulnerability assessment of historical urban centres: case study of the old city centre of Faro, Portugal. *Journal of Risk Research*, **19**(5), 551–580. DOI: 10.1080/13669877.2014.988285

Makris, N., and Konstantinidis, D., 2003. The rocking spectrum and the limitations of practical design methodologies. *Earthquake Engineering & Structural Dynamics*, **32**(2), 265–289. DOI: 10.1002/eqe.223

Manzini, C. F., Magenes, G., Penna, A., da Porto, F., Camilletti, D., Cattari, S., and Lagomarsino, S., 2018. Masonry Italian Code-Conforming Buildings. Part 1: Case Studies and Design Methods. *Journal of Earthquake Engineering*, **22**(sup2), 54–73. DOI: 10.1080/13632469.2018.1532358

Mauro, A., de Felice, G., and DeJong, M. J., 2015. The relative dynamic resilience of masonry collapse mechanisms. *Engineering Structures*, **85**, 182–194. DOI: 10.1016/j.engstruct.2014.11.021

McGill, W. L., and Ayyub, B. M., 2008. Estimating parameter distributions in structural reliability assessment using the Transferable Belief Model. *Computers & Structures*, Uncertainty in Structural Analysis - Their Effect on Robustness, Sensitivity and Design, **86**(10), 1052–1060. DOI: 10.1016/j.compstruc.2007.05.038

McGuire, R. K., 2004. *Seismic hazard and risk analysis*. Second monograph series. Oakland, Calif: Earthquake Engineering Research Institute.

Mehrotra, A., and DeJong, M. J., 2018. The influence of interface geometry, stiffness, and crushing on the dynamic response of masonry collapse mechanisms. *Earthquake Engineering & Structural Dynamics*, **47**(13), 2661–2681. DOI: 10.1002/eqe.3103

Ministero della Cultura, 2010. *Linee Guida per la valutazione e riduzione del rischio sismico del patrimonio culturale –allineamento alle nuove Norme tecniche per le costruzioni*.

MIT, 2018. *D.M. 17.01.2018 Aggiornamento delle "Norme Tecniche per le Costruzioni."*

MIT, 2019. *Circolare 21 gennaio 2019 , n. 7 C.S.LL.PP. . Istruzioni per l'applicazione dell'«Aggiornamento delle "Norme tecniche per le costruzioni"» di cui al decreto ministeriale 17 gennaio 2018.*

Möller, B., and Beer, M., 2004. *Fuzzy randomness: uncertainty in civil engineering and computational mechanics*. Berlin ; New York: Springer.

Möller, B., Graf, W., and Beer, M., 2000. Fuzzy structural analysis using α-level optimization. *Computational Mechanics*, **26**(6), 547–565. DOI: 10.1007/s004660000204

Möller, B., Graf, W., and Beer, M., 2003. Safety assessment of structures in view of

fuzzy randomness. *Computers & Structures*, **81**(15), 1567–1582. DOI: 10.1016/S0045-7949(03)00147-0

Nale, M., Chiozzi, A., Lamborghini, R., Minghini, F., Rigolin, M., and Tralli, A., 2020. Fragility assessment of unreinforced masonry walls undergoing earthquake-induced local failure mechanisms. In M. Papadrakakis, M. Fragiadakis, and C. Papadimitriou (Eds.), *EURODYN 2020 Proceedings* (pp. 4311–4317). Athens: European Association for Structural Dynamics.

Nale, M., Minghini, F., Chiozzi, A., and Tralli, A., 2021. Fragility functions for local failure mechanisms in unreinforced masonry buildings: a typological study in Ferrara, Italy. *Bulletin of Earthquake Engineering*. DOI: 10.1007/s10518-021-01199-6

National Research Council, 1983. *Committee on the institutional means for assessment of risks to public health*. Washington, DC: National Academy Press.

NRC, 1975. *Reactor Safety Study, an Assessment of Accident Risks* (No. NUREG-75/014) (p. 1975). Washington, D.C.: U.S. Nuclear Regulatory Commission.

Nunziante, L., 2021. Damage to masonry retaining walls caused by capillarity. *Academia Letters*. DOI: 10.20935/AL1854

Oberguggenberger, M., and Fellin, W., 2008. Reliability bounds through random sets: Non-parametric methods and geotechnical applications. *Computers & Structures*, Uncertainty in Structural Analysis - Their Effect on Robustness, Sensitivity and Design, **86**(10), 1093–1101. DOI: 10.1016/j.compstruc.2007.05.040

Oberkampf, W. L., Helton, J. C., Joslyn, C. A., Wojtkiewicz, S. F., and Ferson, S., 2004. Challenge problems: uncertainty in system response given uncertain parameters. *Reliability Engineering & System Safety*, Alternative Representations of Epistemic Uncertainty, **85**(1), 11–19. DOI: 10.1016/j.ress.2004.03.002

Panteli, M., and Mancarella, P., 2015. Influence of extreme weather and climate change on the resilience of power systems: Impacts and possible mitigation strategies. *Electric Power Systems Research*, **127**, 259–270. DOI: 10.1016/j.epsr.2015.06.012

Papa, E., and Taliercio, A., 2005. A visco-damage model for brittle materials under monotonic and sustained stresses. *International Journal for Numerical and Analytical Methods in Geomechanics*, **29**(3), 287–310. John Wiley & Sons, Ltd. DOI:

10.1002/nag.415

Papathanassiou, G., Mantovani, A., Tarabusi, G., Rapti, D., and Caputo, R., 2015. Assessment of liquefaction potential for two liquefaction prone areas considering the May 20, 2012 Emilia (Italy) earthquake. *Engineering Geology*, **189**, 1–16. DOI: 10.1016/j.enggeo.2015.02.002

Paté-Cornell, M. E., 1996. Uncertainties in risk analysis: Six levels of treatment. *Reliability Engineering & System Safety*, Treatment of Aleatory and Epistemic Uncertainty, **54**(2), 95–111. DOI: 10.1016/S0951-8320(96)00067-1

Patelli, E., 2017. COSSAN: A Multidisciplinary Software Suite for Uncertainty Quantification and Risk Management. In R. Ghanem, D. Higdon, and H. Owhadi (Eds.), *Handbook of Uncertainty Quantification* (pp. 1909–1977). Cham: Springer International Publishing. DOI: 10.1007/978-3-319-12385-1_59

Patelli, E., Alvarez, D. A., Broggi, M., and de Angelis, M., 2014. An integrated and efficient numerical framework for uncertainty quantification: application to the NASA Langley multidisciplinary Uncertainty Quantification Challenge. *16th AIAA Non-Deterministic Approaches Conference*, AIAA SciTech Forum (Vols. 1-0). American Institute of Aeronautics and Astronautics. DOI: 10.2514/6.2014-1501

Patelli, E., Tolo, S., George-Williams, H., Sadeghi, J., Rocchetta, R., De Angelis, M., and Broggi, M., 2018. OpenCossan 2.0: an efficient computational toolbox for risk, reliability and resilience analysis. Florianopolis Brazil.

Pedroni, N., Zio, E., and Cadini, F., 2017. Advanced Monte Carlo Methods and Applications. *ASCE-ASME Journal of Risk and Uncertainty in Engineering Systems, Part A: Civil Engineering*, **3**(4), 02017001. DOI: 10.1061/AJRUA6.0000921

Penna, A., 2015. Seismic assessment of existing and strengthened stone-masonry buildings: critical issues and possible strategies. *Bulletin of Earthquake Engineering*, **13**(4), 1051–1071. DOI: 10.1007/s10518-014-9659-0

Penna, A., Morandi, P., Rota, M., Manzini, C. F., da Porto, F., and Magenes, G., 2014. Performance of masonry buildings during the Emilia 2012 earthquake. *Bulletin of Earthquake Engineering*, **12**(5), 2255–2273. DOI: 10.1007/s10518-013-9496-6

Pitilakis, K., Crowley, H., and Kaynia, A. M. (Eds.), 2014. *SYNER-G: Typology*

Definition and Fragility Functions for Physical Elements at Seismic Risk. Geotechnical, Geological and Earthquake Engineering (Vol. 27). Dordrecht: Springer Netherlands. DOI: 10.1007/978-94-007-7872-6

Pozzati, P., 1977. *Teoria e Tecnica delle Strutture* (Vol. 2–I). Torino, Italy: UTET.

Priestley, M. J. N., 1985. Seismic behaviour of unreinforced masonry walls. *Bulletin of the New Zealand Society for Earthquake Engineering*, **18**(2), 191–205. DOI: 10.5459/bnzsee.18.2.191-205

Rechard, R. P., 1999. Historical Relationship Between Performance Assessment for Radioactive Waste Disposal and Other Types of Risk Assessment. *Risk Analysis*, **19**(5), 763–807. John Wiley & Sons, Ltd. DOI: 10.1111/j.1539-6924.1999.tb00446.x

Rechard, R. P., 2000. Historical background on performance assessment for the Waste Isolation Pilot Plant. *Reliability Engineering & System Safety*, **69**(1), 5–46. DOI: 10.1016/S0951-8320(00)00023-5

ReLUIS, 2020. *Uso dei software di calcolo nella verifica sismica degli edifici in muratura* (No. ReLUIS 2019-WP10) (p. 372). Naples, Italy: ReLUIS.

Roca, P., Cervera, M., Gariup, G., and Pela', L., 2010. Structural Analysis of Masonry Historical Constructions. Classical and Advanced Approaches. *Archives of Computational Methods in Engineering*, **17**(3), 299–325. DOI: 10.1007/s11831-010-9046-1

Rocchetta, R., 2018. *Robust Computational Frameworks for Power Grid Reliability, Vulnerability and Resilience Analysis* (PhD Dissertation). Liverpool: University of Liverpool.

Rocchetta, R., Broggi, M., and Patelli, E., 2018. Do we have enough data? Robust reliability via uncertainty quantification. *Applied Mathematical Modelling*, **54**, 710–721. DOI: 10.1016/j.apm.2017.10.020

Romano, F., Ganduscio, S., and Zingone, G., 1993. Cracked Nonlinear Masonry Stability under Vertical and Lateral Loads. *Journal of Structural Engineering*, **119**(1), 69–87. American Society of Civil Engineers. DOI: 10.1061/(ASCE)0733-9445(1993)119:1(69)

Rosin, J., Butenweg, C., Cacciatore, P., and Boesen, N., 2018. Investigation of the

seismic performance of modern masonry buildings during the Emilia Romagna earthquake series: Untersuchungen des seismischen Verhaltens von modernen Mauerwerksbauten während der Erdbebenserie in der Emilia Romagna. *Mauerwerk*, **22**(4), 238–250. DOI: 10.1002/dama.201800013

Rota, M., Penna, A., and Magenes, G., 2010. A methodology for deriving analytical fragility curves for masonry buildings based on stochastic nonlinear analyses. *Engineering Structures*, **32**(5), 1312–1323. DOI: 10.1016/j.engstruct.2010.01.009

Sahlin, S., 1971. *Structural Masonry*. Englewood Cliffs, N.J.: Prentice-Hall.

Saisi, A., Binda, L., Cantini, L., and Tedeschi, C., 2008. Experimental study on the damaged pillars of the Noto Cathedral. *Learning from Failure Long-term Behaviour of Heavy Masonry Structures*, International Series on Advances in Architecture (pp. 109–123). WIT Press.

Saloustros, S., Pelà, L., Contrafatto, F. R., Roca, P., and Petromichelakis, I., 2019. Analytical Derivation of Seismic Fragility Curves for Historical Masonry Structures Based on Stochastic Analysis of Uncertain Material Parameters. *International Journal of Architectural Heritage*, **13**(7), 1142–1164. DOI: 10.1080/15583058.2019.1638992

Saltelli, A., 2008. *Global sensitivity analysis: the primer*. Chichester, England; Hoboken, NJ: John Wiley.

Sandoval, C., Roca, P., Bernat, E., and Gil, L., 2011. Testing and numerical modelling of buckling failure of masonry walls. *Masonry Research and Practice*, **25**(12), 4394–4402. DOI: 10.1016/j.conbuildmat.2011.01.007

Savoia, M., 2002. Structural reliability analysis through fuzzy number approach, with application to stability. *Computers & Structures*, **80**(12), 1087–1102. DOI: 10.1016/S0045-7949(02)00068-8

Savoia, M., Mazzotti, C., Ferracuti, B., Ferretti, F., and Tilocca, A. R., 2016. *Relazione riassuntiva e indicazioni tecnico operative*. Realizzazione di indagini sperimentali in situ su pareti di edifici in muratura nei comuni colpiti dal sisma del 2012 (p. 40). Bologna: CIRI.

Schenk, C. A., and Schuëller, G. I., 2005. *Uncertainty Assessment of Large Finite Element Systems*. Lecture Notes in Applied and Computational Mechanics (Vol. 24).

Berlin/Heidelberg: Springer-Verlag. DOI: 10.1007/11673941

Schöbi, R., 2017. *Surrogate models for uncertainty quantification in the context of imprecise probability modelling* (PhD Dissertation). Zurich, CH: ETH Zurich.

Schöbi, R., Sudret, B., and Marelli, S., 2017. Rare Event Estimation Using Polynomial-Chaos Kriging. *ASCE-ASME Journal of Risk and Uncertainty in Engineering Systems, Part A: Civil Engineering*, **3**(2). DOI: 10.1061/AJRUA6.0000870

Shafer, G., 1976. *A Mathematical Theory of Evidence*. Princeton University Press. DOI: 10.2307/j.ctv10vm1qb

Shawa, O. Al, de Felice, G., Mauro, A., and Sorrentino, L., 2012. Out-of-plane seismic behaviour of rocking masonry walls. *Earthquake Engineering & Structural Dynamics*, **41**(5), 949–968. DOI: 10.1002/eqe.1168

Silva, V., Akkar, S., Baker, J., Bazzurro, P., Castro, J. M., Crowley, H., Dolsek, M., et al., 2019. Current Challenges and Future Trends in Analytical Fragility and Vulnerability Modelling. *Earthquake Spectra*. DOI: 10.1193/042418EQS101O

Simões, A. G., Bento, R., Lagomarsino, S., Cattari, S., and Lourenço, P. B., 2019a. Fragility Functions for Tall URM Buildings around Early 20th Century in Lisbon. Part 1: Methodology and Application at Building Level. *International Journal of Architectural Heritage*, 1–24. DOI: 10.1080/15583058.2019.1618974

Simões, A. G., Bento, R., Lagomarsino, S., Cattari, S., and Lourenço, P. B., 2019b. Fragility Functions for Tall URM Buildings around Early 20th Century in Lisbon, Part 2: Application to Different Classes of Buildings. *International Journal of Architectural Heritage*, 1–17. DOI: 10.1080/15583058.2019.1661136

Simões, A. G., Bento, R., Lagomarsino, S., Cattari, S., and Lourenço, P. B., 2020. Seismic assessment of nineteenth and twentieth centuries URM buildings in Lisbon: structural features and derivation of fragility curves. *Bulletin of Earthquake Engineering*, **18**(2), 645–672. DOI: 10.1007/s10518-019-00618-z

SIMULIA, 2006. *ABAQUS Finite element analysis*. Maastricht, NL.

Sobol, I. M., 1993. Sensitivity estimates for nonlinear mathematical models. *Mathematical Modeling and ComputationalExperiment*, **1**(4), 407–414.

Sorrentino, L., AlShawa, O., and Decanini, L. D., 2011. The relevance of energy damping in unreinforced masonry rocking mechanisms. Experimental and analytic investigations. *Bulletin of Earthquake Engineering*, **9**(5), 1617–1642. DOI: 10.1007/s10518-011-9291-1

Sorrentino, L., Cattari, S., da Porto, F., Magenes, G., and Penna, A., 2019. Seismic behaviour of ordinary masonry buildings during the 2016 central Italy earthquakes. *Bulletin of Earthquake Engineering*, **17**(10), 5583–5607. DOI: 10.1007/s10518-018-0370-4

Sorrentino, L., D'Ayala, D., de Felice, G., Griffith, M. C., Lagomarsino, S., and Magenes, G., 2016. Review of Out-of-Plane Seismic Assessment Techniques Applied To Existing Masonry Buildings. *International Journal of Architectural Heritage*, 1–20. DOI: 10.1080/15583058.2016.1237586

Sorrentino, L., Liberatore, L., Liberatore, D., and Masiani, R., 2014. The behaviour of vernacular buildings in the 2012 Emilia earthquakes. *Bulletin of Earthquake Engineering*, **12**(5), 2367–2382. DOI: 10.1007/s10518-013-9455-2

Sorrentino, L., Masiani, R., and Griffith, M. C., 2008. The vertical spanning strip wall as a coupled rocking rigid body assembly. *Structural Engineering and Mechanics*, **29**(4), 433–453. DOI: 10.12989/sem.2008.29.4.433

Spanos, P. D., and Koh, A., 1984. Rocking of Rigid Blocks Due to Harmonic Shaking. *Journal of Engineering Mechanics*, **110**(11), 1627–1642. DOI: 10.1061/(ASCE)0733-9399(1984)110:11(1627)

Spillatura, A., Fiorini, E., Bazzurro, P., and Pennucci, D., 2014. Harmonization of vulnerability fragility curves for masonry buildings. *Second European Conference on Earthquake Engineering*.

Squassina, A., 2011. Murature di mattoni medioevali a vista e resti di finiture a Venezia. *Arqueología de la Arquitectura*, **0**(8), 239–271. DOI: 10.3989/arqarqt.2011.10015

Stucchi, M., Meletti, C., Montaldo, V., Crowley, H., Calvi, G. M., and Boschi, E., 2011. Seismic Hazard Assessment (2003-2009) for the Italian Building Code. *Bulletin of the Seismological Society of America*, **101**(4), 1885–1911. DOI: 10.1785/0120100130

Sun, X., Kirchdoerfer, T., and Ortiz, M., 2020. Rigorous uncertainty quantification and design with uncertain material models. *International Journal of Impact Engineering*, **136**, 103418. DOI: 10.1016/j.ijimpeng.2019.103418

Suzuki, A., and Iervolino, I., 2017. Italian vs. worldwide history of largest PGA and PGV. *Annals of Geophysics*, **60**(5). DOI: 10.4401/ag-7391

The Mathworks Inc., 2016. MATLAB - MathWorks. *www.mathworks.com/products/matlab*. Retrieved from http://www.mathworks.com/products/matlab/

Tomassetti, U., Graziotti, F., Sorrentino, L., and Penna, A., 2019. Modelling rocking response via equivalent viscous damping. *Earthquake Engineering & Structural Dynamics*, **48**(11), 1277–1296. DOI: 10.1002/eqe.3182

Tonon, F., and Bernardini, A., 1998. A random set approach to the optimization of uncertain structures. *Computers & Structures*, **68**(6), 583–600. DOI: 10.1016/S0045-7949(98)00079-0

Tralli, A., Alessandri, C., and Milani, G., 2014. Computational Methods for Masonry Vaults: A Review of Recent Results. *The Open Civil Engineering Journal*, **8**(1), 272–287. DOI: 10.2174/1874149501408010272

Vaculik, J., and Griffith, M. C., 2017. Out-of-plane load–displacement model for two-way spanning masonry walls. *Engineering Structures*, **141**, 328–343. DOI: 10.1016/j.engstruct.2017.03.024

Valente, M., and Milani, G., 2018. Seismic response and damage patterns of masonry churches: Seven case studies in Ferrara, Italy. *Engineering Structures*, **177**, 809–835. DOI: 10.1016/j.engstruct.2018.08.071

Vamvatsikos, D., and Cornell, C. A., 2002. Incremental dynamic analysis. *Earthquake Engineering & Structural Dynamics*, **31**(3), 491–514. DOI: 10.1002/eqe.141

Verstrynge, E., Schueremans, L., and Van Gemert, D., 2011. Time-dependent mechanical behavior of lime-mortar masonry. *Materials and Structures*, **44**(1), 29–42. DOI: 10.1617/s11527-010-9606-8

Verstrynge, E., Schueremans, L., Van Gemert, D., and Hendriks, M. A. N., 2011. Modelling and analysis of time-dependent behaviour of historical masonry under high

stress levels. *Engineering Structures*, **33**(1), 210–217. DOI: 10.1016/j.engstruct.2010.10.010

Wang, P., Lu, Z., and Tang, Z., 2013. An application of the Kriging method in global sensitivity analysis with parameter uncertainty. *Applied Mathematical Modelling*, **37**(9), 6543–6555. DOI: 10.1016/j.apm.2013.01.019

Wang, Z., and Kiureghian, A. D., 2017. Orthogonal Plane Sampling for High-Dimensional Reliability Analysis. *ASCE-ASME Journal of Risk and Uncertainty in Engineering Systems, Part A: Civil Engineering*, **3**(3). DOI: 10.1061/AJRUA6.0000901

Wei, P., Lu, Z., and Song, J., 2014. Extended Monte Carlo Simulation for Parametric Global Sensitivity Analysis and Optimization. *AIAA Journal*, **52**(4), 867–878. DOI: 10.2514/1.J052726

Whittaker, A., Atkinson, G., Baker, J., Bray, J., Grant, D., Hamburger, R., Haselton, C., et al., 2011. *Selecting and Scaling Earthquake Ground Motions for Performing Response-History Analyses*.

Wu, Y.-T., 1994. Computational methods for efficient structural reliability and reliability sensitivity analysis. *AIAA Journal*, **32**(8), 1717–1723. DOI: 10.2514/3.12164

Xu, C., and Gertner, G. Z., 2008. Uncertainty and sensitivity analysis for models with correlated parameters. *Reliability Engineering & System Safety*, **93**(10), 1563–1573. DOI: 10.1016/j.ress.2007.06.003

Yim, C.-S., Chopra, A. K., and Penzien, J., 1980. Rocking response of rigid blocks to earthquakes. *Earthquake Engineering & Structural Dynamics*, **8**(6), 565–587. DOI: 10.1002/eqe.4290080606

Yokel, F. Y., 1971. Stability and Load Capacity of Members with No Tensile Strength. *Journal of the Structural Division*, **97**(7), 1913–1926. American Society of Civil Engineers. DOI: 10.1061/JSDEAG.0002954

Zadeh, L. A., 1968. Probability measures of Fuzzy events. *Journal of Mathematical Analysis and Applications*, **23**(2), 421–427. DOI: 10.1016/0022-247X(68)90078-4

Zadeh, L. A., 1975. The concept of a linguistic variable and its application to approximate reasoning—I. *Information Sciences*, **8**(3), 199–249. DOI: 10.1016/0020-

0255(75)90036-5

Zio, E., 2007. *An introduction to the basics of reliability and risk analysis*. Series on quality, reliability & engineering statistics. Singapore ; Hackensack, N.J: World Scientific.

Zio, E., 2013. *The Monte Carlo Simulation Method for System Reliability and Risk Analysis*. Springer Series in Reliability Engineering. London: Springer London. DOI: 10.1007/978-1-4471-4588-2

Zio, E., 2018. The future of risk assessment. *Reliability Engineering & System Safety*, **177**, 176–190. DOI: 10.1016/j.ress.2018.04.020

Zuccaro, G., and Cacace, F., 2012. Seismic vulnerability assessment of the masonry buildings based on the probability of occurrence of the main collapse mechanisms. Damage Vulnerability Curves vs. PGA. (pp. 1–10). Presented at the 15th WCEE, Lisboa (Portugal).

Zuccaro, G., and Cacace, F., 2015. Seismic vulnerability assessment based on typological characteristics. The first level procedure "SAVE." *Soil Dynamics and Earthquake Engineering*, **69**, 262–269. DOI: 10.1016/j.soildyn.2014.11.003

Zuccaro, G., Dato, F., Cacace, F., De Gregorio, D., and Sessa, S., 2017. Seismic collapse mechanisms analyses and masonry structures typologies: a possible correlation. *Ingegneria Sismica*, **34**(4), 121–149.

Zuccaro, G., Dolce, M., de Gregorio, D., Speranza, E., and Moroni, C., 2016. La scheda CARTIS per la caratterizzazione tipologico- strutturale dei comparti urbani costituiti da edifici ordinari. Valutazione dell'esposizione in analisi di rischio sismico. *Proceedings of the GNGTS* (pp. 281–287). Presented at the GNGTS 2015.

Zuccaro, G., and Papa, F., 2004. MEDEA: A multimedia and didactic handbook for seismic damage evaluation. *XXXIX European Seismological Commission General Assembly* (pp. 215–220). Presented at the XXXIX European Seismological Commission General Assembly, Potsdam, Germany: GeoForschungsZentrum & Potsdam University.